THE ORIGIN OF THE NCHANGA COPPER-COBALT DEPOSITS OF THE ZAMBIAN COPPERBELT

A thesis presented for the degree
of Doctor of Philosophy

By Ross McGowan

School of Ocean and Earth Science

Faculty of Science

University of Southampton

May 2003

University of Southampton

DECLARATION

This PhD thesis by

Ross McGowan

has been produced whilst registered for postgraduate studies under the supervision of the following persons:

Supervisors:	Dr. Stephen Roberts University of Southampton
	Dr. Robert P. Foster Exploration Consultants Ltd.
Chair of Advisory Panel:	Prof. Carl L. Amos University of Southampton
Member of Advisory Panel:	Dr. Andrew J. Barker University of Southampton

It is based on work carried out by the above named author, unless otherwise stated, and has not been submitted, in any form, for another degree.

Ross McGowan

UNIVERSITY OF SOUTHAMPTON

ABSTRACT

FACULTY OF SCIENCE

SCHOOL OF OCEAN & EARTH SCIENCE

Doctor of Philosophy

THE ORIGIN OF THE NCHANGA COPPER-COBALT DEPOSITS OF THE ZAMBIAN COPPEBELT

By Ross McGowan

The Zambian Copperbelt is arguably the most significantly mineralized Neoproterozoic basin on earth, preserving a truly spectacular scale of mineralization, with in excess of one billion tonnes of ore at ~2.7% copper extracted to date and major cobalt accumulations. The origin of these deposits, of which Nchanga is one of the largest, has been intensely debated for over six decades, yet the driving forces that generated this system are poorly understood, in particular the relationship between tectonics, palaeo-fluid circulation, and ore deposition.

The structural evolution of Nchanga involved: (i) early, pre-Katangan extension, represented by high-angle structures within the Basement, followed by (ii) inversion on high-angle structures (against stable granite block) and internal thrust-propagation fold development within the basal part of the Katangan sequence (Lower and Upper Roan Groups). This most likely took place during the main phases of the Lufilian Orogeny (550 to 560 Ma), and was strongly controlled by competence contrasts between different lithologies. High-grade mineralization is spatially associated with major structures, and the majority is hosted by shale-capped quartzo-feldspathic units that have undergone recrystallization and potassic hydrothermal alteration, indicated by a mineral assemblage of phlogopite-sericite-quartz (± dolomite, tourmaline and rutile). Ore mineralogy consists of diagenetic/early pyrite (that possibly replaced earlier anhydrite) replaced by disseminated and fracture-related chalcopyrite and bornite, which has subsequently undergone replacement by chalcocite. Carrollite (Co) appears to overprint primary chalcopyrite and bornite where present, but precedes the chalcocite. Supergene oxidation of mineralization is represented by abundances of malachite and chrysocolla.

Fluid inclusion data, in combination with alteration mineral assemblages and whole-rock geochemistry, have identified a potential ore-forming fluid of medium temperature (pressure-corrected: 300° to 310°C within faults and 220° to 240°C within ore zones; T_H = 230° to 240°C and 160° to 180°C respectively), high salinity (30 to 38 equivalent wt% NaCl), and near-neutral to slightly acidic pH (5-7), that contained significant quantities of Mg and Ca, as well as Cu and Co. Oxygen isotope analysis has revealed $\delta^{18}O_{fluid}$ (SMOW) signatures of +2.7‰ to +10.3‰ (calculated with corrected temperatures), which are consistent with basinal brines that have undergone significant water-rock interaction. The $\delta^{34}S$ (CDT) of diagenetic pyrites within black shale ranges form –1‰ to –17‰, typical of bacterially reduced seawater sulphate. By contrast, the copper sulphides range from –1‰ to +18‰, which is more representative of thermochemical reduction of a sulphate-enriched fluid. This is supported by the $\delta^{13}C$ (PDB) of dolomite alteration around ore with values of –5.6‰ to –8.3‰, indicative of a component of organic carbon, compared to dolomites of the Upper Roan, which yield $\delta^{13}C$ typical of marine carbon of +1.5‰ to +2.5‰.

These new data highlight the link between processes occurring during basin evolution and ore formation. A new model is proposed involving the migration of copper- and cobalt-rich brines into shale-capped methane-rich arenites, during basin inversion, with precipitation of sulphides on thermochemical reduction of the sulphate-enriched fluid. The brine, generated deep within the host basin, most probably became highly saline, Mg-, Ca-, and sulphate-rich, and suitably oxidizing for the effective transport of copper and cobalt as tetrahedral complex chloride ions, during dissolution of evaporites, leaching metals from Basement during migration to the margins of the deforming basin.

TABLE OF CONTENTS

APPENDICES (ON CD ROM)

APPENDIX A BOREHOLE AND SAMPLE LISTS

A1 List of boreholes
A2 Sample lists

APPENDIX B GEOCHEMICAL DATA

B1 Mineral chemistry of Nchanga phlogopites
B2 ACME Laboratories Ltd analytical procedures
B3 ACME Laboratories Ltd detection limits
B4 ACME Laboratories Ltd geochemical data
B5 XRF data
B6 Isocon method for interpretation of XRF data
B7 Accuracy and precision of geochemical data

APPENDIX C FLUID INCLUSION DATA

C1 Calibration of Linkam 600 heating/freezing stage
C2 Fluid inclusion thermometric data

APPENDIX D STABLE ISOTOPE DATA

D1 Oxygen isotope data
D2 Conventional and laser sulphur isotope data
D3 Carbon and oxygen isotope data of dolomites
D4 Accuracy and precision of isotope data

APPENDIX E THESIS PHOTOGRAPHS

LIST OF FIGURES

LIST OF TABLES

ACKNOWLEDGEMENTS

Firstly thanks must go to my supervisors, Dr Stephen Roberts and Dr Bob Foster, for their advice throughout the project and their invaluable criticisms and comments during the preparation of this thesis. Thanks must also go to Dr Adrian Boyce for advice concerning stable isotope work and the preparation of manuscripts and the thesis.

The Fermor Award of the Geological Society of London funded the majority of the author's studies. In addition, Anglo American provided financial and logistical support during fieldwork in Zambia. Stable isotope work was funded by a NERC Isotope Geosciences Laboratory Grant (IP/755/0302) and carried out using the facilities at the Scottish Universities Environmental Research Centre (SUERC).

Support and advice from the following is acknowledged during time spent in Africa: Nick Franey, Dr Mike Buxton, Jon Woodhead, and Peter Mann (Anglo American and Zamanglo Prospecting Ltd.), Dr Dave Coller (ERA Maptec), Dr SK Chakroboty, Kevin Palmer, and Phashion Chabaya (formerly KCM and ZCCM), Dave Armstrong (Mopani Mines), Dr Bruce Nesbitt, Noel McNee, Mike Richards, and Jeames McKibben (Equinox Resources).

The following people have offered advice during completion of studies in the UK: Dr Andy Barker, Dr Damon Teagle, Professor Martin Palmer, Dr Ian Croudace, Dr Jim Andrews, Dr Clive Boulter, Nicola Holland, and Dr Jon Evans (University of Southampton), Dr Kevin Leahy (Exploration Consultants Ltd.), and Dr Jamie Wilkinson (Imperial College, London). Practical support at the University of Southampton from Bob Jones, Jon Ford, Dr Richard Pearce, Ross Williams, and Barry Marsh is also acknowledged.

Finally, thanks must go to family and friends for their support throughout the last three and a half years, in particular my mother for financial support in the later stages, and Kristina for help with some aspects of the final version of this thesis.

CHAPTER 1:

INTRODUCTION

CHAPTER 1: INTRODUCTION

1.1 Rationale

Sediment-hosted copper deposits are one of the world's most important sources of copper, with their essential characteristics of consistent grades and lateral continuity making them a much sought after exploration target. The Zambian Copperbelt, as arguably the most significantly mineralized Neoproterozoic basin on Earth, is no exception. By far the most significant metal concentrations are the copper-cobalt deposits, the origin of which have been debated for over six decades (Darnley, 1960; Whyte & Green, 1971; Garlick, 1972; Annels, 1974; Binda, 1975; Van Eden, 1974; Annels *et al.*, 1983; Sweeney *et al.*, 1986, 1991; Sweeney & Binda, 1989, 1994; Molak, 1995). These deposits preserve a truly spectacular scale of mineralization with in excess of a billion tonnes of ore at ~2.7% copper extracted to date (MMMD, 1998) and major cobalt accumulations. However, our understanding of the driving forces behind these systems does not reflect their importance, in particular the relationships between tectonics and the processes occurring during host-basin evolution, and palaeo-fluid circulation, and the role they play in ore formation.

Current research and exploration activity in Zambia represents the significant interest now being given to the whole region. This research project is one of several now being carried out on the Copperbelt. Its primary aim is to determine the controls of mineralization for the Nchanga group of deposits (Zambian Copperbelt) and to generate a new genetic model to account for their origin. Various aspects of ore genesis have been tested, including: (i) source of various components such as metals, sulphur, and ore-forming fluids, (ii) migration of fluids on a basin-scale to deposit-scale, and (iii) the controls on the deposition of metals and sulphides. Presented here are the results of field-based studies and follow up petrographic, palaeo-fluid, and stable isotope work that further our understanding of the genesis of these world-class copper and cobalt resources. The model presented in this thesis represents a significant re-interpretation of the genesis of a major component of Copperbelt mineralization and has important implications, not only for our understanding of the processes responsible for the production of such spectacular metal concentrations in the crust, but also for future exploration initiatives in the area.

1.2 Objectives

The principal objectives of this study are:

- To understand the geology of the Nchanga deposits, in particular the structural evolution of the host-rock package.
- To determine the relationships of copper and cobalt mineralization to lithology and structure from macro- to micro-scale.
- To determine the petrography and paragenesis of the ore mineral assemblages.
- To investigate the associated wallrock alteration and geochemistry and the implications for fluid chemistry.
- To determine the p-t-x conditions of fluids within the host-rock package, through the study of fluid inclusions, and potentially sample the ore-forming fluid.
- To investigate the stable isotope characteristics of ore sulphides and associated gangue minerals to constrain the geological fluid reservoirs contributing to the mineralization.

1.3 Location

The Copperbelt region of Zambia (Fig. 1.1) is located north of the capital Lusaka, adjacent to the Democratic Republic of Congo border. The Zambian Copperbelt itself (Fig. 1.2) is a strip of land approximately 50 kilometres wide and 140 kilometres long, stretching from Chililabombwe (Konkola Mine) in the north to Ndola in the south, and contains the majority of major copper and cobalt deposits of the region.

1.4 Methodology

This study has been concentrated on the Nchanga area and group of deposits situated around the town of Chingola. In total 12 weeks were spent in the field at Nchanga completing a number of tasks, including:

- Field mapping of open pit and underground geology and ore sequences
- Logging of boreholes through ore sequences
- Reconstruction of mine sections
- Hand specimen sampling for follow up analytical work in Southampton
- Down-hole 'groove' sampling for geochemical analysis

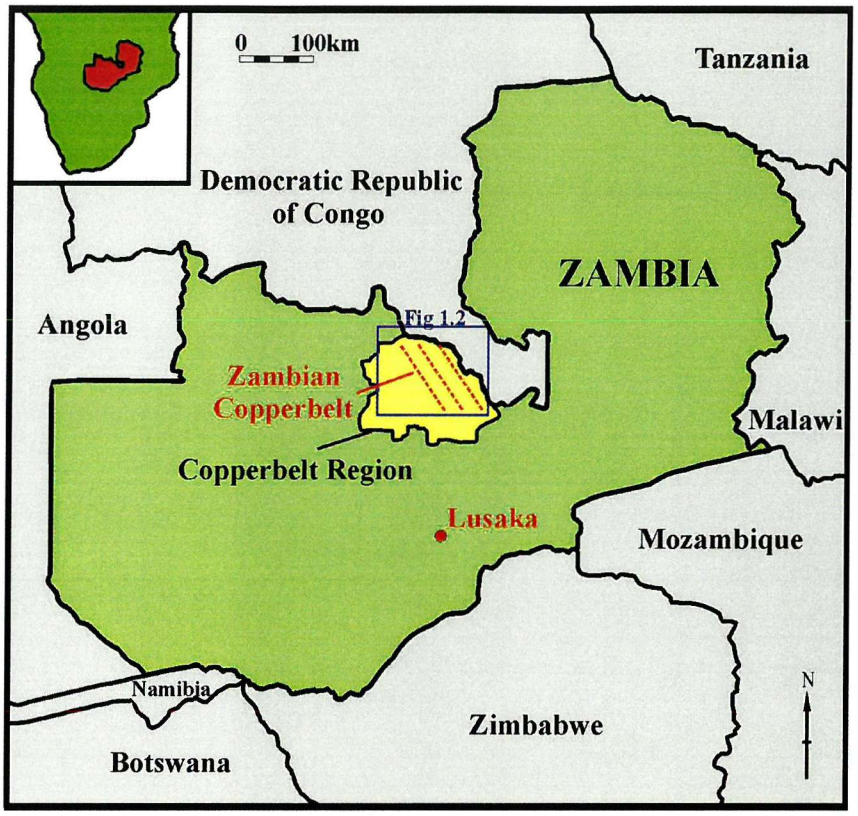

Figure 1.1: Map of Zambia showing the Copperbelt region and the Zambian Copperbelt.

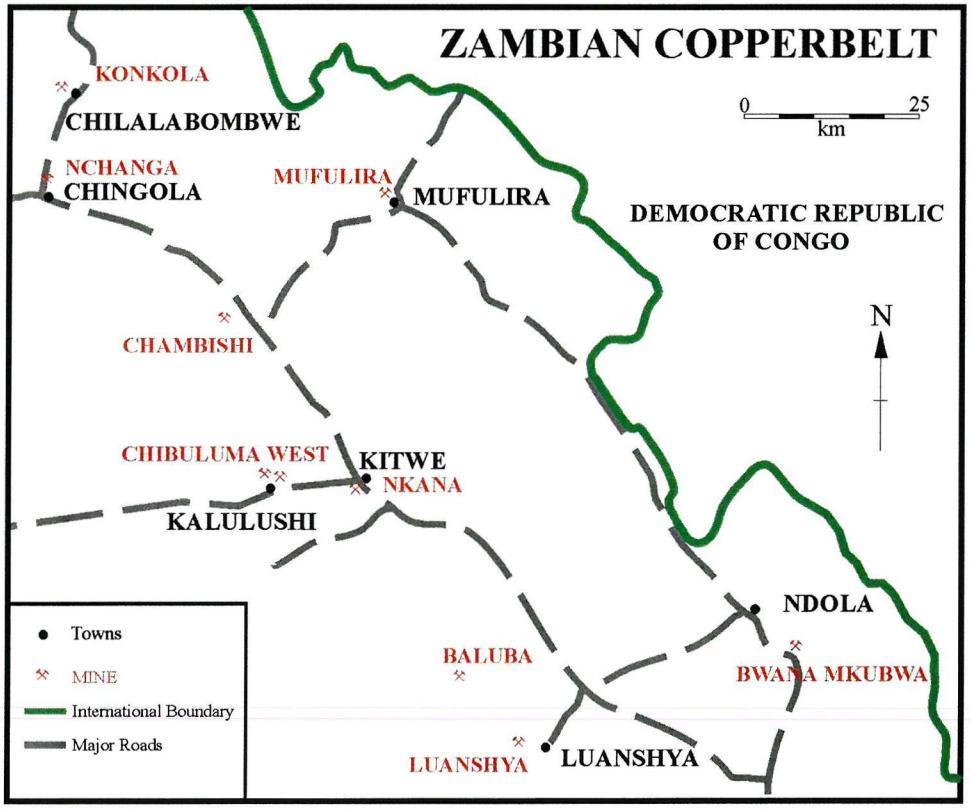

Figure 1.2: Map of Zambian Copperbelt showing the major mines, towns, and roads of the region.

Subsequent work completed at Southampton University and the Scottish Universities Environmental Research Centre (SUERC) included:

- Detailed petrographic analysis of sulphide ores and Nchanga lithologies
- X-Ray fluorescence spectrometry of selected samples for geochemical suite analysis
- Palaeo-fluid/fluid inclusion analysis of Nchanga quartz veins
- Stable isotope analysis (sulphur, oxygen, and carbon) of selected sulphides, quartz veins, and carbonates

1.5 Thesis outline

The basis for any ore deposit study is to first constrain the geology (stratigraphy, structure, and metamorphism), and then to study the mineralization, hydrothermal alteration, and stable isotope and fluid inclusion characteristics with respect to these observations. Therefore the thesis has been constructed around this concept (Fig. 1.3). The geology and mineralization is described in details from large scale (Chapter 2: Regional geology), to deposit scale (Chapter 3: Geology and mineralization of the Nchanga area), and finally down to micro-scale to deal with the petrographic nature of the Nchanga sequence (Chapter 4: Ore mineralogy and wallrock alteration). The final results chapter (Chapter 5: Palaeo-fluid and stable isotope analysis) presents fluid inclusion and stable isotope analyses that aimed to test specific hypotheses and questions that have arisen during the Nchanga study. A discussion of the data presented in chapters 3 to 5, and the implications of those results for ore genesis is covered in Chapter 6, followed by conclusions, implications for future exploration, and recommendations for future work in Chapter 7.

1.6 Previous work at Nchanga

Considering the significant size of the Nchanga deposits and the fact that they constitute a major component of Copperbelt mineralization, there are few detailed descriptions of their geology and genesis, apart from the reviews by McKinnon & Smit (1961) and Fleischer *et al.* (1976), in comparison to some of the other major deposits such as Konkola, Chambishi, and Mufulira. Some previous authors (e.g. Daly *et al.*, 1984; Molak, 1995) have focused on the structural features that can be observed in the Nchanga open pits, yet there appears to be few studies that have taken into account the combined structural, alteration, ore, fluid inclusions, and stable isotope characteristics for this major copper and cobalt accumulation.

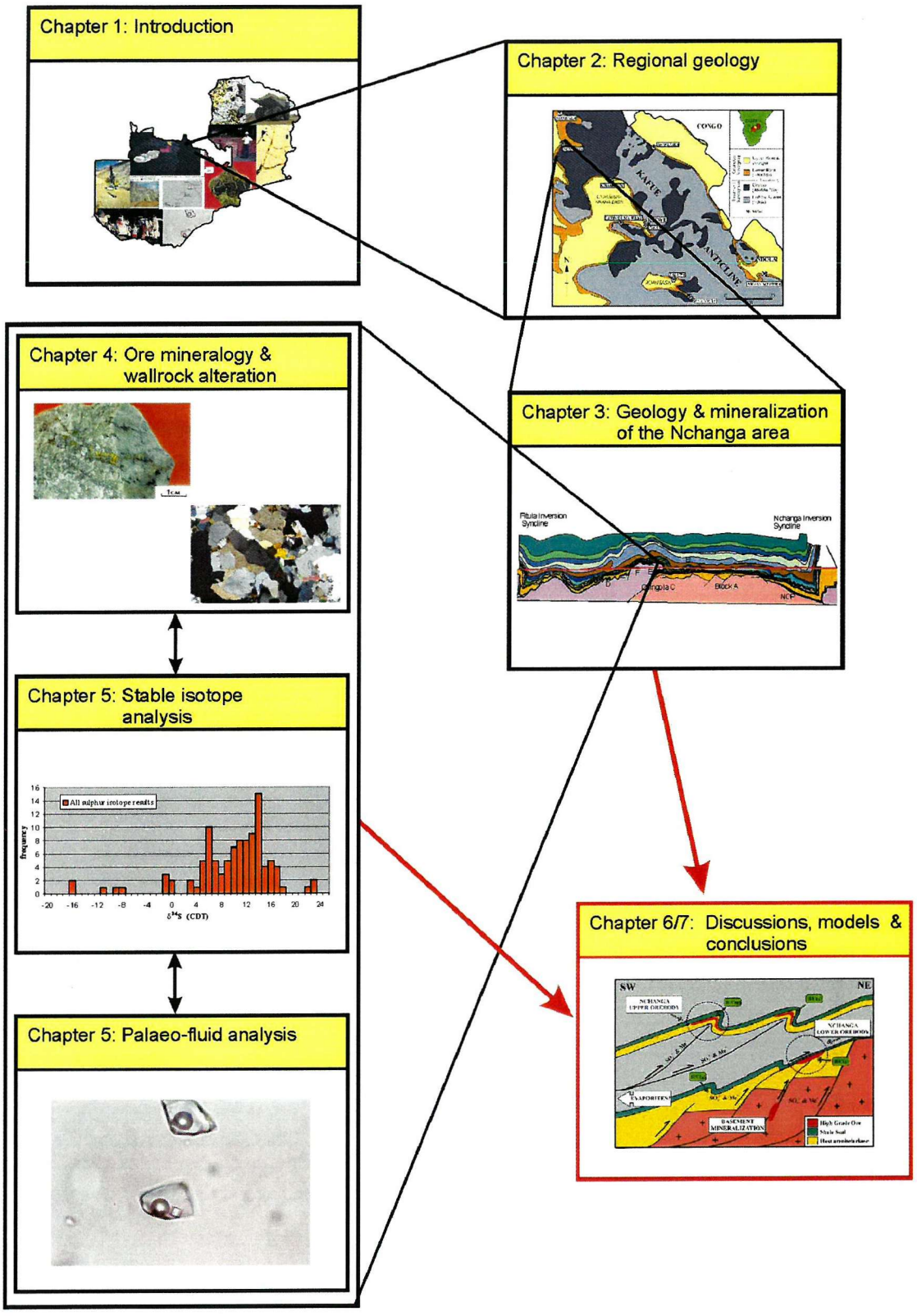

Figure 1.3: Diagrammatic summary of the Nchanga-based study and outline of this thesis.

1.7 Sediment-hosted copper deposits

Sediment-hosted copper deposits are a large and diverse class of deposit that includes some of the richest copper concentrations in the world, with common metal associations of cobalt and silver, and more minor occurrences of zinc, gold, lead, and iron (Fig. 1.4; Kirkham, 1976; Gustafson & Williams, 1981). Two of the most famous deposits are the Kupferchiefer of Poland and the Zambian Copperbelt, both of which contain deposits that are classed as 'giant copper deposits' (Gustafson & Williams, 1981). They are commonly located within fault-controlled sedimentary basins, in predominantly rift environments located in both intracontinental and continental-margin settings, with ages of mineralization ranging from Proterozoic to younger (Gustafson & Williams, 1981; Jowett, 1989; Lefebvre & Alldrick, 1996), with Proterozoic rocks being the hosts to a greater number of deposits than any other age, although this spans a large time period of 1930 Ma (Kirkham, 1989). Generally they consist of chalcopyrite, chalcocite and bornite (with pyrite outside of ore zones) within reduced horizons (shales, sandstones, and carbonates) near to oxidation-reduction boundaries, which are typically underlain by red-bed sandstones containing evaporite sequences (Lefebvre & Alldrick, 1996; Binda 1994; Kirkham, 1976; Maiden *et al.*, 1984; Oszczepalski, 1989). In most cases host rocks have not been subjected to metamorphism, although in Zambia greenschist facies grade is recorded (Fig. 1.4). There is generally no association with volcanic rocks. Kirkham (1989) emphasized the evaporite-copper association within arid and semi-arid environments by presenting plots of the distribution of both copper and evaporite deposits around the world, which appear to show a strong coincidence (Fig. 1.4). Gustafson & Williams (1981) went further and described the close association of many stratiform copper deposits with both gypsum and anhydrite, including the Zambian Copperbelt, Mount Isa, McArthur River, Kupferschiefer, Redstone River, and the Irish Pb-Zn deposits, and suggested that they provide a major source of sulphur (later fixed as sulphides), high salinity, and potential fluid pathways (through dissolution).

The timing of mineralization, the sources of fluids and fluid migration, the source of metals, the source of sulphur, and the trapping mechanism of copper, in the genesis of these major ores has often been a point of contention in studies of individual deposits wherever they are in the world (Kirkham, 1976; Brown, 1981). The views have generally been divided between syngenetic and epigenetic models, although in the last two decades mineralization during diagenesis has been proposed as the favoured timing for introduction of copper (and other base metals) into sedimentary host rocks (Kirkham, 1989).

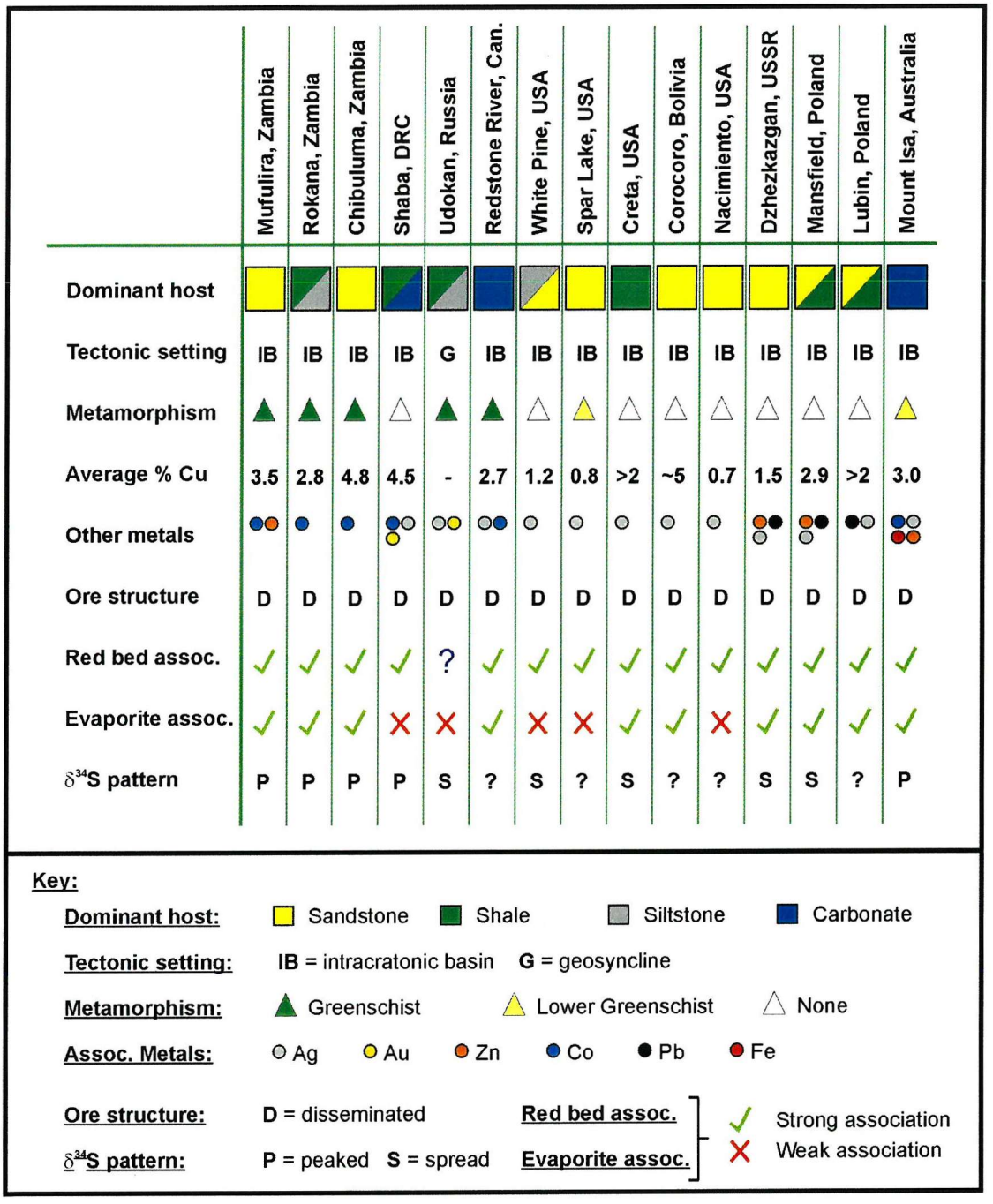

Figure 1.4: Summary of main characteristics of some major sediment-hosted copper deposits, including the Mufulira and Chibuluma deposits of the Zambian Copperbelt (modified from Gustafson & Williams, 1981).

Further detailed information on classification, distribution, geology, and genesis of sediment-hosted copper deposits is covered in the comprehensive reviews of Gustafson & Williams (1981) and Boyle *et al.*, (1989). Aspects of genesis of sediment-hosted copper deposits are discussed with reference to the Nchanga deposits in Chapter 6.

CHAPTER 2:

REGIONAL GEOLOGY

CHAPTER 2: REGIONAL GEOLOGY

2.1 Tectonic setting of the Zambian Copperbelt

The Zambian Copperbelt forms the southeastern part of the 900km-long Neoproterozoic Lufilian Arc (Figs. 2.1 & 2.2), a Pan-African fold belt (approximately 550Ma) that extends northwards into the Democratic Republic of Congo (Cahen & Snelling, 1966; Clifford, 1967, Daly *et al.*, 1984; Porada & Berhorst, 2000) and links with the Damara Belt of Namibia (Hunter & Pretorius, 1981; Unrug, 1983; Coward & Daly, 1984). This fold belt contains the Precambrian sediments of the Katangan Supergroup and the majority of the Cu-Co deposits of Zambia and the D.R.C. (Daly *et al.*, 1984). The Lufilian Arc (Fig. 2.3) is bounded to the northwest by the Kasai Shield; to the north and northeast by the Kibaran Belt and Bangwelu Block; to the east by the Irumide Belt of Kibaran age (1300-1000Ma); and to the south by the Mwembeshi Shear Zone (Ackermann & Forster, 1960; De Swardt & Drysdall, 1964; Unrug, 1983; Porada & Berhorst, 2000). The western boundary is covered by post-Katangan sediments (Unrug, 1983). The Zambezi Belt was defined by Unrug (1983) as "the region south of the Mwembeshi Shear zone and north of the Zimbabwe Craton not affected by Pan-African tectono-thermal processes." The Lufilian Arc is reported to have formed during the collision of the Angola-Kalahari and Congo-Tanzania Plates and accompanying NE-directed thrusting at 560-550Ma (Porada & Berhorst, 2000). The Mwembeshi Shear zone has been interpreted by some previous authors as the structure that separates the two plates (Unrug, 1983; Daly, 1986; Kampunzu & Cailteux, 1997), although this is rejected by Porada & Berhorst (2000).

2.2 Stratigraphy of the Zambian Copperbelt

The stratigraphy of the Zambian Copperbelt is summarized in Figure 2.4. The Basement Complex consists of the Lufubu System (the oldest rocks of the Copperbelt area), the Muva System (rarely exposed on the Copperbelt) overlying the basement, and granitic rocks which intrude the Lufubu but are mostly older than the Muva, with the exception of the Nchanga Red Granite (Mendelsohn, 1961; Fleischer *et al.*, 1976). The lowermost units of the Katangan Supergroup (Lower and Upper Roan Groups of the Mine Series) are exposed in mines and rare outcrops, whereas the Kundulungu sedimentary rocks only occur locally on the

Copperbelt (Mendelsohn, 1961). The Lower Roan Group, the dominant ore-bearing sequence, occurs in structural basins, separated by outcropping pre-Katangan basement highs (Cailteux *et al.*, 1994), where the sediments rest with an angular unconformity on the granites and schists of the Basement Complex.

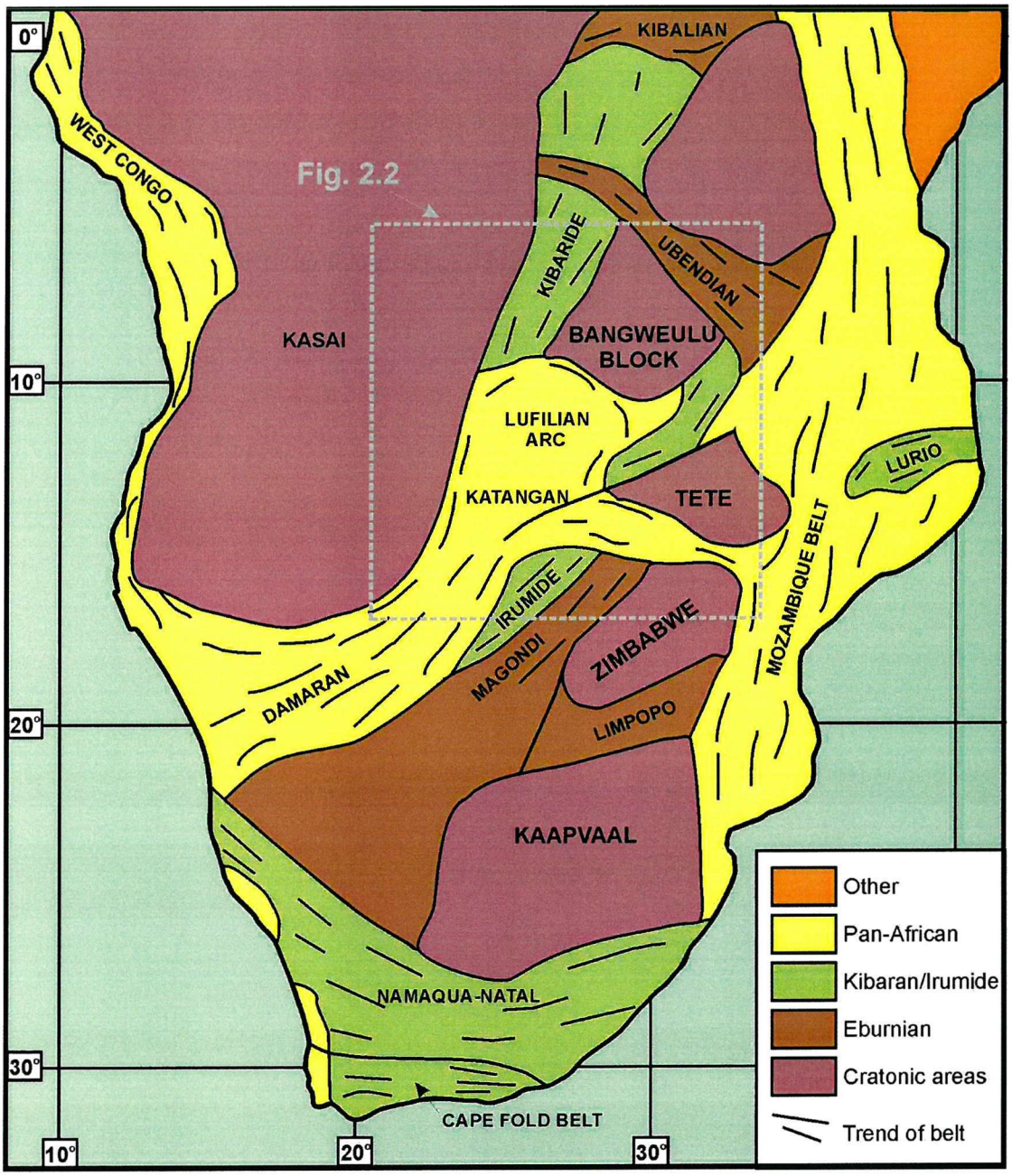

Figure 2.1: Major cratons and fold belts of central and southern Africa (Duane & Saggerson, 1995)

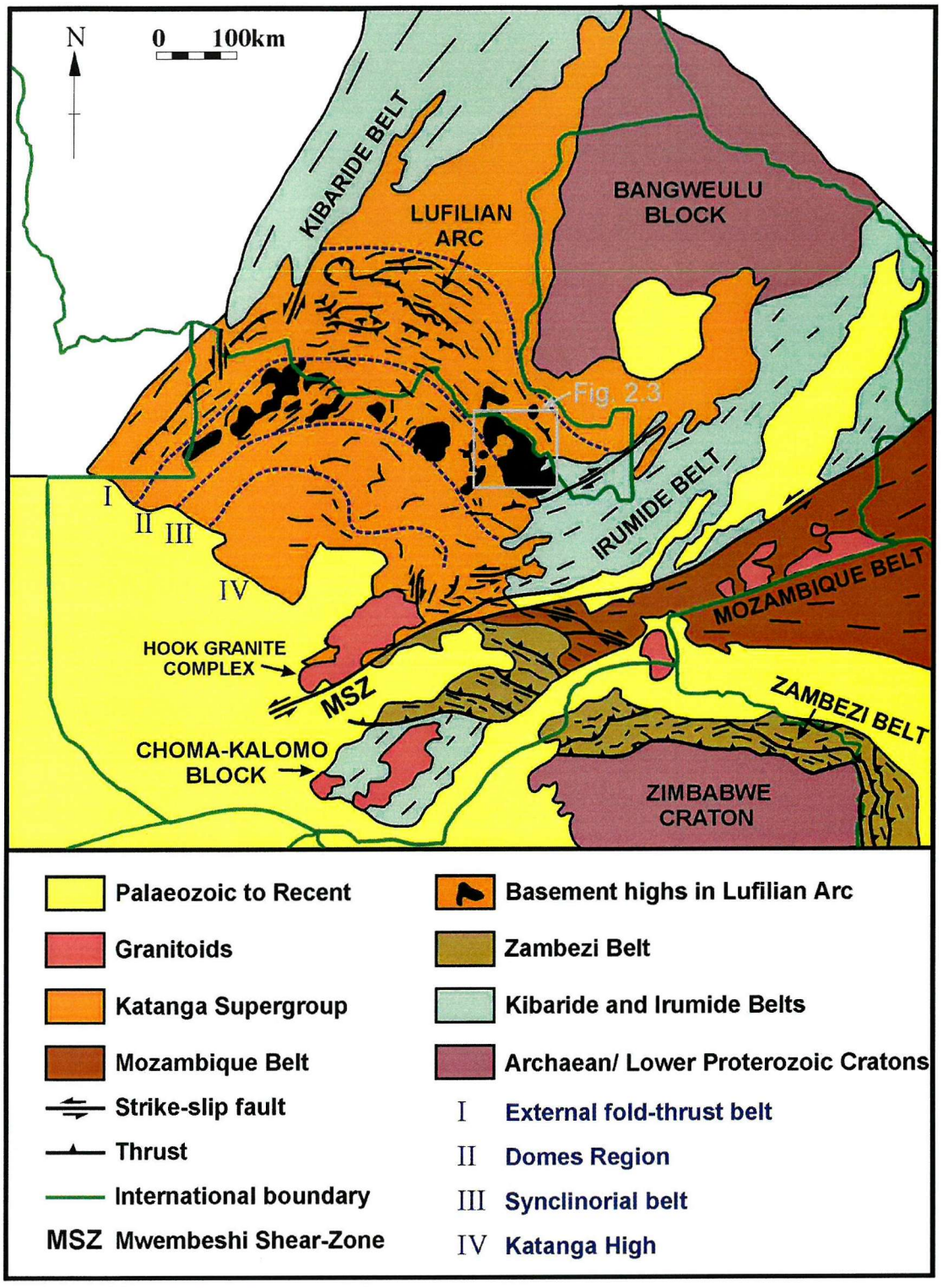

Figure 2.2: Tectonic setting of Zambia and the Lufilian Arc (Porada, 1989; Binda & Porada, 1995).

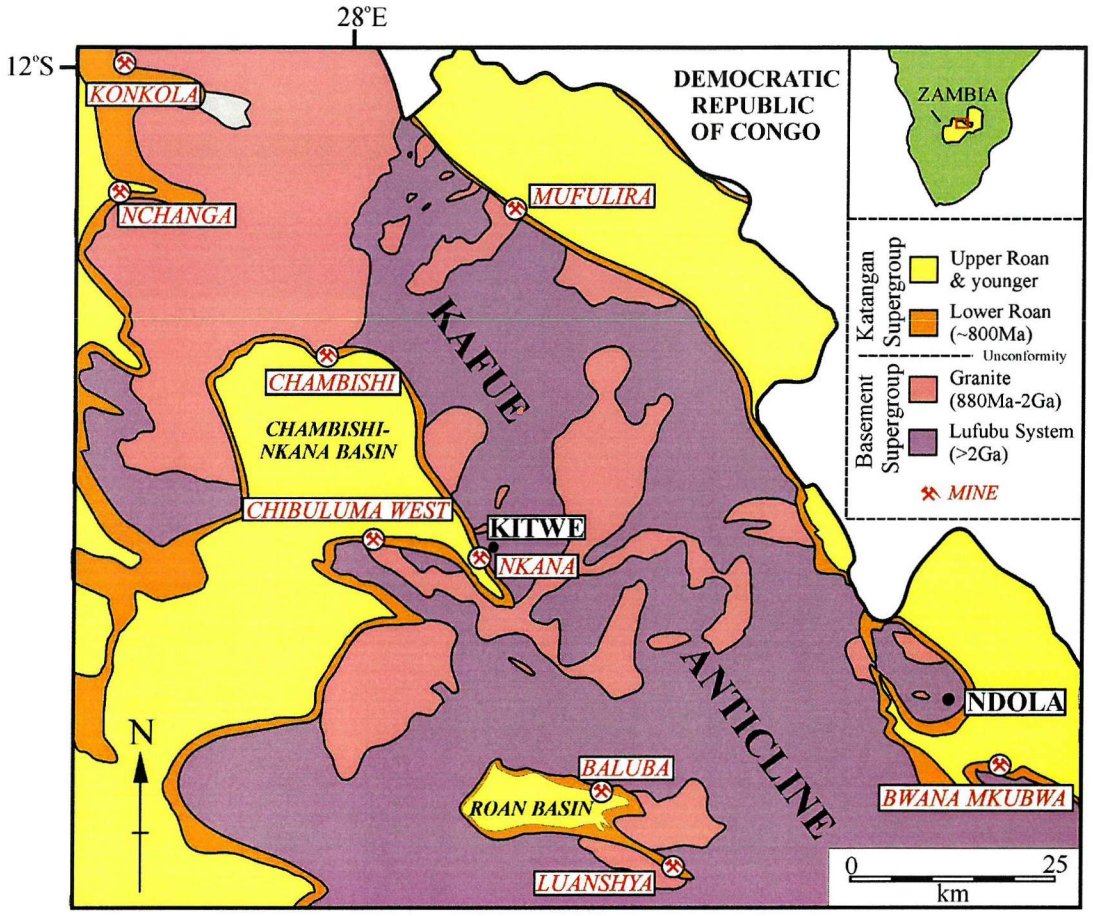

Figure 2.3: Geological map of the Zambian Copperbelt showing the Katangan sedimentary rocks exposed on the flank of the Kafue Anticline and the major towns and mines of the region (modified from Fleischer *et al.*, 1976).

2.2.1 Basement Complex

The quartz-mica schists and gneisses of the Lufubu System comprise the oldest rocks on the Copperbelt (Mendelsohn, 1961), dated at >2 Ga, and have been intruded by granites. They mainly consist of dark grey to green biotite-muscovite-quartz-schists or biotite gneisses, and locally are extensively foliated. Granites that intrude the basement show zircon ages of 1975 and 1750 Ma for the Mufulira and Roan Antelope granites respectively (Cahen *et al.*, 1970), 1882 ±20 Ma for the Luina Dome, Shaba (Ngoyi *et al.*, 1991), 863 Ma for the Lusakan Granite (Barr *et al.*, 1977), 877 ±11 Ma for the Nchanga Red Granite, considered as the youngest granite on the Copperbelt (Armstrong *et al.*, 1999). These data suggest that the Lufubu schists are Eburnean (~2000 Ma) or older. Mendelsohn (1961) claimed that much of the older granite was generated by granitization of the Lufubu Schists. Granites of the Hook Granite Complex, south-west of the Copperbelt, record even younger zircon ages of 559 ± 18 and 566 ± 5 Ma, which appear to equate to the age of granite plutonism in the Damara Belt of Namibia, supporting some form of tectono-thermal link between these two regions during Pan-African orogenesis (Hanson *et al.*, 1993).

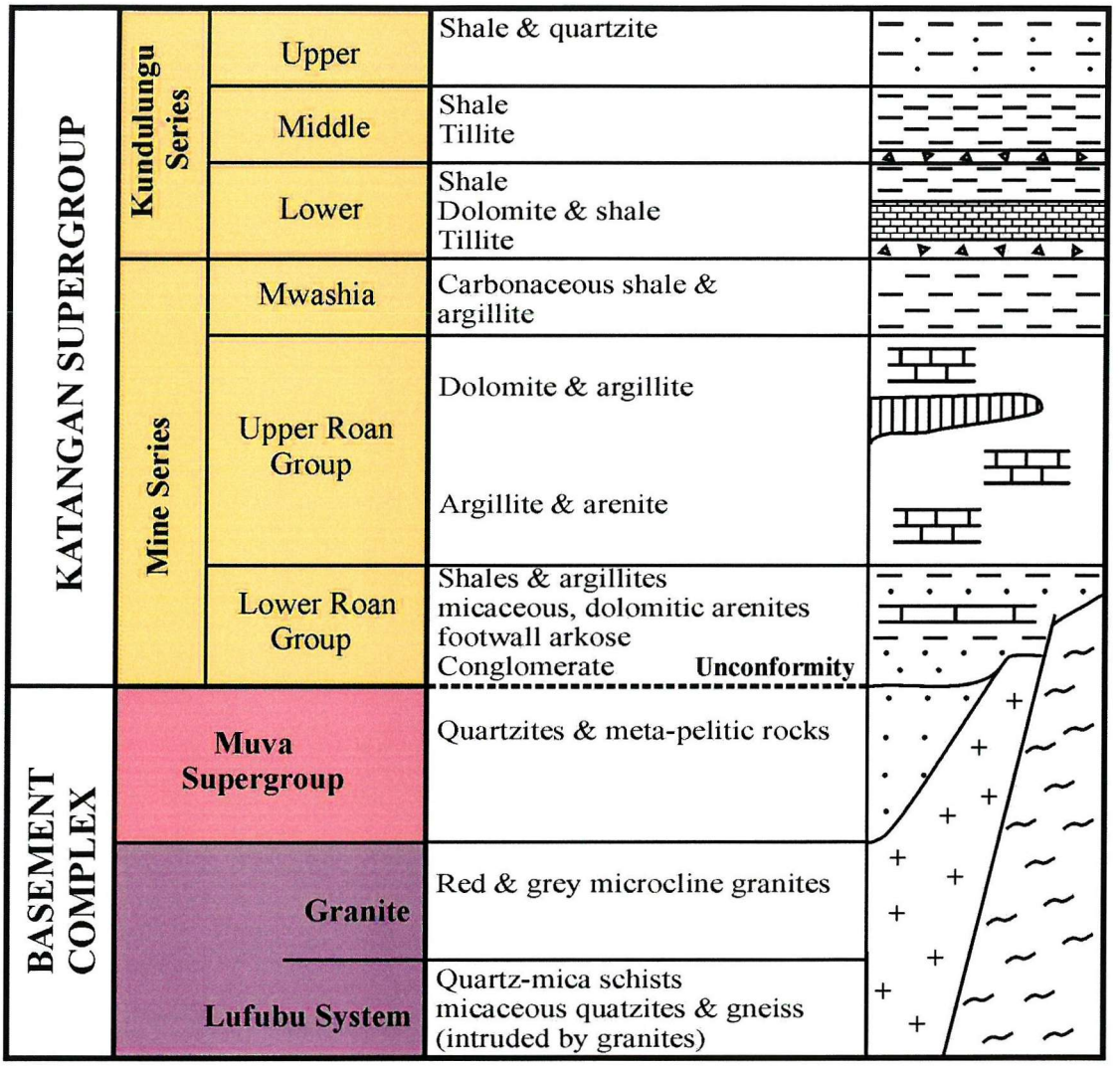

Figure 2.4: Stratigraphy of the Zambian Copperbelt and major lithologies (summarized from Mendelsohn, 1961; Drysdall *et al.*, 1972; Binda & Mulgrew, 1974; Fleischer *et al.*, 1976).

2.2.2 Katangan Supergroup

The sediments of the Katangan Supergroup are well described in the available literature compared with the rocks of the Basement Complex, in particular the Lower and Upper Roan Groups of the Mine Series (Fig. 2.4), which are the hosts to all the major occurrences of copper and cobalt. The maximum age for the Katangan is constrained by the U-Pb 877 ± 11 Ma age of the Nchanga Red Granite; zircons in the overlying basal arkoses have been dated at 880 Ma and 1800-2000 Ma suggesting that the Roan was derived from the Nchanga Red Granite or correlatives as well as from older basement (Armstrong *et al.*, 1999). The Mine Series, ranging in thickness from 800m to 2000m, has a well-defined sequence. This passes upwards from basal continental clastics (deposited in response to marine incursion across a continental landscape) to accumulations of shallow argillaceous marine clastics to mixed

carbonate platform sequence (mainly dolomitic units) and finally to the carbonaceous shales of the Mwashia Group (Mendelsohn, 1961; Simmonds, 1998). The trend of palaeo-shorelines has been interpreted as NW-SE from studies at Luanshya and Chambishi (Garlick, 1961b) and Mufulira (Van Eden & Binda, 1972). The upper units of the Katanga Supergroup, preserved in deeper parts of the basins (away from mines), are less well known.

The Lower Roan Group of rocks that host the copper and cobalt of the Zambian Copperbelt has in the past been subdivided into five formations (Table 2.1): the 'Footwall Formation,' the 'Ore Shale,' the 'Hangingwall Formation,' the 'Chingola Dolomite' and the 'Shale with Grit' Formation (based on observations made at Luanshya Mine by Binda & Mulgrew (1974), although recognized at each Copperbelt deposit). The Lower Roan is then conformably overlain by the dolomites and dolomitic shales of the Upper Roan Group and the black carbonaceous shales of the Mwashia Group (Cailteux *et al.*, 1994). It must be kept in mind that these formation names are mining terms and do not necessarily represent the true lithology. Binda (1994) alternatively subdivided the Lower and Upper Roan Groups into three lithostratigraphical divisions (summarized in Table 2.2) and this report uses this subdivision to avoid use of misleading mining terms: the Siliciclastic Unit (equivalent to the 'footwall formation'); the Mixed Unit (equivalent to the 'ore-shale'); and the Carbonate Unit (all units overlying the 'ore-shale' but below the Mwashia Group). In addition to the main lithologies (Tables 2.1 & 2.2), anhydrite is common, both as lenses and scattered beds within the Lower Roan sediments (in particular within the Mixed Unit).

Although the stratigraphy has been described in detail for individual deposits, often using different terms to describe units, Binda & Mulgrew (1974) presented a detailed correlation of the Lower Roan units on the western side of the Kafue Anticline, and Binda (1994) and Binda & Mulgrew (1974) correlated these with the Lower Roan at Mufulira on the eastern side (Fig. 2.5). The result is that the inter-deposit sequence of the Lower Roan appears to correlate well, if the stratigraphic classification of units at each deposit is correct. The variable thickness of the Siliciclastic Unit, where near palaeo-highs may be thin and may contain only one conglomerate unit, but further away may be several hundred metres thick and contain up to three conglomerate units (Fig. 2.5).

KATANGAN	MWASHIA GROUP		
	UPPER ROAN		
	LOWER ROAN	Shale with Grit Formation	Coarse arenites and some argillites
		Chingola Dolomite	Yellow-brown dolomite with minor interbedded argillites
		Hangingwall Formation	Cross-bedded 'quartzites' (feldspathic arenites) and argillites becoming more dolomitic and schistose towards the top.
		Ore Shale	Argillaceous units (locally carbonaceous), arenites and dolomitic horizons
		Footwall Formation	Footwall sandstone – feldspathic arenite Footwall 'quartzites' – up to 300m of clean feldspathic arenites Basal conglomerate – variable thickness
BASEMENT			

Table 2.1: Subdivisions of the Lower Roan Group, unconformably overlying the Pre-Katangan basement (summarized from: Mendelsohn, 1961; Binda & Mulgrew, 1974; Clemmey, 1974; Fleischer *et al.*, 1976; Cailteux *et al.*, 1994)

2.2.3 Interpretation of regional stratigraphy

The sedimentary succession of the Katangan Lower Roan sequence can be interpreted on the basis of transgressive and regressive marine phases over a continental (basement) landscape:

- Early transgression over basement topography and deposition of footwall siliciclastics.
- A major transgression over the whole of the Copperbelt (towards the NE), with truncation of basement highs, development of evaporites, and subsequently the deposition of deeper-water facies of the 'ore-shale' horizon.
- Oscillations of the shore-line causing deposition of the arenites, argillites and dolomites of the Mixed Unit.

(summarized from Binda & Mulgrew, 1974; Diederix, 1977).

KATANGAN	MWASHIA GROUP		
	UPPER ROAN	Carbonate Unit (365-670m)	Dolostone and interbedded dolomitic shales (± anhydrite beds)
	LOWER ROAN	Mixed Unit (150-250m)	Carbonate rocks Argillite, siltstone and arkosic sandstone (± anhydrite beds)
		Siliciclastic Unit (0-500m)	Sandstone and siltstone (red beds) Hematitic arkosic conglomerate
BASEMENT			

Table 2.2: Subdivisions of the Lower and Upper Roan Groups, unconformably overlying the Pre-Katangan basement that will be used in this report (summarized from Binda, 1994).

2.2.4 Igneous rocks

Igneous rocks are not a major component of the Copperbelt Katangan sequence. No volcanic rocks have been described from the Lower Roan at any of the major deposits. Gabbros have been recognized intruding the Upper Roan carbonates (Tembo *et al.*, 1999), and Annels (1974, 1984) described 'amphibolite' sills in the Upper Roan. Simmonds (1998) reported irregular sill-like gabbros within the Upper Roan and Mwashia Groups that 'comprise part of a major bimodal magmatic province, localised by rift faults during deposition of the Kundulungu Supergroup.' These sills have also been identified at the Chibuluma West Deposit where they have been described as multiple intrusions of syenitic to gabbroic composition that have been extensively altered to scapolitized amphibolitic rocks (Whyte & Green, 1971).

The lithostratigraphy is discussed in greater detail in Chapter 3 where the geology of the Nchanga deposits is described.

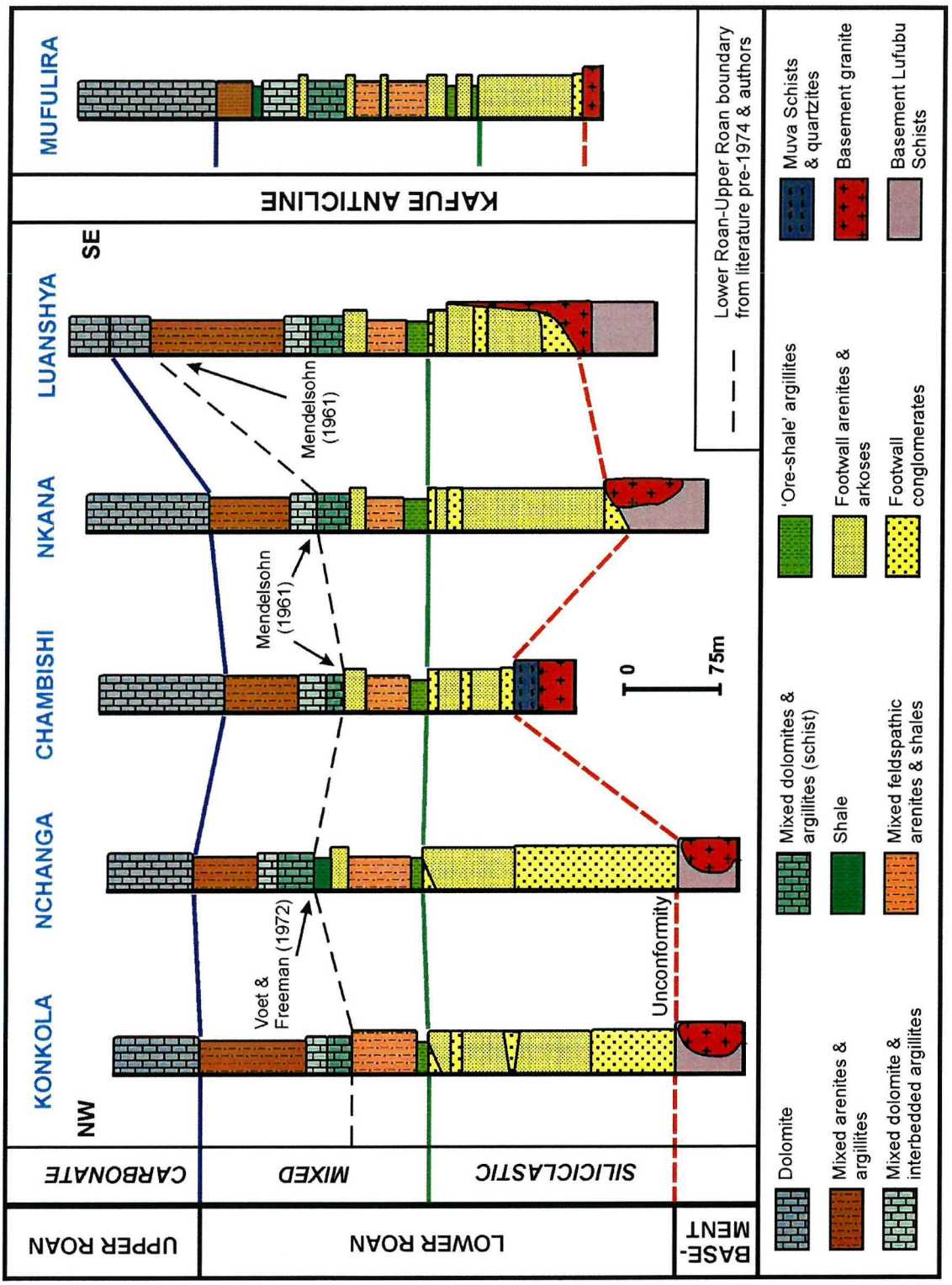

Figure 2.5: Stratigraphic correlation of the Lower Roan Group of the Katangan Supergroup on the western flank of the Kafue Anticline, including a comparison with the Mufulira deposit on the eastern side (modified from Binda & Mulgrew, 1974 and Binda, 1994).

2.2.5 Lithostratigraphic correlation with the Katangan sequence in the D.R.C.

Cailteux *et al.* (1994) presented a lithostratigraphic correlation between the Katangan Supergroup of the Zambian Copperbelt and the Shaba region of the Democratic Republic of Congo (Table 2.3). The 'Groupe des Mines" (equivalent to the Mines Series in Zambia) occurs mostly as allochthonous sheets overlying younger rocks of the Kundulungu. With two apparently different tectonic settings, correlation has always been somewhat controversial, promoted by the fact that D.R.C. orebodies occur in carbonate host-rocks (Upper Roan?) whereas the deposits of Zambia are hosted predominantly by siliciclastic units. The 'Roches Argilo-Talqueuses' (R.A.T.) is the oldest unit of the allochthonous succession and corresponds to the Siliciclastic Unit of Zambia. Both the R.A.T. and Dipeta Group form tectonized thrust sheets/nappes associated with prominent breccias containing fragments of the Mines Group.

<table>
<tr><td rowspan="7">KATANGAN S.GROUP</td><td colspan="4">KUNDULUNGU</td></tr>
<tr><td colspan="2">D.R.C.</td><td colspan="2">ZAMBIA</td></tr>
<tr><td rowspan="4">Roan Supergroup</td><td>Mwashya Group</td><td colspan="2">Mwashia Group</td></tr>
<tr><td rowspan="2">Dipeta Group</td><td rowspan="2">Carbonate Unit</td><td>Upper Roan</td></tr>
<tr><td rowspan="2">Mixed Unit</td><td rowspan="3">Lower Roan</td></tr>
<tr><td>Mines Group (Series des Mines)</td></tr>
<tr><td colspan="2">R.A.T.</td><td>Siliciclastic Unit</td></tr>
<tr><td colspan="4">KIBARAN & PRE-KIBARAN BASEMENT</td></tr>
</table>

Table 2.3: Simplified lithostratigraphic correlation of the Katangan Supergroup of the Zambian Copperbelt and the D.R.C. (modified from Cailteux *et al.*, 1994).

2.2.6 Tectonic setting of sedimentation

The geotectonic setting of the Zambian Copperbelt and mechanisms of basin evolution are important when considering genetic models for the mineralization and relative timing of ore-forming processes. It is widely accepted that the setting was intracratonic (Binda, 1994). However, debate on the mechanism that controlled sediment accumulation ranges from rifting to slow subsidence models. Annels (1984) claimed that the Copperbelt is stratigraphically related to a Proterozoic intracratonic rift, developed during episodes of cratonic basic magmatism in central Africa from 1400 to 900 Ma (simultaneous with the formation of the Kibaride and Irumide mobile belts) and the associated extension and fracturing of the continental crust (Watson, 1973). It is also suggested that a 'hot-spot' occurred at the south-eastern margin of the Congo Craton where a triple junction developed, the failed arm of which extended into the area of the Zambian Copperbelt and promoted subsidence and sedimentation (± metallogenesis). These events occurred at approximately 900 Ma, about the time that deposition of Lower Roan sediments is now thought to have commenced (Armstrong *et al.*, 1999). The evidence for an intracratonic rift (Annels, 1984) includes the location of the amphibolite or gabbro sills (described above) and the characteristic sequence of rift sediments, i.e. evaporites and cyclic sedimentation. The geometry of the basement is explained as a complex structure of uplifted and downfaulted blocks controlling the palaeo-topography, over which the Lower Roan sediments were draped. These were then folded into steeply inclined folds during the Lufilian Orogeny. Wendorff *et al.* (2000) also suggested that rifting of a continental block and a major marine transgression led to the deposition of the Roan, suggesting that the Katangan sequence is the sedimentary record of a complete 'Wilson Cycle' of continental and shallow marine clastics succeeded by platform carbonates (Kampunzu *et al.*, 1993; Tembo *et al.*, 1999). However, Binda (1994), whilst admitting that most Phanerozoic basins with sedimentary sequences similar to the Copperbelt formed as a result of early extension (Kingston *et al.*, 1983), dismissed any fracturing and rifting of the crust in the Copperbelt due to lack of evidence, including the absence of basaltic magmatism, ophiolites, linear dyke swarms, and magnetic anomalies. The closure of the basin was marked by north-directed thrusting and minor south-verging back-thrusts (Kampunzu & Cailteux, 1999; see below).

2.3 Tectonics and structure of the Zambian Copperbelt

The dominant control on the outcrop pattern of the Copperbelt is the Kafue Dome (Kafue Anticline), a major NNW-striking basement culmination off which the Katangan sediments dip both to the east and west (Daly *et al.*, 1984). The Zambian Copperbelt formed its present fold and thrust-belt character during the Damara-Lufilian-Zambezi Orogen (Daly, 1986;

Unrug, 1988, 1989; Porada, 1989; Hanson *et al.*, 1988; Simmonds, 1998; Hitzman, 2000). Cailteux *et al.* (1994) claimed that the Katangan rocks were affected by three tectono-thermal events: the Lomamian (~950 Ma), the Lusakan (~850-950 Ma) and the Lufilian (~650-600 Ma) Orogenies. However, the Lower Roan has been dated at 877 ± 11 Ma (Armstrong *et al.*, 1999), which suggests that the Katangan rocks have only been subjected to Lufilian orogenesis. The Lufilian Orogeny has been dated at 656-503 Ma (Cahen *et al.*, 1984), although Hanson *et al.* (1993) proposed that the main stage of deformation of Copperbelt sequences occurred at 560-550 Ma based on age determinations on the Hook Granite and related syntectonic rhyolites in the Mwembeshi Shear Zone (Porada & Berhorst, 2000). Unrug (1988, 1989) subdivided the Lufilian Arc into two broad zones: a northern zone (which contains the D.R.C.) of tightly folded, thin-skinned thrust sheets of weakly to non-metamorphosed Katangan strata (Hitzman, 2000) and a southern or inner zone containing the Zambian Copperbelt. This southern zone was further subdivided by Porada (1989) into four structural belts, with the Zambian Copperbelt located in the Domes region (Fig. 2.2).

Coward & Daly (1984), Daly *et al.* (1984), and Daly (1986) interpreted the Kafue Anticline (Fig. 2.3) as a hangingwall ramp above a deep decoupling zone (Fig. 2.6). They suggest that deep-rooted structures cut up through the Basement, with dominant transport direction and vergence to the northeast, forming the culmination. Hitzman (2000) reported that the Katangan sequence is folded parallel to the axis of the Kafue Anticline, with structures displaying vergence to the north east, and that the basement rocks of the Zambian Copperbelt do not display any evidence of the fold-thrust event that has affected the Katangan rocks. This suggests that the Basement Supergroup and Katangan Supergroup were locally decoupled during Lufilian-age deformation. Porada (1989) also proposed detachments within the Katangan stratigraphy and in part of the Domes region west of the Copperbelt (Fig. 2.2). Cosi *et al.* (1992) described a detachment at the Basement-Katangan contact and NE-directed thrusting within the Katangan sequence. A similar relationship was noted at Chambishi by Hitzman (2000). Hitzman (2000) also proposed the presence of major thrust structures, with NE-directed transport, to explain the changes in metamorphic grade from northeast (lower greenschist) to southwest (upper greenschist-lower amphibolite; Fig. 2.7). The southwest vergence of some structures is attributed to local backthrust development (Daly *et al.*, 1984).

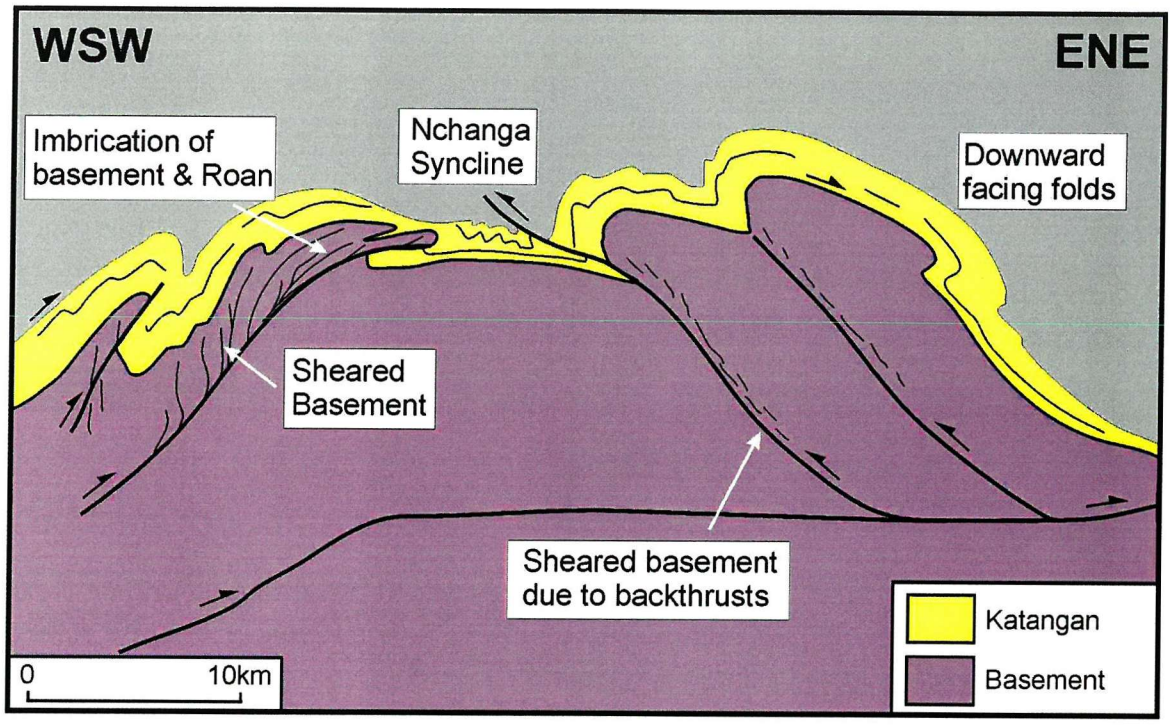

Figure 2.6: Schematic cross-section of the northern part of the Kafue Anticline, invoking NE-directed thrusts as the major control on the basement culmination (Daly *et al.*, 1984).

2.4 Metamorphism

The rocks of the Basement Supergroup have been subjected to greenschist facies metamorphism, slightly higher grade than the sediments of the Katanga Supergroup. (Mendelsohn, 1961). The basement underwent pervasive, retrogressive metamorphism during the folding of the Katangan cover during the Lufilian Orogeny (Mendelsohn, 1961; Fleischer *et al.*, 1976). The most common metamorphic minerals are reported to be sericite and biotite.

The Katangan rocks were deformed and metamorphosed mainly during the Lufilian Orogeny (~650-500 Ma) to greenschist facies (Simmonds, 1998). Extensive recrystallization of the clastic sediments of the Lower Roan has taken place, in particular of the sandstones which have been converted to arenites, and sedimentary structures are mostly destroyed (Mendelsohn, 1961). In addition, the argillaceous and carbonate rocks have been recrystallized. The main metamorphic minerals, observed by Darnley (1960), Mendelsohn (1961), and Fleischer *et al.* (1976), are biotite and sericite, accompanied by scapolite and minor tourmaline, chlorite, tremolite-actinolite, epidote, and apatite. The presence of scapolite within the Lower Roan sediments (in particular within the Mixed Unit) is further evidence of the former presence of evaporites within the sequence (Hitzman, 2000). Mendelsohn (1961) reported that the metamorphism and subsequent growth of new minerals probably took place without the addition of material from an external source. Hitzman (2000) proposed the

change in metamorphic grade across the Copperbelt from the lowest grades at Konkola and Mufulira (lower greenschist) to the highest grades at Luanshya (upper greenschist/amphibolite; Fig. 2.7).

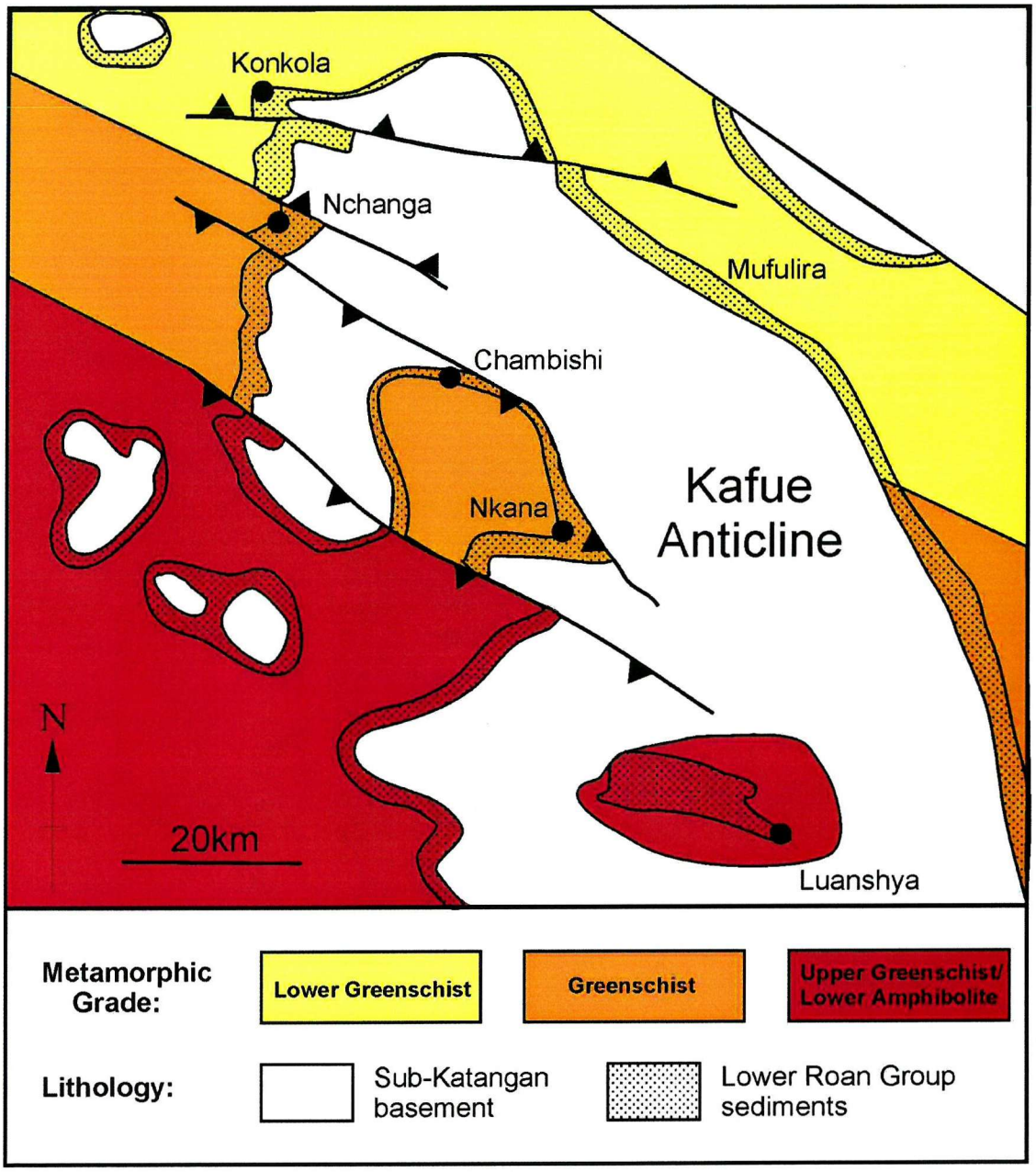

Figure 2.7: Schematic geological map of the Zambian Copperbelt showing the distribution of metamorphic grades and the proposed position of major thrust structures based on the metamorphic zones (modified from Hitzman, 2000).

2.5 Copper and cobalt mineralization

The majority of the copper and cobalt of the Zambian Copperbelt is confined to the arenites, shales, and carbonate rocks of the Mixed and Siliciclastic Units of the Lower Roan Group. However, mineralization has also been observed in basement rocks (Pienaar, 1961; Wakefield, 1978) although this has not yet been exploited, and Upper Roan units. Where mineralization is observed in the Lower Roan, it is reported to be mainly hosted by reduced sediment facies, in particular shales (in places carbonaceous, e.g. Nchanga). Fleischer *et al.* (1976) claimed that 60% of mineralization is shale-hosted and 40% is arenite- and arkose-hosted. It has also been suggested that deposits on the western side of the Kafue Anticline are predominantly 'ore-shale'-hosted, whereas those on the eastern side are arenite- or arkose-hosted (Fleischer *et al.*, 1976; Annels, 1989). However, the majority of mineralization at Nchanga, Chambishi, and Chibuluma, all on the western side of the Kafue Anticline, is found within arenites.

The common ore minerals are chalcopyrite, bornite, and chalcocite (± pyrite and pyrrhotite), with carrollite being the major cobalt-bearing sulphide (Mendelsohn, 1961). Cobalt is also enriched in pyrite, calcite and feldspar in some units. As well as primary sulphides, a range of secondary copper minerals can occur within copper orebodies, the principal ones being chalcocite, malachite, cuprite and chrysocolla (± tenorite and native copper; Mendelsohn, 1961). At Nchanga, copper can be enriched within phyllosilicates (mainly phlogopite), and this has been termed 'vermiculite' or 'refractory' ore (Bassett, 1958; Fisher & Notebaart, 1976; Notebaart, 1978).

The primary sulphide orebodies are often tabular and have considerable strike lengths (up to 2km). The sulphide mineralization itself can be found in a variety of styles, the most common of which are:

- Sulphides as fine disseminations, streaks, or aggregates within host rocks, generally parallel to bedding (Mendelsohn, 1961).
- 'Sulphide beds' such as those at Chibuluma (Whyte & Green, 1971).
- Quartz-carbonate lenses containing sulphides, generally orientated parallel to bedding as at Chambishi (Annels, 1989).
- Sulphides along cleavage surfaces or within syn-tectonic metamorphic quartz (± carbonate) veins (Hitzman, 1998).

Mendelsohn (1961) and Fleischer *et al.* (1976) presented descriptions of mineralization at each of the major ore deposits on the Copperbelt in detail.

2.5.1 Distribution of orebodies

There is a clear alignment of the major orebodies of the Copperbelt in a trend parallel to the Kafue Anticline (Fig. 2.3), in particular of the deposits on the western side through Luanshya, Nkana, Chambishi, Nchanga, and Konkola, but also of those on the eastern side through Mufulira and Ndola (Bwana Mkubwa). Although many researchers agree on this alignment, the interpretation has variously been explained in relation to a deep structural feature and an ancient shoreline. The orebodies themselves are preserved in synforms (of folded Katangan stratigraphy) around and within basement inliers (Unrug, 1989) and occur in sometimes steeply dipping strata. These have been interpreted in the past as former small basins into which the host sediments were deposited, but later exaggerated by folding, thus invoking a strong palaeo-topographical control on both Lower Roan deposition and localization of sulphide mineralization (Mendelsohn, 1961).

2.5.2 Origin of Zambian Copperbelt mineralization

The controversy surrounding the origin of Zambian Copperbelt mineralization has focused on the timing and nature of the principal ore-forming processes; whether the mineralization was introduced syngenetically with the host sediments; during early diagenesis, before compaction of the host sediments; or epigenetically, following lithification of the host sequence. The various models are introduced below.

The model that has been most widely accepted over the last sixty years is the syngenetic model, which involves the input of sediment and dissolved metals into a marginal marine environment and the precipitation and zonation of copper sulphides relative to palaeo-shorelines below the oxygenated zone, in response to reduction of seawater by bacterial activity (Garlick, 1961a, 1972; Binda & Mulgrew, 1974; Clemmey, 1974; Sweeney & Binda, 1994). The strongest argument for this model is the zonal distribution of sulphides, widely reported on the Copperbelt, where different sulphides are interpreted as having precipitated relative to their distance from palaeo-shorelines and their solubility (Fig. 2.8; Garlick, 1961a; Garlick, 1972; Fleischer *et al.*, 1976). This is classically a chalcocite (near-shore)-bornite-chalcopyrite-pyrite (deeper) zonation. Some other lines of evidence presented for this model include: the lateral extent and reported disseminated nature of sulphides (Garlick, 1976; Whyte & Green, 1971); the association of copper grades and tidal patterns (Clemmey, 1974);

and mechanically transported copper sulphide grains from Mufulira (Voet & Freeman, 1972; Binda, 1975).

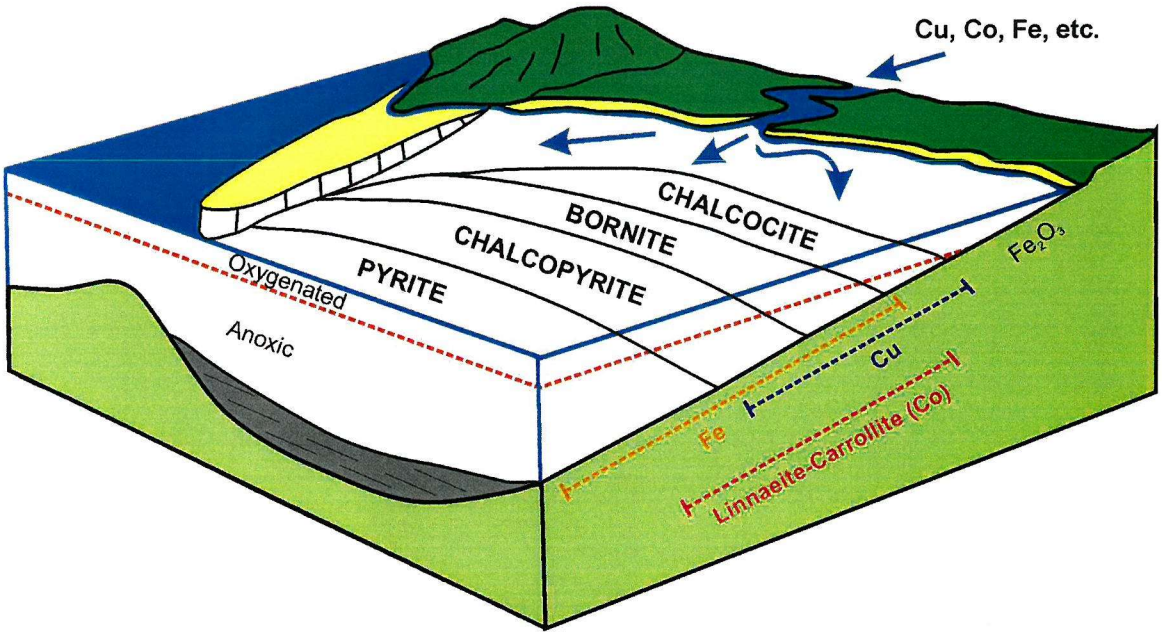

Figure 2.8: Mineral zoning of sulphides relative to distance from palaeo-shorelines (Fleischer *et al.*, 1976).

The diagenetic model was introduced to take into account the processes that must have occurred following deposition of the host sediments but prior to significant compaction, and are really an extension of the syngenetic model. Sweeney & Binda (1994) called this a pre-compaction model. It involves the precipitation of sulphides as copper-rich solutions migrate through porous, unconsolidated sediments during diagenesis (Van Eden & Binda, 1972; Sweeney & Binda, 1989, 1994). Support for this model includes evidence that copper was introduced prior to compaction of the host sediments (from 'lateral secretion veins'), and evidence that sulphides were subsequently remobilized during metamorphism (Garlick, 1961a, 1972).

A number of exhalative, hydrothermal models involved sulphide precipitation from copper-rich hydrothermal solutions that found their way into variably consolidated cover sequences via deep basement structures (Darnley, 1960; Annels, 1984, 1989; Annels & Simmonds, 1984). The relationship between cobalt orebodies and intrusive amphibolite orebodies on the west of the Kafue Anticline was noted by Annels (1974) and Annels *et al.* (1983), and led to the suggestion that the two were genetically related. Annels (1984) claimed that Katangan sedimentation took place in a narrow rift bounded to the north by the Kafue Anticline and to the south by the depositional edge of the 'ore-shale' (Sweeney & Binda, 1994). Fractures may have acted as suitable channels of basaltic magma, and associated copper-rich hydrothermal

fluids found their way into unconsolidated sediments or were extruded directly onto the sea floor (Annels, 1984). Annels (1989) recorded temperatures of 142-213°C for veins related to sulphides. He used this as evidence to suggest that sulphides precipitated when copper-rich hydrothermal fluids ascended along fractures and faults and encountered reduced sulphur within suitable host rocks. Darnley (1960) also suggests that a hidden magma body must have been involved in the generation of the extensive mineralization of the Copperbelt. He favours a 'pre-metamorphic hypogene' model, whereby magmatic solutions (escaping from a magma chamber with high water- and volatile- content) migrated to the surface and mingled with surface waters during Katangan sedimentation, and believed that during subsequent compaction of the sediments, connate waters mixed with magmatic copper-rich solutions were squeezed out, with precipitation of sulphides occurring within suitable host rocks on encountering organic matter. Principal conduits for the magmatic solutions were probably unconformities or vertical structures within the basement (Darnley, 1960). The evidence for this model includes the association of ore with 'abnormal metasomatism' of the host sediments, indicated by sericitization and tourmalinization of Lower Roan rocks. Basinal brines have been identified as playing a role in the generation of many sediment-hosted base metal deposits. Lefebvre (1989) suggested that Mg- and Cu- (and Co)-rich brines found their way into the Lower Roan host rocks via rift fractures in the Shaba Province of the Democratic Republic of Congo. He envisaged this as 'post-sedimentary addition of copper (and cobalt) to former pyrite-rich sediments.

Finally, recent epigenetic models involve the role of migrating, copper-rich, basinal brines or metamorphic fluids being introduced into the Lower Roan during regional Lufilian tectonism. This model has been suggested to explain the relationship between Lufilian-age thrusting and Copperbelt mineralization (Molak, 1995; Simmonds, 1998). Early epigenetic, hydrothermal models (e.g. Davidson, 1931) involved the granites of the Copperbelt being intrusive into the Katangan sediments and the source of mineralizing fluids, based on evidence such as mineralized veins within the granites themselves and ore horizons. Molak (1995) noted the association of phyllosilicate development, and enrichment in copper and cobalt with shear and thrust structures. This lead him to envisage a 'shear zone' model for the Copperbelt deposits, involving the generation of major shear zones, and simultaneous influx of copper and cobalt-rich fluids (also rich in K, Ba, and Na) during several major tectonic and metamorphic episodes of the Lufilian Orogeny. Lefebvre (1989) claimed that later polymetallic mineralization (Cu, Co, U) within syntectonic fractures was superimposed on to pre-existing copper concentrations in the Shaba Province of the Democratic Republic of Congo.

2.6 Summary

- The copper-cobalt deposits of the Zambian Copperbelt are contained within the Lufilian Arc, a Neoproterozoic Pan-African fold belt, and hosted by the sedimentary Katangan Supergroup.

- The Katangan sediments (maximum age of 877 Ma) were deposited in response to marine incursion across a continental landscape, represented by basement rocks ranging in age from 877 to 2000 Ma, and consists of basal clastics overlain by shales, sandstones, and carbonates.

- The Katangan sedimentary rocks have been subjected to greenschist facies metamorphism and are exposed on the flank of the Kafue Anticline, a basement culmination that was developed during regional (Lufilian-age) compression (550-50 Ma) and associated NE-directed thrusting.

- Copper-cobalt orebodies are commonly located within preserved geosynclines between outcropping basement highs. Common ore minerals are chalcopyrite, bornite, and chalcocite hosted within shales or arenites in a variety of styles, including disseminations, veins, and fractures.

- The exact timing of ore formation is a controversial issue, and previous models have advocated syngenetic, diagenetic, or epigenetic mineralization.

CHAPTER 3:

GEOLOGY & MINERALIZATION OF THE NCHANGA AREA

CHAPTER 3: GEOLOGY AND MINERALIZATION OF THE NCHANGA AREA

3.1 Introduction

The first deposit to be discovered in the Nchanga area was the River Lode deposit by James J. Beaton in 1923 (McKinnon & Smit, 1961). Presently, the Nchanga mining licence, situated between Konkola and Chambishi mines around the town of Chingola (Fig. 1.2), occupies an area of 111km^2, and consists of two operating underground mines, a total of eight open pits (two currently in operation), and two additional, as of yet unexploited, orebodies (Luponelo, 2001). This chapter provides a detailed description of the geology of the Nchanga deposits, including presentation of a section constructed across the Nchanga area and macro-scale structural observations made during field mapping and core-logging.

3.2 General characteristics

The mineralization at Nchanga is hosted by arenites and shales of the Lower Roan Group of the Neoproterozoic Katangan Supergroup. The general stratigraphy (Fig. 3.1) consists of Nchanga Red Granite (dated at 877 ± 11 Ma by Armstrong *et al.*, 1999) intruded into older Lufubu Schist. These rocks are grouped together under the 'Basement Complex,' and are overlain by conglomerates and arkoses/arenites (of the Siliciclastic Unit), mixed shales, arenites, and dolomites (of the Mixed Unit), and then by Upper Roan dolomites (of the Carbonate Unit; Binda, 1994). The Katangan rocks infill an irregular basement topography and subsequently developed their fold and thrust character during the Lufilian Orogeny (Molak, 1995; Simmonds, 1998), the most notable structure being the asymmetric Nchanga Syncline to the north of the stable Nchanga Red Granite block (Fig. 3.2). Three orebodies are exploited (Fig. 3.1): the Lower Orebody, hosted by footwall arkoses and arenites and the overlying carbonaceous shale unit ('Lower Banded Shale'); the Intermediate Orebody, hosted by a minor feldspathic arenite unit (the 'Pink Quartzite'); and the Upper Orebody (currently the main source of ore at Nchanga), hosted by a feldspathic arenite unit and base of overlying shale ('The Feldspathic Quartzite' and the 'Upper Banded Shale'). The dominant ore minerals are bornite, chalcopyrite, chalcocite and carrollite (Co) as sulphides, malachite as the main copper carbonate, and chrysocolla, and cuprite as oxides. In addition, there are occurrences of 'vermiculite' ore (Notebaart, 1978) in which copper is contained within phyllosilicates,

mainly within the 'Banded Sandstone' and 'Dolomitic Schist' units. This has been termed the 'Chingola Refractory Ore.'

3.3 Stratigraphy

The stratigraphy of the Nchanga area and the location of the major ore occurrences (Nchanga Lower, Intermediate, and Upper Orebodies) are summarized in Figure 3.1, which includes the mining terms (in inverted commas) that have been used for many years. For example the term 'quartzite' is widely used, whereas the correct lithological name should be arenite based on the feldspar content (Pettijohn *et al.*, 1987). Descriptions of the unmineralized lithology of each unit are presented below using the Nchanga Mine terms for individual lithological units (e.g. 'Lower Banded Shale;' Fig. 3.1). However, the correct lithological descriptions must be noted. The sequence described below can be traced across the entire Nchanga area.

3.3.1 Basement Complex

The green biotite-muscovite-quartz-schists or biotite-gneisses of the Lufubu System (> 2 Ga) are considered to be of sedimentary origin as no volcanic beds have been discovered (McKinnon & Smit, 1961). No economic concentrations of copper have been found within the Lufubu Schists, and outcrop in the immediate Nchanga area is relatively poor, hence little is known about them. They mainly consist of quartz (up to 70%) and mica (and very rare microcline or albite), with accessory carbonates, iron oxides, and tourmaline (Mendelsohn, 1961). Garnetiferous chlorite-schists have also been described from the Kafue Valley (Jackson, 1932), intruded by younger granites, the youngest of which is the Nchanga Red Granite (877 ± 11 Ma; Armstrong *et al.*, 1999).

Three varieties of granite that intrude the Lufubu Schists have been described from the Nchanga area: the dark, biotite-rich Nchanga Dark Granite, the Nchanga Grey Granite and the Nchanga Red Granite (McKinnon & Smit, 1961). The Nchanga Dark Granite is the oldest and consists of a high proportion of biotite, with large crystals of microcline, albite and oligoclase set in a finer groundmass of quartz and feldspar (O'Meara, 1959). Accessory minerals include apatite, muscovite, sphene, tourmaline, carbonate, magnetite, and pyrite, with traces of chalcopyrite, digenite, bornite and chalcocite (O'Meara, 1959). It has been interpreted as granitized sediment in order to explain the high biotite and minor sulphide contents that are thought to be original constituents of the pre-altered rock (McKinnon & Smit, 1961).

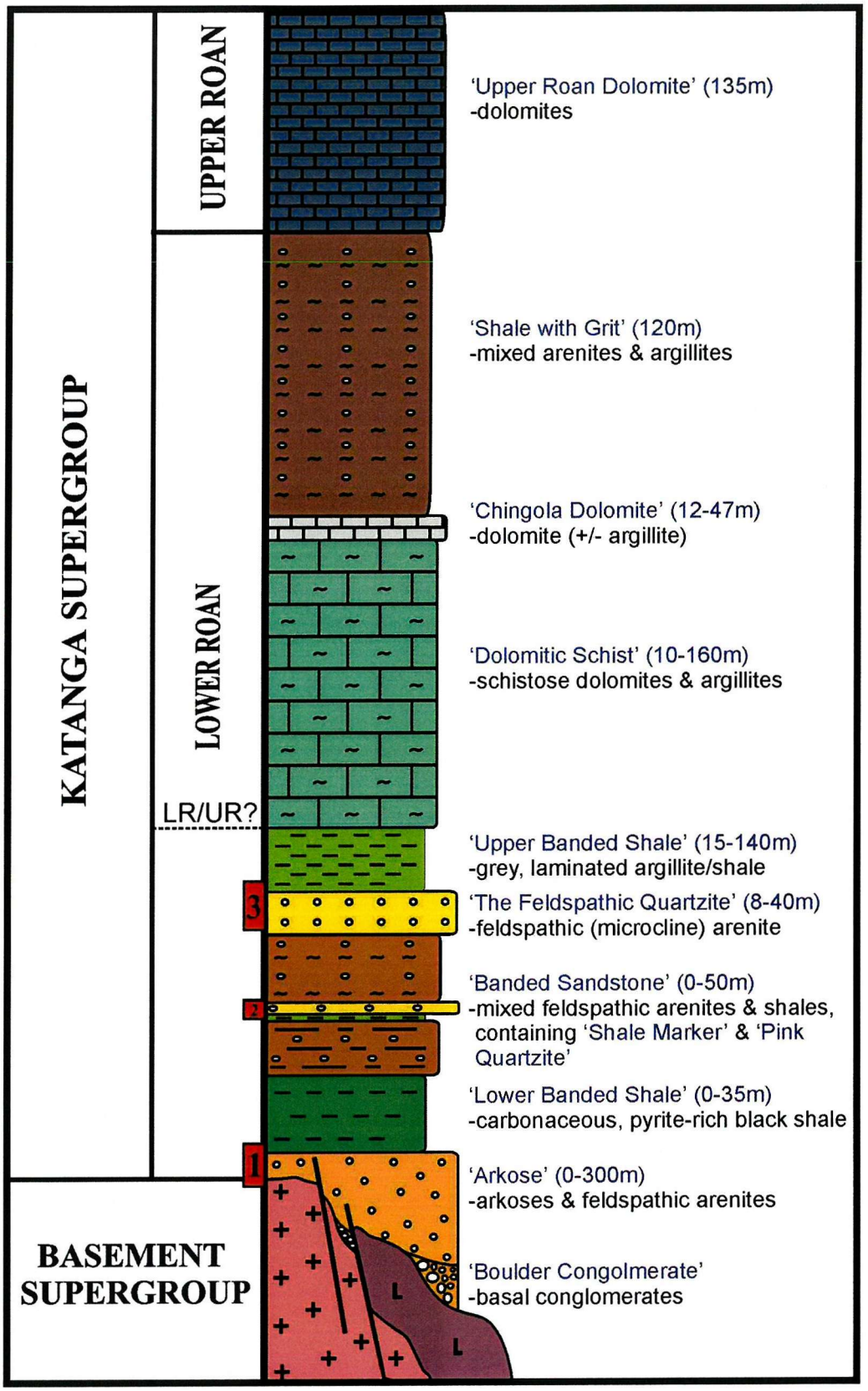

Figure 3.1: Stratigraphy of the Nchanga deposits showing the major lithologies and mining terms that have been used, and the stratigraphic location of major orebodies: (1) Lower Orebody, (2) Intermediate Orebody, and (3) Upper Orebody (thickness variations from Diederix, 1977).

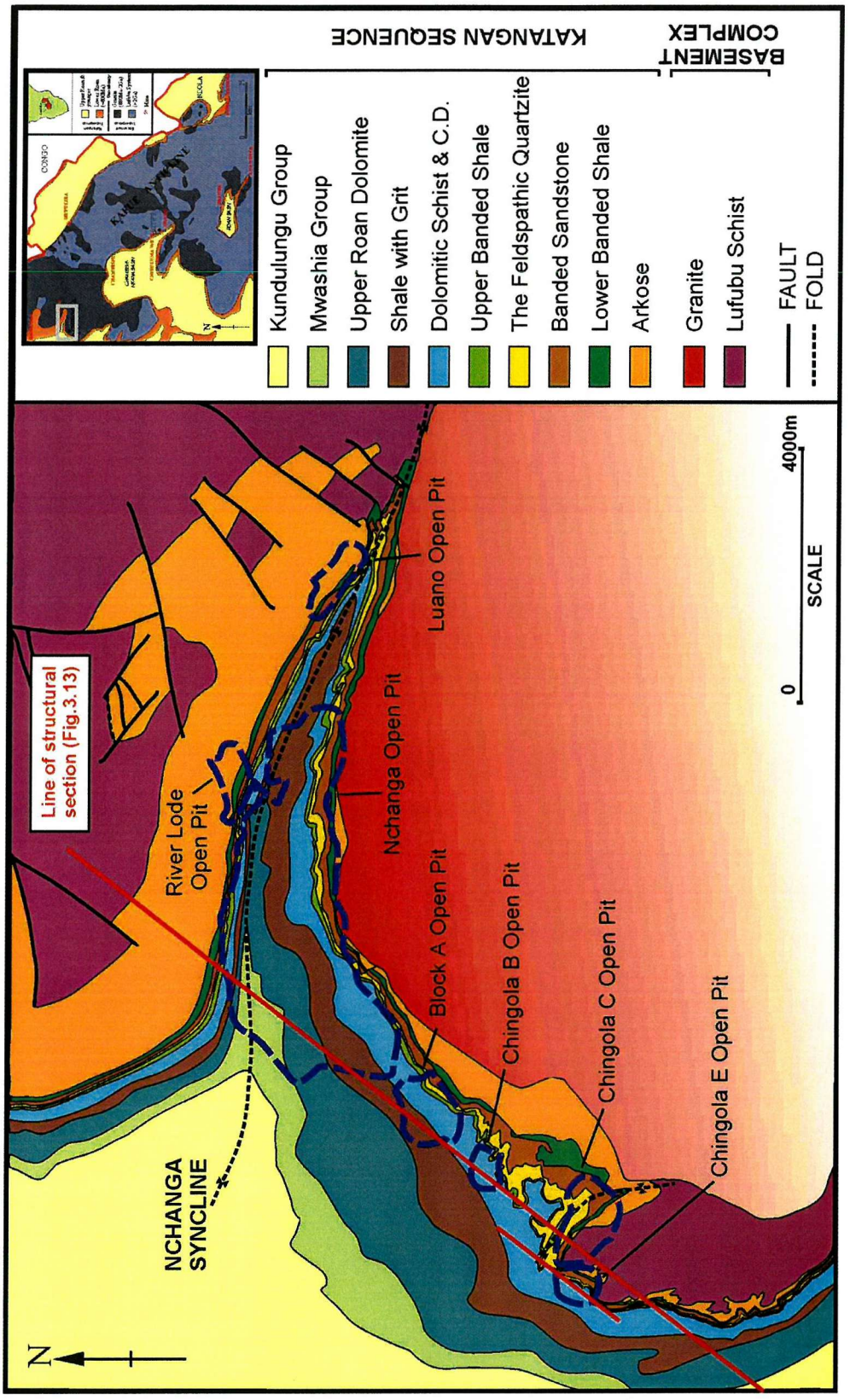

Figure 3.2: Geological map of the Nchanga area with the main open pits of the Nchanga mining licence, in particular the Nchanga Open Pit exploiting the shallow, north dipping Lower Roan units of the south limb of the asymmetric Nchanga Syncline (modified from Diederix, 1977).

The Nchanga Grey Granite consists of coarse microclines in a groundmass of quartz, plagioclase (altered to sericite), epidote, and minor biotite (McKinnon & Smit, 1961). The grey variety has been intruded by the Nchanga Red Granite (Fig. 3.3A), a potassic, coarse-grained, pink granite containing interlocking grains of quartz (~40%), microcline (micro-perthitic; ~30-35%), and albite (10-15%) with minor biotite and muscovite (Fig. 3.3B). Accessory minerals include sericite, magnetite, hematite, tourmaline, and zircon (± epidote). McKinnon & Smit (1961) additionally reported occurrences of allanite, fluorite, apatite, sphene and carbonate, and Diederix (1977) described aplite veins, also from the Nchanga Red Granite.

The composition of a parent magma reflects the various sources of the magma components (Pitcher, 1979). Based on the classification of granite types by Chappell & White (1974) and White & Chappell (1977), the Nchanga Red Granite falls in the S-type category (metasedimentary source). This is determined using distinctive geochemical properties such as Na_2O and K_2O contents, and specific mineral components. Based on the classification of granitoid rocks by Streckeison (1976), the Nchanga Red Granite lies in the 'monzo-granite' field, tending towards the boundary with the 'syeno-granite' field where plagioclase content is low. Using geochemical data and the discrimination plots of Harris & Inger (1986), Pepper (1999) claimed that these granites formed in a syn- to post-collisional setting. However, using the same data and the discrimination plot of Pearce *et al.* (1984), the data occupy the field of granites that formed 'within plate.' If they did form in a collisional setting, then a pre-Katanga event (the Nchanga Red Granite is older than the Katangan sediments, see above) must have triggered the plutonism.

3.3.2 Katangan Supergroup

Footwall Arkoses

The contact between the Nchanga Red Granite and overlying footwall conglomerates and arkoses was first described as an unconformity by Garlick & Brummer (1951). The contact is visible in the main access ramp to the Nchanga Open Pit, where there are sub-rounded boulders of a finer grained quartz-sericite rock immediately above the granite, apparently sourced from a pre-Katanga basement rock. Also, on the south limb of the Nchanga Syncline granite slabs (up to 5m) are suspended in overlying arkose (McKinnon & Smit, 1961). The contact was intersected in boreholes NOP 741 and NOP 708 and shows no evidence of a tectonized boundary. This footwall sequence infills an irregular fault-block basement topography with an unconformable contact (Figs. 3.4), with basal conglomerates grading upwards to arkoses and arenites. The thickness of the arkose varies considerably, controlled

by the topography of the pre-Katangan surface (McKinnon & Smit, 1961). Loading of coarse quartz and feldspar grains into finer, more argillaceous layers (Fig. 3.5A) and cross-bedding indicate that the arkose beds have not been overturned. The arkose consists of coarse quartz and pink feldspar (microcline) in a finer groundmass of quartz and feldspar, with accessory magnetite, zircon, sphene, and tourmaline (Fig. 3.5B). Sericite and biotite are common components, as is phlogopite, which is particularly abundant towards the top of the unit and adjacent to fault zones (see Chapter 4). The arkose appears more like Lufubu Schist where extensive shearing and alteration has taken place. Towards the top of the unit, the arkose becomes progressively more disrupted and altered, indicated by the increasing alteration of feldspars (to sericite), bleaching of the lithology, and, in places, abundance of phlogopite.

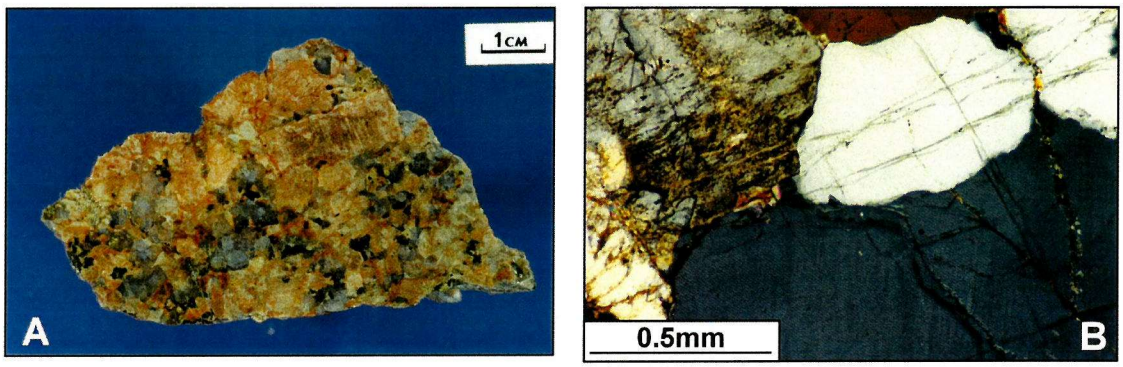

Figure 3.3: (A) Hand specimen photograph of a typical Nchanga Red Granite sample (NOP 12); (B) Photograph of a thin section of typical Nchanga Red Granite in crossed-polars (NOP 12).

Figure 3.4: Field photograph of the granite – arkose contact in Nchanga Open Pit where fault-block granite topography (Nchanga Red Granite) is overlain by north-dipping beds of arkose (looking SE, Nchanga Open Pit).

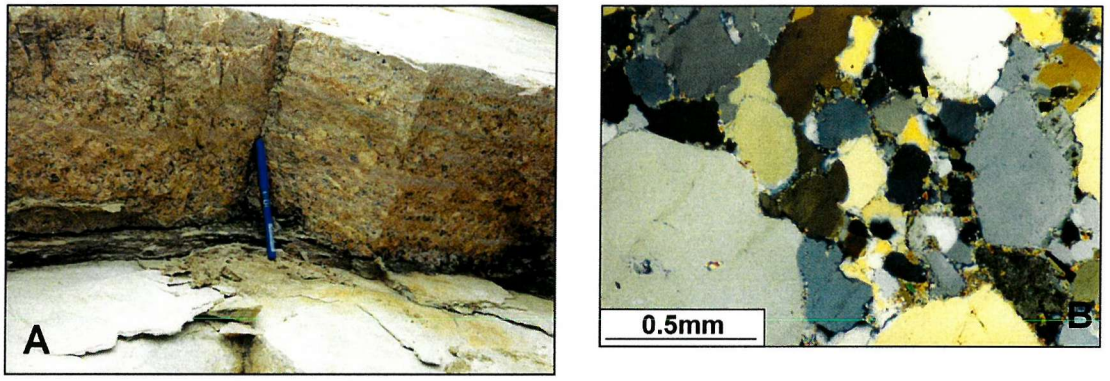

Figure 3.5: (A) Field photograph of the bedded nature of arkose, with coarse quartz and feldspar grains loading into softer, argillaceous material (looking W, Nchanga Open Pit); (B) Photograph of a thin section of typical unmineralized arkose in crossed polars (CB4, Nchanga Open Pit).

Contact between 'Arkose' and 'Lower Banded Shale' ('Transition')

This contact, previously termed a 'Transition' unit and described as an evaporite collapse breccia (Stanton, 1966), is used to denote a sequence of soft, incoherent rocks occurring between recognizable underlying arkose and overlying carbonaceous shale (Figs. 3.6A & B; Diederix, 1977). In reality, the 'Transition' represents deformation, alteration, and intense weathering of the arkose and shale on either side of a tectonized contact (more so on the arkose side; Fig. 3.6B; see section 3.5) and is used here in that context. However, the existence of evaporite beds prior to deformation cannot be ruled out. This contact zone or 'Transition' can be up to 18m thick. The fact that the 'Transition' occurs at the contact between Nchanga Red Granite and 'Lower Banded Shale,' where the arkose is absent, is further support for this unit not being a true transition from arkose to shale.

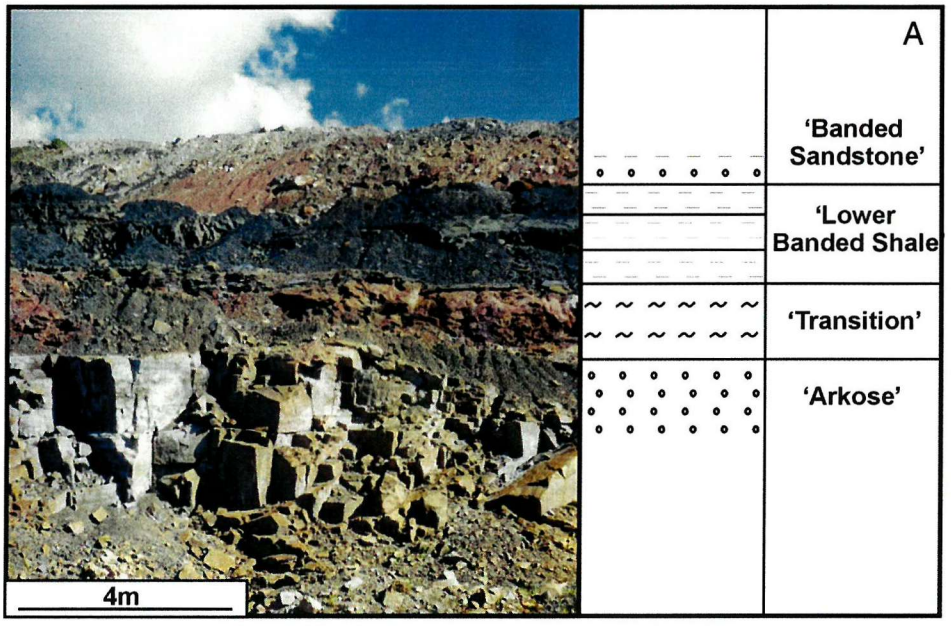

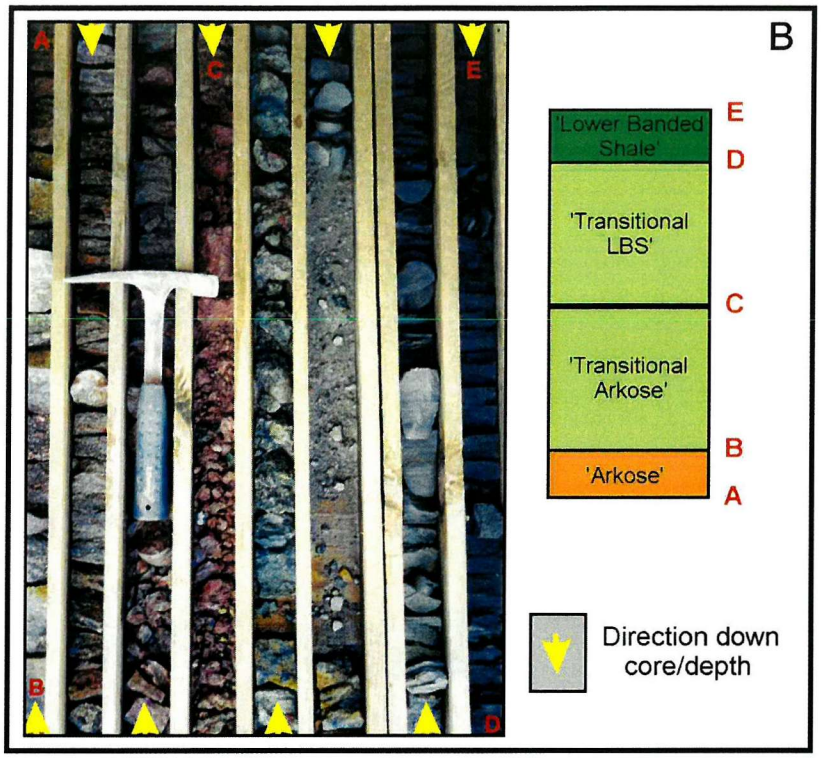

Figure 3.6: Photographs of the contact between arkose and overlying carbonaceous shale, marked by alteration and deformation of lithologies on either side: (A) Soft, incoherent rocks in between recognizable arkose and shale (looking S, Nchanga Open Pit), and (B) the contact from borehole NOP 741 (Nchanga Open Pit).

'Lower Banded Shale' (LBS)

The 'Lower Banded Shale' (equivalent to the 'ore-shale') is, in its unaltered form, a black (sometimes grey), fine-grained, carbonaceous, laminated shale, consisting of quartz (~30%), feldspar (~20%) and sericite (~20%), deposited in reducing conditions (Fig. 3.7A & B). The other main components are carbonaceous matter (>20%) and pyrite, with accessory zircon and tourmaline (McKinnon & Smit, 1961). In one case, diagenetic anhydrite nodules within the shale were found to be replaced by a later pyrite phase (Borehole NOP 827), indicating that more abundant evaporites may once have been present within the unit. Minor, more quartzitic layers commonly occur within the shale and are normally 1 to 10cm thick. Bleaching of the shale occurs towards the lower contact with the arkose and towards the upper contact with the 'Banded Sandstone.' The upper contact is marked by a thin unit of microcrystalline quartz (0-6m), interpreted as a product of leaching above dolomitic and quartzose horizons (Diederix, 1977).

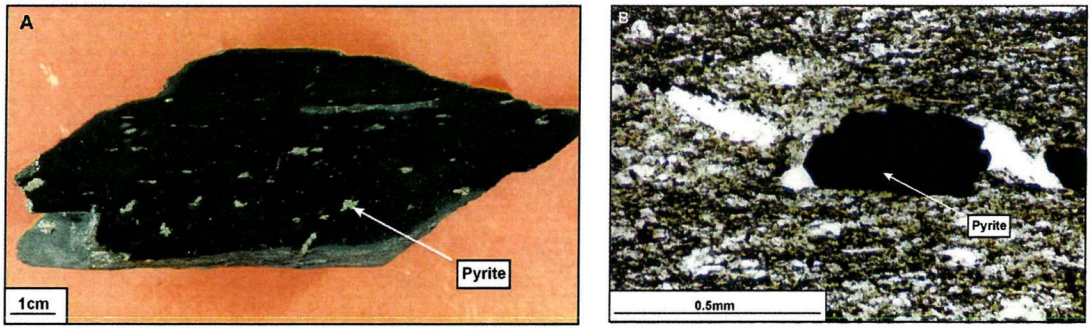

Figure 3.7: (A) Hand specimen photograph of the black, carbonaceous, pyrite-rich shale overlying the footwall arkose unit (NOP 86, 'Lower Banded Shale'); (B) Photograph of thin-section of the shale showing fine-grained nature and quartz, feldspar and sericite components in crossed-polars (NOP 86, Nchanga Open Pit).

'Banded Sandstone' (BSS)

The 'Banded Sandstone' has been subdivided into a Lower (BSSL) and Upper (BSSU) unit by the 'Shale Marker' and 'Pink Quartzite.' It is highly disrupted and deformed, and the original lithologies are rarely observed. In Block A Open Pit, a lack of alteration and only minor disruption reveals a more competent feldspathic sandstone or arenite, showing ripple structures (Fig. 3.8), and minor interbedded argillites. The main components are quartz, feldspar, and sericite, with abundant phlogopite and dolomite in some parts (particularly in the 'Upper Banded Sandstone'), and minor malachite, hematite and scapolite.

Figure 3.8: Field photograph of an unaltered and relatively undeformed section of 'Banded Sandstone' with sedimentary structures preserved (looking N, Block A Open Pit).

'The Feldspathic Quartzite' (TFQ)

A competent feldspathic arenite, composed mainly of quartz (~50-60%) and microcline feldspar (~20-30%; ± dolomite, phlogopite, sericite) overlies the deformed rocks of the 'Banded Sandstone.' It is a white to pale grey, medium-grained rock (Fig. 3.9A & B), that normally contains greater than 20% feldspar, and in places carbonaceous material (Darnley, 1960). Cross-bedding is widely reported from this unit (McKinnon & Smit, 1961; Diederix, 1977) but was not observed by the present author, probably due to the extensive recrystallization of the detrital components that has taken place. Like the top of the arkose unit, the base of the 'Feldspathic Quartzite' is sometimes referred to as a 'transitional unit,'

but only where it is marked by a dark zone of dolomite-phlogopite-quartz rocks (similar in composition to the 'Banded Sandstone' below). This zone is more accurately interpreted as a sheared and altered part of the quartzite (and underlying sandstone) and not a true lithological transition.

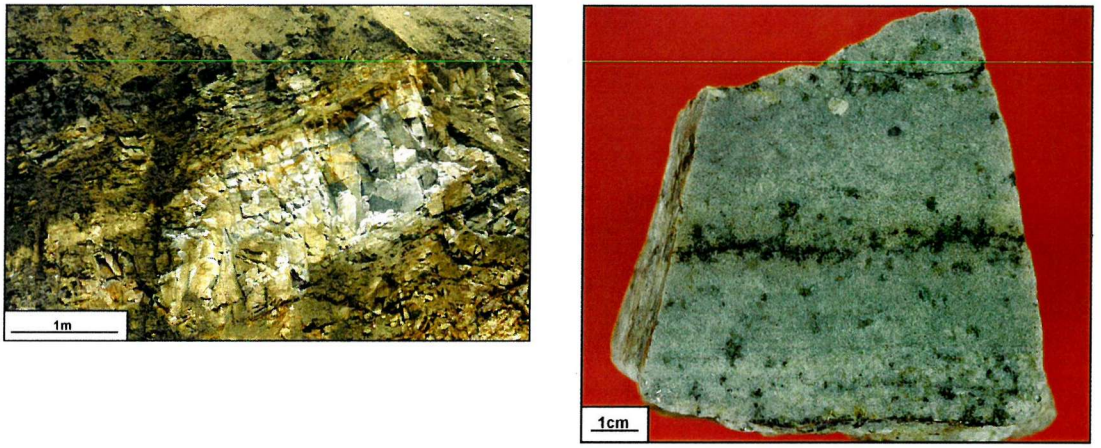

Figure 3.9: (A) Field photograph of exposed feldspathic arenite (looking E, Nchanga Open Pit); (B) Hand specimen photograph of the arenite (A), the host to Upper Orebody sulphides (NOP123, Nchanga Open Pit).

'Upper Banded Shale' (UBS)

This shale unit overlying the feldspathic arenite is a fine-grained, grey to brown laminated shale consisting of quartz, microcline feldspar, and sericite/muscovite and is commonly interbedded with fine arenite layers (Fig. 3.10; borehole NOP 741). It has also been termed a phyllite by previous authors (Diederix, 1977). In places it is bleached towards its lower contact with the 'Feldspathic Quartzite,' and towards its upper contact with the dolomites and argillites it becomes progressively more interbedded with the dolomites (Fleischer *et al.*, 1976). In Nchanga Open Pit, there appear to be two distinguishable lithologies within the UBS - a soft, micaceous dolomitic unit with scapolite, and a more competent, quartz-rich dolomitic horizon.

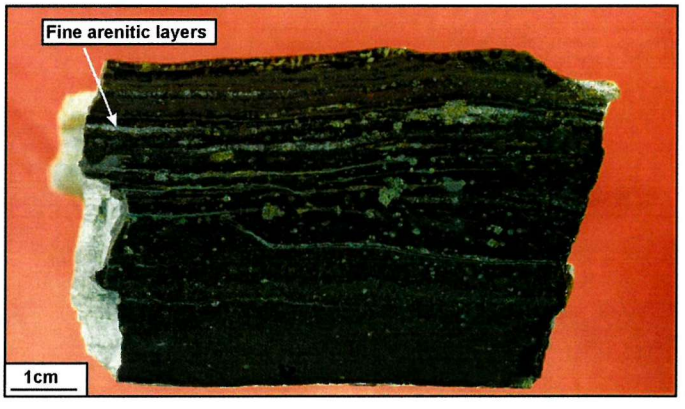

Figure 3.10: Hand specimen photograph of an 'Upper Banded Shale' sample showing fine, interbedded arenite layers (NOP 68, Nchanga Open Pit).

'Dolomitic Schist' (DS) and 'Chingola Dolomite' (CD)

There has been some debate as to whether this contact of shale and dominantly dolomitic units above represents the Lower Roan – Upper Roan boundary. Some authors believe it does (Mendelsohn, 1961) whereas in more recent publications the boundary has been put at the base of the Upper Roan Dolomite unit, much higher up in the sequence (Binda & Mulgrew, 1974). This unit is an alternating sequence of competent dolomite beds (0.2 – 2m thick, ± quartz and phlogopite) and much less competent, deformed dolomite-phlogopite schists (0.1 – 1m thick; Fig. 3.11). The crystalline dolomite of the 'Chingola Dolomite' caps this schist succession, and has been described as a light-coloured quartzose and talcose dolomite (Diederix, 1977).

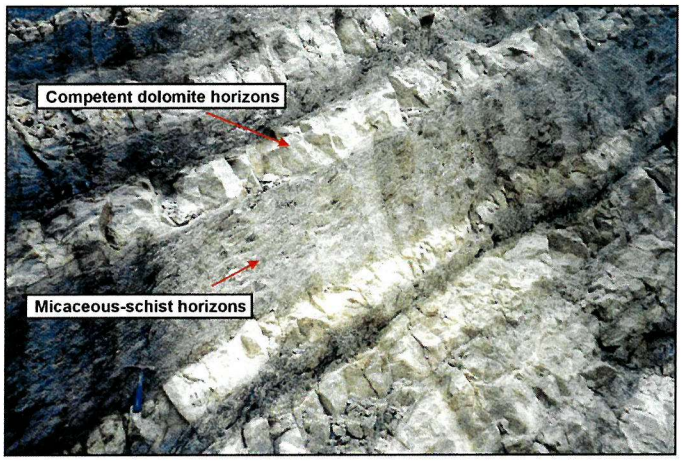

Figure 3.11: Field Photograph of interbedded dolomites and dolomitic-mica schists of the 'Dolomitic Schist' unit (looking E, Nchanga Open Pit).

'Shale with Grit' and 'Upper Roan Dolomite'

A mixed unit of argillites and fine- to medium-grained feldspathic sandstones overlies the dolomite and schist units. The top of this succession and base of the Upper Roan Dolomite was considered as the Lower-Upper Roan boundary by Binda & Mulgrew (1974). The Upper Roan Dolomites consist of interbedded dolomites and minor argillaceous units, where anhydrite is commonly encountered (Diederix, 1977).

3.3.3 Intrusive rocks

Previous literature describes a 'lamprophyre' dyke (Diederix, 1977) or a metamorphosed gabbro (Fleischer *et al.*, 1976) intruding the Lower Roan sediments in the Nchanga Open Pit. It is a largely unconsolidated phlogopite-quartz-scapolite schist (Fig. 3.12) containing sulphides, with minor amounts of muscovite and rutile, associated with a fault zone that only extends to the top of the granite. Dalgleish (1977) reported that the rocks bear little resemblance to true lamprophyres. Diederix (1977) claimed that this 'dyke' intrudes as high into the stratigraphy as 'The Feldspathic Quartzite' and that another one, underground at Chingola Lower Orebody, only intrudes the Nchanga Red Granite. However, there is no evidence in the field that this schist is an intrusion, and no such rocks have been seen by the present author within the Lower Roan sequence (see section 3.5).

Gabbroic bodies intruding Upper Roan rocks and younger sequences are reported from areas west of Nchanga, generally forming sill-like structures. These are considered to be younger than the regional folding event (Diederix, 1977).

Figure 3.12: Hand specimen photograph of fault-related phlogopite-quartz-scapolite schist, previously interpreted as a 'lamprophyre' dyke (NOP 47, Nchanga Open Pit).

3.3.4 Sedimentary setting

The sediments of the Zambian Copperbelt were deposited in marine basins. There are reported to be two basins (Fig. 2.3): the Roan Basin containing the Luanshya and Baluba orebodies, and a much larger basin, defined by the outcrop of the Lower Roan that forms the outer rim, represented by a number of preserved interconnecting synclines (Fleischer *et al.*, 1976), of which the Nchanga Syncline is just one. The sediments are generally thought to have been deposited in differentially-subsiding, intra-cratonic, rift basins (Simmonds, 1998). Rifting of the continental block and a major marine transgression resulted in the deposition of a thick sequence of basal continental clastics and shallow marine deposits, succeeded by mixed carbonate platform (hypersaline) lagoonal, evaporite sequences (Simmonds, 1998; Wendorff *et al.*, 2000). The Nchanga sequence, described above, is consistent with this setting, with the arkose sequence as the basal continental clastics that appear to be sourced from granite similar in composition to the Nchanga Red Granite. The 'Mixed Unit' of shales, sandstones, dolostones ('Lower Banded Shale' to 'Dolomitic Schist' units), and minor evaporites represents a sequence of shallow marine sediments deposited in a paralic basin (Wendorff *et al.*, 2000) during marine regressions and transgressions, whereas the thick sequence of Upper Roan dolomites (with varying amounts of anhydrite) represents the platform carbonates.

3.4 Metamorphism

The basement has been subjected to a higher grade of metamorphism than the overlying Katangan sedimentary rocks (Fleischer *et al.*, 1976). Recrystallization of detrital components (in particular quartz) and growth of new minerals has taken place. O'Meara (1959) listed a number of minerals that have been reported from the Roan sedimentary rocks, including quartz, sericite, microcline, tourmaline, rutile, scapolite, biotite, and dolomite. However, early descriptions of lithology and metamorphism do not adequately take into account those processes that must have occurred during structural evolution of (and associated fluid migration within) the host package (see section 3.5). The Lufubu Schists and certain units of the Katangan sequence (e.g. the 'Banded Sandstone') are locally extensively deformed with the development of phyllosilicate-rich shear-zones, where biotite and dolomite are structurally related. The timing of this deformation in relation to peak metamorphism is not known.

The Lufubu Schists contain variable amounts of quartz, chlorite, biotite, muscovite, and red garnet (Fleischer *et al.*, 1976). Within the Nchanga Red Granite, a variety of metamorphic minerals have been described, including fluorite, biotite, red garnet, and micro-perthites indicating albite alteration of microcline feldspars (this study; Garlick, 1973; Fleischer *et al.*, 1976). This has led some authors to believe that basement rocks were once subjected to temperatures as high as amphibolite facies, and that the lack of some of these minerals (e.g. red garnets) in the overlying Katangan succession is indicative of a pre-Katangan metamorphic event (Garlick, 1973). However, Fleischer *et al.* (1976) believed that subsequent low-grade metamorphism of the entire sequence (post-Katangan) caused widespread retrograde metamorphism of the basement, with higher-grade indicators only locally preserved.

The Katangan sequence has been metamorphosed to greenschist facies during deep burial and tectonism (Fleischer *et al.*, 1976), with the most common minerals being biotite, sericite, and scapolite. Recrystallization of quartz is common, particularly within arenite units. Biotite (mostly the magnesium-rich variety phlogopite) is well developed in deformed horizons (e.g. the 'Banded Sandstone' and 'Dolomite Schist' units) and is clearly associated with structural features (see section 3.5). Sericite is more widespread but is most common in argillaceous units. Scapolite is also mostly restricted to argillaceous units and to the 'lamprophyre' fault gouge in the Basement rocks and is common within the 'Banded Sandstone' and 'Dolomitic Schist' units. Dolomite is also common, often associated with the phlogopite. The metamorphism and hydrothermal alteration of the Lower Roan rocks are discussed in more detail in Chapters 4 and 6.

3.5 Structural Geology

There are two structural domains of the Nchanga area: (1) the flat granite horst block onto which the Katangan sediments were deposited; and (2) the fold geometry of the overlying Katangan Supergroup which is controlled by the development of thrust-folds that were generated at tip lines to blind local thrusts and detach within the Lower Roan sequence. Two distinct structural regimes have been recognized: a weakly deformed zone consisting of basement Nchanga Red Granite and overlying footwall siliciclastics, and a moderately to tightly folded zone of meta-sediments of the Katangan succession (excluding footwall arkoses; Fig. 3.13). Early extension (D1 deformation – pre-Katangan) was followed by (and promoted) deposition of the Katangan sediments. Subsequent compression (D2 deformation) as part of the regional Lufilian Orogeny, largely affected the Lower and Upper Roan Groups (above footwall siliciclastics), during which the basement granite acted as a stable buttress.

The current study was involved with the construction of a structural section across the Nchanga area carried out by ERA Maptec (Dublin) and Zamanglo geologists in 2001 (a simplified and interpretative version by the present author is presented in Fig. 3.13). As the majority of structures mapped in the field have strike orientations of SE-NW, the section was constructed SW-NE to show the main features of the geology, but perpendicular section lines across deposits would be required to further constrain the structural geology. The following descriptions of structural features at individual locations should be read in relation to the main interpretative structural cross-section (Fig. 3.13).

3.5.1 D1 deformation: Pre-Katangan extension

Pre-Katangan extension is represented in the stable granite block by high-angle fault structures (e.g. Fig. 3.4) with one main east-west strike direction (average dip of 80°; Fig. 3.14), associated with deformation and wallrock alteration. There are also a high number of minor north-south structures that are found within both the granite and the overlying arkose unit (average dip of 80°; Fig. 3.14). However, as the majority of open pit faces with exposed granite trend east to west, there is a bias in the measurement of the minor north-south structures.

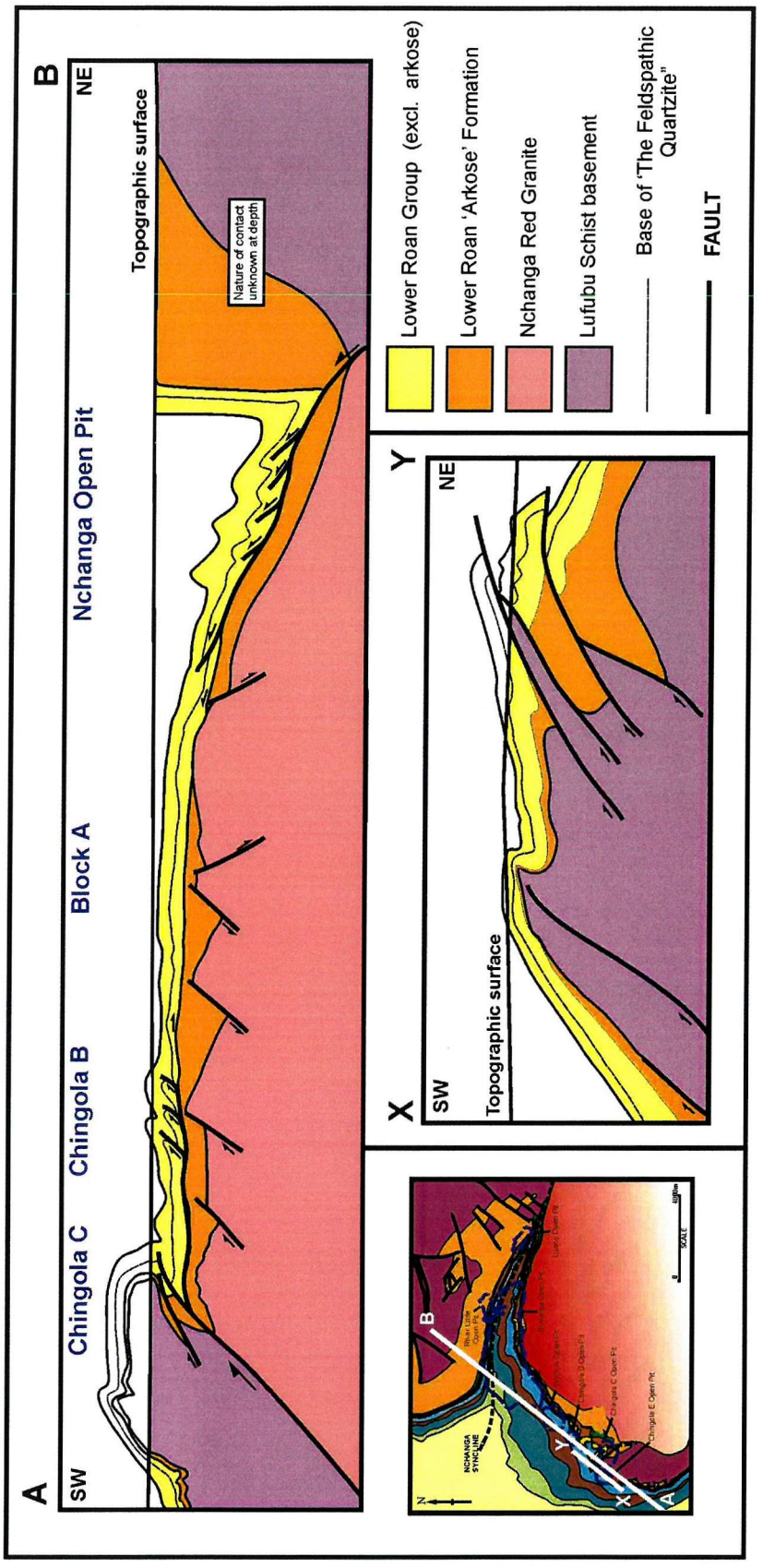

Figure 3.13: Simplified interpretative structural section constructed SW-NE across the Nchanga area (explained in section 3.5.4; interpreted from Coller & Wani, 2001).

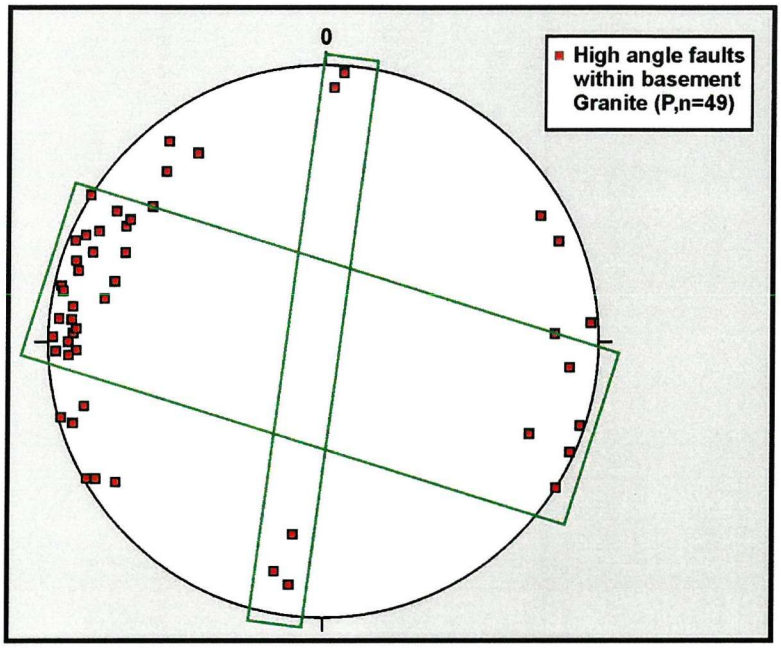

Figure 3.14: Stereographic projection of poles to fault planes in the granite basement of Nchanga Open Pit.

The east-west-striking structures (Fig. 3.4) show evidence of normal movement and pre-date the deposition of the Katangan Supergroup. These are interpreted as early extensional structures that formed an irregular fault-block topography that was syn- or post-tectonically infilled during the deposition of the footwall arkoses. One of these structures (and associated phlogopite-rich fault gouge) has been interpreted as a 'lamprophyre' dyke (see section 3.3.3). In fact, this phlogopite-rich material occurs at the intersection of two extensional faults, a major one trending 244° and dipping 55° SE, and a more minor structure trending 010° and dipping 85° E.

High-angle structures with the same orientations are also observed within the footwall arkose sequence, with the same bias in data collection (Fig. 3.15). However, bearing in mind the field relations of structures and overlying arkose, it is unclear as to whether these are representative of extension during or following the deposition of the arkose sequence or reactivation of granite structures (now represented in the arkose) during later compression. The structures in the arkose are not represented in the shales and less competent units above.

3.5.2 D2 deformation: Post-Katangan compression

Post-Katangan compression is represented by early, transgressive, bed-parallel shears and detachments to internal (within Lower Roan) fault-propagation fold structures that control the geometry of the Katangan sequence (Fig. 3.13). Across the Nchanga area, transport direction and vergence of thrusts and folds is to the north-east (Chingola C, Chingola B) but across the Block A area (Fig. 3.13) this changes to dominantly southwest-verging (Nchanga Open Pit), due to the influence of the southward-verging Nchanga Syncline (Coller & Wani, 2001.)

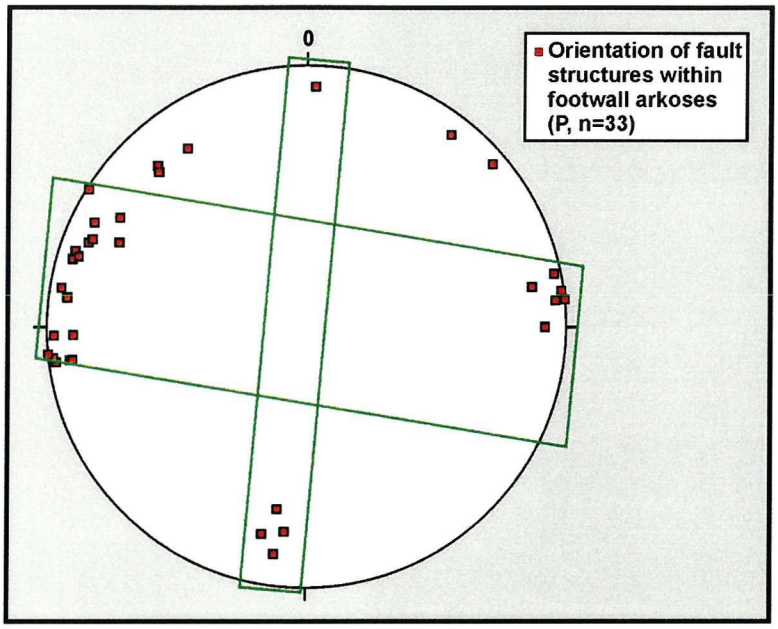

Figure 3.15: Stereographic projection of mapped structures within the footwall arkoses of Nchanga Open Pit (poles to fault planes).

Molak (1995) and Daly *et al.* (1984) both recognized major shear-zones within the Katangan sequence at Nchanga and interpreted them as compressional structures, and at Chambishi, Hitzman (2000) reported a similar feature where a decollement formed the tectonized contact between a weakly deformed footwall (including basement and footwall siliciclastic rocks) and a tightly folded Katangan sequence. Molak (1995) claimed that asymmetric folding has not only affected the Lower and Upper Roan rocks, but also basement formations, although not necessarily at Nchanga. The main evidence for both these structural features is discussed below, based on field mapping and interpretation of structural data, core-logging, and work with mine sections and their structural interpretation (in collaboration with ERA Maptec and Anglo American geologists).

Evidence for inversion structures and basement thrusts

Perhaps the most striking feature of the structural section across the Nchanga area is the wedge of basement Lufubu Schist that has been thrust over the Nchanga Red Granite at Chingola C (Fig. 3.13). This has formed a recumbent anticline structure that roots back to a steep thrust in the basement (Fig. 3.16; Coller & Wani, 2001), in front of which, and as a direct result of which, an imbricate fan thrust system has developed at Chingola B. It is interpreted here as a granite-bounding extensional fault that has been reactivated during subsequent compression for two reasons: (i) the high-angle nature of the thrust, and (ii) the fact that it occurs at the Lufubu Schist-Nchanga Red Granite contact. Equally striking on the SW-NE section is the thickness of the footwall arkose succession on the north limb of the Nchanga Syncline (also evident from geological maps such as Fig. 3.2 and logged in borehole L128 from the Luano orebody).

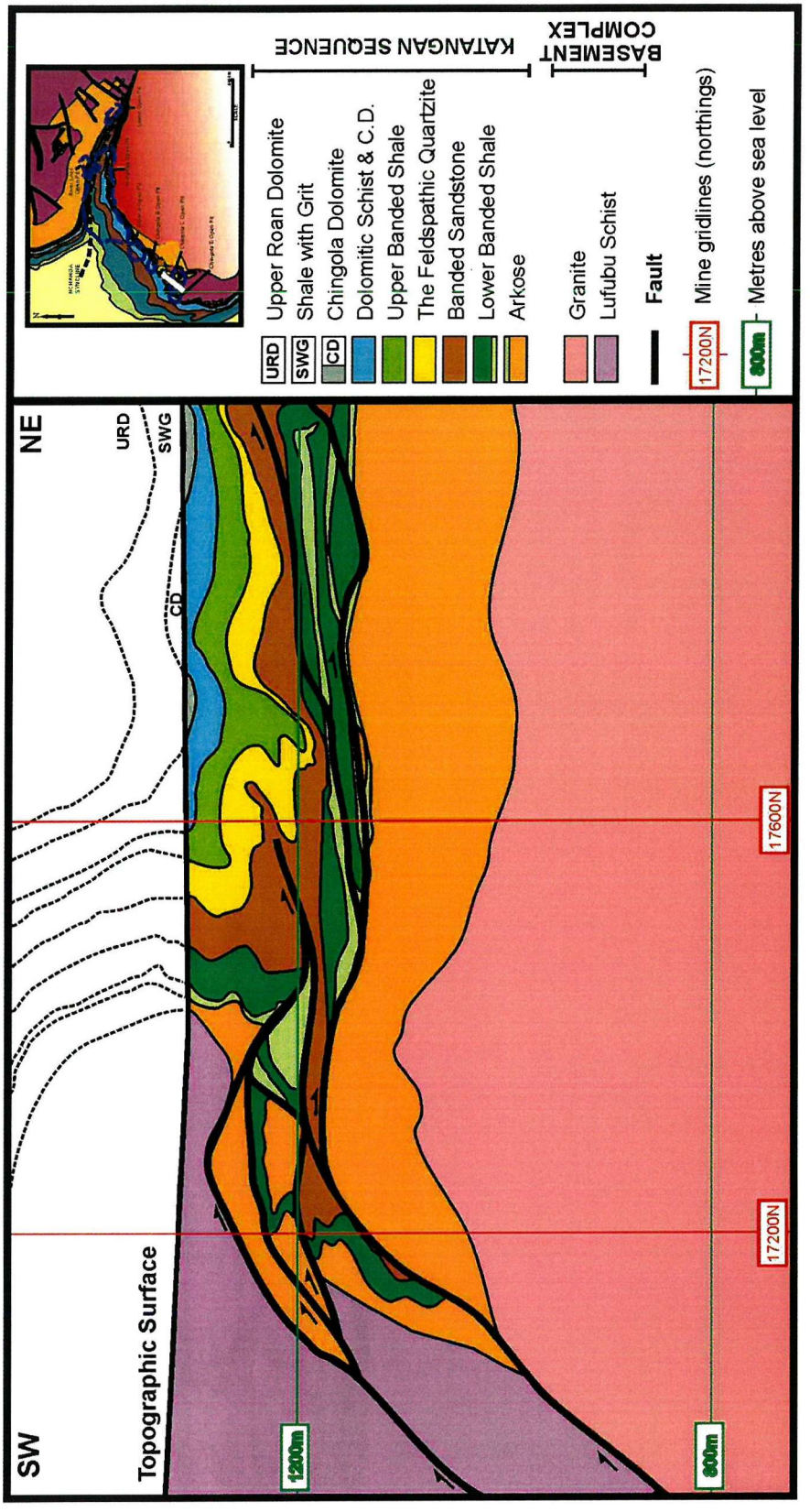

Figure 3.16: Geology of the Chingola C deposit where a NE-verging recumbent anticline structure has developed where basement schists are thrust over Lower Roan stratigraphy (refer to Fig. 3.13 for large-scale view).

Borehole L128 does not intersect the arkose-basement contact but still has a thickness of at least 265m (compared with 0 to 60m on the south limb). This has also been interpreted as a major inversion feature, where a thick arkose sequence to the north of the Nchanga Red Granite has been pushed upwards during the development of the Nchanga Syncline (Fig. 3.17). Coller (2000) suggested that the geometry of the syncline, with its steep to overturned limb, indicates a fold that has developed above a north-dipping reverse fault. In most cases, minor extensional structures do not appear to have been reactivated as thrusts (e.g. Chingola B, Block A). However, at Chingola E, Daly *et al.* (1984) described interleaving of basement granite and Lower Roan sedimentary units, where basement wedges have been emplaced (by thrusts) into and have folded the Lower Roan sediments above (XY, Fig. 3.13). They reported a strong L/S deformation fabric within the basement and a mineral stretching lineation that plunges to the SW, and cited these observations as convincing evidence that thrusts climb from the basement and displace Lower Roan units as opposed to thrusts only affecting the sedimentary cover.

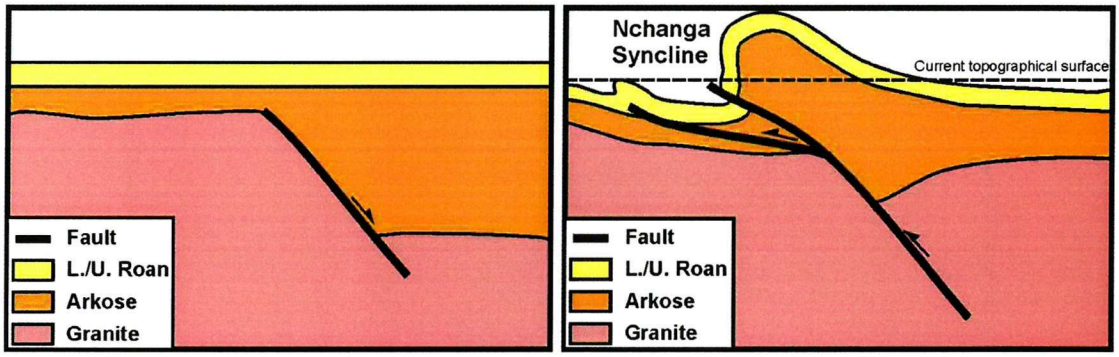

Figure 3.17: Suggested process of inversion of a granite-bounding extensional structure beneath the Nchanga Syncline, to explain the thickness of arkose on the north limb. The extensional fault is reactivated as a high-angle thrust and a major fault-propagation fold (incorporating the thick arkose succession) develops above the reactivated fault. A more shallow shortcut fault may have developed from the high-angle structure (now beneath the Nchanga Syncline). Breakthrough of the high-angle fault may or may not occur, but if it does, the most likely point of displacement is across the vertical limb of the fold (weakest point).

Evidence for internal detachments and fault-propagation folds

The fold geometry of the Lower Roan package, from the top of the arkose sequence to the Upper Roan Dolonites, is controlled by internal fault-propagation fold structures that detach within or near the 'Lower Banded Shale.' These structures are well developed at Chingola B (Fig. 3.18; NE-verging) and the Nchanga Open Pit (Fig. 3.19; S/SW-verging), and explain the often dramatic increase in intensity of folding and horizontal thickening from arkose to upper units. At Chingola B, the folds are overturned to the northeast and plunge to the northwest,

and are controlled by thrusts that dip approximately 20-40° to the southwest and indicate no more than 40m displacement (Fig. 3.20).

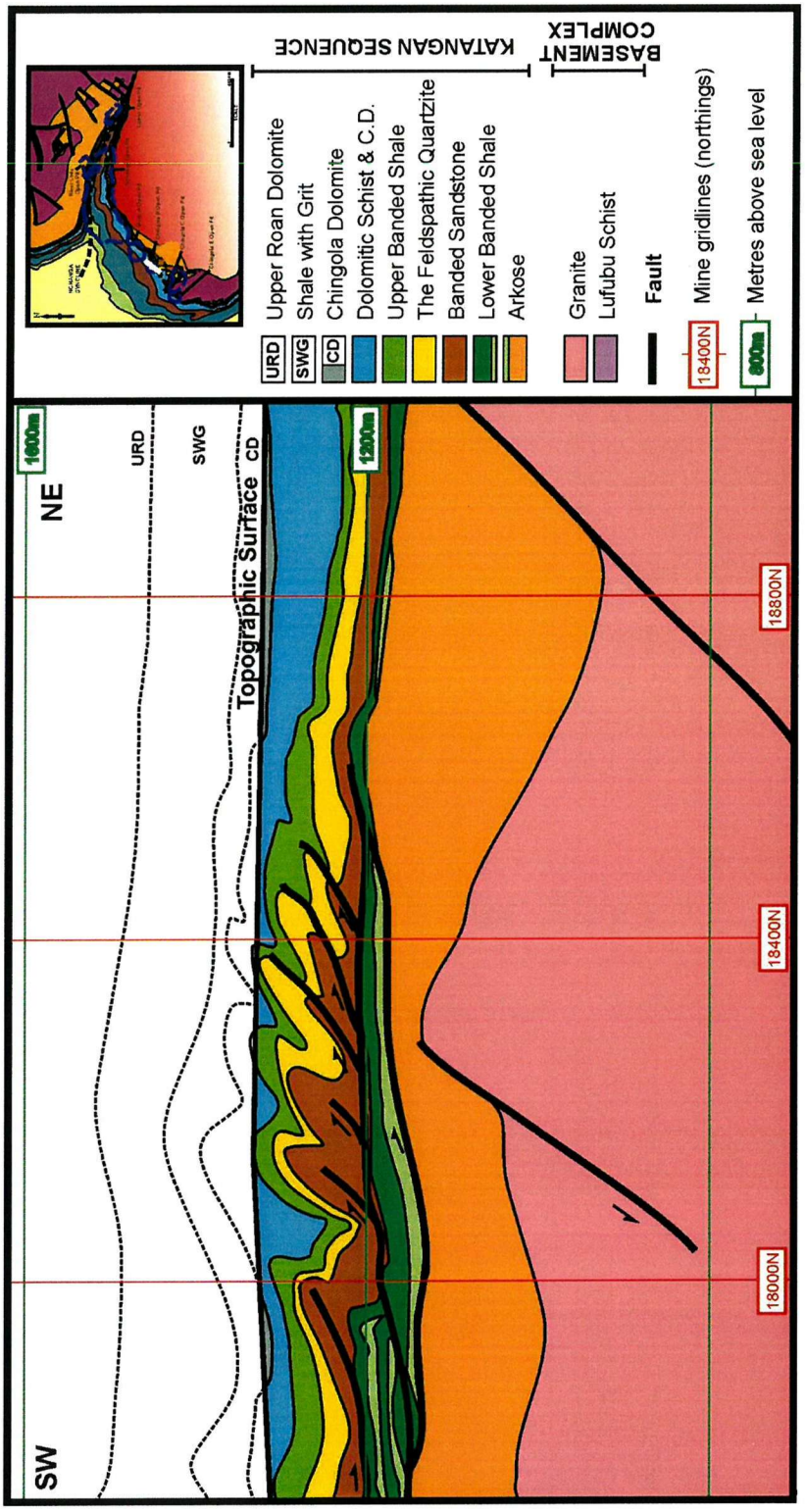

Figure 3.18: Geology of the Chingola B area where a NE-verging fold-thrust duplex has developed ahead of, and as a direct result of, the thrust-related recumbent anticline at Chingola C (refer to Fig. 3.13 for large-scale view).

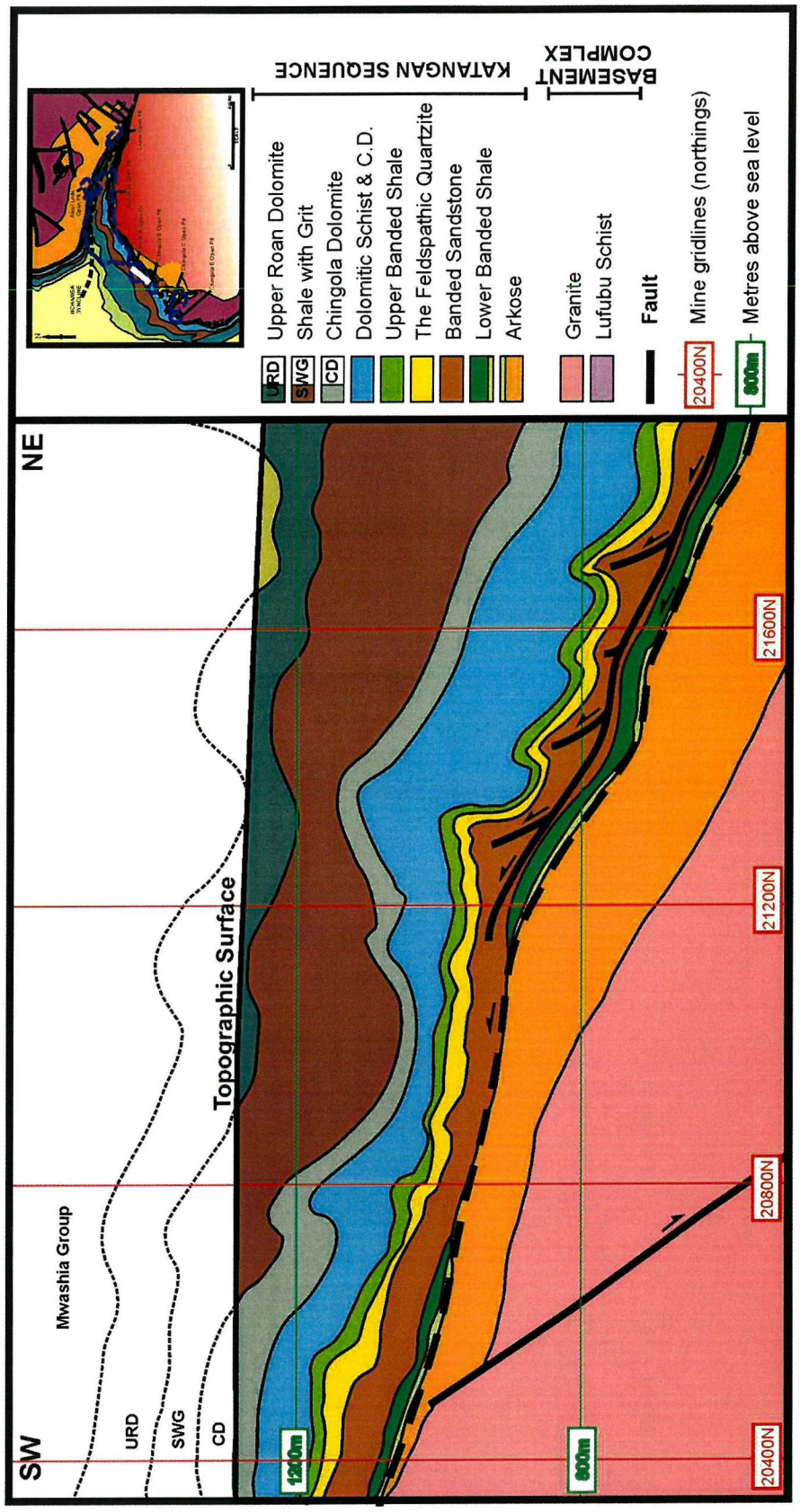

Figure 3.19: Geology of the Nchanga Open Pit deposit showing detachments within the Lower Roan sequence and related fold structures controlling the fold geometry.

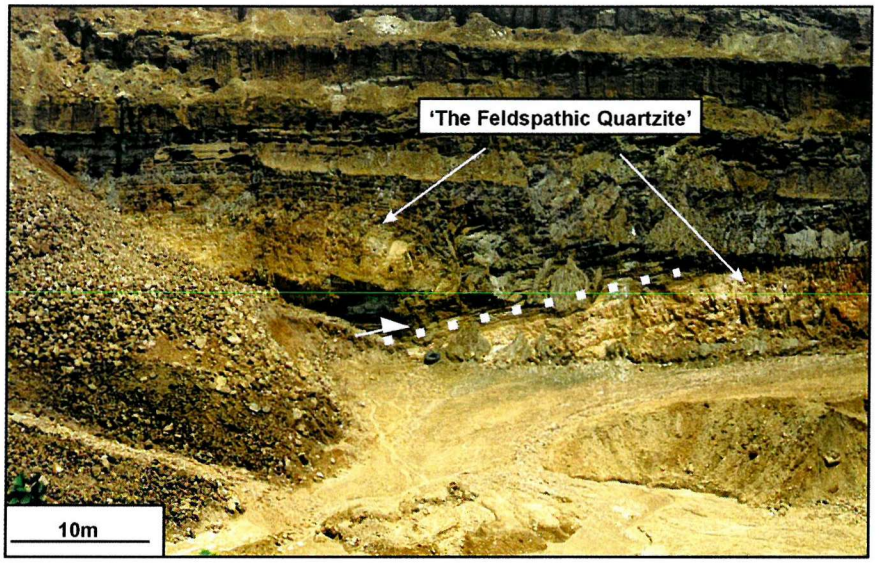

Figure 3.20 Field photograph of a thrust that controls the development of a detachment fold within the Lower Roan sequence (looking NW, Chingola B Open Pit).

These structures root back to a detachment at the top of the arkose, indicated by a zone of extensive deformation and alteration at Chingola B underground (Fig. 3.21). Minor displacement of beds, within less competent Lower Roan units, also show evidence of reverse movement (Fig. 3.22). The geometry of the internal folds at Nchanga Open Pit is similar, yet they show vergence and transport direction to the SSW or SW, and in some cases develop double hinges and box-type geometries (Fig. 3.23; Coller, 2000). They also detach somewhere between the base of the 'Lower Banded Shale' and 'Banded Sandstone' units. Fold breakthough by thrust faults is common, and is recognized during detailed logging of core, where the faults cause local repetition of the competent 'Feldpsathic Quartzite' (Fig. 3.24; borehole NOP 760), thus providing further evidence of the folds being controlled by the thrusts.

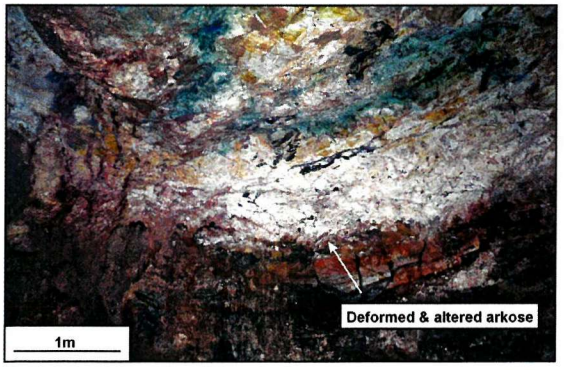

Figure 3.21: Photograph of a major zone of deformation and alteration at the top of the arkose unit, interpreted here as a detachment between arkose and overlying stratigraphy (looking N/NW, Chingola B Underground).

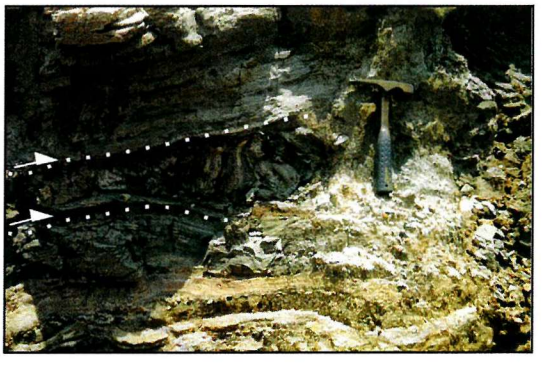

Figure 3.22: Field photograph of small reverse faults within the 'Banded Sandstone' unit and local rotation of beds (Chingola B Open Pit).

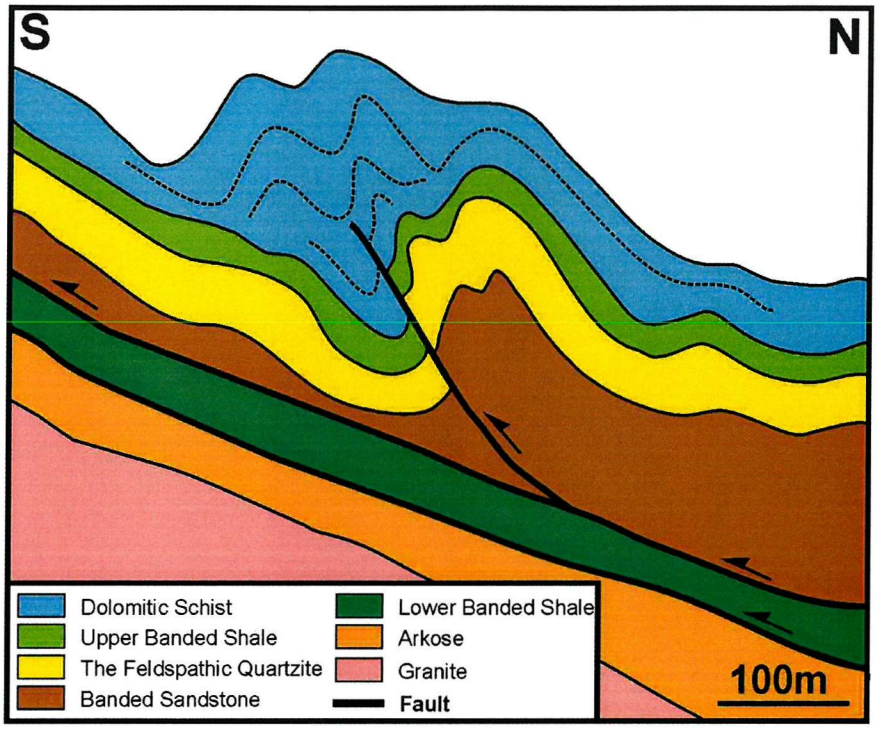

Figure 3.23: Simplified diagram of part of the south limb of the Nchanga Syncline (simplified from mine section 27E, Nchanga Open Pit).

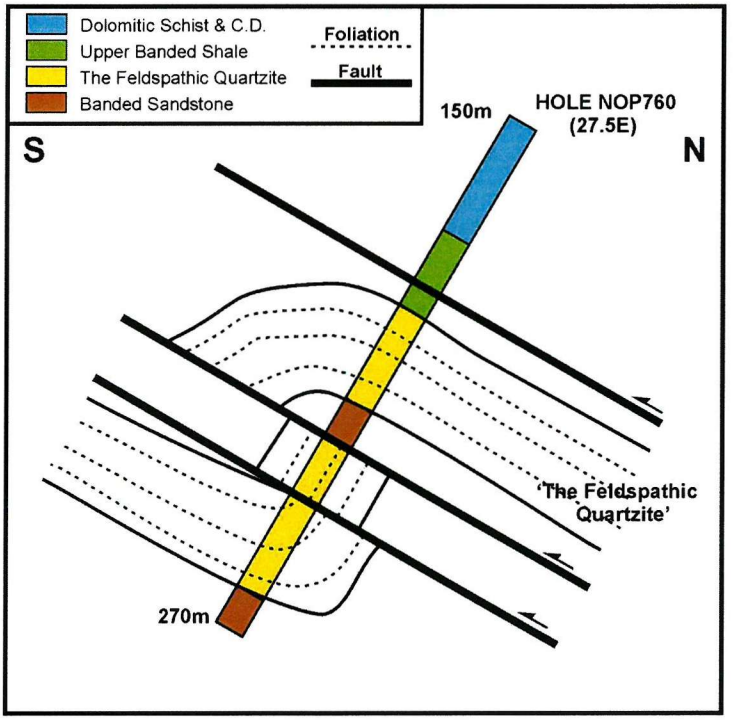

Figure 3.24: Schematic interpretation of borehole NOP 760 where local repetition of arenite units across fold zones suggests that thrusts control the fold development and geometry.

A structure contour plot of the top of 'The Feldspathic Quartzite' unit (Fig. 3.25), on to which are plotted the fold axes of the footwall synclines and hangingwall anticlines to the southward-verging folds and thrusts in the Nchanga Open Pit, gives some insight into the development of these fault-propagation folds (Coller & Wani, 2001). There is only one major detachment fold occurring on the north-dipping south limb of the Nchanga Syncline, although there are several to the west of the open pit where the main section line cuts through (Fig. 3.13 & 3.19). This diagram shows that there are three main (thrust-controlled) folds with similar strike directions of WNW-ESE, which are essentially the same structure. These main zones of displacement are thought to be linked by relay zones of smaller structures, which have taken up the displacement that has occurred on the larger thrusts/folds (Coller, 2000).

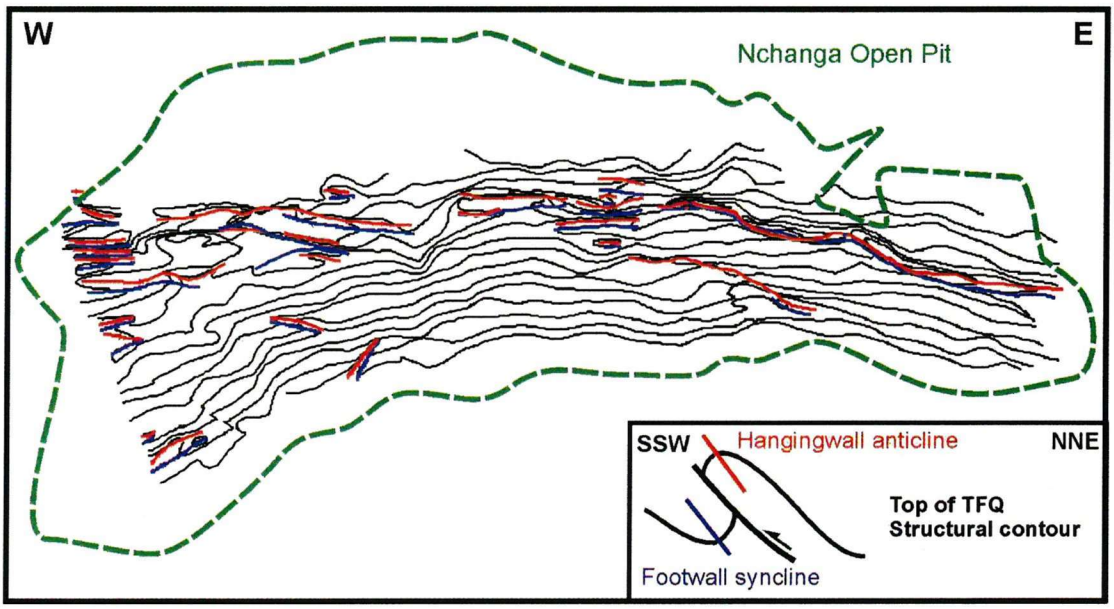

Figure 3.25: Structure contour plot of the top of the upper arenite unit, showing axes of folds, related to the development of the fault-propagation folds on the south limb of the Nchanga Syncline (modified from Coller & Wani, 2001). A number of structures occur on the south limb of the Nchanga Syncline to the west, but to the east only one fault-propagated fold is developed.

Across the Nchanga area, layer-parallel detachments (also termed decoupling horizons by Daly *et al.*, 1984) appear to have developed at three main stratigraphic points: (i) at the top of the arkose unit; (ii) at the top of the 'Lower Banded Shale' unit or within the 'Banded Sandstone' unit; and (iii) at the top of the 'Upper Banded Shale' unit. This interpretation is mainly based on the observed disruption and alteration of the lithologies at these particular depths, represented in the arkose by the increasing intensity in truncation and fracturing of feldspar grains towards the top of the unit. Within the Block A deposit, formations above the 'Lower Banded Shale' are much less deformed than in the other deposits due to lack of the fault-propagation fold structures evident at Chingola B (Fig. 3.26). However, the contact between the footwall arkoses and overlying shales is still marked by deformation and

alteration, and exposure of the contact in the open pit reveals flat-lying arkose beds overlain by highly contorted shale beds, suggesting that the detachments described above extend further northwards into Block A.

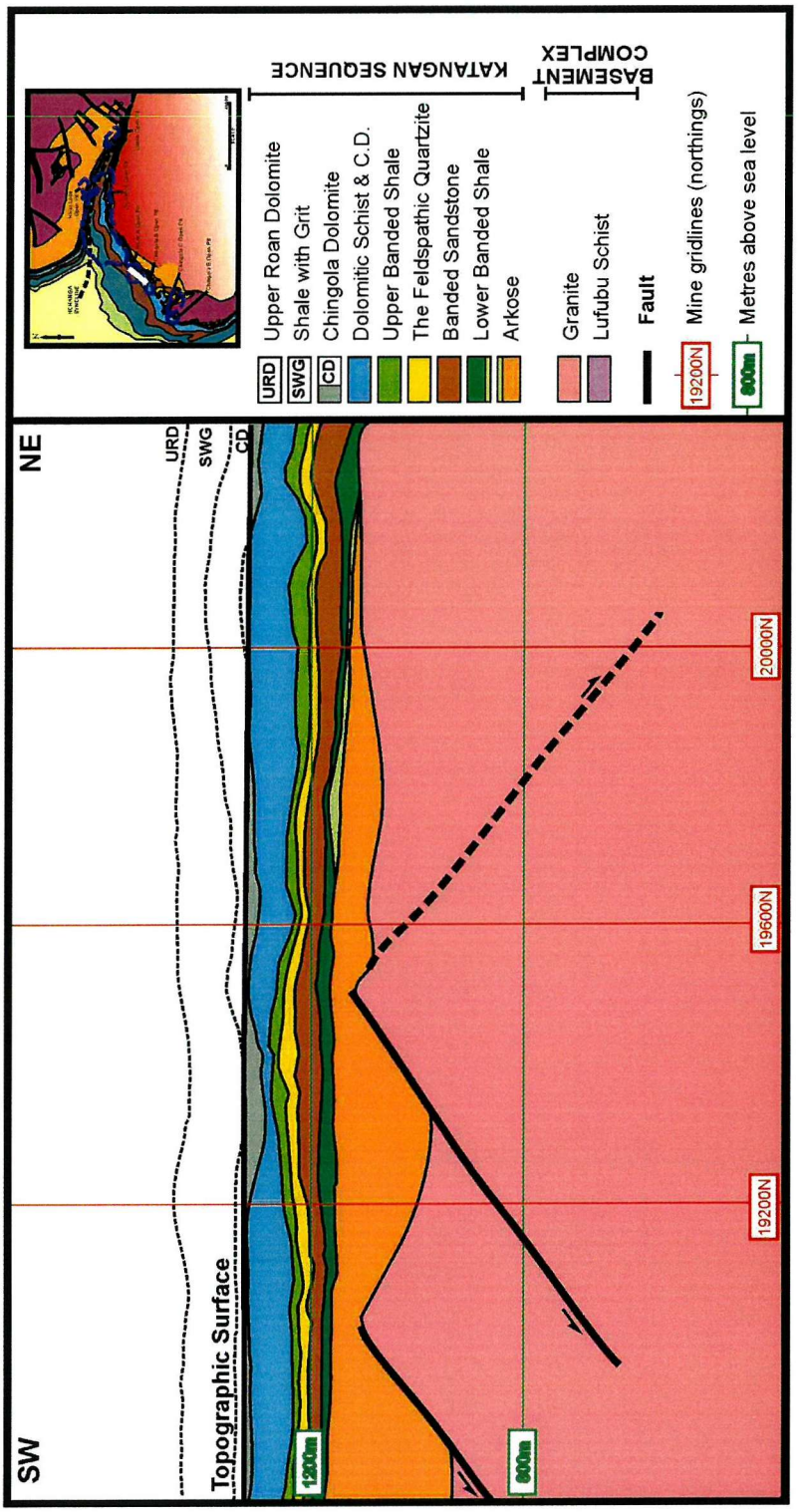

Figure 3.26: Geology of the Block A deposit showing the absence of the thrust-fold structures of Chingola B. The geology is relatively flat-lying, although there is field evidence that layer-parallel structures are present.

Structural fabrics reveal information about the structural geology of Nchanga. However, distinguishing between true bedding and these fabrics is hampered not only by the extensive shearing but also by the recrystallization of certain lithologies, in particular the less competent ones. For example, the section of 'Banded Sandstone' in borehole NOP 777 preserves no original sedimentary structures but only an intense shear fabric. Molak (1995) suggested that many of the laminar structures present in sheared rocks may not be sedimentary features but vein systems that develop during ductile or brittle-ductile shear deformation. Structural mapping and collated data from Nchanga Open Pit (data diagrammatically summarized in Figs. 3.27 and 3.28) support these interpretations. A consistent pattern in the data is an observed steeper foliation (S_1; represented by fractures in arenites) cutting a more shallow bedding (S_0). The foliation/cleavage is related to the thrust-controlled detachment folds described above.

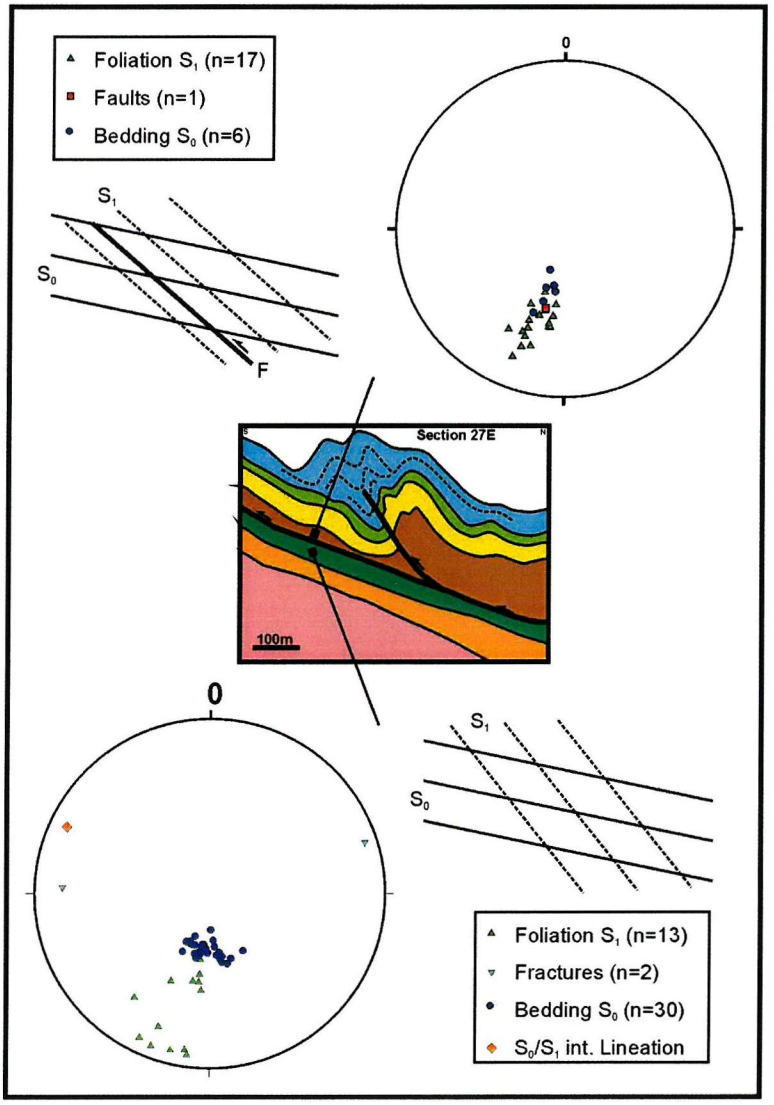

Figure 3.27: Stereographic projection of structural data (poles) recorded from 'Lower Banded Shale' and 'Banded Sandstone' units (Nchanga Open Pit).

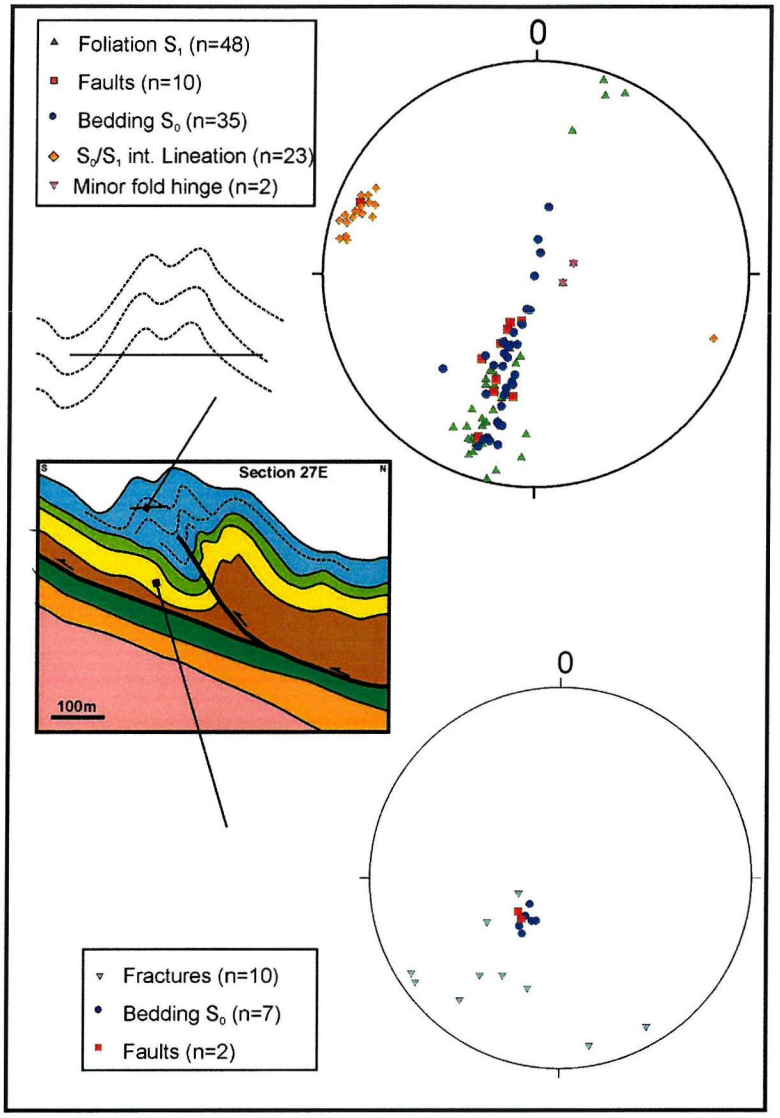

Figure 3.28: Stereographic projection of structural data (poles) recorded from 'The Feldspathic Quartzite' and 'Dolomite Schist' units (Nchanga Open Pit).

The thrust structures themselves can be observed in the Nchanga and Chingola B Open Pits and preserved in core. Exposure of the 'Banded Sandstone' unit in the Nchanga Open Pit and within most boreholes shows phlogopite-dolomite-quartz (± scapolite)-rich shear-zones at various levels within the unit (their vertical position being controlled by proximity to fault-propagation folds). They are associated with local extensive deformation (Fig. 3.29) and a strong planar fabric that in some cases appears to be sub-parallel to bedding, but in others is clearly steeper than the bedding (Fig. 3.27). Difficulties in recognizing bedding within the 'Banded Sandstone' are common with the high degree of deformation that has taken place.

Further evidence for thrusting at Nchanga is the presence of low-angle shear zones within the Lower Roan host package. The dark 'transitional' unit at the base of the 'Feldspathic Quartzite' has been revealed here as a dolomite-phlogopite-quartz shear zone. In addition

Diederix (1977) claimed that this 'transition' zone only occurs beneath the thrust-fold zones described above. This unit is most probably a thrust shear-zone that comes into contact with the 'Feldspathic Quartzite' in the vicinity of thrust-fold zones. Molak (1995) described 'extensive shear-zones composed mainly of phyllosilicates and locally rich in sulphide mineralization' as evidence for high shear strain mostly restricted to the Lower Roan package. Exposure of the folded dolomitic schist unit in Nchanga Open Pit (Section 27E) reveals strongly sheared, isoclinal fold structures and bed-parallel shear zones (Fig. 3.30). These 'shear folds' appear to fold a planar schist fabric (Coller, 2000) that is parallel to fold transport direction (and bedding?). Alignment of abundant micas (mostly phlogopite) aids identification of shear structures, including the minor stacking of thin dolomite beds within the 'Dolomitic Schist' unit along south-verging thrusts (cm scale) in borehole NOP 741.

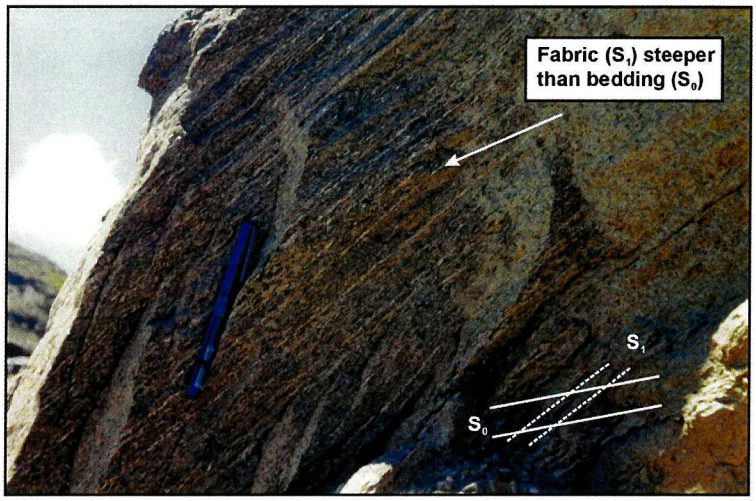

Figure 3.29: Field photograph of extensively sheared 'Banded Sandstone' that displays foliation cross-cutting a more shallow bedding (looking SE, Nchanga Open Pit).

The features described above have also been recognized by previous workers on the Nchanga deposits. Molak (1995) described the asymmetric detachment folding above a decoupling horizon parallel to bedding and located somewhere within the Lower Roan package, although he claimed that the thrusts root back into the basement as opposed to the detachment itself. Likewise, Daly *et al.* (1984) observed the bedding-parallel shear zones that they also interpreted as bedding-parallel thrust surfaces or 'decoupling horizons', and suggest that the 'Lower Banded Shale' has been followed by thrusts as a preferred plane of slip. However, Daly *et al.* (1984) described ENE-verging asymmetric folds above the Lower Roan detachment in the Nchanga Open Pit, whereas field observations during this study all indicate S/SW vergence in this one deposit. De Swardt (1962) also noted thrust structures (and associated banded 'mylonitc' rocks) from Nchanga.

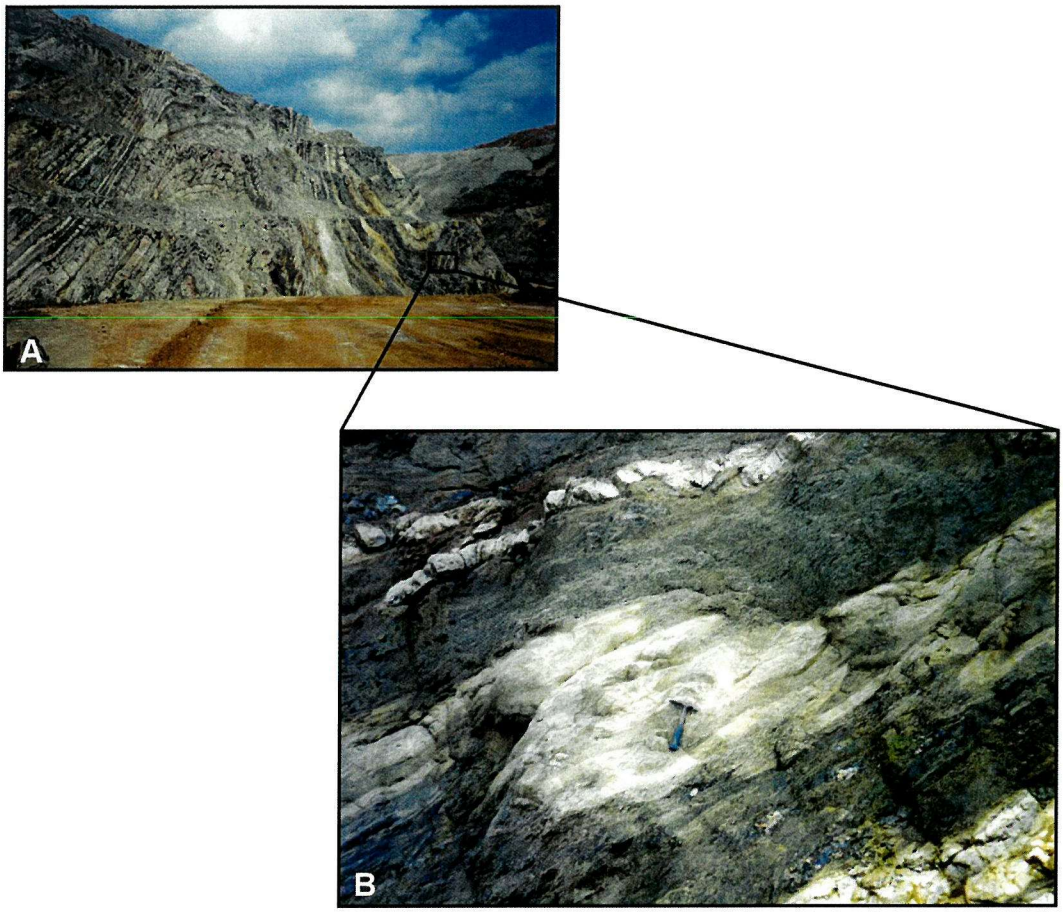

Figure 3.30: Field photograph of 'Dolomite Schist' exposure in Nchanga Open Pit, showing isoclinal folds and bed-parallel shearing developed on the limbs of a detachment fold (looking E).

The Nchanga Syncline

Intersection lineations and minor fold axes indicate that the fault-propagation folds have WNW-ESE-striking fold axes that plunge approximately 11° to the WNW. This not only appears to be the fold orientation of the minor detachment folds but also the large Nchanga Syncline, suggesting that the two fold events were related to the same compressional phase. The bed-parallel shear zones and associated detachment folds were subsequently folded around the 12km long asymmetric Nchanga Syncline, the largest structure at Nchanga that plunges to the WNW (also noted by Daly *et al.*, 1984). Coller (2000) recognized two cleavages with the same SE strike as bedding: (1) a flat-lying fabric (sub-parallel to bedding) associated with extensive phyllosilicate development (phlogopite) and (2) a steeper cleavage that cuts and modifies the flat-lying fabric suggesting it is later (with no phyllosilicate development). These two fabrics may relate to the fault-propagation folds and Nchanga Syncline respectively.

The structural features of the north limb of the Nchanga Syncline support the idea that the fault-propagation folds developed prior to the Nchanga Syncline. The River Lode Orebody (not studied as part of this project) and the Luano Orebody are both situated on this steeply-dipping north limb (Fig. 3.2), and are approximately 3km apart. Observations of mine sections and borehole L128 from the Luano Open Pit (and the description of the River Lode Orebody by Diederix, 1977) reveal the same structural discontinuity around the 'Lower Banded Shale' unit. Arkose and shale units are simply steeply dipping, whereas younger units (stratigraphically above) are folded into tight isoclinal folds (Fig. 3.31). Diederix (1977) suggested that early, tectonic, asymmetric folds have been tightly compressed into these isoclinal structures at a later stage. They are interpreted here as north-verging structures (synchronous with those developed on the south limb) that were re-folded during the development of the Nchanga Syncline. Garlick & Haldane (1976) described overturned, folded beds of 'Lower Banded Shale' and 'Banded Sandstone' dipping 60° to the northeast, where the axial planes of the folds are also overturned, and the fold axes plunge west and trend parallel to the general strike and to the fold axis of the Nchanga Syncline. These observations suggest that the layer-parallel shearing, associated decoupling of stratigraphy (at the 'Lower Banded Shale' as described above for the south limb), and the generation of fault-propagation folds occurred before (or at early stages of) the development of the Nchanga Syncline.

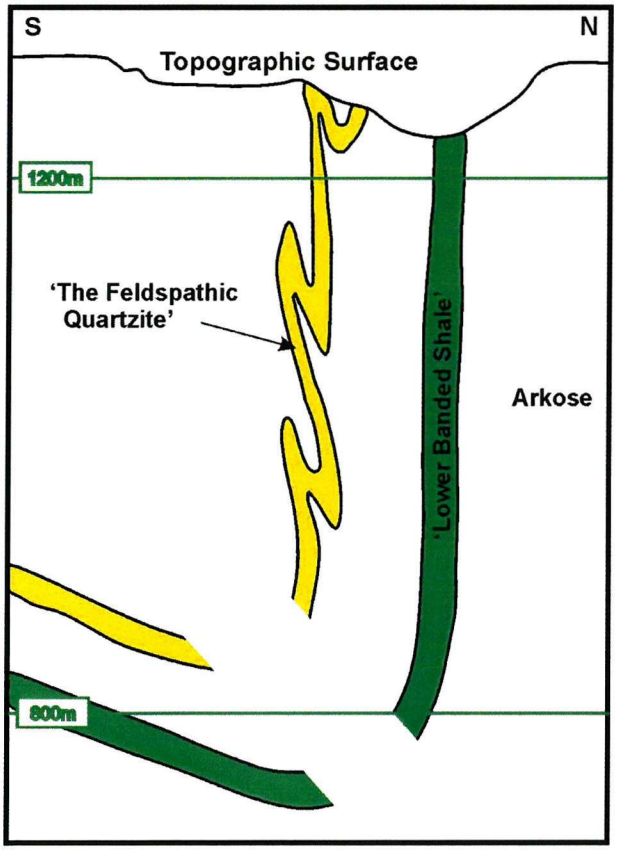

Figure 3.31: N-S cross-section through the River Lode Open Pit showing the steeply-dipping to vertical north limb of the Nchanga Syncline (modified from Diederix, 1977). The bottom of the syncline is omitted as there is no evidence to indicate whether the syncline continues around to the south limb or a fault has broken through.

3.5.3 Veins

Veins are more common at Nchanga than previously described in the available literature. In many units veins are easy to recognize, but in the quartz-rich arenite units the occurrence of veins is most easily observed in thin section. This section deals with the most common vein-types and locations, with further detail provided in Chapter 4 when discussing ore mineralogy and hydrothermal alteration.

Steeply dipping veins within basement and footwall siliciclastic unit

Numerous high-angle veins are associated with the high-angle extensional structures described in section 3.5.2, ranging in width from 2cm to 70cm (Fig. 3.32). These are most commonly quartz (± carbonate or microcline) and are associated with wallrock brecciation and alteration (see Chapter 4). Other components of the veins include hematite and limonite. At least one vein (sample NOP 17) completely encloses altered wallrock ('crack seal') suggesting more than one phase of vein development. High-angle veins, like the structures with which they are associated, are terminated at the upper contact of the footwall arkose sequence. The nature of the veins at the contact between basement granite and overlying arkose is unknown.

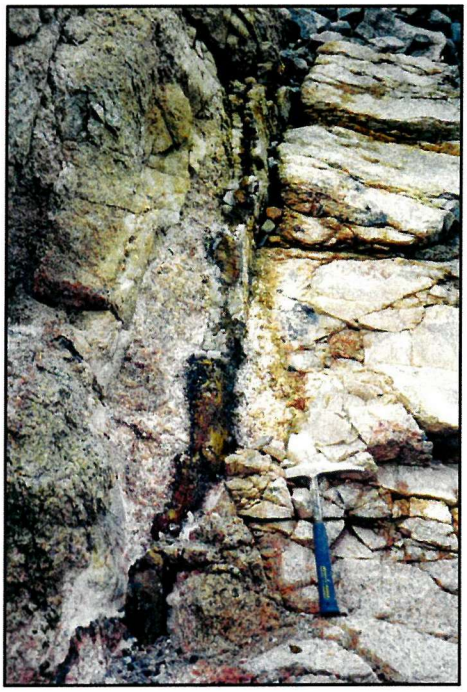

Figure 3.32: Field photograph of high-angle quartz vein associated with extensional structure within the granite basement (looking S, Nchanga Open Pit).

Veins within Lower Roan sequence

As well as the high-angle veins described above, the footwall arkoses also contains lower-angle veins, associated both with low-angle structures (e.g. Chingola C) and with the detachment at the top of the arkose unit. Often, veins within the detachment are themselves deformed and reduced to quartz breccia and overlain by a silicified zone at the base of the shale. Within the overlying shale unit, fine quartz (± pyrite) veins (< 1cm thick) trend parallel to and locally cross-cut bedding (Fig. 3.33). The orientation at which the veins cross-cut bedding is similar to that of the foliation (Fig. 3.27). Layer-parallel (bedding-parallel)

phyllosilicate shear zones developed within the 'Banded Sandstone' and 'Dolomitic Schist' units are associated with quartz-dolomite veins. None of these veins have been observed cross-cutting the shear fabric and hence are considered to have formed at the same time, although subsequent deformation of the veins has taken place. At Chingola B Open Pit, a major quartz vein and associated alteration marks the location of a thrust fault that displaces the upper units of the Lower Roan (Fig. 3.34).

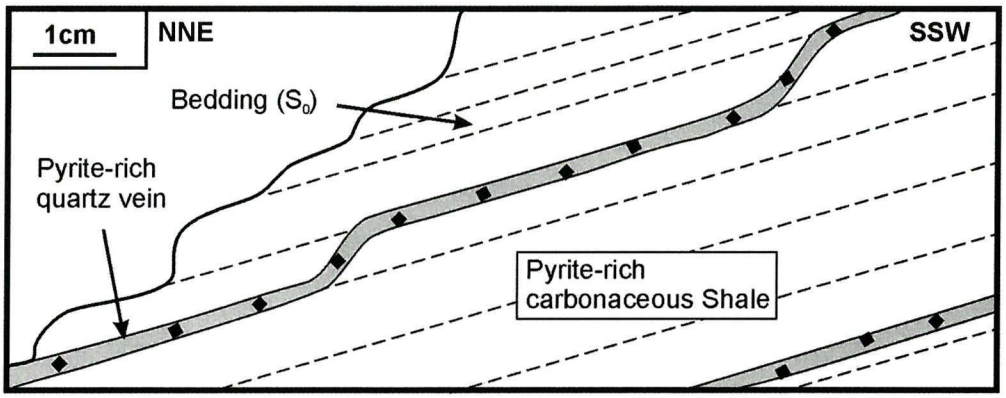

Figure 3.33: Schematic sketch of relationship of quartz veins to bedding within the 'Lower Banded Shale' unit (Nchanga Open Pit).

Figure 3.34: Field photograph of thrust fault and associated quartz vein within the Lower Roan (looking ESE, Chingola B Open Pit).

Veins are also common within arenite units, although mostly with a similar mineralogy to the wallrock and zones of recrystallization of detrital components. They are often better observed in thin section. Many of these veins appear to be parallel or sub-parallel to bedding, although McKinnon & Smit (1961) described veins transverse to bedding that terminate at ore boundaries. They are mostly quartz-dolomite (± sulphide) veins (rarely with microcline), the same composition as the wallrock feldspathic arenite (Fig. 3.35). For this reason, they have been interpreted in the past as lateral secretion veins formed during remobillization of the host-rock components (Garlick, 1972). At Chingola B, extensional veins within competent units at fold hinge zones that formed during compression are observed in the field. These

veins may have formed in similar circumstances, so appearing to terminate at ore boundaries (which are the lithological contacts of the 'Feldspathic Quartzite') and explaining their high-angle intersection with bed-parallel features.

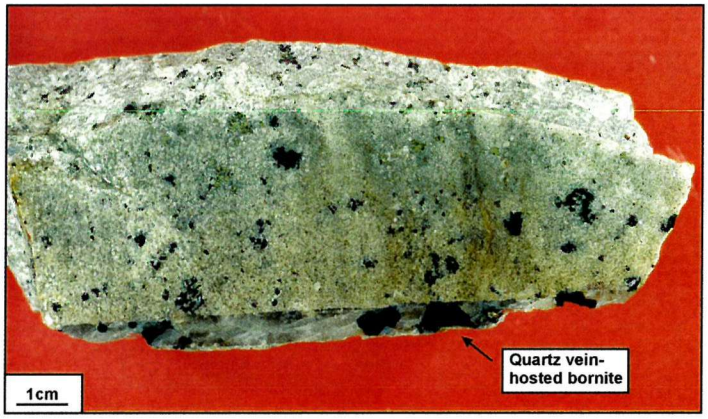

Figure 3.35: Hand-specimen photograph of quartz-dolomite-bornite vein within the 'Feldspathic Quartzite' unit (NOP 111, Nchanga Open Pit).

3.5.4 Structural evolution of Nchanga

Below are some of the sequential key events that took place at Nchanga to generate the structural features outlined above. Following the intrusion of the Nchanga Red Granite into the older Lufubu Schists at 877 Ma (Armstrong *et al.*, 1999), an early basin-forming extensional tectonic phase formed an irregular fault block topography on to which the footwall arkoses were deposited. It is likely that extension continued during deposition of the arkose perhaps explaining the minor high-angle structures within the footwall but not in the overlying stratigraphy.

At this stage, there are two possible processes: (1) basin inversion where early extensional faults are reactivated as high-angle thrusts; and (2) thrust and fold development within the Katangan cover not involving early structures or basement rocks. Here, basin inversion is favoured, as indicated above. Inversion tectonics involves a switch from extension to compression, such that extensional basins are contracted and become regions of positive relief (McClay & Buchanan, 1992). The architecture of thrust systems in inverted extensional basins is often controlled by the pre-existing extensional faults (Cooper & Williams, 1989; McClay *et al.*, 1989). The geometry of such systems is commonly more complicated than simple thrust systems and can vary from small, high-angle thrusts in basins that have undergone small amounts of contraction to large, low-angle thrust systems that override and obliterate the pre-existing extensional fault geometry (McClay & Buchanan, 1992). Based on the observations at Nchanga, the latter is more plausible. One other interesting feature of inverted basins is the fact that not all extensional structures are reactivated, indeed only a few

may show signs of reverse movement (McClay & Buchanan, 1992). This certainly appears to be the case at Nchanga, where there is little evidence for inversion on many structures, apart from the ones that bound the granite block to the north and south.

At some point during the early stages of compression (and basin inversion), bed-parallel thrusts (decollements) developed within a layer-cake stratigraphy, strongly controlled by the competence difference between certain horizons. For example, the contact between the thick, competent sequence of arkose and overlying, less competent shale was a preferred plane of slip. This may have been aided by an evaporite horizon that once existed at that contact. Within the South Pyrenean fold and thrust belt, evaporite horizons act as suitable sites for the development of decollements, with thrusts ramping up from oldest to the youngest evaporite (Verges *et al.*, 1992). As the decollements progressed, at some point the fault would have started to cut up through stratigraphy. Then a process termed 'fault-propagation folding' (Suppe & Medwedeff, 1990) occurs, which explains the common association of asymmetric folds with one steep or overturned limb adjacent to thrust faults. Folds form and grow at the tips of propagating thrust faults, often resulting in footwall synclines and hangingwall anticlines to the thrusts. The detachment folds described above from Chingola B and Nchanga Open Pit are considered to be this type of structure. Suppe and Medwedeff (1990) proposed three models: (1) the folds form first; (2) the faults form first; and (3) contemporaneous folding and faulting. At Nchanga, the faulting and folding are not considered to be two distinct processes, with early thrusting and related folding (and subsequent break-through of structures through some folds) being favoured. However, it must be noted that faulting followed by folding (of less competent units) can also form the hangingwall anticline structures, often called drag-folds (Suppe & Medwedeff, 1990).

The folds would have continued to grow at the tip of the thrust fault as the fault itself progressed (sequential development of a fault-propagation fold is shown in Fig. 3.36). Certain lithologies fold much more readily than others, and at some point the thrust may have impinged on a unit that would not fold as easily as others. At this point, the fault locked, stress built up, and inevitably breakthough occurred, either along the synclinal axial surface, along the anticlinal axial surface, or somewhere within the steep limb where most extensive fracturing of the brittle unit takes place (Suppe & Medwedeff, 1990). At this stage footwall collapse would have occurred. If this model is applied to Nchanga, bearing in mind the known stratigraphy, units such as the 'Banded Sandstone' would preferentially fold, whereas 'The Feldspathic Quartzite' would act in a brittle manner, and intersection of a thrust with the arenite would promote eventual breakthrough (Fig. 3.29). However, the process may be more

complicated than this and breakthough may be achieved along multiple low-angle structures and not just one thrust.

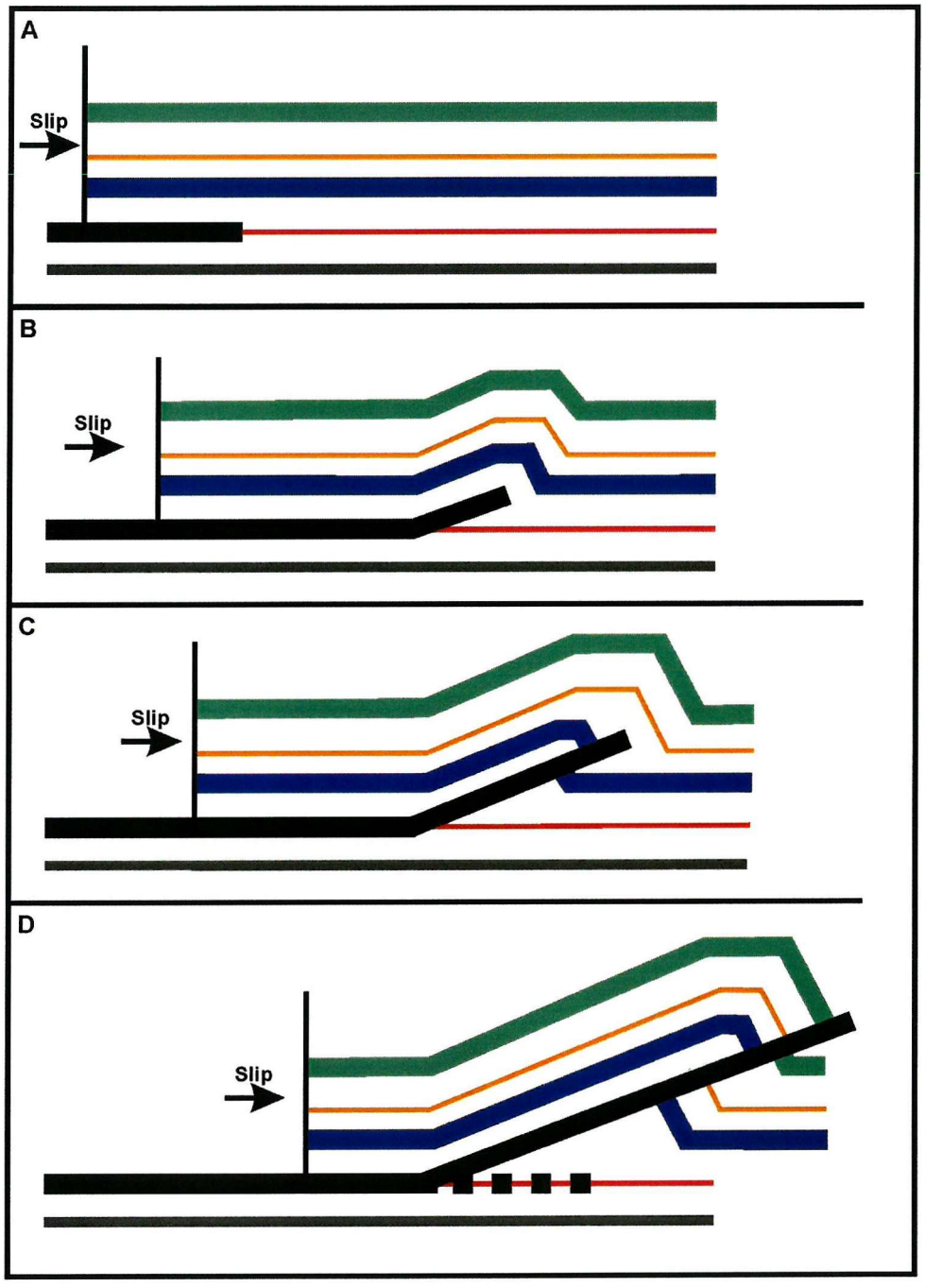

Figure 3.36: Sequential development of fault-propagation fold leading to formation of thrust-fold duplex at Nchanga: (A) development of a bed-parallel decollement and associated slip; (B) propagation of fault cutting up through stratigraphy and the folding of horizons above in response; (C) further propagation growth of fault-propagation fold above the fault, with displacement of some horizons nearer to the original basal decollement; (D) fault propagates further, sticks, and then breaks through the high-angle limb of the fold where fractures are most extensive. The fault then dies out and slip and further deformation continues along the original decollement surface and above process is repeated (simplified from Suppe & Medwedeff, 1990).

Following fold breakthrough (and subsequent footwall collapse), the propagating thrust would have died out and displacement continued along the basal detachment to which the thrusts root back, with the development of new fault-propagation folds. Hence, structures that are furthest towards their vergence direction are younger than those 'behind' them. Therefore, at Nchanga and in particular Chingola B (Fig. 3.18), the most northeasterly folds are the youngest. Major reactivation of extensional structures resulted in the generation of some of the larger structures, such as the Nchanga Syncline to the north of the Nchanga Red Granite, and the Chingola C recumbent anticline to the south. There is no evidence at this stage to confirm whether basement structures, other than the granite-bounding ones (e.g. Chingola B, Block A), have been inverted.

In reality, there are no separate chronological fault, fold, and reactivation phases. They are all part of the same D2 compression of the Katangan sequence. Which process is occurring at each locality at the same time is controlled by a number of factors: including the competence and thickness of units being deformed, the proximity to the granite-bounding structures, and the position north or south of the Nchanga Red Granite block. The latter is important as south-verging structures within the Nchanga Syncline are thought to relate to backthrusts (caused by inversion on the granite-bounding extensional fault on the north side of the Nchanga Red Granite). For example, the north-verging thrusts (and folds) on the south side of the granite within the dominantly north-transporting compressional regime were probably generated before those that verge southwards on the north side. The most likely timing for the D2 compression is during the Lufilian Orogeny (Daly *et al.*, 1984).

3.6 Mineralization

There are three economic concentrations of copper (and cobalt) at Nchanga: the Lower Orebody (copper only), hosted at the top of arkose unit and base of overlying shale; the Intermediate Orebody (copper only), a relatively minor occurrence within the 'Pink Quartzite' in the 'Banded Sandstone' unit; and the Upper Orebody (copper and cobalt) hosted mostly within 'The Feldspathic Quartzite' unit but also occurring in the base of the overlying shale (Figure 3.37). The main sources of ore are the Lower and Upper Orebodies. Nchanga mineralization consists of a range of ore minerals including chalcopyrite, bornite and chalcocite as sulphides, malachite and chrysocolla (with minor cuprite and native copper) as supergene minerals. The only source for the cobalt appears to be carrollite, a cobalt-nickel sulphide, although cobaltiferous pyrite has been described from other Copperbelt deposits (Mendelsohn, 1961). Pyrite can be common within ore zones and within some of the black

shale horizons. The ore minerals themselves occur in a variety of styles including disseminated blebs, bed-parallel streaks, and within minor fractures and veins. In addition to the typical orebodies described above, other anomalous concentrations of copper occur as the 'vermiculite' orebodies (Bassett, 1958) where copper is hosted within micas (as part of the mica lattice). This is mostly hosted within the 'Banded Sandstone' unit, particularly the upper part.

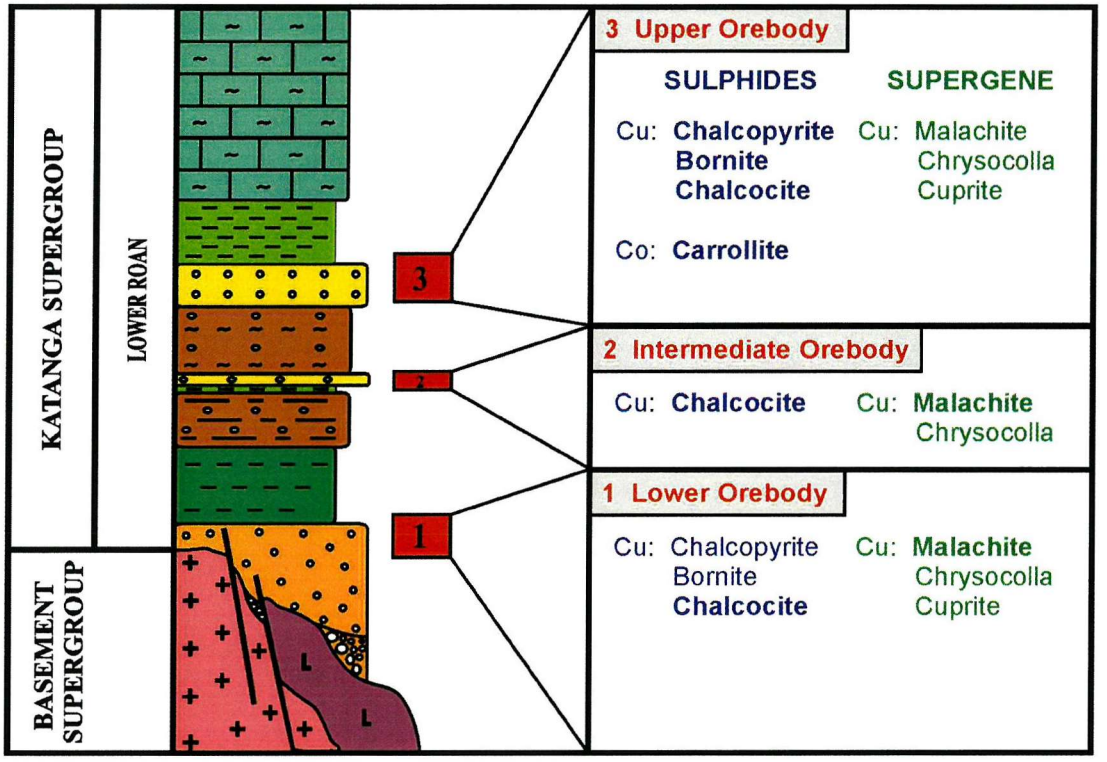

Figure 3.37: Stratigraphic location of economic orebodies at Nchanga, showing the main ore minerals found within those zones.

Typical grades for the Lower Orebody are 2 to 3% copper over 6-10m representing the contact zone between arkose and overlying 'Lower Banded Shale.' For the Upper Orebody, copper grades average approximately 2.5 to 3%, with cobalt grades reaching as high as 1% within cobalt-rich zones. The 'vermiculite' ore generally contains 1 to 2% (copper only).

3.6.1 Macro-scale distribution of mineralization

The general location of copper (and cobalt) ores are illustrated by the projection of high-grade orebodies to surface on a geological map of the Nchanga area (Figs. 3.38 & 3.39). High-grade Lower Orebody mineralization occurs within each of the individual deposits. However, Upper Orebody mineralization only occurs where the internal detachment-related folds within the Lower Roan have developed at Nchanga Open Pit and Chingola B (refer to Figs. 3.18 & 3.19). The cobalt mineralization of the Upper Orebody is only found within the Nchanga

Open Pit. The main Nchanga Open Pit Lower and Upper Orebodies display considerable lateral (> 3km) and down-dip (up to 1km) extent of mineralization.

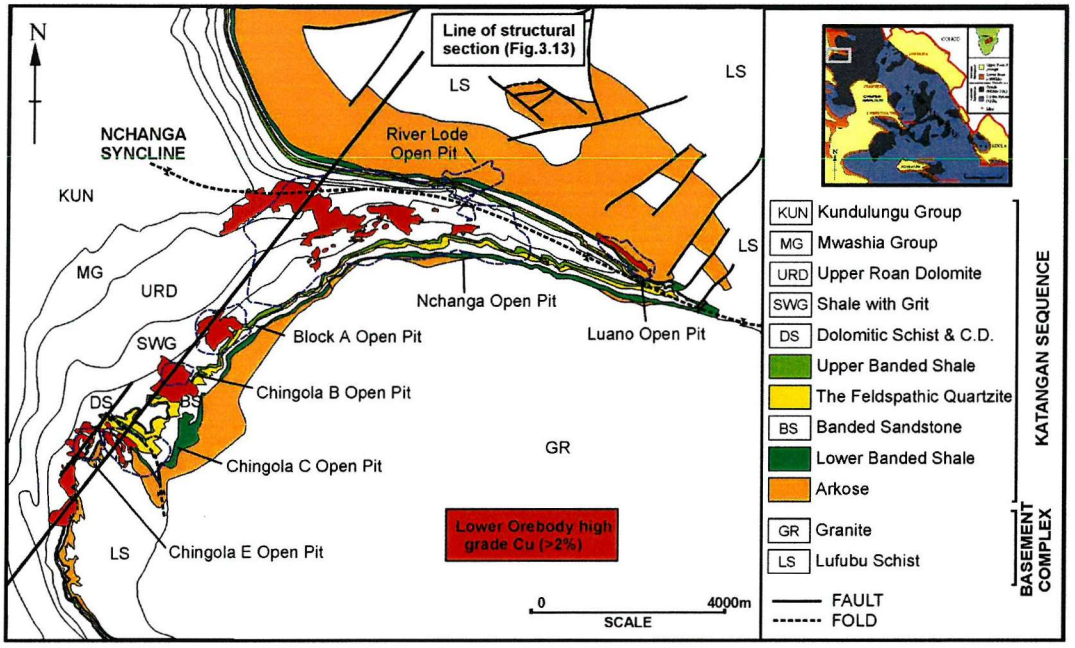

Figure 3.38: High-grade Lower Orebody mineralization in the Nchanga area projected to surface.

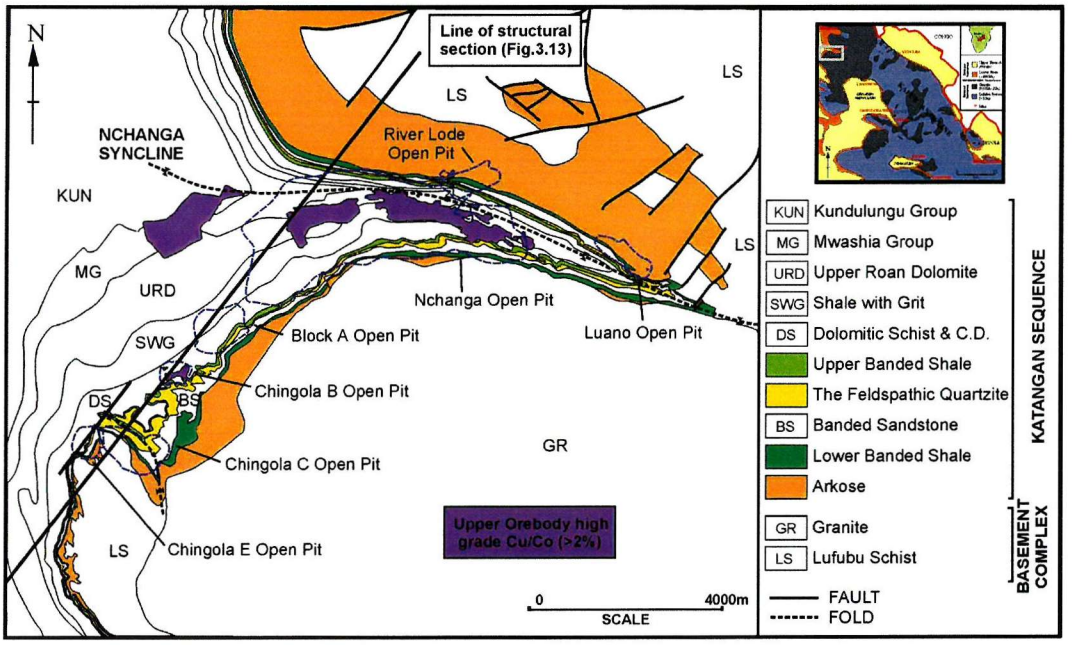

Figure 3.39: High-grade Upper Orebody mineralization in the Nchanga area projected to surface.

Nchanga mineralization is continuous along the SW-NE section through the Nchanga area (Fig. 3.13), from Chingola F, D, and E to Chingola C (Fig. 3.40), Chingola B (Fig. 3.41), Block A (Fig. 3.42) and the Nchanga Open Pit (Fig. 3.43). These adjoining sections reveal no truly barren gaps in mineralization for a distance of over 5km. Note that the lower cut-offs

used in figures 3.38 and 3.39 are approximately 2% (Cu), compared to a cut off of 0.01% (100ppm) for the sections.

As well as the lateral or horizontal continuity of mineralization, the sections also reveal the vertical extent of copper concentrations from Basement rocks, through the Lower Roan host package to the dolomite formations. In particular, the distribution of mineralization at Chingola B, Block A, and Nchanga Open Pit (Figs. 3.41, 3.42, & 3.43) indicates that, although economic concentrations of copper are restricted to the two main stratigraphic horizons described above, low-grade copper can be found within any Lower Roan rocks. In addition to this, a striking feature at the Chingola B mine (fig. 3.41) is the low-grade copper in Basement Nchanga Red Granite, and the transgressive nature of the mineralization. There is a strong structural control on this distribution of copper, evident at Block A (Fig. 3.42) where the vergence of structures appears to change from NE-verging at Chingola B to S/SW-verging at Nchanga Open Pit (see section 3.5). Where this change in vergence occurs, the geometry of the low-grade copper plumes also changes, mirroring the structures. In many cases, the lower limit of the low-grade copper (extending downwards within the arkose towards the Basement contact) is unknown as many of the boreholes have only been assayed as far as the extent of any visible mineralization.

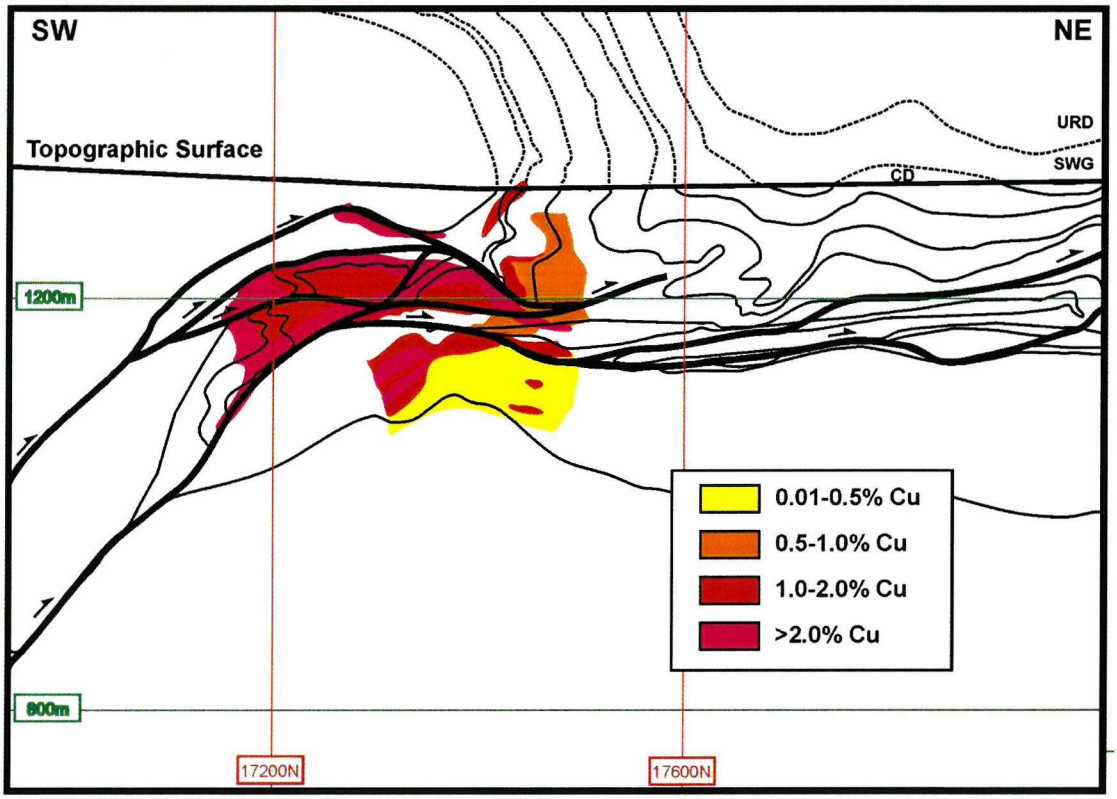

Figure 3.40: The distribution of mineralization at Chingola C (based on copper grade boundaries) plotted on to the section geology (refer to Fig. 3.16). High-grade mineralization is strongly related to thrust structures.

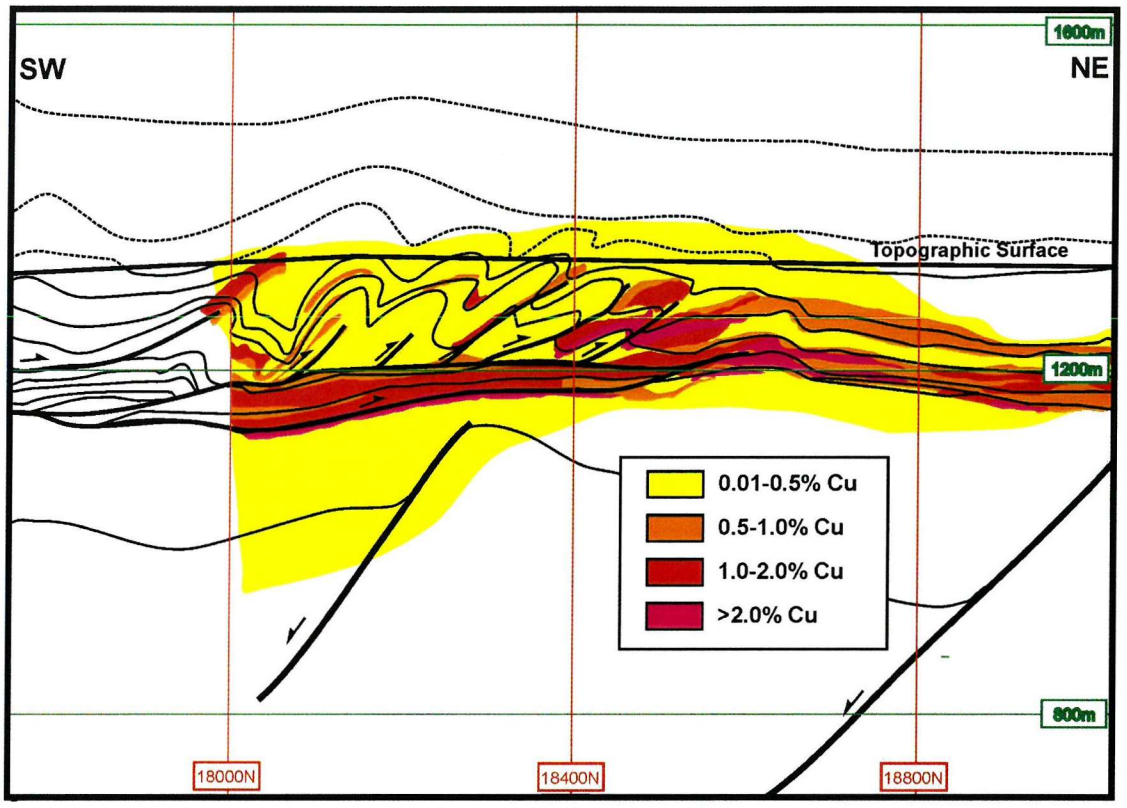

Figure 3.41: The distribution of mineralization at Chingola B (based on copper grade boundaries) plotted on to the section geology (refer to Fig. 3.18). Mineralization is strongly related to the fault-propagation folds and controlling thrusts, as well as basal detachments.

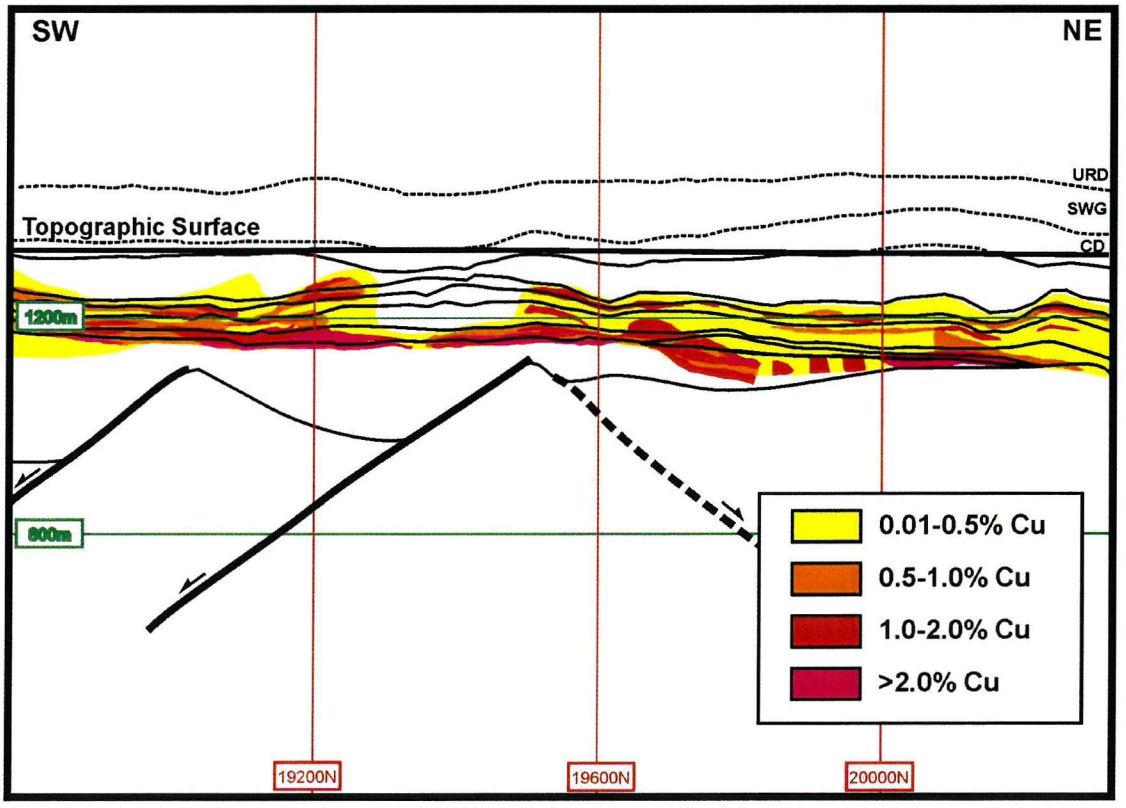

Figure 3.42: The distribution of mineralization at Block A (based on copper grade boundaries) plotted on to the section geology (refer to Fig. 3.26).

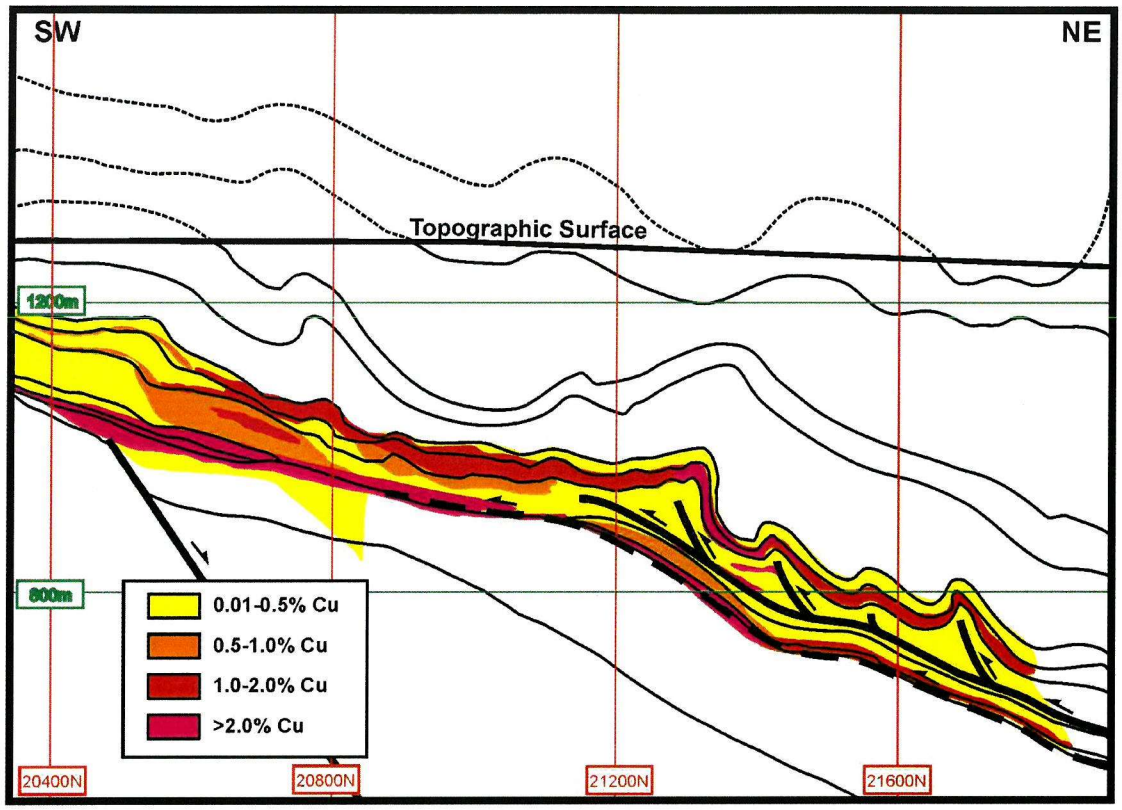

Figure 3.43: The distribution of mineralization at Nchanga Open Pit (based on copper grade boundaries) plotted on to the section geology (refer to Fig. 3.19).

The main concentrations of copper and cobalt mineralization at Nchanga are reviewed below: the Lower, Intermediate, and Upper Orebodies, as well as 'refractory' ore (within micas) and mineralization within the Basement.

3.6.2 The Lower Orebody

The economic Lower Orebody is almost continuous across the Nchanga area, and varies in thickness from 0.5m to 20m. The distribution of mineralization reveals that the high-grade copper is strongly spatially associated with the tectonized contact between the arkose and 'Lower Banded Shale.' The structural control of Lower Orebody mineralization is particularly evident in the sections showing distribution of mineralization at Chingola C (Fig. 3.40) and Chingola B (Fig. 3.41). At Chingola C, high-grade copper mineralization is concentrated in the most tectonized part of the recumbent anticline structure, where thrusts cut up through the basement to the northeast. In fact, high-grade copper (> 2%) appears to follow the structures far more closely than any particular lithology. Likewise, at Chingola B, high-grade copper mineralization follows the layer-parallel structural detachments that have developed within the Lower Roan sequence, in particular at the top of the arkose unit but also within the 'Banded Sandstone.' In addition to this, the transgressive nature of mineralization at the Chingola C, Chingola B, and Block A deposits suggests that it is clearly associated with

transgressive structures (e.g. thrusts). Another structural control on the location of Lower Orebody mineralization may be the pre-Katangan extensional structures in the Basement. Diederix (1977) claimed that the Lower Orebody is not altogether continuous but is localized and controlled by the Basement topography and the presence of the 'Lamprophyre' intrusive. However, the current study has revealed that the Basement topography is controlled by early extensional structures and that the 'Lamprophyre dyke' is actually one of them (section 3.5). Similarly the Lower Orebody reveals a clear increase in copper where a high-angle, extensional fault zone (the 'Lamprophyre dyke') intersects the arkose and overlying shale in both the Nchanga Open Pit (south limb of the Nchanga Syncline) and the River Lode Pit (north limb).

Previous authors have described the mineralization as being mostly shale-hosted. However, the current study has revealed that much of the high-grade copper may actually be hosted within the top part of the arkose unit and along the deformed contact with the overlying shale, often called the 'Transitional Arkose' (Fig. 3.44 & 3.45). This is particularly true where the mineralization consists mostly of malachite (± chrysocolla). High-grade copper can also occur in the 'Lower Banded Shale,' (Fig. 3.46; Block A), yet the boreholes studied from Chingola E (NE 297), Chingola C (NE 529/528), Chingola B (NE 282), Nchanga Open Pit (NOP 716/741) and the Luano deposit on the north limb of the Nchanga Syncline (L 128) all reveal the majority (60-90%) of high-grade copper within the arkose.

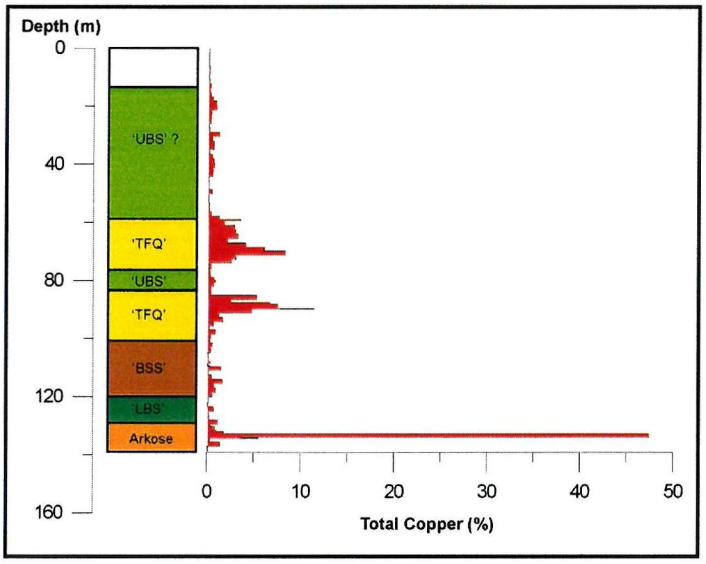

Figure 3.44: Down-hole grades of Cu mineralization (%) from borehole NE 282, Chingola B (assay grades from mine data).

The assay data was not only taken from mine logs of the selected boreholes, but samples were also collected during this study and analysed for copper and cobalt content. Little work was carried out on the Chingola D and F orebodies, as they were unexploited at the time of the study. However, Diederix (1977) reported that much of the mineralization is also hosted within the top part of the arkose unit, and not in the overlying shales. It is worth noting that Lower Orebody mineralization on the north limb of the Nchanga Syncline (Luano) also

occurs at this contact between arkose and shale, even where these units are overturned or vertical. This may suggest that mineralization was introduced prior to development of the Nchanga Syncline.

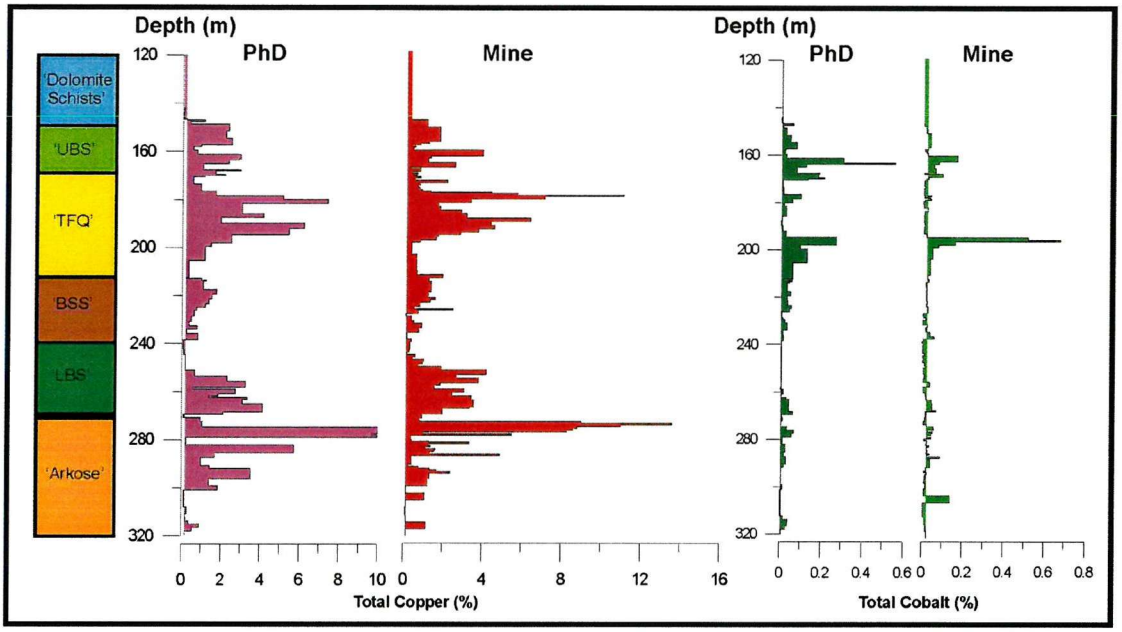

Figure 3.45: Down-hole grades of copper and cobalt mineralization (%) for borehole NOP 716, Nchanga Open Pit (assay grades from mine data are compared to those obtained during PhD study)

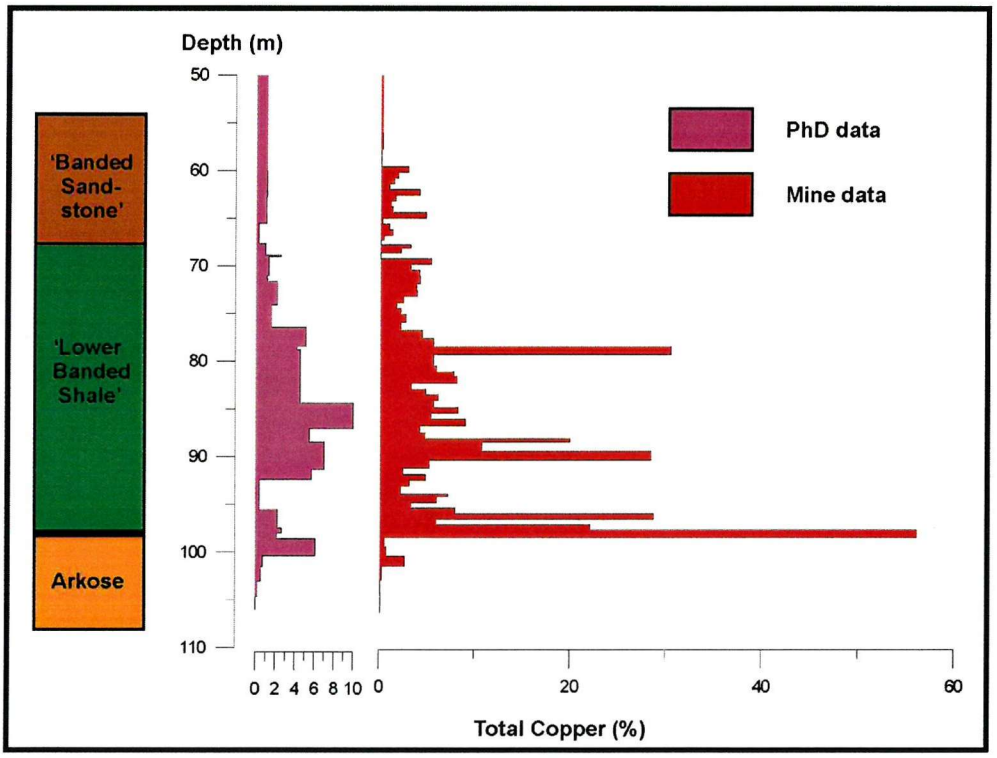

Figure 3.46: Down-hole grades of copper mineralization (%) for borehole NE 515, Block A (assay grades from mine data are compared to those obtained during the PhD study)

The main copper minerals are chalcocite and malachite. High-grade ore normally consists of breccia-, vein-, and fracture-hosted chalcocite and malachite within deformed and altered arkose, between 0m and 20m below the arkose-shale contact (Chingola B, Block A, Nchanga Open Pit, and Luano). Often, the most abundant copper minerals, in particular malachite and chalcocite, occur within the 'Transition' contact zone between arkose and shale. Sulphides are rare within the Lower Orebody, although Diederix (1977) described bornite and chalcopyrite at deeper levels within the arkose, with a supergene zone only occurring much nearer to surface, consisting of malachite, chrysocolla and cuprite. In addition, minor sulphides were observed below the supergene zone in several holes. At Block A, shale-hosted mineralization consists of fine blebs of chalcopyrite and chalcocite clearly associated with the developed cleavage. Diederix (1977) distinguished between a much more sulphide-rich Lower Orebody (chalcopyrite, bornite, chalcocite) on the western side of the south limb of the Nchanga Syncline and a mixed sulphide and malachite orebody on the eastern side. Other minerals that are commonly found with the malachite include chrysocolla and cuprite, normally found with malachite. Pyrite occurs within the 'Lower Banded Shale,' although there is normally an inverse relationship between abundance of copper minerals and pyrite (Block A, Nchanga Open Pit).

Zoning of the mineralization at the Siliciclastic-Mixed Unit boundaries ('Ore-shale') is well described from other Copperbelt deposits (Mendelsohn, 1961; Fleischer, 1984), although not from Nchanga due probably to the supergene modification of the primary sulphides. McKinnon & Smit (1961) recognized zoning of sulphides within the Nchanga Lower Orebody, from a chalcopyrite zone at shallower levels to a bornite-chalcopyrite zone at deeper levels. Lateral zoning may not be common but there is a sense of vertical zoning and McKinnon & Smit (1961) also described a vertical zonation of from arkose to 'Lower Banded Shale,' of chalcopyrite/bornite to chalcopyrite to pyrite (Fig. 3.47) in the central part of the lower orebody on the south limb of the Nchanga Syncline.

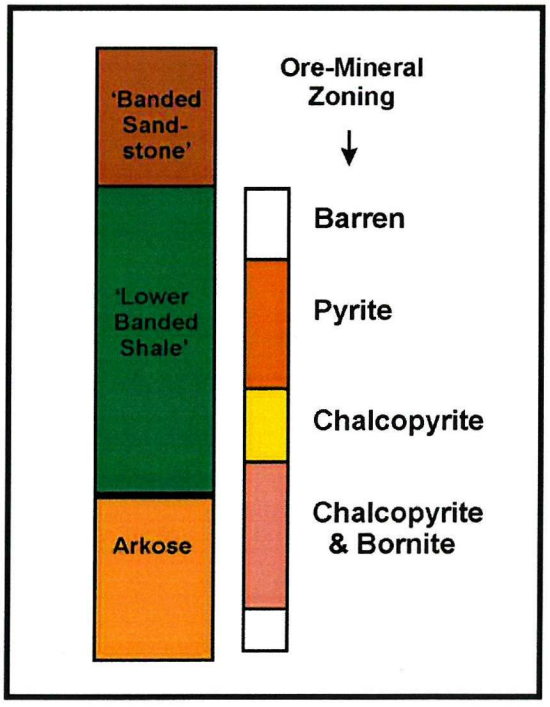

Figure 3.47: Apparent vertical ore-mineral zoning of Lower Orebody (McKinnon & Smit, 1961).

Pyrite is often considered to be part of the primary mineral zoning, but will be shown in Chapters 4 and 5 to be a different phase of sulphide introduction and to have been replaced by copper minerals. Taking into account field evidence and information from mine literature, the zoning of Lower Orebody sulphides is thought to be similar to that suggested by McKinnon & Smit (1961), but with a chalcocite (primary or secondary) zone at the contact between arkose and overlying shale (Fig. 3.48).

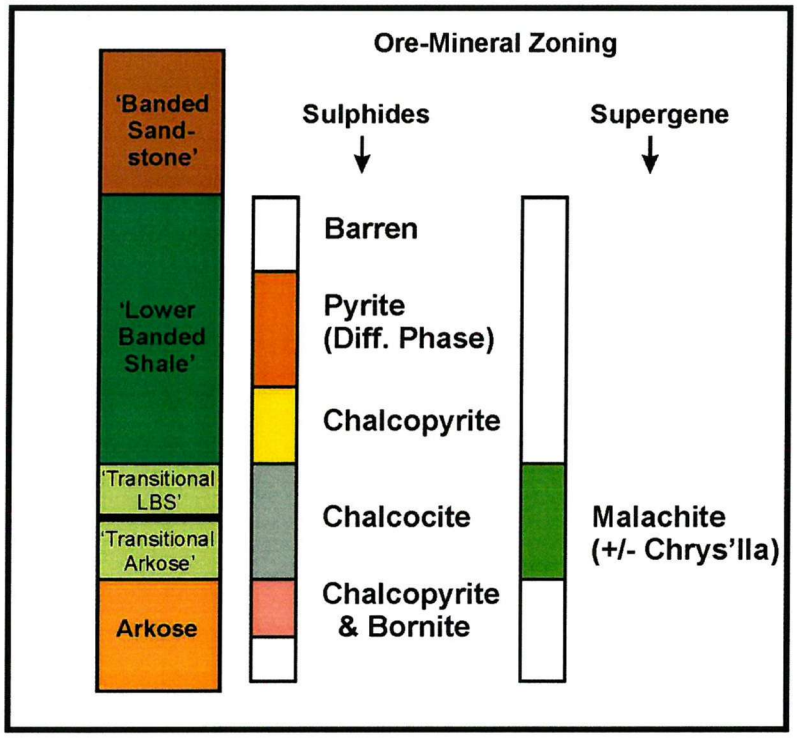

Figure 3.48: Zoning of sulphides for Nchanga Lower Orebody at Nchanga Open Pit and Block A (based on field observations and mine literature) and location of malachite ore within the 'Transition' unit.

There is a clear distinction to be made between sulphides and supergene mineralization at Nchanga. Primary minerals at Nchanga are bornite, chalcopyrite, chalcocite, and pyrite. All copper oxides and carbonates are supergene in origin, including malachite, chrysocolla, and cuprite (chalcocite can be primary as well as secondary). At Nchanga Open Pit, a malachite zone occurs within bleached host rocks (the 'Transition' unit), with sulphides more widespread (Fig. 3.48). This suggests that the malachite (and associated alteration that caused bleaching) is a later supergene feature, replacing and modifying earlier sulphides. Sulphides are more or less restricted to the host rocks described in sections 3.6.3 to 3.6.7, unlike the malachite that can be found in all units, often only as a minor component of late veins or late as fracture- and joint-coatings. Mine assay grades consist of two numbers: total copper (wt %) and acid soluble copper (wt %). Malachite and chrysocolla are acid soluble, whereas sulphides are not, thus the latter value reveals the proportion of supergene minerals within any

sample (Fig. 3.49). As expected from field observations, the Lower Orebody contains a high proportion of 'acid soluble' copper.

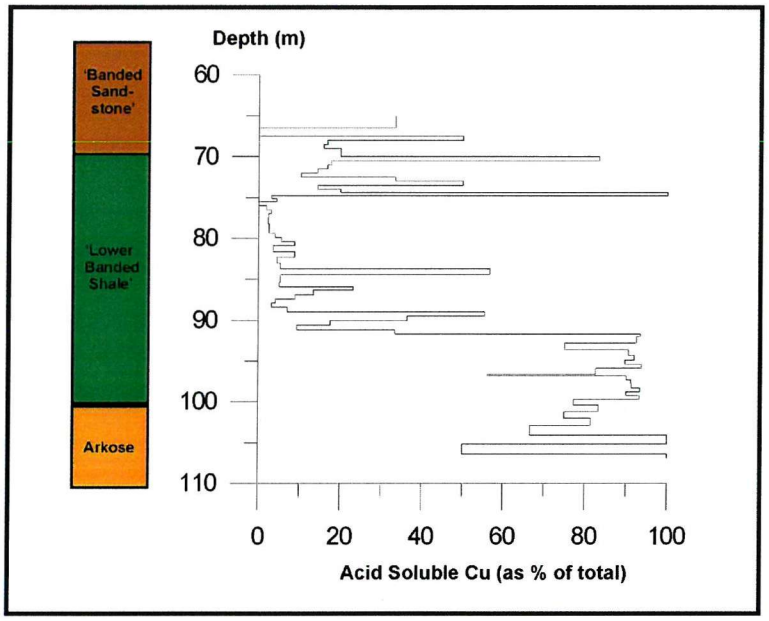

Figure 3.49: Down-hole 'acid-soluble' copper as percentage of total copper for borehole NE 515, Block A. The proportion of 'acid soluble' is much greater (> 80%) around the contact between the arkose and overlying shale (i.e. the supergene zone) as opposed to above where sulphides constitute the bulk of ore minerals (< 30%).

3.6.3 The Intermediate Orebody

Little appears to be known about the Intermediate Orebody, where copper mineralization occurs as malachite or chalcocite hosted within the 'Pink Quartzite' unit on the south limb of the Nchanga Syncline only. Not exposed in the Nchanga Open Pit during this study, it was best developed between section lines 1E and 17E. The bulk of the mineralization, encountered at this stratigraphic level during the present study, consists of malachite (and minor chalcocite) localized along fairly steep fractures within this thin feldspathic arenite. However, observation of borehole NOP 741 revealed small (2mm) blebs of chalcopyrite within the 'Pink Quartzite,' as well as malachite along bed-parallel fractures. Intermediate Orebody grades in NOP 741 reaches 9% total copper.

3.6.4 The Upper Orebody

Upper Orebody mineralization, hosted mostly within the 'Feldspathic Quartzite,' is only present at Chingola B and Nchanga Open Pit where the fault-propagation fold structures have developed internally within the Lower Roan (Figs. 3.41 & 3.43). There is a strong spatial association between these structures and the mineralization, supported by the fact that where there are no thrust-folds at Block A there is no significant Upper Orebody mineralization. In comparison to the Nchanga Open Pit, which is currently the main source of ore from the Nchanga area, the Chingola B Upper Orebody is small. The former is situated on the south limb of the Nchanga Syncline, has an estimated strike length (E-W) of more than 3.5km,

extends to a depth of over 450m, and has an average thickness of approximately 30m. Like Chingola B, it also has the same orientation as the feldspathic arenite, within which it is hosted, dipping gently to the north, but is folded around small detachment-related thrust-fold structures at greater depths (Fig. 3.43).

The Upper Orebody of the Nchanga Open Pit is not only a major source of copper, but also contains local high concentrations of cobalt. Although they are both part of the Upper Orebody, on a large scale there appears to be an inverse relationship between the two (Fig. 3.50). Where cobalt is high-grade (the 'cobalt fold'), copper is lower-grade and vice versa.

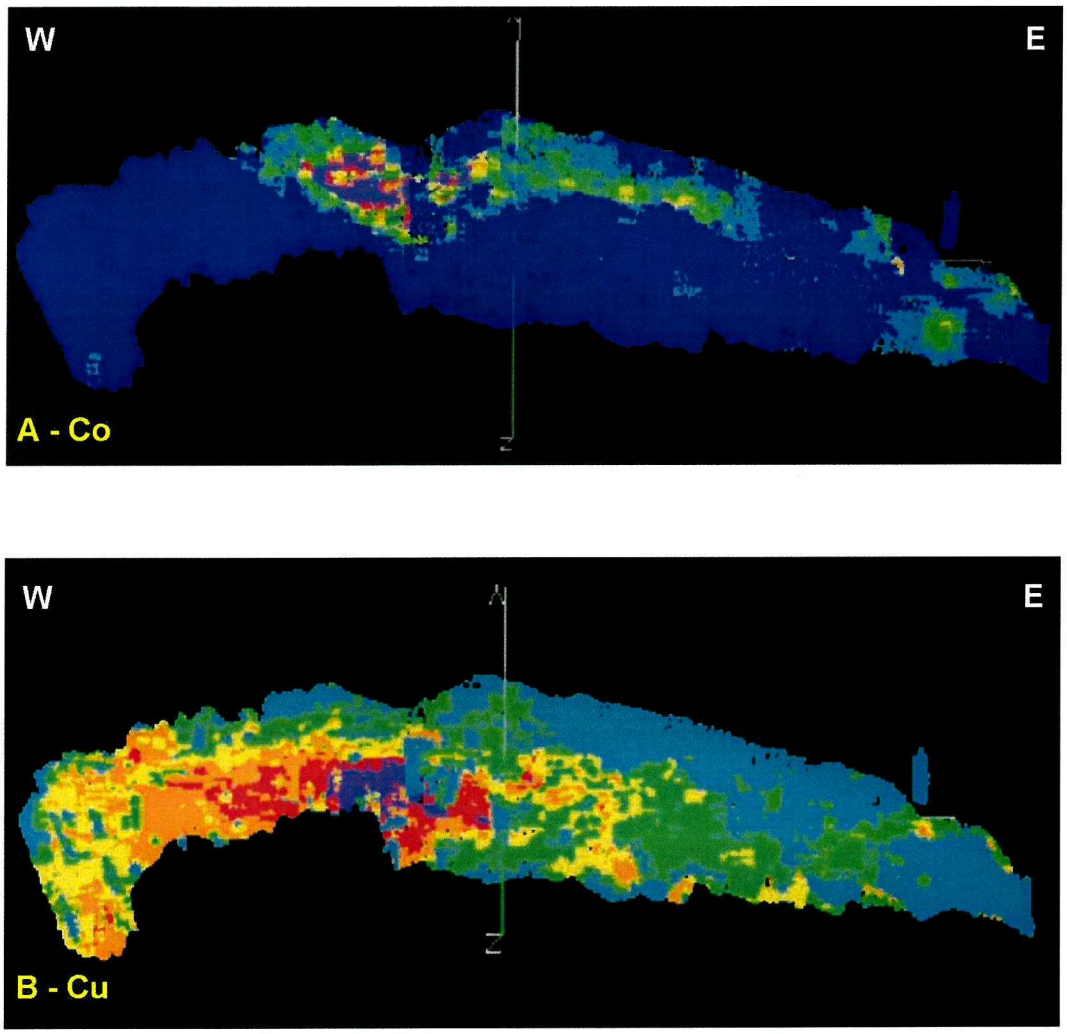

Figure 3.50: Plan view datamine image from Nchanga Open Pit Upper Orebody showing location of high-grade (A) cobalt and (B) copper, and the inverse relationship between the two (Nchanga Mine Geology Department).

However, as boreholes through the cobalt fold area show (Fig. 3.51, NOP 741), there are local higher copper grades within high-grade cobalt ore, just not as extensively developed as high-grade copper orebodies (Fig. 3.45). Borehole NOP 741 also revealed some of the highest

grades of cobalt (up to 1.6% total Co), particularly associated with a number of veins at the top of the 'Feldspathic Quartzite.' Cobalt mineralization is more strongly related to structure than copper, as demonstrated by its close relationship with the thrust-propagation folds.

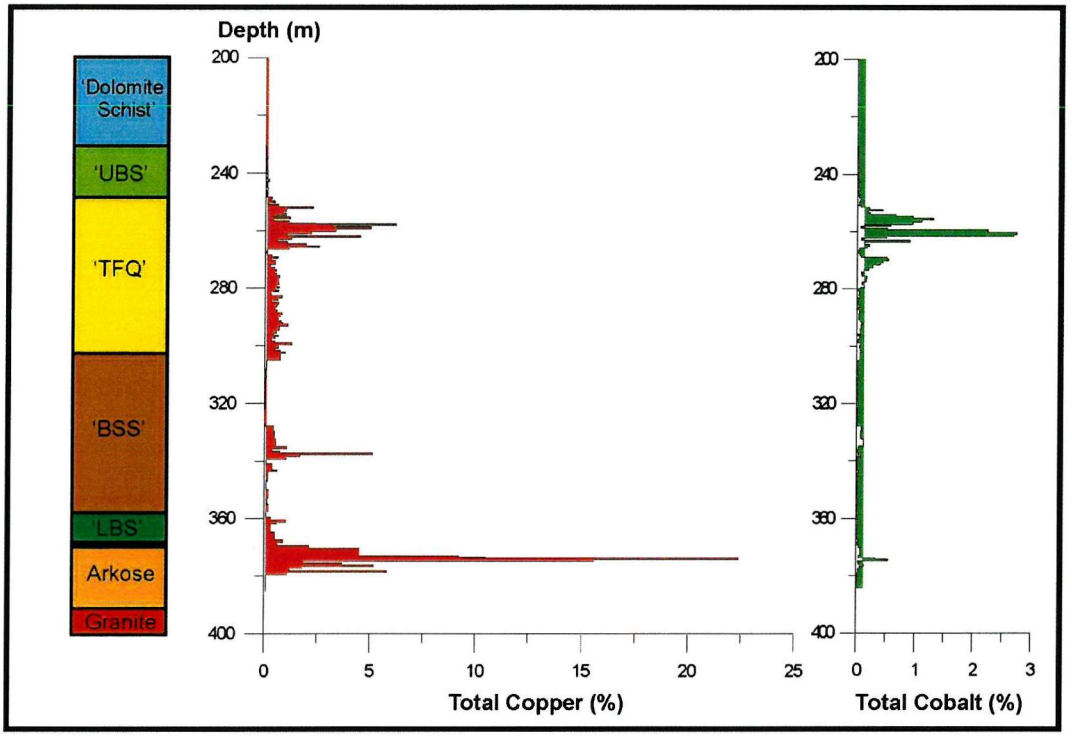

Figure 3.51: Down-hole grades of copper and cobalt mineralization for borehole NOP 741, Nchanga Open Pit (assay grades from mine data).

Unlike the main section line across the Nchanga area (Figs. 3.13 and 3.19), there is only one main thrust-fold developed on the eastern part of the south limb of the Nchanga Syncline. This part of the upper feldspathic arenite folded around this thrust-fold structure is the host for the majority of the cobalt ore. Up-dip of this fold, copper mineralization is extensive; however, down-dip the mineralization fringes out (based on existing data). Related to the maximum development of major thrust-fold zones striking WNW-ESE (described in section 3.5.2), there are three main cobalt orebodies (Fig. 3.52A), which are flanked to the south by two or three major lobes of copper mineralization (Fig. 3.52B). Low-grade gaps between the cobalt orebodies are thought to represent the relay zones (of minor structures) between major thrust-folds. This appears to be the situation within much of the open pit where cobalt mineralization within the fold zone is distinct from extensive copper mineralization southwards and up-dip of the fold zone (schematically represented in Fig. 3.53). High-grade cobalt is indicated by an abundance of carrollite, and although almost always hosted within the 'Feldspathic Quartzite,' in one case (borehole NOP 760) the carrollite occurs within the 'Upper Banded Shale' unit associated with a fault zone (grades of up to 1.1% total cobalt).

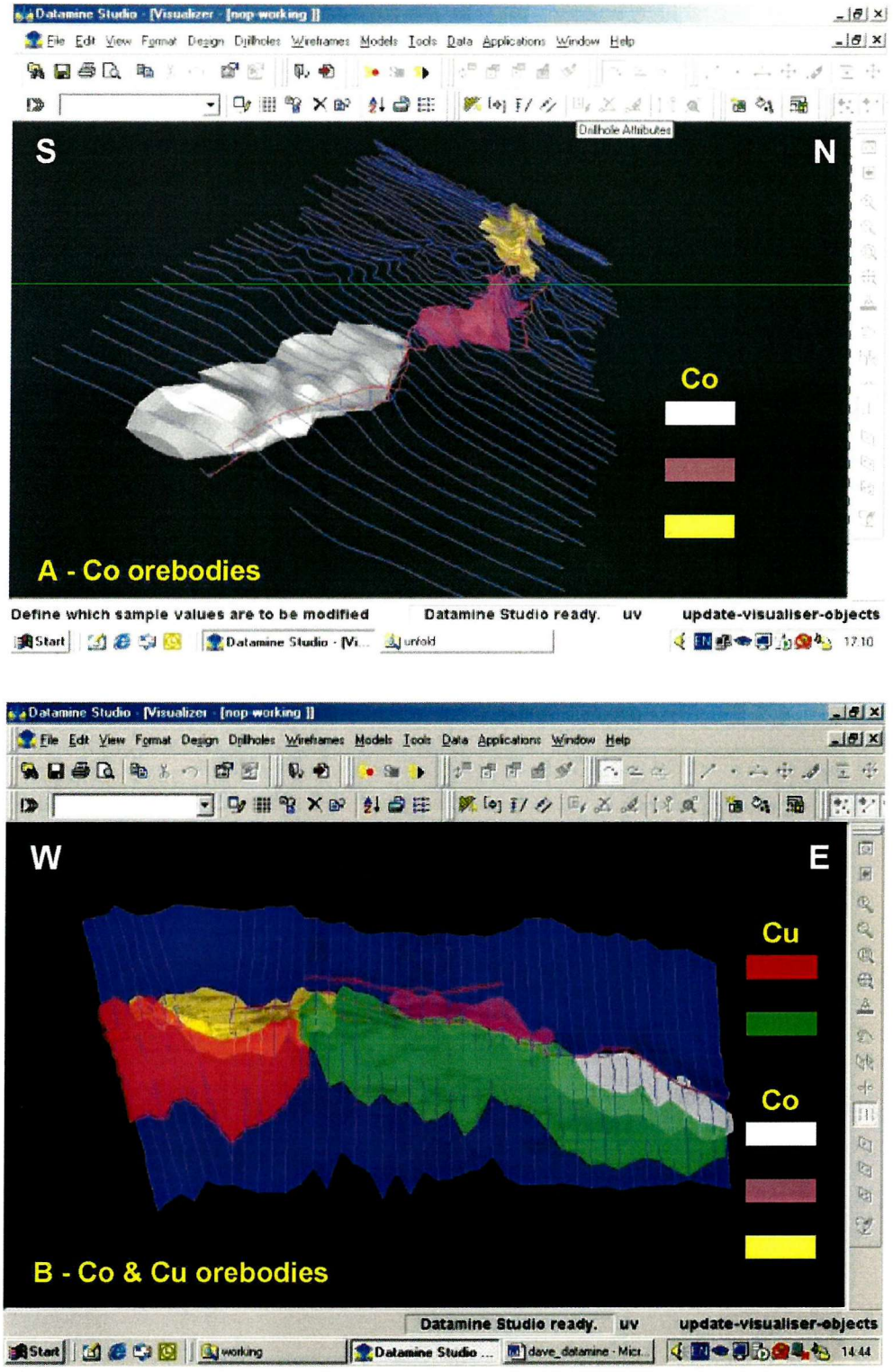

Figure 3.52: Datamine image from Nchanga Open Pit showing structural contours of the top of the 'Feldspathic Quartzite' unit and (A) the location of major cobalt orebodies and (B) cobalt and copper orebodies together (looking W; Nchanga Mine Geology Department).

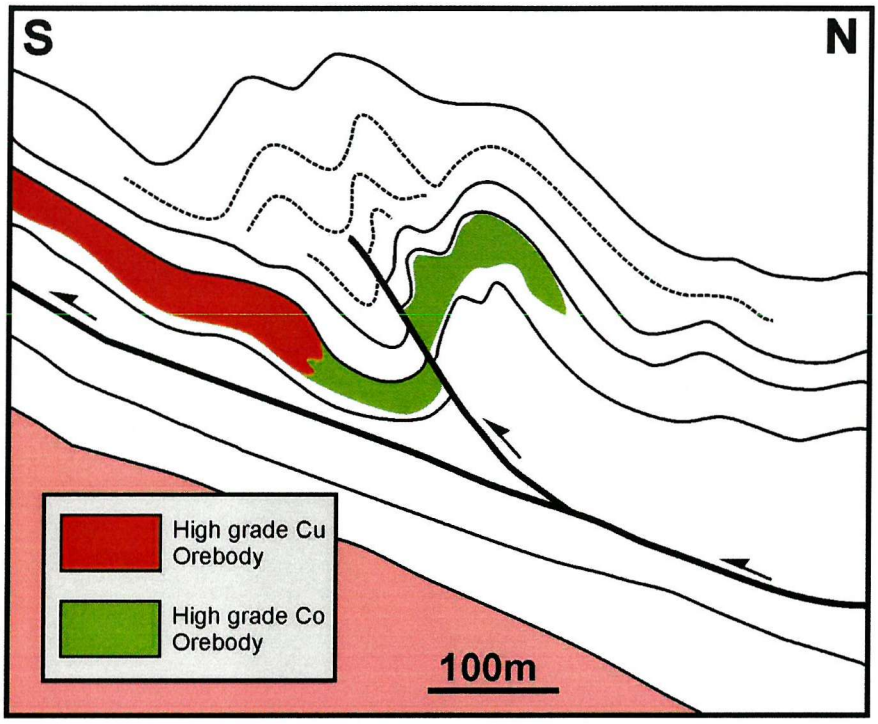

Figure 3.53: Schematic representation of the Nchanga Upper Orebody and high-grade copper and cobalt mineralization of Section 27E (looking W; refer to Fig. 3.23; modified from Nchanga Mine Geology Department sections).

Generally, the base of the arenite is poorly mineralized, with the abundance of copper minerals increasing towards the top of the unit. In fact, the highest grades occur at the top of the arenite unit (and sometimes at the base of the overlying shale; Fig. 3.45), a feature also noted by Diederix (1977), although mineralization mainly consists of oxides (malachite) when in the shale. In some cases (e.g. borehole NOP 741) mineralization stops abruptly at the contact between the arenite and shale. McKinnon & Smit (1961) described sulphide-rich veins that terminate at ore boundaries, suggesting a common origin. Detailed examination of boreholes reveals copper anomalies associated with fault zones outside of the normal host rocks for Upper Orebody mineralization. These are often represented by 'rubble zones' indicating extensive disruption of the wallrock and abundance of phlogopite and are most common in the 'Banded Sandstone,' 'Upper Banded Shale,' and 'Dolomitic Schist' units.

The major ore minerals are bornite, chalcopyrite, chalcocite (copper) and carrollite (cobalt). At Chingola B, mineralization consists of bornite and chalcocite only. Malachite and minor chrysocolla (± cuprite) are sometimes present, with cobalti-calcite encountered on one occasion within sheared 'Banded Sandstone' (borehole NOP 716). The ore minerals themselves are often fracture-related and vein-hosted, and disseminated, in a dolomite-rich feldspathic arenite, often taking on a leached appearance where mineralized. It is worth noting that where copper and cobalt mineralization is low grade (e.g. borehole NOP 770) the host-

rocks often contain pyrite. The Upper Orebody of the Nchanga Syncline shows no vertical zoning. However, there is some sense of a lateral sequence of ore-minerals changing progressively from bornite and chalcocite in the south (chalcocite replaces bornite) to chalcopyrite and then to chalcopyrite and carrollite and finally carrollite in the north. The primary or secondary origin of the chalcocite and relative timing of cobalt with respect to copper are issues that need to be resolved before accepting this as primary zoning and are discussed in Chapter 6. There appears to be no zoning of the Upper Orebody ore-minerals at Chingola B.

3.6.5 Refractory Ore

Within the Nchanga Open Pit, the main locations for refractory ore development (copper only) are within the 'Banded Sandstone' and 'Dolomitic Schist' units below and above the Upper Orebody respectively. The copper in the 'refractory' or 'vermiculite' ore is held in the mica (Diederix, 1977). Although the copper of the ore is not visible when studying hand specimens or thin sections of the host rocks, it is mainly contained within phlogopite (which is visible), tied largely to hydroxyl groups within the interstratified micas (Bassett, 1958). Grades from the refractory orebodies can reach 2% Cu (average 1%), with phlogopites containing 0-8 wt % Cu (Diederix, 1977). Molak (1995) described phyllosilicate-rich shear-zones within the Lower Roan that are copper-rich. Other authors have termed these as 'copper-mica shear-zones' (Nisbett, 1996). In the field, phlogopite is clearly associated with deformation of the host units, usually expressed by the development of layer-parallel and cross-cutting shear-zones within the 'Banded Sandstone' and dolomite schists. Molak (1995) suggested a common origin for both the copper and abundant micas, as both are concentrated into shear-zones. Interestingly, the phlogopite within the granite fault zone ('Lamprophyre dyke') is also cupriferous. Refractory ore has additionally been discovered within the 'Banded Sandstone' at Chingola C, E and F.

3.6.6 Basement mineralization

The main sources of copper ore are described above. However, mineralization also occurs in Basement rocks. In the Nchanga Open Pit, visible sulphides (chalcopyrite) occur within the phlogopite-rich fault gouge associated with an early extensional fault. This is in addition to any copper that may be contained within the micas themselves as refractory ore. No mineralization is found within the adjacent granite wallrock, apart from minor secondary malachite associated with fracture and joint surfaces. The Nchanga Red Granite apparently contains mineralized quartz veins and coarse blebs of chalcopyrite 10km SE of Nchanga Open Pit and, at Nchanga, malachite, chalcopyrite and bornite have been found within quartz-

carbonate veins as well as joint surfaces (Pienaar, 1961). Pienaar (1961) also described bornite, chalcopyrite, chalcocite, and malachite (± cuprite and native copper) from the west of Nchanga Mine, with an average grade of 0.77% Cu, extending down to 9m below the granite-arkose unconformity. At Chingola D, E, and F, Diederix (1977) described copper minerals (identical to those in the arkose) extending downwards into the Lufubu Schists and, at Chingola C, the thrusts that deform the Lower Roan units and root into the basement are also mineralized.

3.6.7 Other metals

The association of other elements with the copper and cobalt is further discussed in Chapter 4. Although other metals are associated with the copper and cobalt of the Lower and Upper Orebodies at Nchanga, they only occur at ppm levels, with the exception of iron.

Iron (Fe)

Iron concentrations depend on the lithology and composition of the measured sample. However, increases occur where there are abundant sulphides and where fault zones are thought to be located. The structural detachment zones at the base and top of the 'Lower Banded Shale' unit are principal zones for fluid flow (until the present day) and are characterized by abundant iron oxides. The Lower Orebody ore, within brecciated arkose, is normally hematite-rich, as well as containing chalcocite and malachite. The most abundant Upper Orebody sulphides are chalcopyrite and bornite, both copper-iron sulphides, and so within these sulphide-rich ore zones iron concentrations increase.

Lead (Pb) and Zinc (Zn)

Although high concentrations of these base metals are known from some sediment-hosted copper deposits, at Nchanga lead and zinc are found in minor amounts, attaining 350 and 200 ppm concentrations respectively within high-grade copper zones only.

Gold (Au)

Gold contents within the Nchanga sediments rarely exceed 20 ppb. However, gold concentrations reach as high as 894ppb and average 445 ppb over 6.5m within some extensively sheared high-grade (with respect to copper) arkose rocks at Chingola C (Borehole NE 529). At Nchanga Open Pit gold contents increase within deformed arkose and the Lower Orebody, from background levels of 2-7 ppb to as high as 140 ppb.

3.7 Summary

Some key points presented in this chapter are summarized below:

- Nchanga mineralization is hosted by the Lower Roan sequence, consisting of basal arkoses overlain by a mixed unit of shales and arenites and subsequently by dolomites, which were deposited on a basement consisting of 2 Ga or older Lufubu Schists that have been intruded by the 877 ± 11 Ma (Armstrong *et al.*, 1999) Nchanga Red Granite.

- The Lower Roan host rocks to copper-cobalt ores have been subjected to greenschist facies metamorphism, represented by varying abundances of phlogopite and sericite and extensive recrystallization of the host quartz component.

- The sedimentary sequence was deposited onto a flat granite horst block (representing pre-Katangan D1 extension) and was subsequently deformed (post-Katangan D2 compression) during the Lufilian Orogeny to form the present fold geometry. During D2 compression, early extensional faults were inverted (in particular the granite-bounding structures) where the granite block acted as a stable buttress. D2 compression is also represented by internal (to Lower Roan) thrust-propagation folds and layer-parallel structural detachments, the geometry and location of which appear to be strongly controlled by the rheological properties of the host succession. Vergence on structures is dominantly to the northeast, but changes to southwest with the influence of the southward-verging Nchanga Syncline.

- There is evidence for a strong structural control on mineralization, where Lower Orebody mineralization is spatially associated with a tectonized contact between the arkose unit and overlying shale, and where Upper Orebody mineralization is only observed where the internal thrust-propagation fold structures have developed. A spatial relationship between high-angle structures within the Basement and high-grade Lower Orebody mineralization is also evident.

- Anomalous concentrations of copper are found throughout the Lower Roan sequence, but economic concentrations exclusively occur within the top parts of arenite/arkose units that are overlain by shales, indicating a degree of stratigraphic control. Cobalt mineralization, however, is found at the same stratigraphic level, but strongly associated with one thrust-propagation fold developed on the south limb of the Nchanga Syncline. Copper mineralization is also associated with several Basement faults and with shear zone (and phlogopite) development within the Lower Roan sequence.

CHAPTER 4:

ORE MINERALOGY & WALLROCK ALTERATION

CHAPTER 4: ORE MINERALOGY AND WALLROCK ALTERATION

4.1 Introduction

The study of ore minerals and their textural relationship to micro-structure, micro-lithological features, metamorphism and hydrothermal alteration of the host rocks is an important step in understanding the origin and post-depositional history of an ore deposit (Craig & Vaughan, 1981). Likewise, the study of hydrothermal alteration is one stage in understanding the properties and origin of hydrothermal fluids that were present within the ore-forming system (Taylor, 1994). In this chapter, hand-specimen and micro-scale observations are presented in order to identify the relative timing of key events in the geological history of the Nchanga ore deposits. Whole rock and mineral geochemistry is used to support petrographic observations and to further understand the alteration and fluid history.

4.2 Ore mineralogy

The sulphide ores of Nchanga are relatively simple, although somewhat complicated by the abundant supergene mineralization and related modification that has subsequently taken place, in particular of the Lower Orebody. The following two sections describe the ore mineralogy from hand-specimen to polished-thin section scale of the various orebodies of Nchanga, as introduced in section 3.5, detailing the different ore minerals and the evidence for the relative timing of the different phases of mineralization. Section 4.2.3 deals with the relationships between micro-lithological and micro-structural features and ore minerals. The wallrock alteration and its association with sulphides is dealt with in section 4.3.

4.2.1 The Lower Orebody – mineralization at the arkose-shale contact

Mineralization at the arkose-shale contact is supergene mineral-rich. For this reason very few primary sulphide minerals and associated textures are observed in hand-specimen or thin-section. Minerals found within this zone are pyrite, bornite, chalcopyrite, chalcocite, malachite and chrysocolla. Relative timing of different sulphides and supergene minerals is identified by replacement textures. However, chalcocite may occur both as a primary and a secondary mineral at Nchanga, and it is not always easy to distinguish between the two. At Nchanga, an early (diagenetic?) pyrite phase is replaced by chalcopyrite, bornite and

chalcocite. In turn, bornite and chalcopyrite are replaced by chalcocite in many cases. Finally, all pre-existing sulphides have been overprinted and replaced by malachite and copper oxides. Whether any enrichment took place during this stage is discussed later in the chapter. The ore mineralogy is described below from earliest to latest phases.

Early pyrite

Pyrite occurs mainly in the 'Lower Banded Shale' but can also be abundant within the 'Transitional arkose' contact zone (noted at the Nchanga Open Pit, Block A, and Chingola C deposits). Within the shale, pyrite occurs as disseminated blebs or streaks that have been orientated along bedding or sometimes cleavage and within quartz veins that are both parallel to and transverse to bedding. Generally the finer pyrite (10-1000μm) takes on an irregular shape when disseminated in the host-rock, whereas within veins coarser, irregular to subhedral pyrite grains (up to 5mm) are common (Fig. 4.1A). Other coarse blebs of pyrite have quartz pressure shadows around them. Within borehole NOP 827 (Nchanga Open Pit) pyrite replaces diagenetic nodular anhydrite within the 'Lower Banded Shale.' Within many samples the majority of pyrite is hosted within these minor quartz veins (80%), with many of the vein-hosted pyrite grains subsequently fractured and broken apart. In addition, slightly coarser, more quartz-rich layers within the shale also contain more pyrite that the surrounding fine-grained shale lithology.

Generally, there is an inverse relationship between the abundances of pyrite and copper sulphides. However, when they do overlap, copper sulphides replace the pyrite (Fig. 4.1B), indicated by examination of high-grade copper ore within the shale at Block A (borehole NE 515). This consists of relatively small (10-100μm) pyrite grains rimmed or totally enclosed by chalcopyrite. Within the chalcopyrite zone (see zonation of Lower Orebody in Fig. 3.51) pyrite, orientated parallel to bedding and within bed-parallel veins, is clearly cross-cut and replaced by chalcopyrite (and minor bornite) which is orientated to a steeper fabric (than bedding) fabric. This is the main line of evidence for copper sulphides being a later (and distinct) phase of mineralization than the pyrite.

Pyrite is not restricted to the 'Lower Banded Shale' (as suggested by McKinnon & Smit, 1961) but can also be found towards the top of the arkose within the 'Transition' unit. Here it consists of sometimes abundant (up to 60% of an individual hand specimen) often euhedral, 0.1-10mm, pyrite grains that have been deformed in a brittle manner (Fig. 4.1C), and were subsequently replaced by chalcocite along fractures (Fig. 4.1D). Due to the extensive deformation and alteration of the arkose towards its upper contact, the relationship of pyrite to bedding or foliation is unclear. Some authors have suggested that this 'Transition' was once

an evaporite layer (McKinnon & Smit, 1961). If this is true and taking into account the evidence here, then it was probably also pyrite-rich, prior to copper mineralization and oxidation, following pyrite replacement of the evaporites.

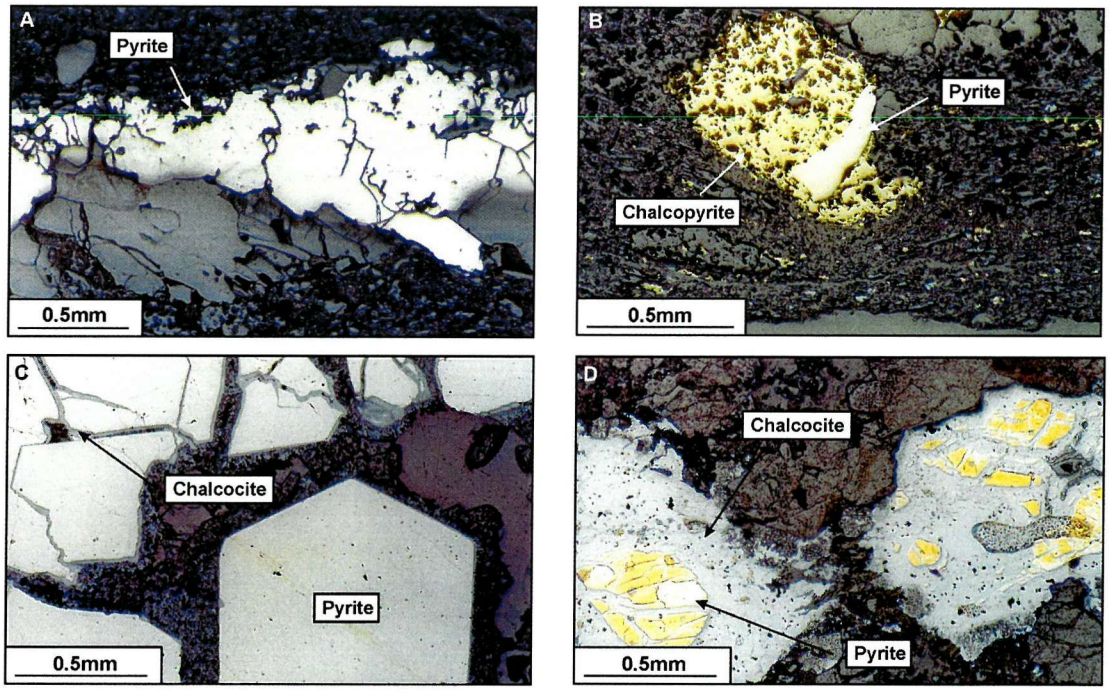

Figure 4.1: Reflected light photographs of pyrite and its relationship to Lower Orebody copper sulphides (sample numbers in brackets): (A) coarse pyrite in a quartz vein, that has subsequently been deformed, within the 'Lower Banded Shale' unit, Block A (NOP90); (B) pyrite enclosed and replaced by chalcopyrite within the 'Lower Banded Shale' unit, Block A (NE515-2). Fine-grained chalcopyrite within the host shale is strongly orientated to the developed fabric; (C) euhedral nature of pyrite grains, that have subsequently fractured and been broken apart, within the 'Transitional Arkose' from borehole NOP346, Nchanga Open Pit (NOP346-1); and (D) near skeletal replacement of once euhedral grains of pyrite by coarse, irregular chalcocite within the 'Transition' unit at Chingola B (CB2).

Main phase copper – bornite and chalcopyrite

Both chalcopyrite and bornite are rare within the Lower Orebody. They were described by McKinnon & Smit (1961) from within the arkose, as disseminations and blebs associated with bedding and also quartz veins. As noted above, copper sulphides replace the earlier phase of pyrite mineralization in the 'Lower Banded Shale' at Block A (the only location where copper sulphides other than chalcocite have been observed in the shale). This mainly consists of pyrite totally enclosed by chalcopyrite (Fig. 4.1B). The relative timing is supported by observation of bedding-related pyrite that is cross-cut by fabric-orientated chalcopyrite and quartz-vein hosted chalcopyrite. Minor bornite can also be present as small (< 50μm) blebs within the fine-grained shale wallrock. The chalcopyrite has clearly been affected by the deformation that has taken place, with chalcopyrite blebs orientated to a developed structural fabric (thought to be formed during the development of the fault-propagation folds described

in section 3.4). However, rather than deformed by the fabric with evidence of a pre-existing orientation, the chalcopyrite appears to follow it. Both chalcopyrite and bornite have only rarely been observed in the arkose during this study. However, at Chingola B, coarse chalcopyrite (> 2cm) was found within the arkose and a fault-related quartz vein at the contact with the overlying shale, extensively replaced along fractures by chalcocite (see below).

Chalcocite

Chalcocite is, by far, the most common copper sulphide within the Nchanga Lower Orebody, although there is some argument as to whether it is primary or secondary. It can occur within both the arkose and shale (see chalcocite zone, Fig. 3.51). The highest grades of copper at Nchanga (up to 20% total copper) and the most abundant chalcocite occur within the top several metres of arkose where it is deformed and altered. It consists of coarse chalcocite (and malachite, see below) infilling a highly altered arkose breccia (Figs. 4.2A & B) or hosted within quartz veins (Fig. 4.2C). Within this zone early well-formed pyrite grains are broken up and fracture-replaced by chalcocite (Fig. 4.ID). At Chingola B chalcocite is common within the arkose, occurring as fracture-related, 0.1-0.8mm, anhedral grains (Fig. 4.2D) that are coarser than the host-rock detrital components. In fact, there appears to be a spatial association between sulphides and grain-size reduction and recrystallization of the quartz component of the host arkose. Within a fault-zone above the main orebody coarse vein chalcopyrite and bornite (> 5cm) is replaced by chalcocite around the edges of grains and along fractures (Figs. 4.2E & F). Within the shale at Block A, below the chalcopyrite zone (see above), chalcocite replaces the chalcopyrite that previously replaced early pyrite (Fig. 4.2G). This is represented by chalcocite (which also is orientated in the direction of the developed foliation) enclosing chalcopyrite, and in some cases totally replacing it. Chalcocite becomes more abundant closer to the contact between the arkose and shale, and in places there is no indication as to whether the chalcocite is a total replacement of earlier sulphides or primary. Certainly at Chingola B, there is no evidence to suggest that the chalcocite is anything but primary. Chalcocite is often closely associated with hematite. At Chingola C, hematite (not chalcocite) occurs as fracture-replacement of pyrite below the chalcocite zone.

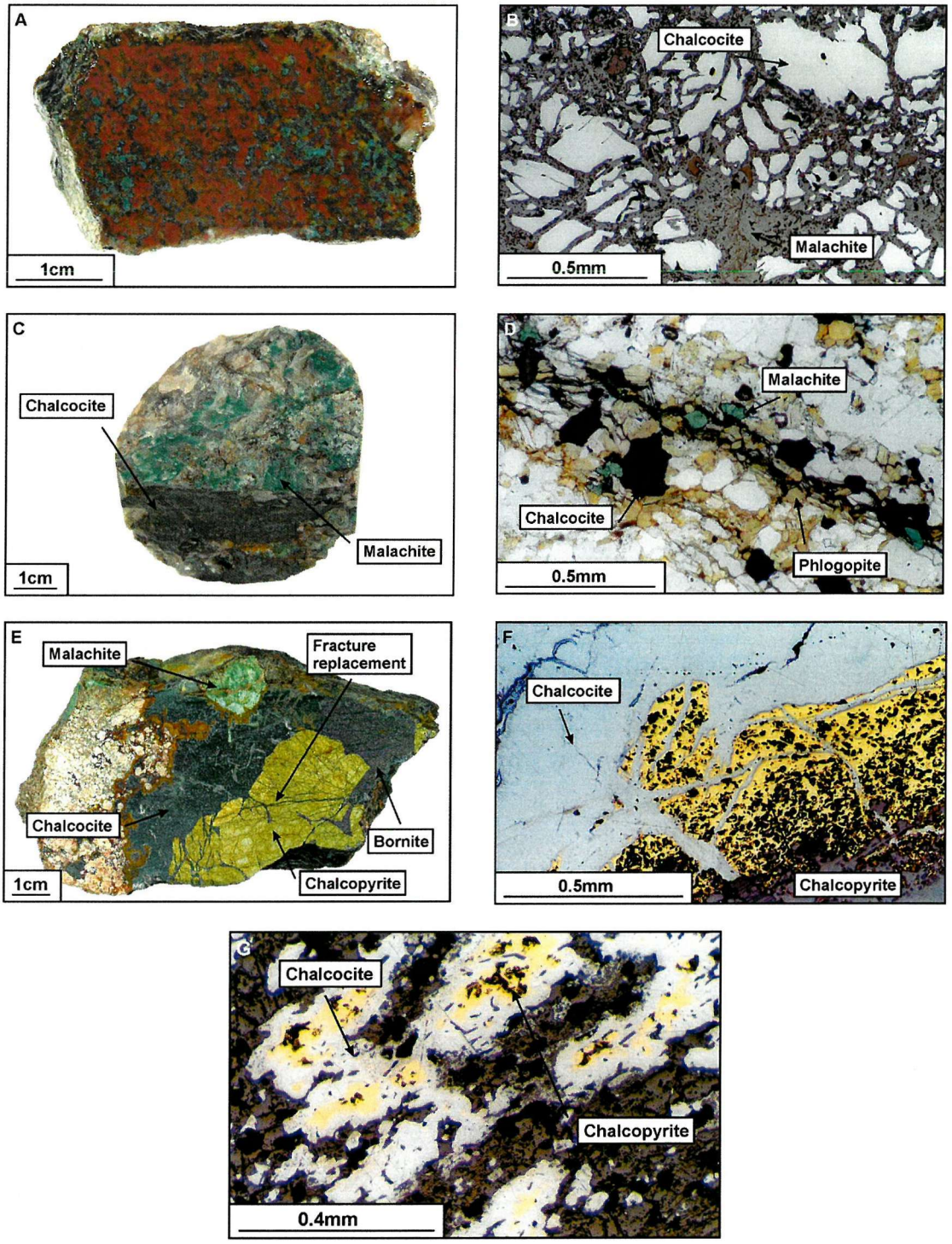

Figure 4.2: Photographs of main copper sulphide mineralogy within the Lower Orebody: (A) chalcocite (+ malachite and hematite) hosted within brecciated arkose material, Nchanga Open Pit (NE515-7); (B) arkose-hosted chalcocite (extensively replaced by malachite and hematite along fractures, see below) in reflected light (NE297-3); (C) chalcocite (+ malachite) hosted within major quartz vein at the contact between arkose and overlying shale from Luano (L128-12); (D) fracture-related chalcocite (+ malachite and phlogopite) within arkose at Chingola B, in plane polarized light (CB7); (E) hand-specimen of coarse vein-hosted chalcopyrite and bornite, replaced by chalcocite, within a Chingola B fault zone (CB9); (F) replacement of chalcopyrite and bornite (of photograph E) by chalcocite in reflected light (CB9); (G) chalcopyrite enclosed and replaced by chalcocite within 'Lower Banded Shale' in reflected light, Block A (NE515-4).

Carbonate and oxide mineralization

The Nchanga Lower Orebody sulphides (including all occurrences of chalcocite, described above) are extensively replaced by supergene minerals and oxides (Fig. 4.3A), in particular malachite, but also minor chrysocolla and cuprite. This is most extensive within the 'Transition' contact zone between arkose and shale (where there are no reported sulphides at Nchanga according to McKinnon & Smit, 1961). Within this zone, malachite replaces the coarse chalcocite mineralization (Figs. 4.3B & C), and also phlogopite at Chingola C and B, Block A, and Nchanga Open Pit (see section 4.3), suggesting that it is the latest phase of copper (or modification of pre-existing ore). Malachite sometimes forms coarse (> 1cm) radiating crystal aggregates (Fig. 4.3D), but can also form irregular, apparently structureless masses or infills fractures (Fig. 4.3E). Malachite of the Nchanga Lower Orebody is strongly associated with iron oxides, mostly hematite (Fig. 4.3F). In many cases, hematite, like malachite, replaces coarse chalcocite mineralization within the 'Transition' zone (Fig. 4.3G), and appears to be part of the same phase of modification of sulphides as the malachite. In other cases, hematite appears to be an earlier phase, where it is replaced by malachite along fractures and around the edges of oxide grains. The main copper oxide mineral is chrysocolla (Fig. 4.3H), which is related to the malachite and is considered here to be part of the same supergene event. It occurs much like the malachite, and has also been found replacing chalcocite and phlogopite (Fig. 4.3I). Malachite (and chrysocolla) also occurs in the 'Lower Banded Shale' in close proximity to the underlying fault contact, either as bed-parallel or bedding-transverse streaks and fractures.

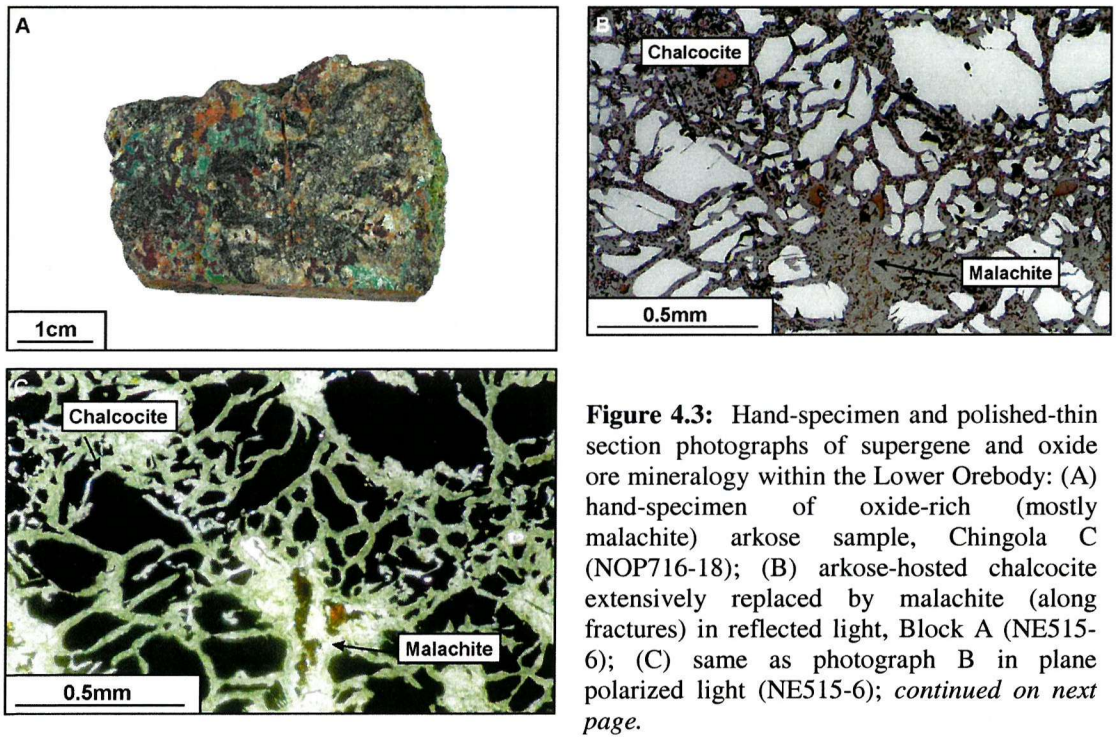

Figure 4.3: Hand-specimen and polished-thin section photographs of supergene and oxide ore mineralogy within the Lower Orebody: (A) hand-specimen of oxide-rich (mostly malachite) arkose sample, Chingola C (NOP716-18); (B) arkose-hosted chalcocite extensively replaced by malachite (along fractures) in reflected light, Block A (NE515-6); (C) same as photograph B in plane polarized light (NE515-6); *continued on next page.*

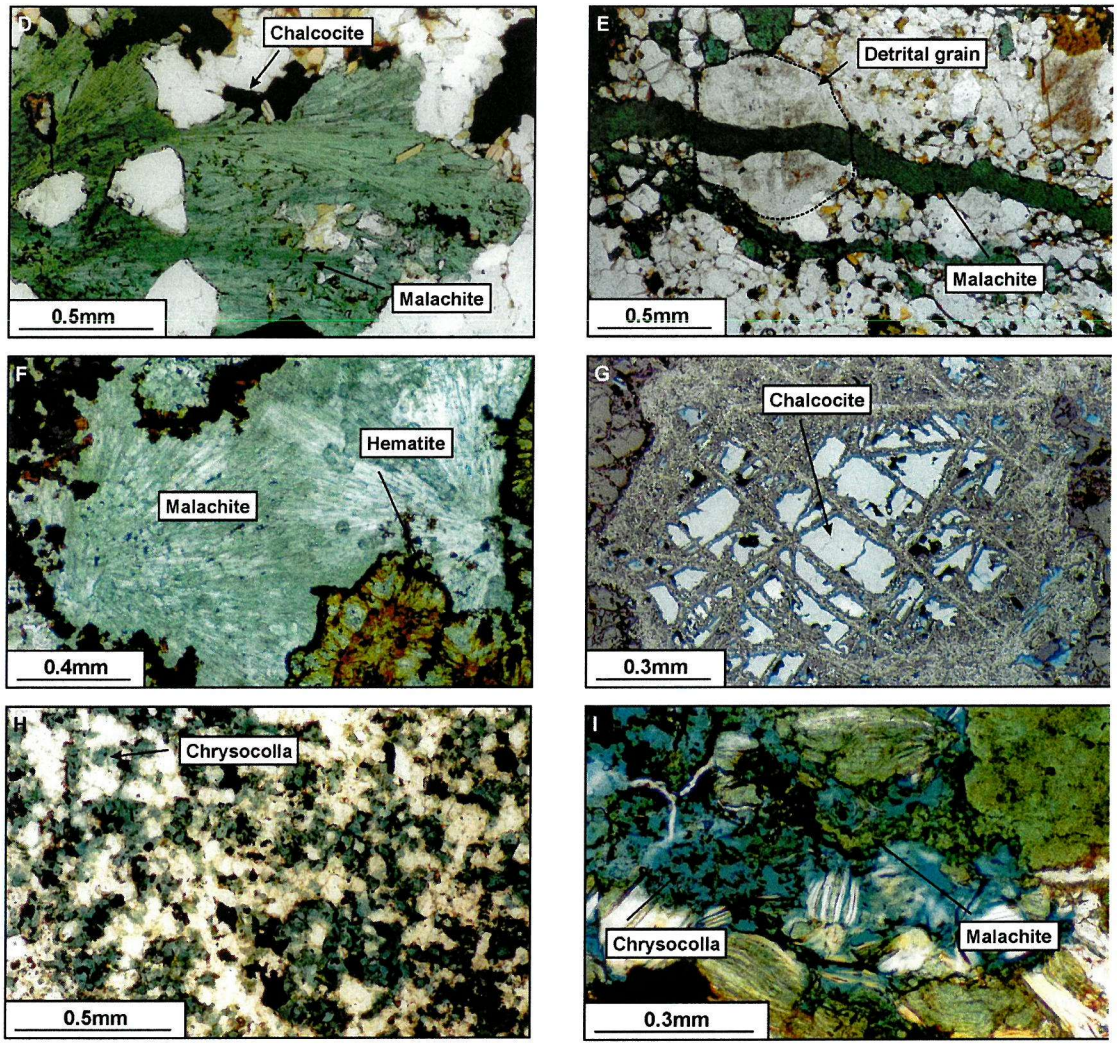

Figure 4.3: *continued* (D) malachite in 'Transitional Arkose' forming an aggregate of radiating malachite crystals in plane polarized light, Nchanga Open Pit (CB7); (E) fracture-related malachite through detrital quartz grain within the arkose in plane polarized light, Chingola B (CB6); (F) photograph illustrating the close relationship of malachite and iron oxide (the latter replaced by the former in some cases; NOP716-4); (G) skeletal replacement of chalcocite by iron oxides, including hematite, in reflected light, Nchanga Open Pit (NOP716-4); (H) abundant chrysocolla (blue-green) within arkose, Chingola B (NOP741-1); (I) close relationship of malachite and chrysocolla both replacing phlogopite and appearing to be of the same supergene phase in plane polarized light, Nchanga Open Pit (NOP716-4).

4.2.2 The Upper Orebody

The Upper Orebody is hosted mainly within the 'Feldspathic Quartzite' and base of overlying 'Upper Banded Shale.' Ore minerals consist of pyrite, chalcopyrite, bornite, carrollite, chalcocite, and minor malachite. As with the Lower Orebody, an early phase of pyrite mineralization is replaced by chalcopyrite, bornite and carrollite, which have subsequently been replaced by chalcocite. Minor overprinting by malachite has taken place. The temporal relationship between copper (bornite and chalcopyrite) and cobalt (carrollite) has been investigated within this zone.

Early pyrite

Coarse (> 2mm), anhedral to subhedral grains of pyrite are replaced by copper and cobalt sulphides within the feldspathic arenite host unit. This is illustrated by copper sulphides totally enclosing and embaying into pyrite or by replacement of pyrite along fractures (Fig. 4.4A & B). Indications are that the pyrite was much coarser that the host detrital components. Pyrite is often more common towards the base of the arenite unit (e.g. borehole NOP 785) suggesting an inverse relationship between copper sulphides and pyrite, as with the Lower Orebody. During this study, very little pyrite was discovered in the overlying 'Upper Banded Shale' unit.

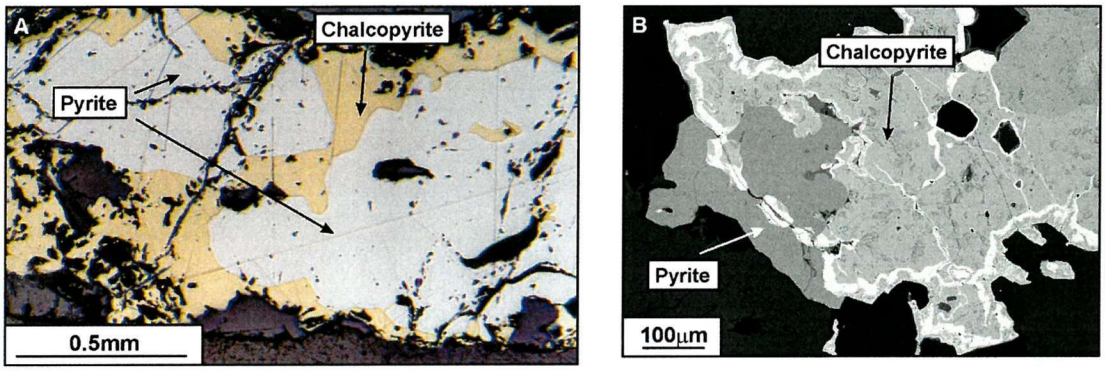

Figure 4.4: Photographs of pyrite within the Upper Orebody of Nchanga Open Pit: coarse pyrite replaced by chalcopyrite along fractures in (A) reflected light (NOP741-20), and (B) a backscattered electron scanning electron microscopy (SEM) image (NOP704-5).

Main phase copper – bornite and chalcopyrite

Bornite is the most common copper sulphide within the Upper Orebody at Nchanga, followed by chalcopyrite. Although not commonly occurring together, minor chalcopyrite-bornite exsolution, occasionally showing basket weave texture, is sometimes observed where they do (Fig. 4.5A & B). Bornite forms irregular, interstitial blebs (0.01-5mm; Fig. 4.5C) within the arenite, which often show chalcocite rims, or occurs within small fractures and bed-parallel quartz-dolomite veins. Chalcopyrite also occurs as anhedral blebs (0.01-5mm), which may or may not be replaced by chalcocite. Chalcopyrite is commonly associated with carrollite-rich zones and is common within quartz-dolomite veins. In general, there are no replacement textures observed between bornite and chalcopyrite: i.e. they appear to have co-precipitated. However, locally, one can appear to replace the other (Fig. 4.5D), but this is rare. Another interesting feature of the Nchanga Upper Orebody is the identical sulphide mineralogy of these quartz-dolomite-sulphide veins and the adjacent wallrock. At Mufulira, for example, bed-parallel bornite mineralization is crosscut by vein-hosted chalcopyrite. However, at Nchanga, if wallrock sulphide is bornite, then so is the vein sulphide.

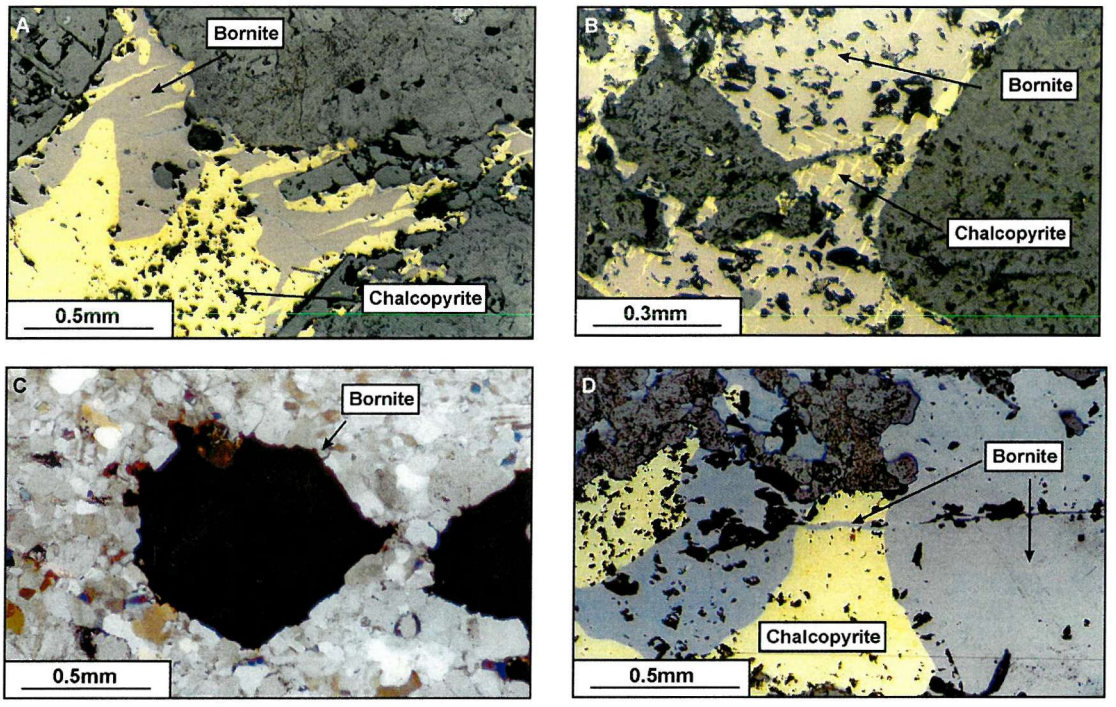

Figure 4.5: Photographs of Upper Orebody main copper sulphides bornite and chalcopyrite: (A) Extensive bornite exsolution in chalcopyrite (or replacement of chalcopyrite by bornite) in reflected light, Nchanga Open Pit (NOP113); (B) minor chalcopyrite exsolution in bornite showing basket weave texture in reflected light, Nchanga Open Pit (NOP124); (C) coarse nature of bornite relative to the grain size of the host-rock arenite in plane polarized light, Nchanga Open Pit (NOP741-16); (D) minor replacement of chalcopyrite by bornite along what may be a fracture in reflected light, Nchanga Open Pit (NOP124).

Main phase cobalt – carrollite

Cobalt mineralization, in the form of carrollite, is restricted to the arenite host-rock within fault-propagation fold zones. It forms coarse (up to 5mm, average 0.5-1mm) subhedral grains or aggregates of grains. Like chalcopyrite and bornite, carrollite normally replaces pyrite where they are found together. The relative timing of copper and cobalt is a contentious issue in the Copperbelt. In some cases they appear to co-exist (Fig. 4.6A), yet in other cases it appears that the carrollite overprints the bornite and sometimes the chalcopyrite (Fig. 4.6B & C), although, this could be a visual result of the different properties of the sulphides, where carrollite forms high-relief, euhedral to subhedral grains with straight edges compared to anhedral, lower-relief bornite or chalcopyrite. On the other hand, the mineral textures can be more ambiguous between chalcopyrite and carrollite (the two are often found together) where local replacement occurs between the two (Fig. 4.6D & E). In general, carrollite shows more replacement textures, suggesting that locally it is later, than copper sulphides.

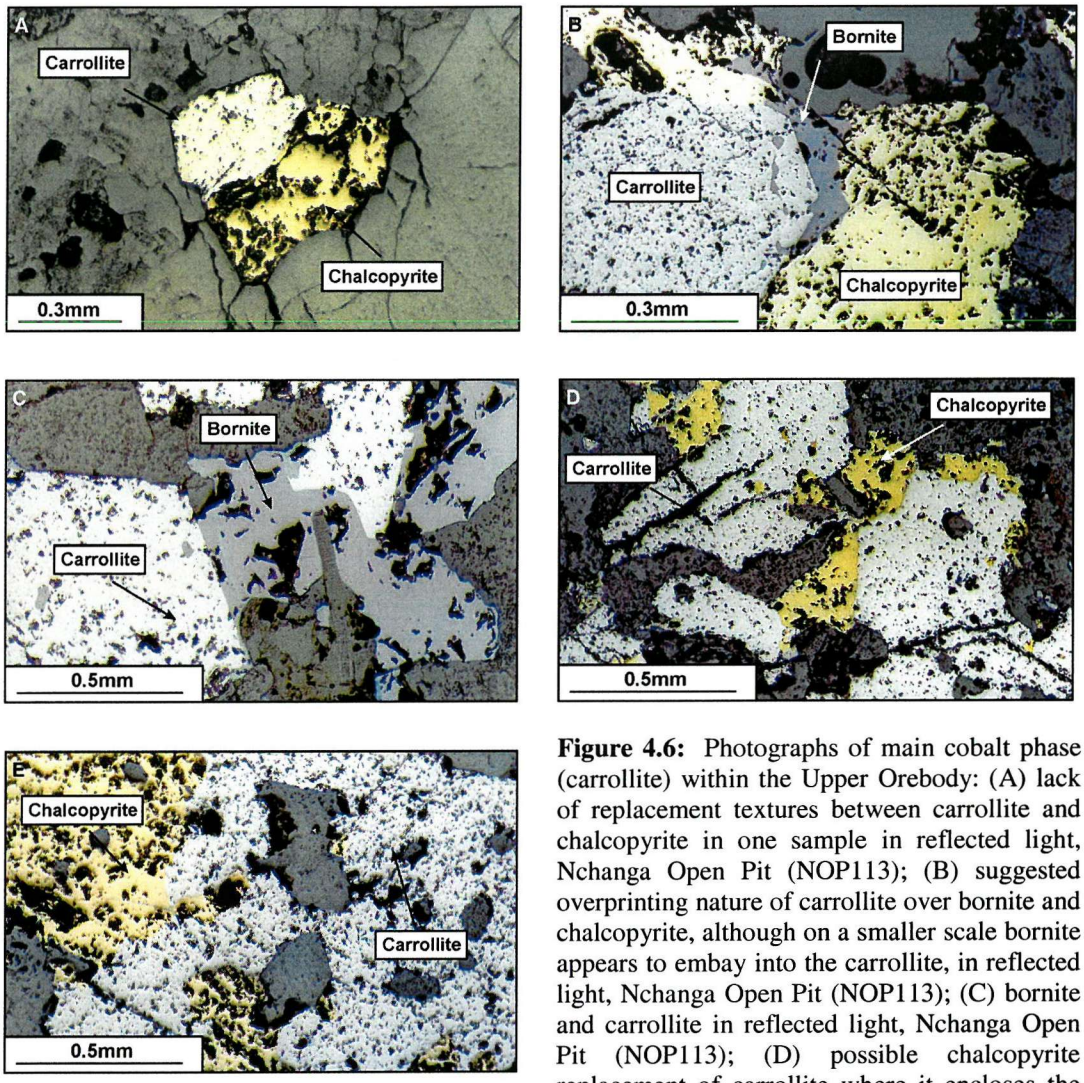

Figure 4.6: Photographs of main cobalt phase (carrollite) within the Upper Orebody: (A) lack of replacement textures between carrollite and chalcopyrite in one sample in reflected light, Nchanga Open Pit (NOP113); (B) suggested overprinting nature of carrollite over bornite and chalcopyrite, although on a smaller scale bornite appears to embay into the carrollite, in reflected light, Nchanga Open Pit (NOP113); (C) bornite and carrollite in reflected light, Nchanga Open Pit (NOP113); (D) possible chalcopyrite replacement of carrollite where it encloses the cobalt ore mineral in reflected light, Nchanga Open Pit (NOP124); (E) strong suggestion of carrollite replacement of chalcopyrite where the former cross-cuts the latter, in reflected light, Nchanga Open Pit (NOP741-19).

Chalcocite

Although chalcocite is common within the Upper Orebody, the majority, if not all of it, replaces earlier copper-iron sulphides (chalcopyrite and bornite). This normally consists of chalcocite rims on chalcopyrite or more commonly bornite, and replacement along fractures. This ranges from minor replacement, with a small proportion of chalcocite compared to bornite (Fig. 4.7A & B), to much more extensive or total replacement (Fig. 4.7C). Chingola B Upper Orebody, previously described as a chalcocite orebody, actually consists of almost total replacement of bornite by chalcocite, with only rare indicators of the precursor sulphide preserved (Fig. 4.7C). Where chalcocite replacement of sulphides occurs in the chalcopyrite-carrollite zones, preferred replacement of chalcopyrite has taken place, and only minor modification of the carrollite (Figs. 4.7D & E). In this present study, no primary chalcocite

(i.e. not a replacement product of bornite or chalcopyrite) has been observed. Covellite, although rare, sometimes appears with the chalcocite and also replaces bornite or chalcopyrite (Fig. 4.7F).

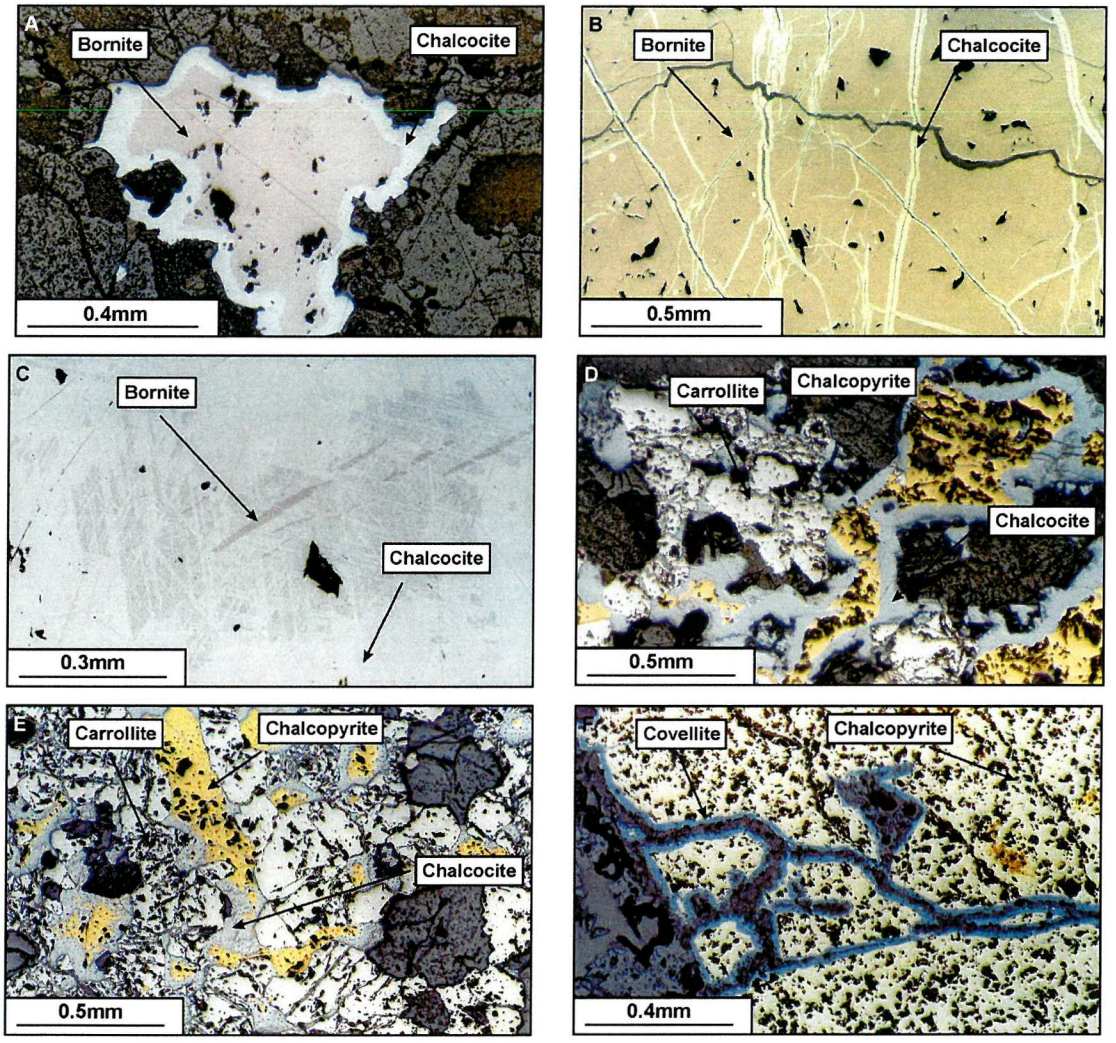

Figure 4.7: Reflected light photographs of secondary chalcocite within the Upper Orebody: (A) chalcocite rim around a bornite grain indicating minor replacement, Nchanga Open Pit (NOP674-3); (B) minor fracture replacement of vein-hosted bornite by chalcocite, Nchanga Open Pit (NOP99); (C) almost total replacement of bornite by chalcocite with only traces of the precursor sulphide preserved, Chingola B (NOP282-8); (D) and (E) selective replacement of chalcopyrite by chalcocite, with only minor modification of carrollite, Nchanga Open Pit (NOP708-3 and NOP760-1); (F) replacement of chalcopyrite by covellite (associated with malachite) along minor fractures, Nchanga Open Pit (NOP741-16).

Late pyrite

In one sample, from borehole NOP 769, pyrite occurs within a quartz vein that appears to cross cut the layer-parallel fabric, which in this case may be bedding. As no copper sulphides occur within the same sample, the exact time relation with respect to main phase mineralization is unknown, and is discussed further in terms of sulphur isotope signatures in section 5.4.

Carbonate and oxide mineralization

Malachite is rare within the Upper Orebody, but where present replaces copper sulphides, coats fractures or occurs within some minor veins. Where chalcocite replaces bornite or chalcopyrite, iron oxides, in particular hematite, are common, which show no replacement textures with the chalcocite. In rare cases hematite does replace chalcocite (that itself is replacing bornite or chalcopyrite) around the edges of grains (Fig. 4.8A & B).

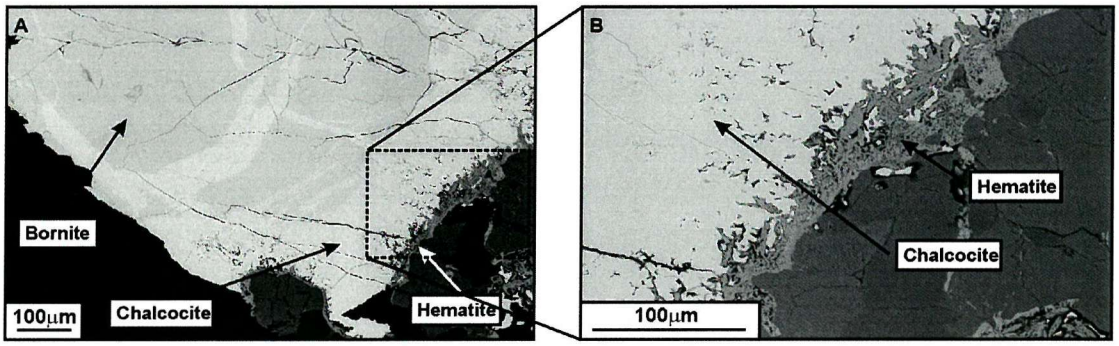

Figure 4.8: Backscattered SEM image of bornite, chalcocite, hematite mineralogy within the Upper Orebody, showing chalcocite (that replaces bornite) itself replaced at the edges of grains by hematite, Nchanga Open Pit (NOP716-19): (A) large scale view, (B) close up of edge of grain.

4.2.3 Micro-relationships of ore minerals to host lithology and structure

The micro-scale observation of ore minerals, and their relationship to the host lithology or microstructure is critical to understanding the timing of mineralization. Clearly, the stratabound mineralization of the Nchanga deposits indicates a strong stratigraphic control in the case of both orebodies, with the majority concentrated within the Lower Roan sediments, in particular the contact between arkose/arenite lithology and overlying shale. However, on a much smaller scale, the ore minerals, described above, are intimately associated with micro-structural features, as shown below, as well as being classically disseminated.

Within the arkose and arenite units, the fracture-related nature of the ore is the most prominent feature, in particular within the Upper Orebody, where there are obvious examples of fracture-related sulphides (Figs. 4.9A to C). Detailed examination of what appears to be stratiform, bedding-orientated mineralization within the arkose (e.g. at Chingola B; Fig. 4.9D) also turns out to be clearly fracture-related on a much smaller scale (Fig. 4.9E). In addition to this, there is a clear grain size reduction of the detrital quartz and feldspar grains relative to the ore minerals nearer to the arkose-shale contact. This is associated with extensive recrystallization of the host quartz component. There are also many examples of fracture-related sulphides transecting single detrital quartz or feldspar grains (Figs. 4.9F to I) as well

as the more obvious, larger-scale, sulphide-filled fractures (Fig. 4.9J & K). Vein-hosted sulphides also occur within the arenites. Apart from obvious veins (e.g. Fig. 3.35), a common feature is primary sulphides surrounded by coarser and more euhedral quartz grains, sometimes identified in hand specimen (Fig. 4.10A), but particularly clear in thin section (Fig. 4.10B). These may be interpreted either as veins or recrystallization of the host lithological components, the latter often referred to as 'lateral secretion veins' (Garlick, 1961) as 'vein' components are identical to the host rock.

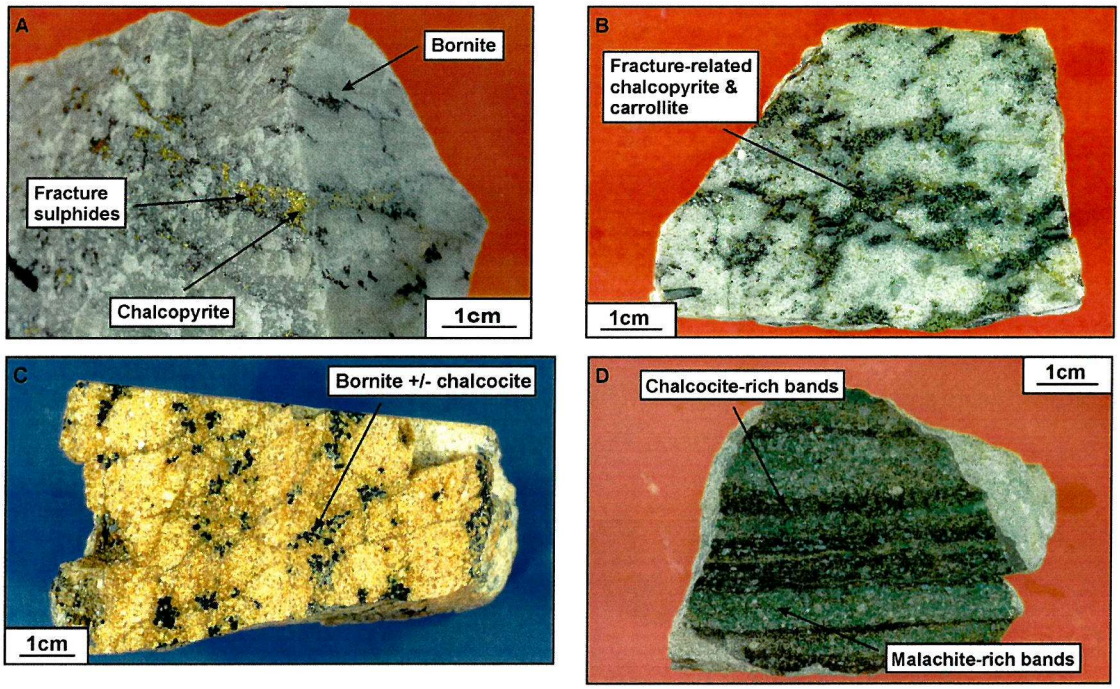

Figure 4.9: Hand-specimen and polished-thin section examples of fracture-related ore minerals within the arkose and 'Feldspathic Quartzite-TFQ' units, Nchanga Open Pit: (A) fracture-related chalcopyrite and bornite within the 'TFQ' unit (NOP118); (B) fracture-related chalcopyrite and carrollite within the 'TFQ' unit (NOP113); (C) bornite (± chalcocite) blebs linked by small (< 1mm) fractures within the Upper Orebody (NOP127); (D) apparent stratiform mineralization within the arkose of the Chingola B Lower Orebody (CB7); (E) actual fracture-related nature of the ore mineralization of photograph D in plane polarized light (CB7); *continued on next page.*

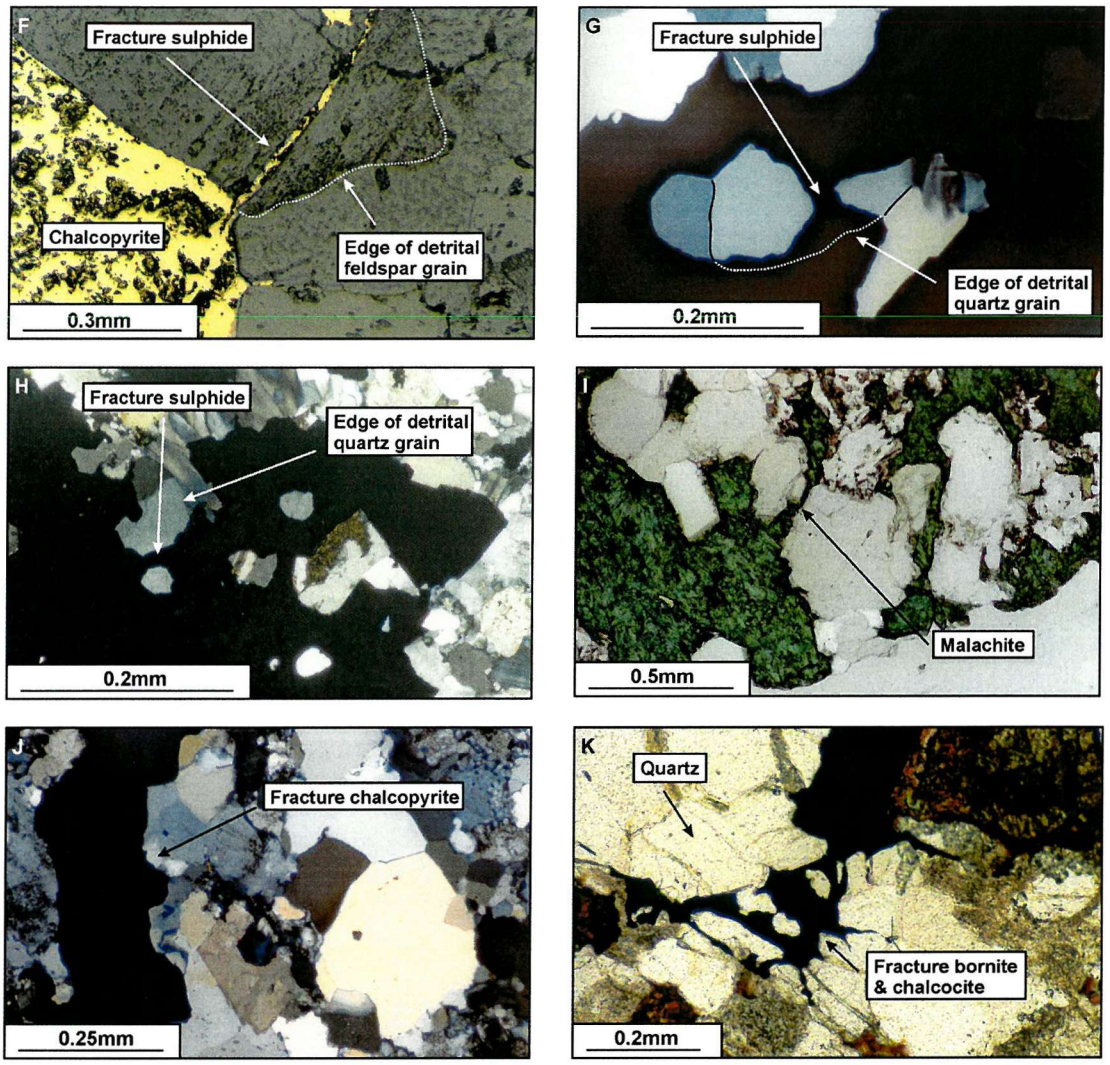

Figure 4.9: *continued* (F) fracture-controlled chalcopyrite in a detrital feldspar grain within the 'TFQ' in reflected light (NOP109); (G) and (H) fracture-controlled chalcopyrite and carrollite respectively in detrital (recrystallized) quartz grains within the 'TFQ' in plane polarized light (NOP741-20 and NOP NOP760-1); (I) fracture malachite through a detrital feldspar grain within arkose, in plane polarized light (CB6); (J) fracture that is infilled with chalcopyrite within the 'TFQ' in plane polarized light (NOP111); (K) fracture bornite and chalcocite within detrital (recrystallized) quartz from the 'TFQ' unit, in plane polarized light .

Within the basal part of both the 'Lower' and 'Upper Banded Shale' units there is evidence for the structure-related nature of the ore minerals. As well as pyrite being concentrated into small quartz veins, chalcopyrite (± bornite) is in places also be fracture- or vein-related (Fig. 4.11A & B). Copper sulphides are commonly orientated along the developed fabric, which is normally steeper to bedding as shown in section 3.5.2), indicated by the examination of hand-specimens (Fig. 4.11C & D) and polished-thin sections (Fig. 4.11E & F). In the 'Lower Banded Shale' of Nchanga Open Pit and Block A, bedding is clearly identified by coarser arenite layers. Although sulphides are clearly more abundant around these layers, they are strongly orientated parallel to and along a fabric and small structures (< 5mm) that deform the layers (Fig. 4.11G).

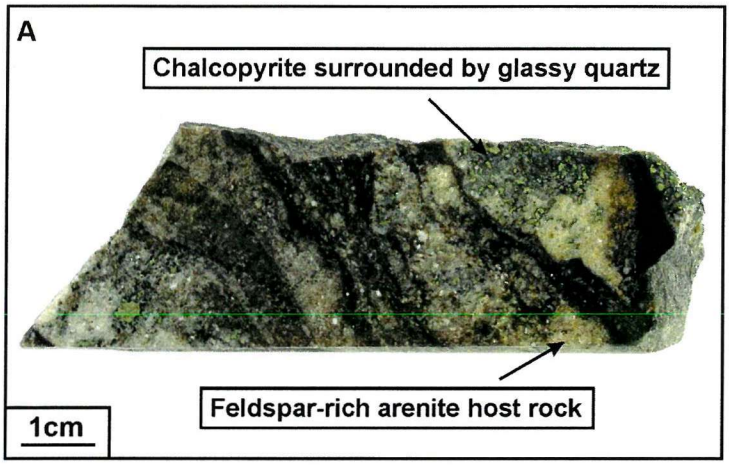

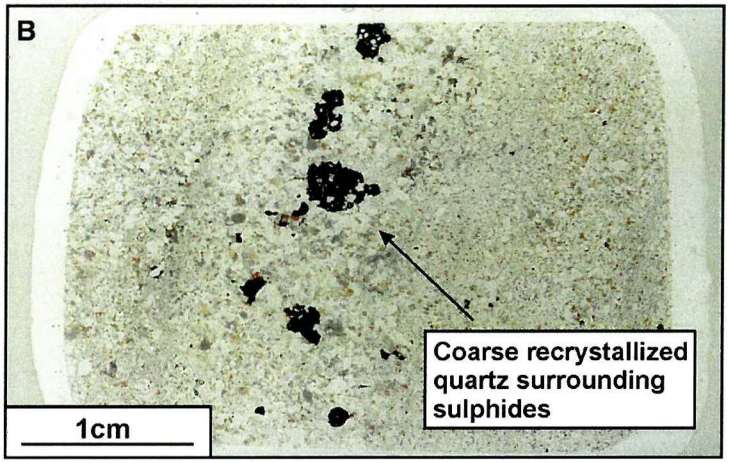

Figure 4.10: Micro-scale evidence for vein-related ore minerals within the 'Feldspathic Quartzite' unit, Nchanga Open Pit: (A) in hand-specimen where darker, glassy quartz (compared to pinkish feldspar-rich host rock) surrounds ore minerals (NOP741-25); and (B) in thin-section (different sample) where there is a clear coarser-grained, quartz abundance around ore minerals (NOP716-7).

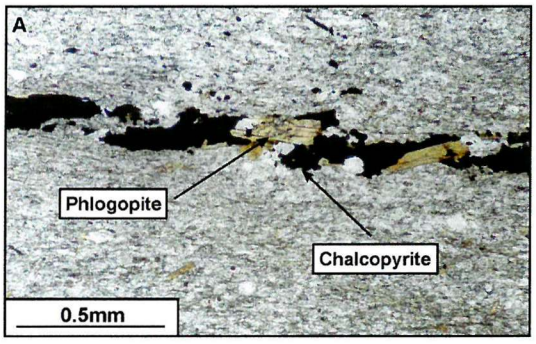

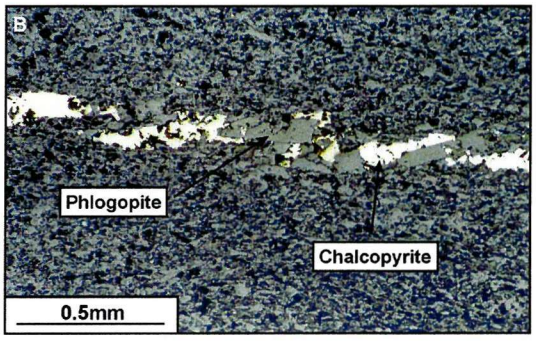

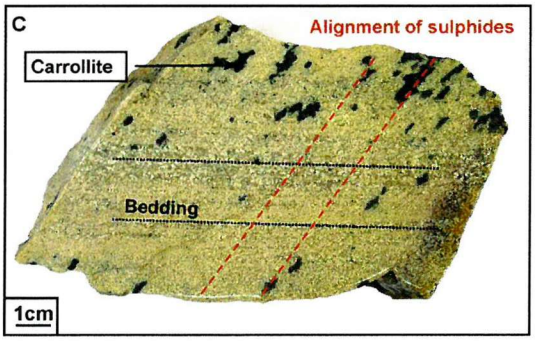

Figure 4.11: Relationships between micro-structure and ore minerals within the 'Lower' and 'Upper Banded Shale' units that overlie the Lower and Upper Orebodies: (A) and (B) chalcopyrite hosted within a quartz-phlogopite fracture/vein within the 'Upper Banded Shale' in plane polarized and reflected light respectively, Nchanga Open Pit; (C) hand specimen showing carrollite within the 'Feldspathic Quartzite' that is aligned to a structural fabric which is steeper than bedding; *continued on next page.*

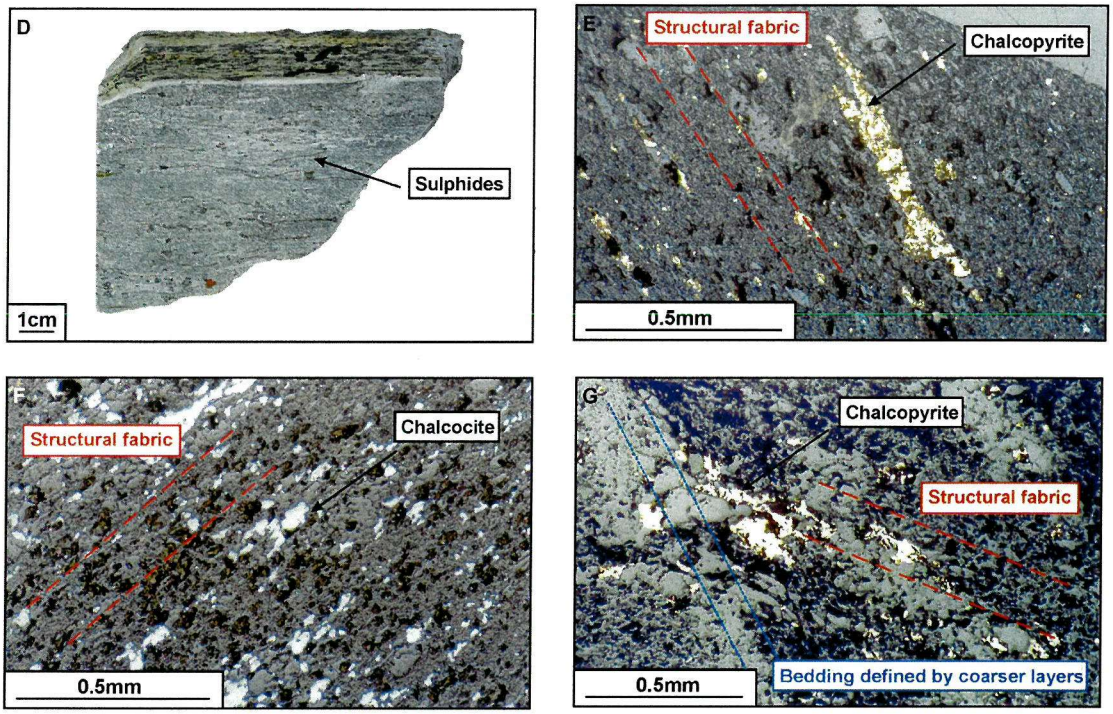

Figure 4.11: *continued* (D) hand-specimen example of chalcopyrite aligned to a developed fabric and associated with small (1-3cm long) micro-faults which cross-cut bedding within the 'Upper Banded Shale,' Nchanga Open Pit; (E) and (F) clear orientation of sulphides to the developed structural fabric within the 'Lower Banded Shale' in reflected light, Block A (NE515-2 and NE515-4); (G) chalcopyrite associated with an arenite layer (original bedding) but strongly controlled by a developed structural fabric within the 'Lower Banded Shale' in reflected light, Block A (NE515-2).

4.3 Wallrock alteration

Hydrothermal alteration is strongly associated with the mineralization of both the Upper and Lower Orebodies at Nchanga. The most dominant alteration minerals are phlogopite, sericite, quartz, and dolomite (± tourmaline and K-feldspar). In fact, it is difficult to find a hand specimen (other than from the granite or base of the arkose unit) that hasn't undergone some form of alteration or mineralization. The following sections detail the various alteration minerals that have been observed at Nchanga, their distribution, their relationship to the ore minerals described above, the mineral chemistry of selected micas, and whole rock geochemical data related to the alteration described. These data provide information on the extent of fluid-rock interaction within the ore-zones and structurally affected zones, and also the nature of fluids that may be involved.

4.3.1 Alteration assemblages: their distribution and relationship to ore minerals

Below are the alteration assemblages that have been identified within the Nchanga host-rock package at key locations from basement rocks to mineralized zones.

Basement rocks

Hydrothermal alteration within Basement granite, that overprints a recrystallized original granitic composition, is associated with high-angle extensional structures (and veins), described in section 3.5.1 and 3.5.3. The alteration consists mainly of small, 0.2mm, randomly orientated blades of phlogopite, which, in the case of a fault gouge that has previously been referred to as a 'lamprophyre dyke,' constitute 70% of the rock (Fig. 4.12). Other minerals present within this assemblage are scapolite (~ 5%), that occurs as often coarse, anhedral grains that appear to overprint the other components, rutile (~ 2%), as well as chalcopyrite and bornite (< 1%). This intensity of alteration has only been encountered in the one location. More normal alteration associated with minor quartz veins and high-angle veins within the arkose unit consist of minor phlogopite (± sericite) immediately adjacent to the vein. Field observations of the fault gouge reveals aggregates of K-feldspar around the quartz veins associated with the fault zone. It is not known whether this is an alteration feature, associated with the vein-forming process.

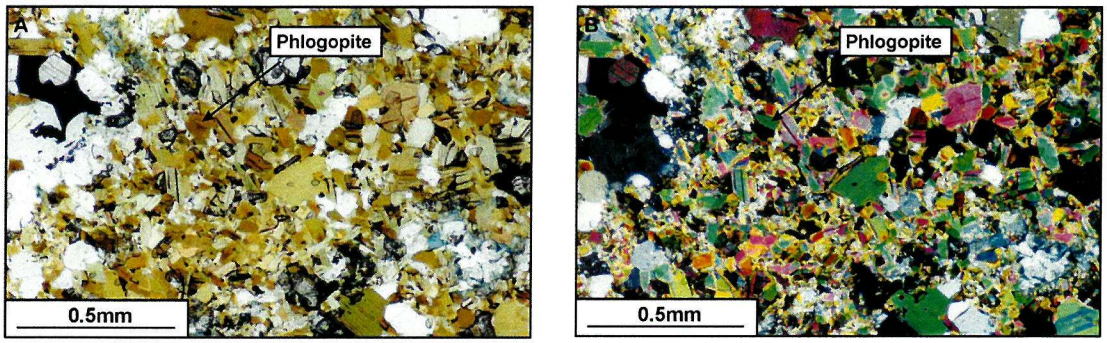

Figure 4.12: Photographs of a thin-section of phlogopite-rich fault gouge within the Basement granite showing mica abundance: (A) PPL and (B) XPL (NOP47, Nchanga Open Pit).

Lower Orebody

Hydrothermal alteration within the arkose unit increases in abundance towards its upper contact with the 'Lower Banded Shale' unit. This is mainly shown by the amount of phlogopite, which increases dramatically in close proximity to mineralization. Less abundant alteration minerals include sericite, rutile, and quartz (± dolomite, tourmaline, and chlorite). The phlogopite is the most significant alteration mineral and can constitute up to 40% of high-grade copper- and cobalt-rich rocks, normally occurring as 0.05-1mm blades (Fig. 4.13A). The phlogopite is strongly related to the presence of copper, and hence is most abundant within the 'transition' contact zone between the arkose and overlying shale. Below this zone, phlogopite appears to be strongly fracture-related (often with ore minerals; Fig. 4.13B); yet in the shale above the contact only minor phlogopite has been observed during this study.

Sericite alteration is widespread within the arkose and shale, and occurs as very fine-grained replacement of the microcline feldspar component (± clay alteration; Fig. 4.13C) as well as coarser grains between recrystallized quartz grains and infilling small fractures (Fig.4.13D). In hand specimen, this sericitic alteration, often accompanied by silicification, is represented by strong bleaching of the wallrock (where oxidized mineralization occurs). This is especially evident in the 'Lower Banded Shale,' where carbonaceous material has been removed and sericite is abundant (Fig. 4.13E & F). Rutile is a common component (~ 1%) of many Nchanga specimens, always occurring as aggregates of very small needles (0.01-0.1mm), and minor pale grey chlorite may also be found within the highly altered contact zone. Minor dolomite was found within the 'transition' contact zone in only two samples, and appears to be a rare component of the alteration assemblage (or one that has been removed subsequently). Euhedral, detrital tourmalines (0.2-0.8mm) are common within the arkose, and many of them show a clear irregular overgrowth of paler tourmaline. Coarse muscovite flakes may be present within altered rocks in the vicinity of Lower Orebody mineralization.

In terms of the relative timing of ore and alteration minerals, the following observations are significant:

- Malachite post-dates the phlogopite, indicated by the replacement of the latter by malachite (and associated iron oxides) along cleavage and around the edges of phlogopite grains (Fig. 4.13G & H). In addition phlogopite is spatially associated with the chalcocite but not necessarily with the malachite.
- Oxide mineralization and malachite are strongly related to the bleaching of host rocks, suggesting that they are also related to the sericite alteration and silicification. In fact the coarser sericite appears to be related to sulphides (although not as strongly as the phlogopite), whereas the very fine-grained sericite alteration of feldspars may be related to oxide or malachite development.
- There have been no replacement textures observed between ore sulphides and phlogopite; instead there appears to be a strong spatial association between the two, with the abundance of alteration minerals decreasing away from the principal zone of mineralization at the arkose-shale contact.
- Muscovite overprints the ore sulphides as in the Upper Orebody (see below)

The other feature strongly related to wallrock alteration and fluid-rock interaction is the recrystallization of detrital components that has taken place. This mainly occurs with quartz, which often exhibits a polycrystalline nature with 120° dihedral angles (Fig. 4.13I), although it is not known how much of this is 'new' quartz vein material rather than recrystallization of

detrital quartz. This appears to be more common and extensive towards the top of the arkose unit, although certainly more widespread (vertically) than both copper mineralization and phlogopite alteration.

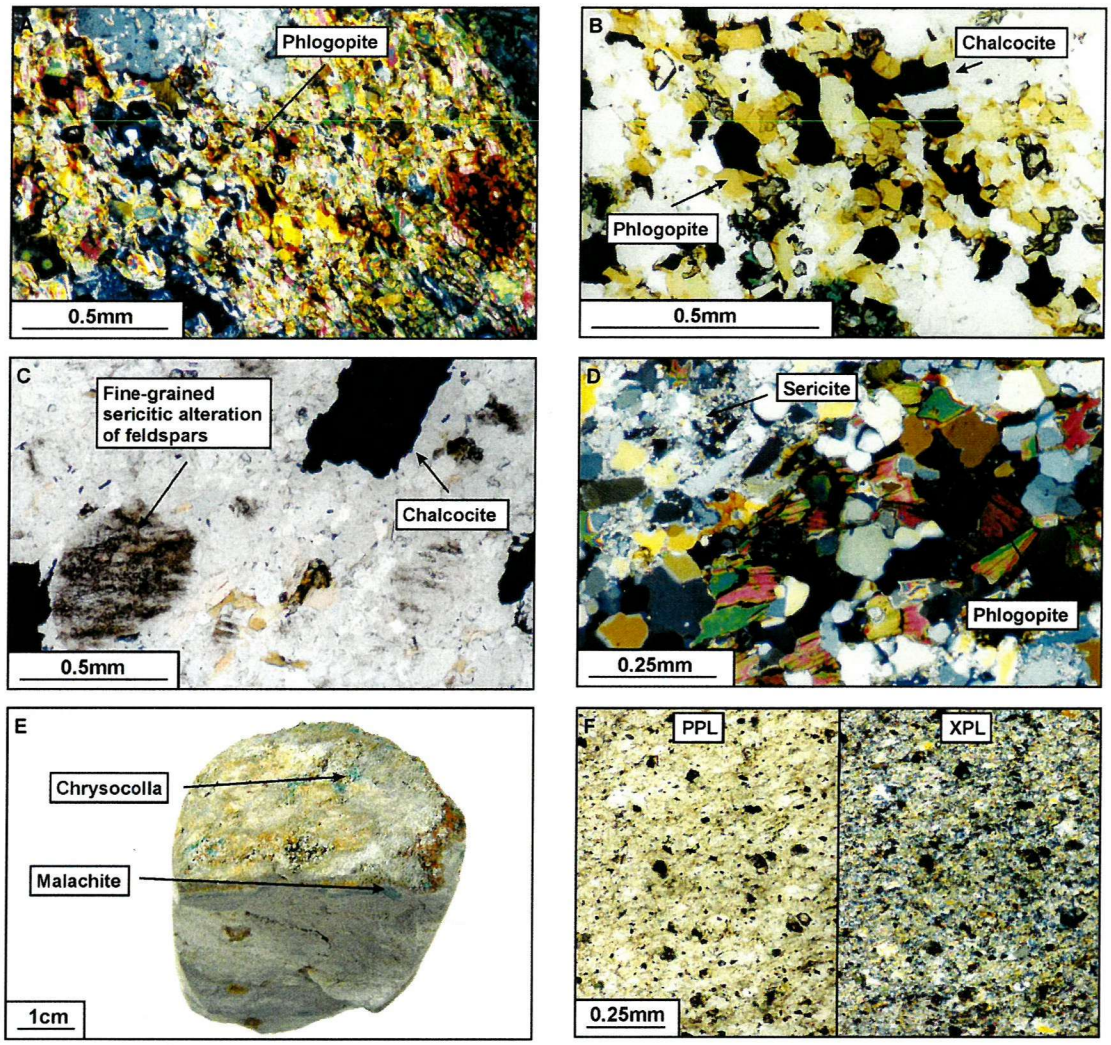

Figure 4.13: Photographs of alteration within Lower Orebody samples and the relationship with mineralization: (A) abundant phlogopite within brecciated arkose at the Nchanga Open Pit 'transition' contact zone (NOP716-3); (B) arkose-hosted fracture-related phlogopite associated with chalcocite within Chingola B Lower Orebody (CB7); (C) extremely fine-grained sericitic replacement of detrital microcline grains within the arkose unit; (D) fine-grained sericite associated with phlogopite alteration within mineralized and brecciated arkose rocks (NOP716-2); (E) hand specimen photograph of altered and oxidized 'Lower Banded Shale' sample (compare with the unaltered version in Fig. 3.7A); (F) thin-section photograph of the sample in Fig. 4.13E (compare with the unaltered version in Fig. 3.7B); *continued on next page.*

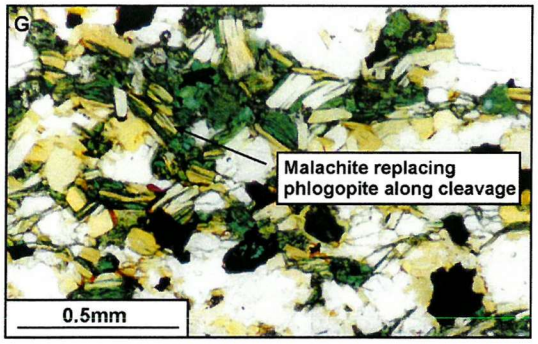

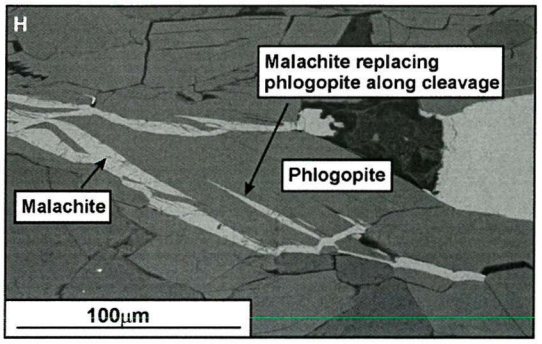

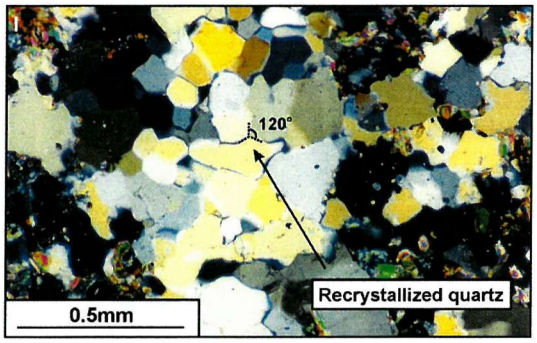

Figure 4.13: *continued* (G) replacement of phlogopite by malachite along cleavage and around the edges of grains within an oxidized Lower Orebody sample from Chingola B (CB7); (H) back scattered SEM image of malachite replacement of phlogopite along cleavage and around grains (CB7); (I) recrystallized nature of host quartz grains showing 120° dihedral angle in many cases (CB6).

'Banded Sandstone' shear-zones

The shear zones related to low-angle thrusts within the 'Banded Sandstone' unit (that lead to the development of the fault-propagation folds) are associated with considerable phlogopite and dolomite abundances. Previous authors have described this unit as originally (pre-deformation) mica-rich (McKinnon & Smit, 1961), but within the shear zones phlogopite content can attain 40-50%. These rocks consist of foliated phlogopite and euhedral dolomite (25-35%) and quartz (10-20%) orientated strongly in the direction of shearing (Fig. 4.14). Scapolite can be a common constituent of these shear zone rocks (<5%), often as coarse, irregular grains that appear to overprint the other components (Fig. 4.14).

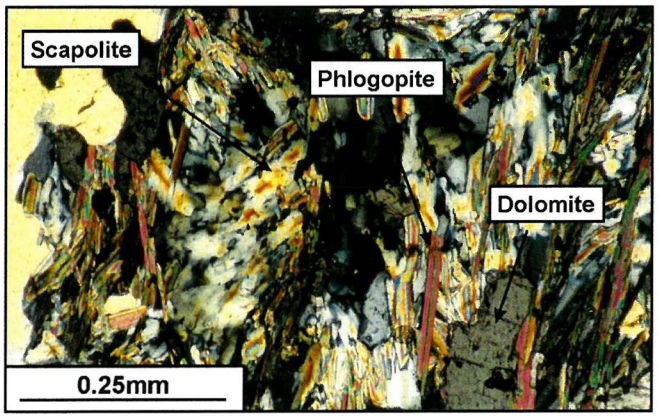

Figure 4.14: Shear zone phlogopite and dolomite within the 'Banded Sandstone' unit, Nchanga Open Pit (NOP61).

Upper Orebody

At Nchanga no unmineralized sections of 'The Feldspathic Quartzite' were observed during the current study. Therefore, this makes understanding the alteration that may or may not have taken place within this unit more difficult. This arenite is commonly dolomite-rich (ranging from 5 to 30%), where the dolomite is accompanied by phlogopite (0-10%), quartz, and sericite (0-10%) in varying amounts and possibly by rutile and K-feldspar (microcline). Other minerals that have been identified within 'The Feldspathic Quartzite' are muscovite, chlorite, and iron oxides, although not all of them are temporally related. Recrystallization of the host quartz component is common, often strongly related to the ore minerals (see 4.2.3).

Within mineralized arenite (where no oxidation of the ore minerals has taken place and where there is no malachite and chrysocolla and very little iron oxide) the dominant alteration minerals are dolomite, phlogopite, sericite, and rutile. The host arenite takes on a pale grey, bleached appearance but phlogopite-rich zones are much darker. The dolomite itself ranges from subhedral grains (0.1-0.5mm; Fig. 4.15A) to much coarser, irregular patches (often >1mm; Fig. 4.15B). It occurs either interstitial to the recrystallized host quartz component or fracture related across detrital grains. Phlogopite is often in close association with the dolomite (Fig. 4.15 C, D & E) and individual grains (0.04-0.3mm) are nearly always orientated in a similar direction, as are the subhedral dolomite crystals and the recrystallized quartz grains. Sericite, as in the Lower Orebody, is represented by fine-grained (15-50μm) distinguishable sericite, and the extremely fine-grained 'dirty' alteration (<5μm) of detrital microcline feldspar grains. Interestingly, like the 'Lower Banded Shale' above the Lower Orebody, the 'Upper Banded Shale' above this host arenite is often bleached for several metres. In both cases sericite is common within the shale, and any carbonaceous material has been removed. Rutile is a common component of most mineralized samples, commonly occurring as several individual grains or aggregates of fine, 10-100μm, needles. K-feldspar (microcline) could be added to this alteration assemblage. Within some samples (e.g. those from NOP 741) there appears to be aggregates of microcline grains associated with sulphides and coarse recrystallization of the host quartz component. It is not clear whether this is a detrital, recrystallization, or alteration feature at this stage.

Samples of the host arenite, within which precursor sulphides are replaced by chalcocite and malachite and iron oxides (including hematite), contain a slightly different alteration assemblage. The very fine-grained 'dirty' alteration of feldspars is much more extensively developed (Fig. 4.15F) and only minor phlogopite (1-4%) is normally observed. Minor chlorite is sometimes present, often associated with any iron oxides. In hand-specimen the host rock takes on a much darker appearance, presumably due to the iron minerals now

abundant (Fig. 4.9C). No dolomite is found within any of these oxidized specimens but rutile is still present (~ 1%). The only other mineral present is muscovite, normally occurring as 0.2 to 1mm grains. Both the iron oxide minerals and muscovite clearly replace the sulphides, including chalcocite, the muscovite overprinting opaque minerals (Fig. 4.15G).

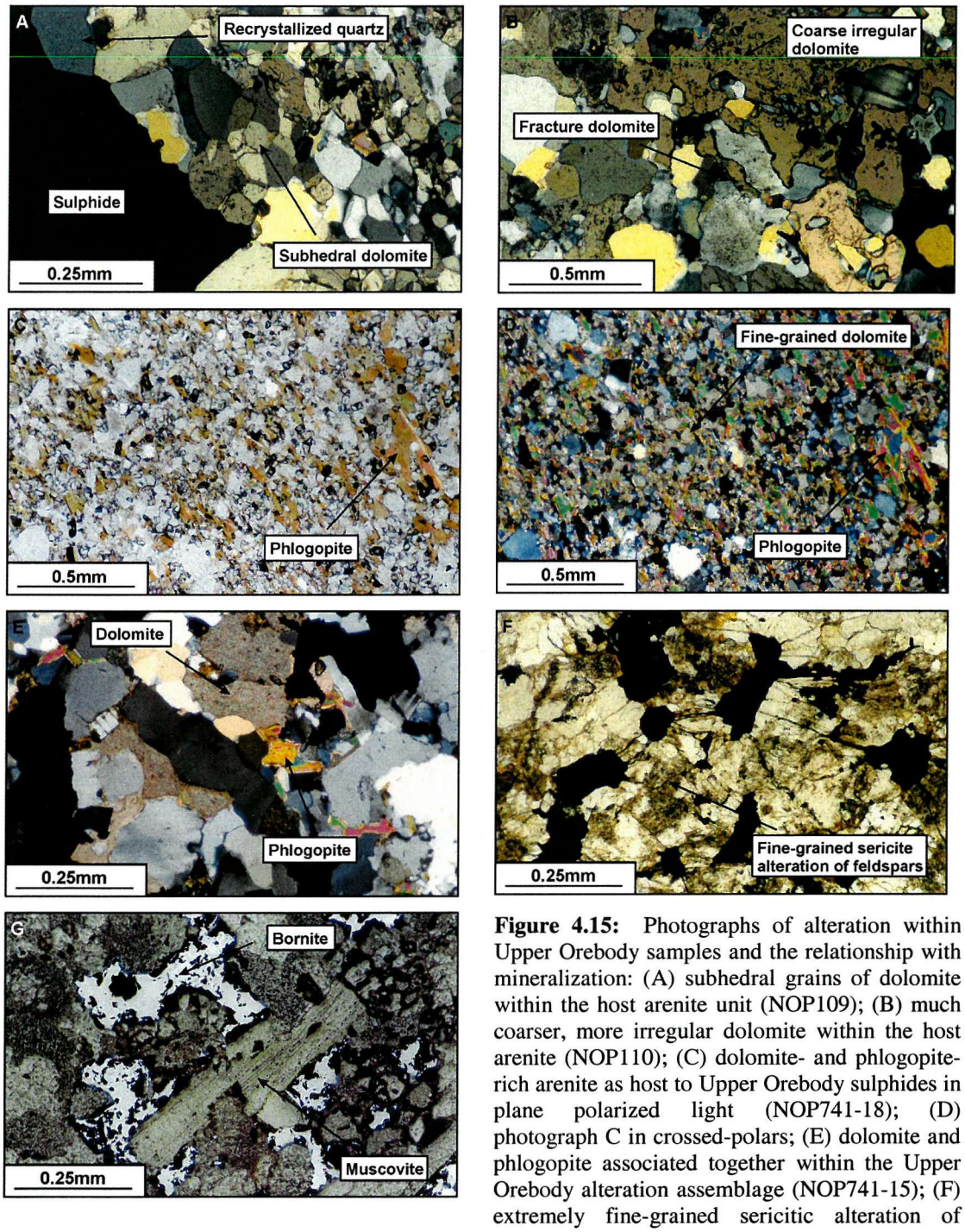

Figure 4.15: Photographs of alteration within Upper Orebody samples and the relationship with mineralization: (A) subhedral grains of dolomite within the host arenite unit (NOP109); (B) much coarser, more irregular dolomite within the host arenite (NOP110); (C) dolomite- and phlogopite-rich arenite as host to Upper Orebody sulphides in plane polarized light (NOP741-18); (D) photograph C in crossed-polars; (E) dolomite and phlogopite associated together within the Upper Orebody alteration assemblage (NOP741-15); (F) extremely fine-grained sericitic alteration of detrital microcline feldspars within the host arenite unit (NOP109); (G) coarse muscovite grain replacing primary bornite within the Upper Orebody (NOP111).

Although the distribution of this alteration is not very well understood, its does appear that the dolomite and phlogopite are spatially associated with the fault-propagation folds described in Chapter 3. This is mainly deduced from identification of these minerals within samples from boreholes that intersect these fault-fold structures (e.g. NOP 741 and 760) and not in boreholes that occur further south (up dip) of the structures (e.g. NOP 716). Therefore there also appears to be the same association between cobalt and dolomite/phlogopite, although copper-rich samples can also be dolomite-rich. Another association, that may be significant, is an inverse relationship between dolomite abundance and chalcocite replacement of bornite or chalcopyrite. In general, where there is major chalcocite replacement of bornite or chalcopyrite within the Upper Orebody, dolomite is not a major component of the alteration assemblage. Yet, within many of the samples containing bornite and chalcopyrite that hadn't been extensively replaced by chalcocite, dolomite was a major alteration mineral.

A summary of the main alteration assemblages at the key locations, described above, is presented in Fig. 4.16. The relative timing of ore precipitation and hydrothermal alteration of the host rocks is discussed in Chapter 6.

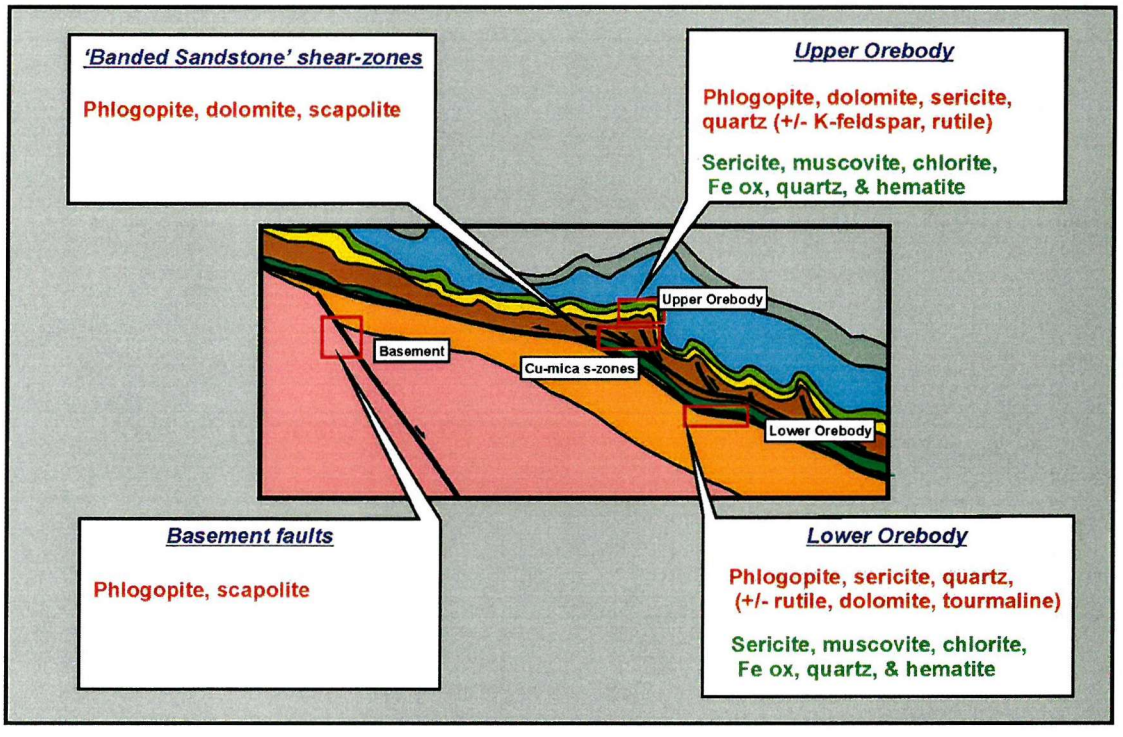

Figure 4.16: Locations and summary of details of the key alteration assemblages described in section 4.3.1 (alteration associated with primary copper and cobalt sulphide mineralization in red, alteration associated with modification of pre-existing sulphides in green for the Lower and Upper Orebodies).

4.3.2 Paragenetic sequencing

The following mineralization phases and associated alteration events have been recognized at Nchanga (Table 4):

Phase of mineralization	(1) Diagenetic sulphide	(2) Main phase Cu & Co	(3) Secondary Cu	(4) Supergene processes
Ore minerals	pyrite	bornite chalcopyrite (± chalcocite)	chalcocite	malachite chrysocolla
Alteration minerals	-	phlogopite quartz sericite dolomite (± rutile, tourmaline, K-feldspar)	hematite (± other Fe ox's) sericite muscovite chlorite	-

TIME ⟶

Table 4.1: Main phases of mineralization and associated ore and alteration minerals. Numbers (1) to (4) refer to the explanation below.

(1) Much of the pyrite is considered diagenetic in origin, but thought to have precipitated in the later stages of diagenesis as it replaces an earlier diagenetic phase of anhydrite. Certainly there is some quartz vein-hosted pyrite. The timing of this is unknown, except that it appears to precede deformation of the host shale overlying the Lower Orebody. Pyrite within the Upper Orebody appears to be the earliest phase of mineralization, although its timing relative to deformation is unknown.

(2) The main phase of copper mineralization consists of chalcopyrite and bornite (+ chalcocite for the Lower Orebody), which replaces the earlier phase of pyrite. Upper Orebody carrollite appears, at this stage, to have been introduced synchronous with copper or slightly later. Primary chalcocite is also present within the Lower Orebody. Alteration associated with ore zones dominantly consists of phlogopite-quartz-sericite for the Lower Orebody and phlogopite-dolomite-quartz-sericite for the Upper Orebody. Dolomite is thought to have been a component of Lower Orebody alteration prior to the extensive modification that has taken place and is further discussed in Chapter 6. Accessory minerals may be rutile and tourmaline (and K-feldspar for the Upper Orebody).

(3) Chalcocite commonly replaces the main phase copper ore minerals. It is unclear how much of the Lower Orebody chalcocite is a replacement product and how much is primary. Almost certainly, the majority of chalcocite in the Upper Orebody, and a proportion of that in the Lower Orebody, is simply replacement of precursor bornite and chalcopyrite. There appears to have been no secondary addition of chalcocite to the Upper Orebody, but possibly some to the Lower Orebody. Alteration associated with this replacement of earlier sulphides consists mainly of muscovite, hematite (reflecting release of iron when $CuFeS_2$ is converted to CuS_2), sericite, and minor chlorite.

(4) Leaching and subsequent modification of ore minerals (chalcocite, bornite, and chalcopyrite) has taken place, most likely during supergene processes (mostly within the Lower Orebody). In addition intense leaching of alteration minerals may also have taken place (in particular dolomite) indicated by the major depletion in many components within these samples. Possible supergene enrichment of copper has taken place within the Lower Orebody and malachite is common along late fracture surfaces.

Both orebodies seem very similar in terms of their ore and alteration mineralogy, even though the Lower Orebody appears to have been subjected to more extensive supergene modification. However, it must be kept in mind that at this stage it cannot be confirmed whether Lower and Upper Orebody sulphides formed synchronously, even though the mineralogy and geochemistry suggest that they did.

4.3.3 Mineral geochemistry

Phlogopites from each of the alteration zones, described above, were analysed on the Cameca SX50 WDS electron microprobe (Natural History Museum, London), using polished-thin sections of selected samples to investigate the elemental compositions of the selected micas and potentially determine their origin.

The iron/magnesium ratios of the phlogopites throughout the Nchanga sequence, from basement faults to the Lower, Intermediate, and Upper Orebodies, and to shear zone micas were determined (Table 4.1; Fig. 4.17; data in Appendix B1). The 'granite fault' sample was from the fault gouge associated with a high-angle extensional structure, described in section 3.3.3. Two 'shear zone' samples were selected: one from the 'Banded Sandstone' unit beneath

one of the fault-propagation folds and one from the 'Dolomite Schist' unit. The strict definition of a phlogopite is based on the ratio of magnesium to iron atoms, which must be greater than two to one (Deer *et al.*, 1966; Heinrich, 1946).

Sample location	Average:	FeO (wt%)	MgO (wt%)	Fe/Mg ratio
'Dolomite Schist' shear zone		**4.289**	**22.980**	0.187 (n=8)
Upper Orebody		**4.441**	**21.865**	0.204 (n=13)
'Banded Sandstone' shear zone		**6.110**	**20.913**	0.292 (n=9)
Intermediate Orebody		**5.68**	**20.175**	0.282 (n=4)
Lower Orebody		**9.946**	**19.055**	0.522 (n=13)
Basement fault		**10.209**	**17.931**	0.569 (n=7)

Table 4.2: Average Fe and Mg weight percents and average $^{Fe}/_{Mg}$ ratios for phlogopites from various sample locations throughout the Nchanga sequence. The number of results in each sample group is included in brackets. The mean Fe/Mg ratio for each phlogopite group is taken from an average of all analyses within each sample, and not a ratio of average Fe to average Mg included in this table.

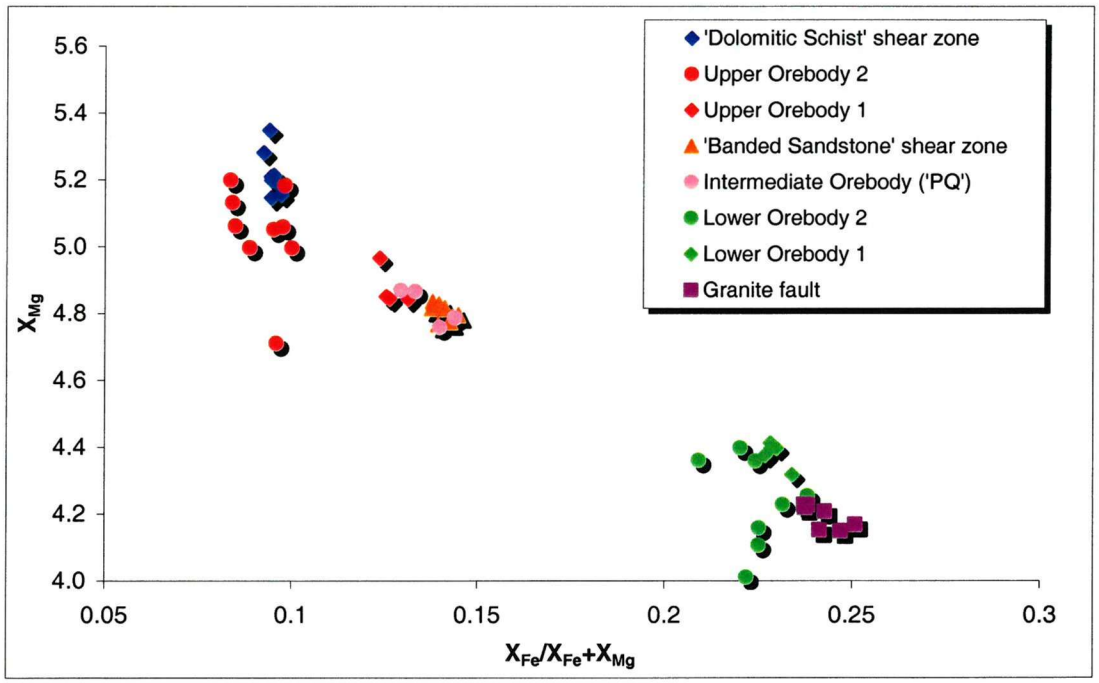

Figure 4.17: Plot of Mg versus Fe/(Fe+Mg) ratios (molecular proportion) of phlogopites from different sections of the Nchanga sequence. The method for this calculation is shown in Table 4.3.

The data clearly shows a progressive decrease in the Fe/Mg ratios from Basement faults through the Lower Orebody and up to the Upper Orebody, with the results from shear-zone phlogopites following the trend. Taking these into account, the individual Fe and Mg data show that this trend is a result of the Fe content of phlogopites decreasing at higher levels in

the sequence (~6 wt% difference in total), matched by an increase in Mg content (~5 wt% difference).

Another interesting feature of the phlogopite chemistry are the high fluorine contents, reaching as high as 4.8 wt%. Phlogopites with high fluorine contents are not rare (Sanz & Stone, 1979; Westrich, 1981). Brimhall & Crerar (1987) investigated the origin of biotites by comparing the ratio of atoms of Mg-Fe and F-OH (the latter is interpreted as the fugacity ratios of HF/H_2O) in phlogopites from contrasting environments using the formula $K_2(Mg,Fe^{2+})_6[Si_6Al_2O_{20}](OH,F)_4$ (Table 4.3). The molecular proportions were calculated using the 'calculation of a mineral formula from a mineral analysis' method in (Deer *et al.*, 1966).

	1	2	3	4	5	6
SiO_2	39.46	40.18	38.57	40.30	39.36	40.90
TiO_2	1.73	1.00	1.41	0.94	1.46	0.74
Al_2O_3	15.17	14.92	14.72	17.88	16.44	16.67
FeO	9.99	9.38	5.54	6.05	5.36	4.27
MnO	0.08	0.13	0.11	0.06	0.06	<0.05
MgO	17.99	18.10	20.23	20.96	21.31	22.96
K_2O	10.57	11.05	10.65	9.99	10.81	9.45
Na_2O	0.08	0.06	0.06	0.26	0.10	0.34
Cl	0.11	0.12	0.05	<0.05	<0.05	0.05
F	1.21	4.52	1.03	0.34	0.18	0.73
Totals	**96.39**	**99.46**	**92.37**	**96.81**	**95.08**	**96.14**
Number of ions in structural formula based on 24 oxygens						
Si	6.2	6.1	6.2	6.1	6.2	6.2
Ti	0.2	0.1	0.2	0.1	0.2	0.1
Al	2.8	2.7	2.8	3.2	3.0	3.0
Fe	1.3	1.2	0.7	0.8	0.7	0.5
Mn	-	-	-	-	-	-
Mg	4.2	4.1	4.9	4.8	5.0	5.2
K	1.1	1.1	1.1	1.0	1.1	0.9
Na	-	-	-	-	-	0.1
Cl	-	-	-	-	-	-
F	3.4	2.2	0.5	0.2	0.1	0.4
OH	0.6	1.8	3.5	3.8	3.9	3.6

Table 4.3: Typical compositions (weight %) of phlogopites from various Nchanga rocks (< = below detection limit): (1) granite fault, (2) Lower Orebody, (3) Intermediate Orebody, (4) 'Banded Sandstone' shear-zone, (5) Upper Orebody, and (6) 'Dolomitic Schist' shear zone. Number of ions in the formula is calculated on the basis of 24 oxygens (Deer *et al.*, 1966). The X_{OH} value is calculated by subtracting the X_F value from 4. (Raw data in Appendix B1).

However, there is some error to be considered in the way that the number of OH ions has been calculated. Normally water would be measured by other methods and the proportion of OH calculated in the way shown above. However, as only the fluorine data is available, it has been calculated by assuming that the number of F and OH atoms would add up to a total of 4

(as they would in a perfect formula for phlogopite). In reality, this would not be the case, as evident from the chemical compositions of some phlogopites presented by Deer *et al.*, (1966), where F and OH ions add up to totals ranging from 3.3 to 4.3. However the method used here has been used by a number of previous authors (Kearns *et al.*, 1980; Petersen *et al.*, 1982; Valley *et al.*, 1982; Belkin *et al.*, 1988). The fluorine data collected in this study (Table 4.3; Fig. 4.18) show high concentrations within the phlogopites sampled from the arkose-hosted Lower Orebody. There is additionally a positive correlation between high fluorine and higher chlorine contents. Unlike the Fe/Mg ratios there appears to be no distinct pattern in the fluorine contents of the phlogopites at Nchanga, only that the phlogopites at the site of the Lower Orebody have much higher fluorine contents than any others. The significance of this is discussed further in Chapter 6.

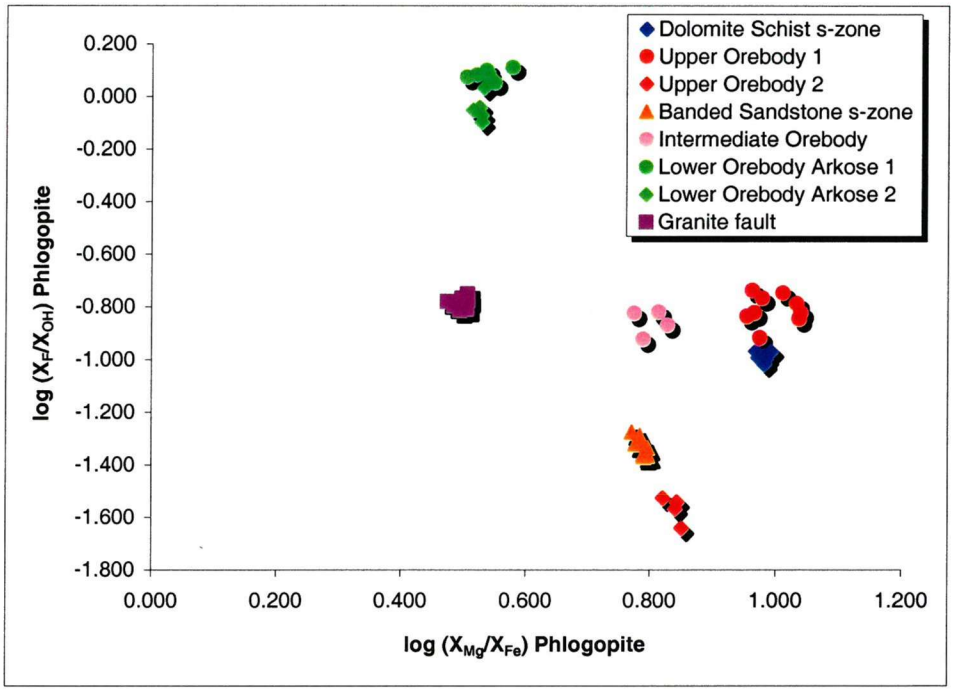

Figure 4.18: The F/OH and Mg/Fe composition of phlogopites from the Nchanga sequence.

Sample location	Average: F (wt%)	Cl (wt%)
'Dolomite Schist' shear-zone	0.768	<0.05
Upper Orebody	0.834	<0.05
'Banded Sandstone' shear-zone	0.368	<0.05
Intermediate Orebody	0.96	<0.05
Lower Orebody	4.339	0.158
Granite fault	1.139	0.109

Table 4.4: Average F and Cl contents (weight %; < = below detection limit) within phlogopites from various locations in the Nchanga sequence.

4.3.4 Whole-rock geochemistry

Whole rock geochemical analysis of selected samples allows the alteration and fluid-rock interaction of the system to be further investigated. Samples (both open pit and core samples) from the Nchanga area were collected and analysed for major and trace elements using X-Ray Fluorescence (XRF; see Appendix B5) analysis. These results were interpreted using the Grant (1986) isocon method (modified from Gresens, 1967) to investigate mobile and immobile elements (Appendix B6). In addition, 153 samples were collected directly from core using a down-hole grooving technique, and analysed at ACME Analytical Laboratories Ltd., Canada by ICP-MS (see Appendix B4).

Down-hole trends and interpretation with respect to ore/alteration mineralogy

Following recognition of the components that may be mobile (Appendix B6), the down-hole trends of these components can be investigated to evaluate the alteration. Four boreholes were sampled by grinding a groove down the side of pieces of core. Any textural, mineralogical, or structural changes in the rock type were noted and a new sample started. The four boreholes chosen were: NOP716 (Nchanga Open Pit Lower Orebody and bornite-rich Upper Orebody); NOP785 (Nchanga Open Pit co-rich Upper Orebody); NE515 (Block A Lower Orebody and sulphide-rich 'Lower Banded Shale'); and NE529 (Chingola C Lower Orebody; see Appendix B4 for raw data).

Down-hole major element concentrations have been plotted for boreholes NOP716 (Lower Orebody and copper-rich Upper Orebody) and NOP785 (cobalt-rich Upper Orebody with minor copper) to investigate down-hole trends compared to those of copper and cobalt (Figs. 4.19 & 4.20). However, care must be taken when dealing with these down-hole trends, as they do not take into account the volume-change effects discussed above. For example, if there is a large increase in copper within ore zones, then there is likely to be a decrease in other components, however this does not mean they have become depleted during the alteration process, just diluted.

At the arkose-shale contact, where high concentrations of copper occur in the Lower Orebody, there is a marked decrease in SiO_2, yet an increase in both Fe_2O_3 and MgO. All other components show little change over this zone. The Fe and Mg increase is most likely due to the presence of sulphides and phlogopite respectively. The significant loss of SiO_2 (~30%) may indicate it being taken into a vein-forming fluid, as quartz veins are common within the contact zone. MnO and TiO_2 are both enriched within altered samples (see isocon plots), Mn probably substituting for Fe and Mg in phlogopites (Deer *et al.*, 1962), and Ti

increasing as a result of rutile abundance, although they show no anomalous concentrations on the down-hole plots. There are no significant variations in concentrations of CaO, Na_2O, K_2O, Al_2O_3, or P_2O_5 on the down-hole plots.

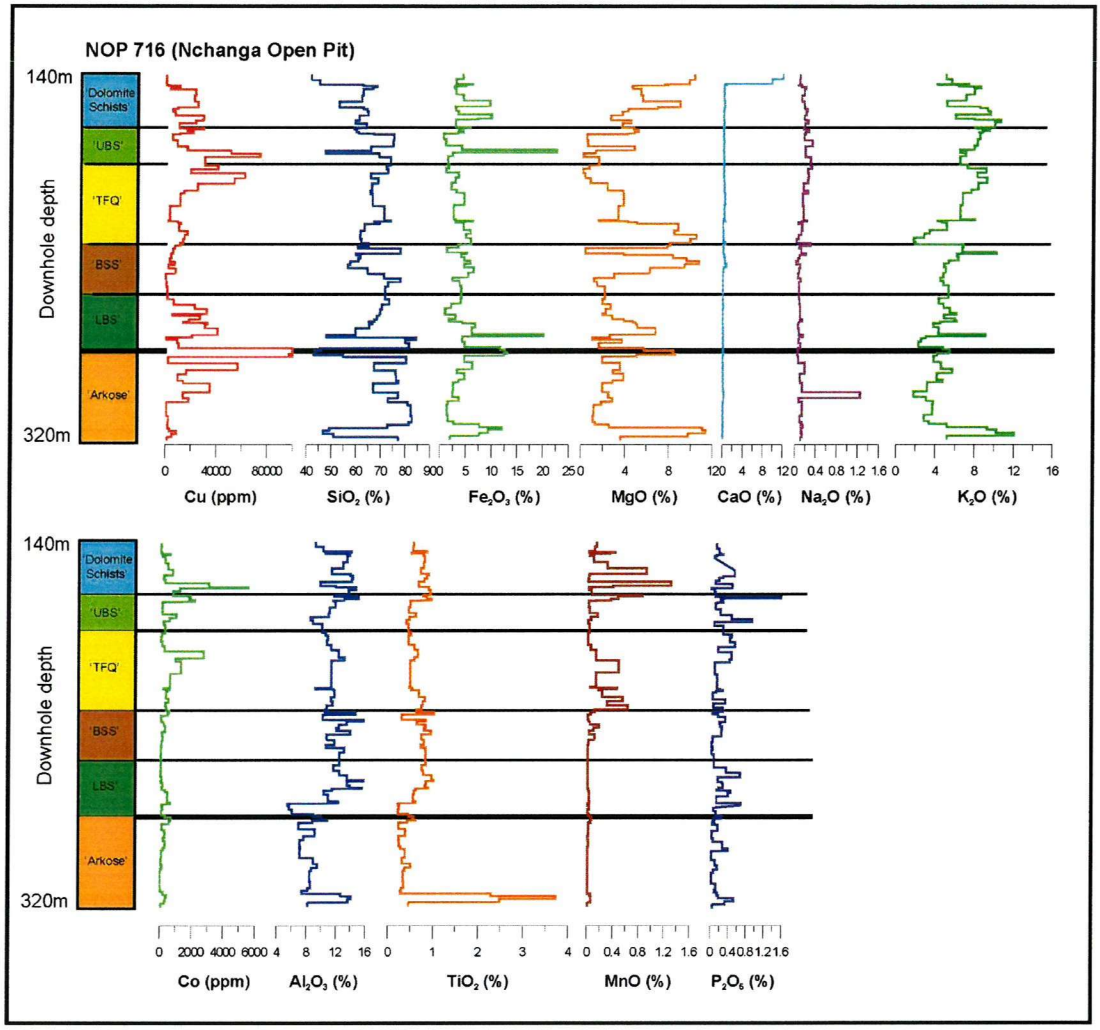

Figure 4.19: Major element concentrations (wt%) plotted with copper and cobalt (ppm) down depth for borehole NOP716, through Lower and Upper Orebodies, Nchanga Open Pit.

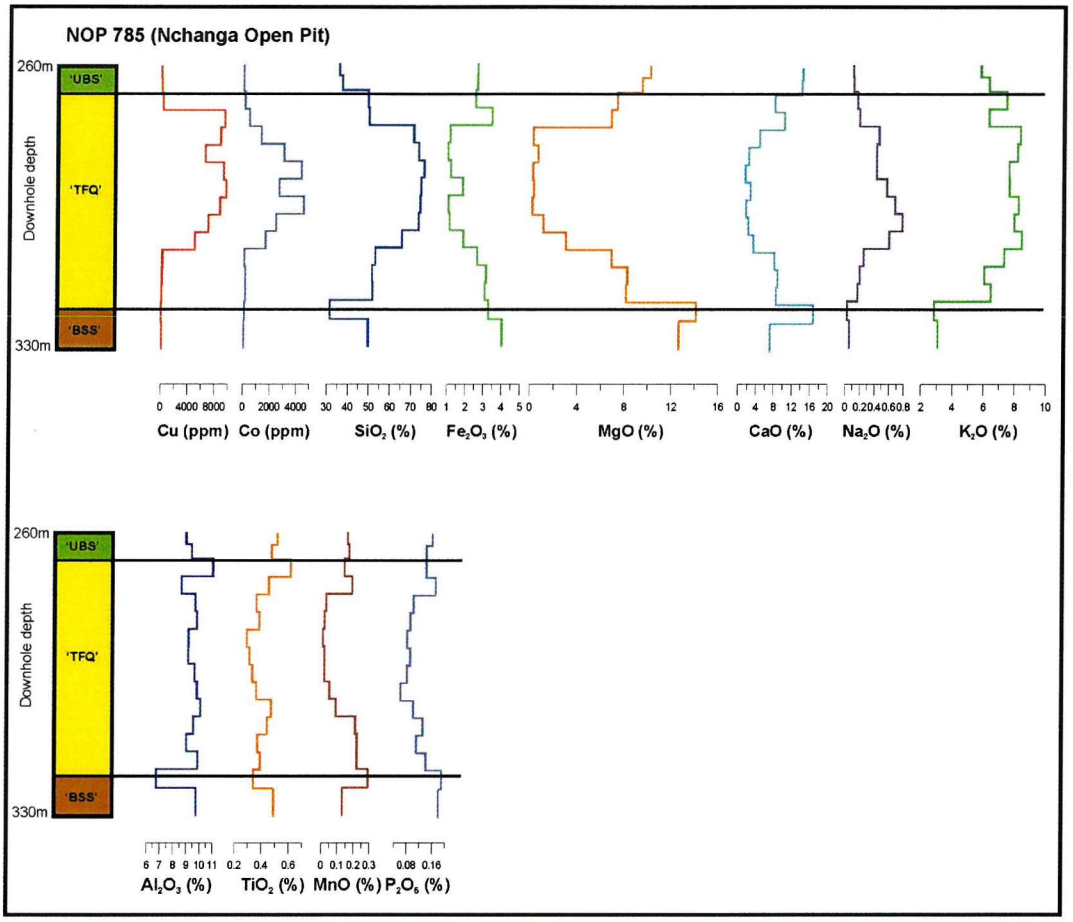

Figure 4.20: Major element concentrations (wt%) plotted with copper and cobalt (ppm) down depth for borehole NOP785, through the Upper Orebody, Nchanga Open Pit.

Selected trace element and base metal concentrations across the Lower Orebody show evidence for enrichment of Mo, Zn, U, As, Bi, Ba, and possibly V (Figs. 4.21, 4.22, & 4.23).

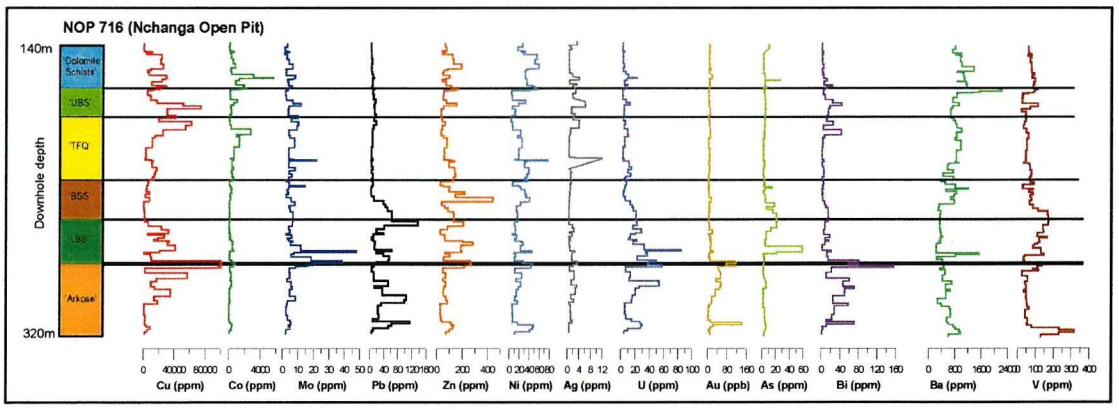

Figure 4.21: Selected base metal and trace element concentrations plotted down depth for borehole NOP716 (Nchanga Open Pit).

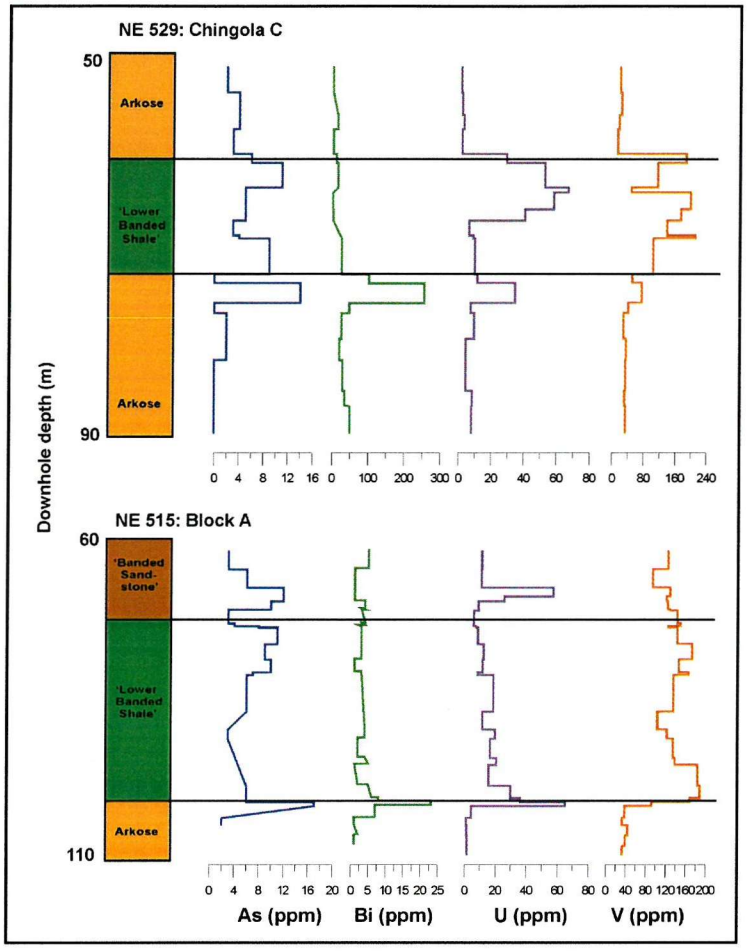

Figure 4.22: As, Bi, U, and V concentrations down depth of boreholes NE529 and NE515 across the Lower Orebody copper zone (Chingola C and Block A respectively).

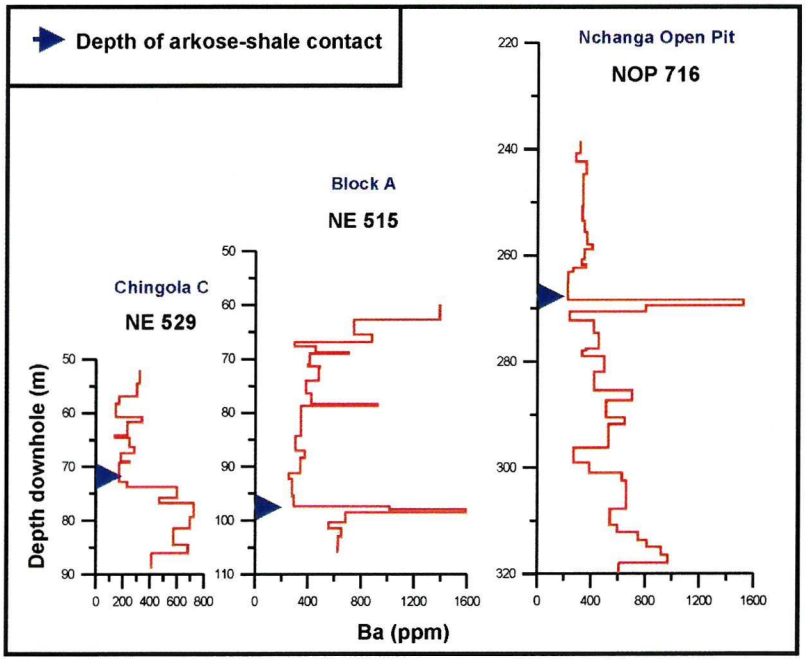

Figure 4.23: Barium concentrations down depth of boreholes NE529, NE515, and NOP716 across the Lower Orebody copper zone showing the exact location of the arkose-shale contact (Chingola C, Block A, and Nchanga Open Pit respectively).

These diagrams appear to show anomalous concentrations of certain elements directly at or just above the arkose-shale contact. Even gold, with average background values of 10-20ppb, increases to over 100ppb at the contact. Pb and Ag normally show very little correlation with Cu, although Zn and Ni often show minor increases in concentration where high-grade copper occurs, either as a part of the sulphides present or in the case of zinc as part of micas. Increases in As, U, Bi, V and Ba are common at the contact zone as shown in detailed plots across it (Figs. 4.22 & 4.23). Whereas with As, Bi and U the anomaly at the contact is very pronounced, with V it is less obvious and represents a broad increase in concentration, often at the base of the overlying shale. Ba concentrations within boreholes NE515 and NOP716 (Fig. 4.23) clearly show marked anomalies at the arkose-shale contact, a feature that was also noted by Sutton & Maynard (2002) in studies at the Konkola North deposit, Zambian Copperbelt. However, Ba appears to be depleted in the overlying shale based on the isocon plots (Appendix B6). Considering the abundance of phlogopite at the contact zone, Ba is thought to be a part of these micas and so taken out of the fluid at this stage. Bi, Mo, and As, are all probably held within sulphides present within the arkose and shale, whereas V is most likely a substitution in micas (Levinson, 1980).

Rare earth element (REE) data from borehole NOP716 (Nchanga Open Pit; Fig. 4.24) reveals only one anomalous concentration. The fact that all the plots are more or less identical suggests that the variations in the REE concentrations are a result of enrichment or depletion of other major components, e.g. SiO_2. Only Eu concentrations at the arkose-shale contact do not correspond with the other elements, and show a clear anomaly at the top of the arkose unit and base of overlying shale, corresponding strongly with high concentrations of copper.

Oxidation of mineralized samples has some effect on the major and trace element geochemistry. In fact, very little is enriched and many more elements are depleted, in particular copper. This suggests that fluid-rock interaction during oxidation may have consisted mainly of leaching of the material already present, hence causing depletion. This data further supports the idea that modification and enrichment of ore minerals took place during supergene processes that affected the Lower Orebody, particularly in close proximity to the ground surface (McKinnon & Smit, 1961). Leaching of copper sulphides may have taken place along with subsequent re-precipitation of malachite at the contact zone between the arkose and shale. It strongly supports the idea that the bleached zones at base of the 'Lower Banded Shale' unit (related to oxides) are a result of this supergene leaching rather than hydrothermal hypogene processes.

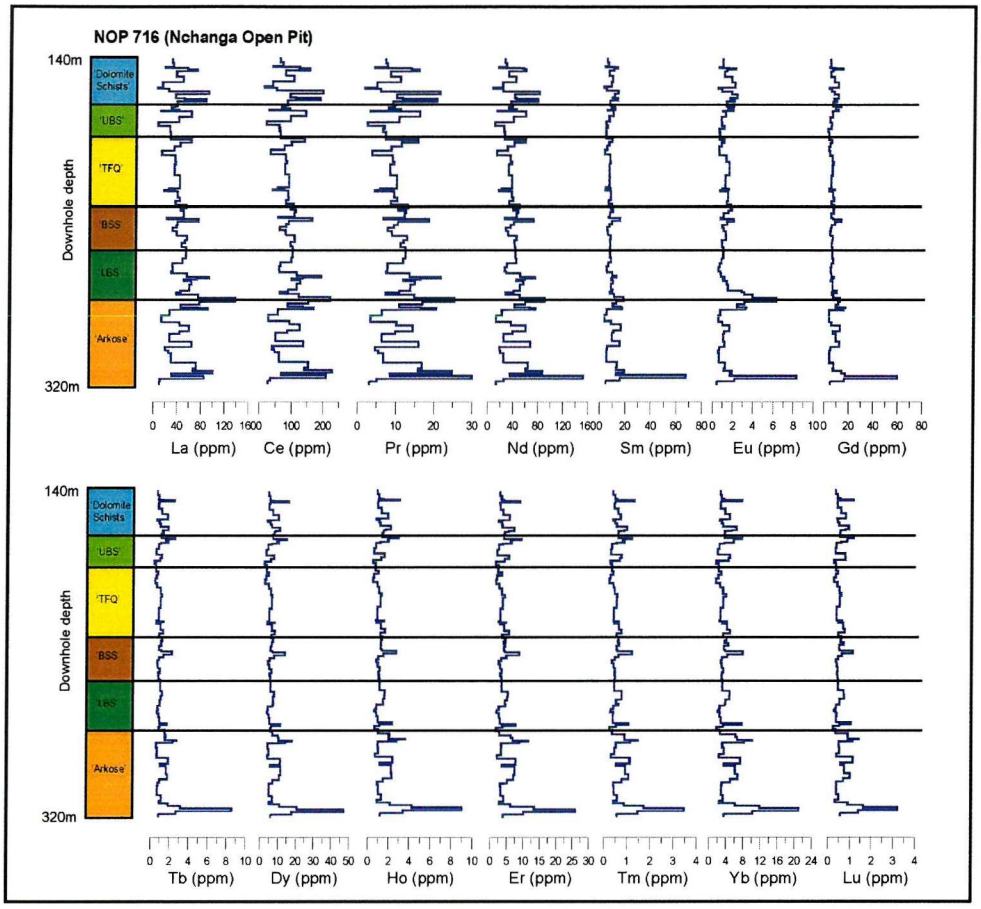

Figure 4.24: Rare earth element (REE) data down depth of borehole NOP716 (Nchanga Open Pit) showing Eu anomaly at the arkose-shale contact where Lower Orebody Cu is concentrated.

Down-hole plots of major element data for the Upper Orebody in boreholes NOP716 (copper-rich; Fig. 4.19) and NOP785 (cobalt-rich: Fig. 4.20) reveal high MgO (and often CaO) concentrations immediately below the high Cu and Co concentrations (i.e. the orebodies). These relate to the dolomite- and phlogopite-rich shear-zones within the 'Banded Sandstone' unit that underlie the host feldspathic arenite. Other major elements concentrations down-hole of NOP716 across the Upper Orebody (Fig. 4.19) reveal few trends in the data.

Within the Co-rich Upper Orebody, NOP785, CaO concentrations (3-9wt%) are high compared to that of other arkose/arenite rocks in the sequence (e.g. the arkose, 0.05-0.5wt%) due to the dolomite alteration within the arenitic host rock. They appear to be related to those of MgO but are not as pronounced, as they are only representative of the dolomite component, whereas the former is also present in phlogopite. MgO concentrations, although high where the phlogopite-rich shear zones occur beneath the orebody, are much lower across the mineralized zone. SiO_2 is also enriched within the host 'Feldspathic Quartzite' and strongly related to copper in borehole NOP785. This is thought to represent the adding of silica by an external fluid and the formation of small quartz veins (that host sulphides) that are observed

in many samples, in particular within fault-propagation fold zones. Na_2O and K_2O show broad increases over the host arenite ('TFQ'), the latter most likely a result of the K-feldspar component within the unit.

There appears to be very little information in the down-hole plots of trace element concentrations across the Upper Orebody (Figs. 4.21 & 4.25).

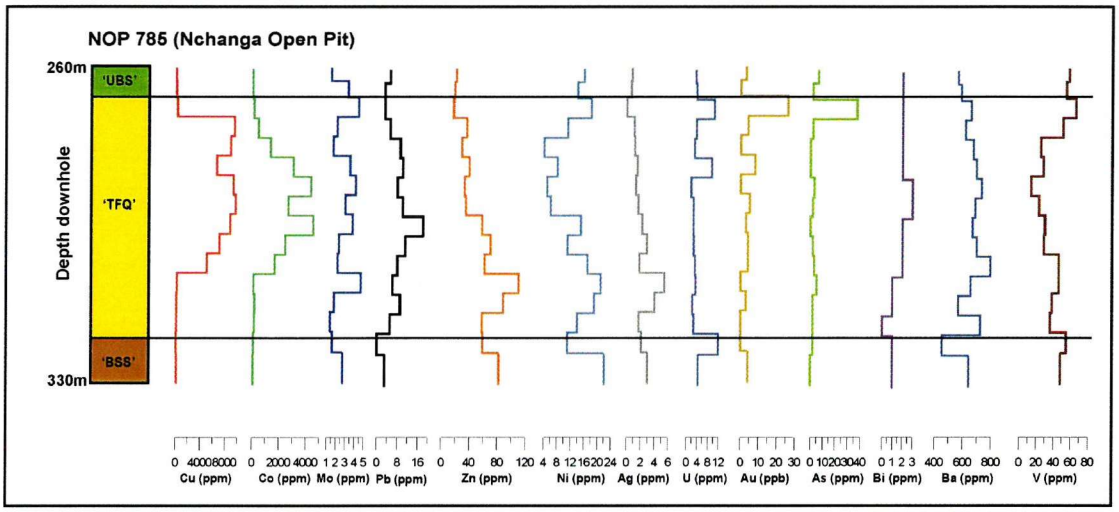

Figure 4.25: Selected base metal and trace element concentrations plotted down depth for borehole NOP785 (Nchanga Open Pit).

4.4 Summary

- A paragenetic sequence has been defined for the sulphide phases observed within both orebodies consisting of diagenetic pyrite replaced by bornite and chalcopyrite (and carrollite for the Upper Orebody) and later-stage chalcocite. Carrollite commonly appears to post-date copper sulphides. Sulphides (in particular within the Lower Orebody) have been overprinted by supergene mineralization consisting mostly of malachite and chrysocolla, indicative of oxidation of primary sulphide mineralization.

- Sulphides appear to be controlled by both lithology and structure, with indications that both natural and fracture-induced porosity promoted the arenaceous units as suitable host rocks. In many cases there is a strong alignment of sulphides to a developed structural fabric rather than any preserved sedimentary features, such as bedding.

- A potassic alteration assemblage has been identified associated with primary mineralization (and thrust structures), consisting mostly of phlogopite, quartz, and

sericite, with varying amounts of dolomite, tourmaline, rutile. Supergene modification of mineralization is accompanied by sericite, hematite, and muscovite.

The following summary statements can be made regarding the whole-rock and mineral geochemistry data presented above:

Lower Orebody:

- There are increases in MgO, Fe_2O_3, TiO_2, Mo, Zn, Bi, U, Ba, V, As, and Eu directly correlating with or as a halo around copper-rich zones.
- The redox boundary between arkose and overlying shale appears to control the abundance of U, Ba, As, V, and Eu.
- Oxidization of primary mineralization (i.e. malachite replacement) is accompanied by depletion in most elements including Cu.

Upper Orebody:

- There are increases in MgO, CaO, and SiO_2 (as well as minor enrichment of TiO_2 and MnO) with copper and cobalt mineralization, in particular significant increases in MgO and CaO immediately below ore zones.
- SiO_2 enrichment within ore zones reflects the addition of quartz to the host rock, mainly in the form of small quartz veins.
- Minor enrichment in U and Zn may have taken place but there appears to be no enrichment in the elements strongly associated with Lower Orebody mineralization, i.e. Bi, Ba, As, V, and Mo.
- There appears to be no significant geochemical differences between the copper- and cobalt-rich Upper Orebodies of boreholes NOP716 and NOP741 respectively.

General:

- Fault zones share many geochemical characteristics with ore zones, including enrichment in Cu (Co), MgO, and Fe_2O_3 (± CaO, MnO, Zn, Ba, Pb).
- 'Banded Sandstone' shear zones show major increases in MgO and CaO, reflecting the dolomite and phlogopite abundance within those zones.
- Although the alteration assemblages are strongly suggesting potassic alteration, there appears to be little information in the K_2O concentrations, possibly a result of small-scale changes being hidden by major concentration changes in MgO, CaO, Fe_2O_3, SiO_2, and Cu.
- The Fe content of phlogopites decreases upwards through the Nchanga system indicated by increasingly Mg-rich micas.

CHAPTER 5:

PALAEO-FLUID & STABLE ISOTOPE ANALYSIS

CHAPTER 5: PALAEO-FLUID AND STABLE ISOTOPE ANALYSIS

5.1 Introduction

Using the tectonic synthesis and detailed petrography (presented in Chapters 3 and 4) as a basis for the isotope analysis, and combining the isotope results with new fluid inclusion data, it is possible to determine the role that hydrothermal processes have played in the development of these hugely significant ore horizons, and critically test the syngenetic and epigenetic hypotheses.

5.2 Fluid inclusion analysis

An understanding of the fluids present within an ore-forming system contributes to our understanding of ore transport and deposition, by revealing such information as ore fluid temperature, pressure, composition, and salinity. Fluid inclusion analysis (in conjunction with oxygen isotope analysis) has been employed, as part of this Nchanga study, to investigate fluid inclusions from within vein quartz (that hosts sulphides) within the Lower and Upper Orebodies, and potentially sample the ore-forming fluid. In addition to this a number of tests were initiated (taking into account the basic assumptions of Roedder & Bodnar, 1997): (1) to compare the fluid inclusions from vein quartz within inverted D1 extensional structures with those within the sulphide-rich quartz veins within the ore zones; (2) to investigate the fluid inclusions within thrust-related vein quartz and compare to those within other vein quartz within the Nchanga sequence; and (3) to investigate any secondary fluids that were present within the Nchanga system (that could have potentially modified existing mineralization or introduced more metals into the system).

5.2.1 Sample selection and method

A total of thirty samples were selected from the groups of vein types outlined above. Following optical examination only eleven were selected for microthermometric analysis (Table 5.1) based on the quality of fluid inclusion populations, on hypotheses to be tested, and on the time available for this stage of the analytical work. Microthermometric analysis of fluid inclusions was carried out using the Linkam THM600 heating/freezing stage at the School of Ocean & Earth Science, University of Southampton. The temperature within the

stage and the state of the inclusion were continually monitored and measured variables included the degree of fill within an inclusion, and the temperatures at which certain phase changes take place (Shepherd *et al.,* 1985): (1) the first melting of the inclusion occurring after freezing (T_{FM}); (2) homogenization of the liquid and vapour (T_H); and (3) when any salt phases homogenize (e.g. halite or sylvite, T_S).

Vein type/location	Mineral	Sample numbers
Basement/arkose extensional structures	Quartz	NOP11, 17, 48
Lower Orebody ('Transition')	Quartz	NE529-6, L128-12, BA2, CB1
Upper Orebody (host sulphides)	Quartz	NOP741-21, 128, 731-13,
Thrust-related ('Banded Sandstone')	Quartz	NOP760-3

Table 5.1: Final selection of samples for fluid inclusion analysis and vein type.

5.2.2 Optical examination of fluid inclusions

Large, primary inclusions are commonly necked, and many that do appear to be undeformed are too small to achieve thermometric analysis. Secondary inclusions are commonly very small and, as a result, most of the fluid inclusion work concentrated on observing as many primary inclusions as possible, within a larger number of samples, and not on the different generations of secondary inclusions within single samples. The distribution, type, and description of quartz-hosted fluid inclusions from each of the vein types are discussed below.

Vein quartz associated with D1 extensional structures (within basement and arkose)

Fluid inclusion populations within basement granite-hosted veins consist of 5-15μm primary inclusions, many (80-90%) containing a halite salt phase (identified by its cubic habit; Shepherd *et al.*, 1985) that normally occupies 5 to 15% of the inclusion volume. The degree of fill typically ranges from 0.85 to 0.98. Other, smaller primary inclusions are two-phase aqueous inclusions, and several halite-bearing or aqueous two-phase inclusions show evidence for CO_2 being present ('bubble within a bubble;' Shepherd *et al.*, 1985). In addition to these, numerous secondary small inclusions (1-5μm) are located in trails. Many of these are two-phase aqueous inclusions, although some do contain salt phases, thought to be halite. Some of the larger inclusions are clearly necked. Within the arkose-hosted veins, primary inclusions are larger (5-40μm), although many of the larger ones (>25μm) are necked (Fig. 5.1A). Slightly smaller inclusions (20μm) are more commonly preserved and many (60-70%) show clear halite daughter phases (Fig. 5.1B); several show possible evidence for an extra daughter phases (Fig. 5.1C). Again, much smaller secondary inclusions, some containing

NaCl phases, are common in trails (Fig. 5.1D). These inclusions are often oblate in shape, compared to the much more irregular-shaped primary inclusions.

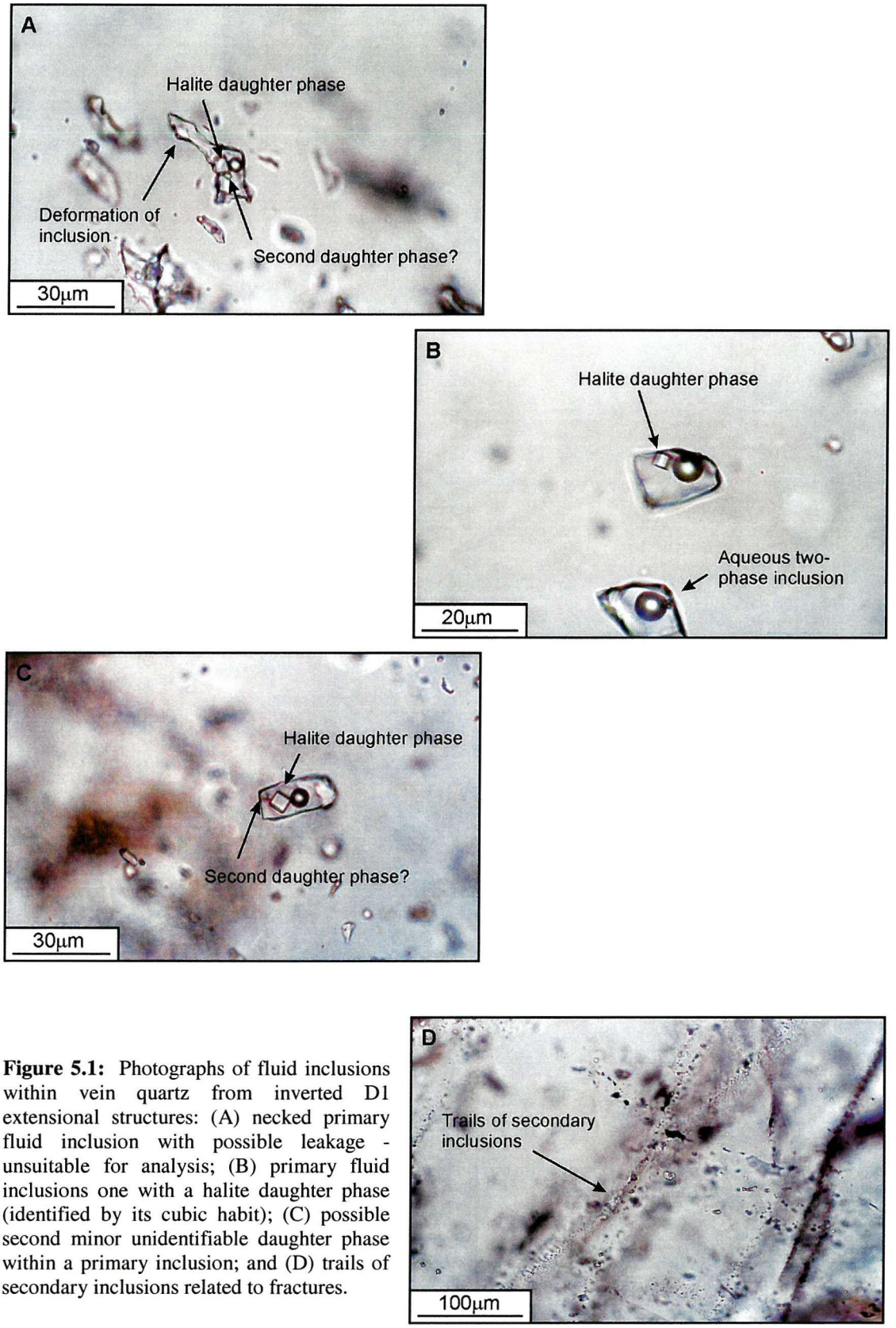

Figure 5.1: Photographs of fluid inclusions within vein quartz from inverted D1 extensional structures: (A) necked primary fluid inclusion with possible leakage - unsuitable for analysis; (B) primary fluid inclusions one with a halite daughter phase (identified by its cubic habit); (C) possible second minor unidentifiable daughter phase within a primary inclusion; and (D) trails of secondary inclusions related to fractures.

Vein quartz within the Lower Orebody ('Transition')

Rare, primary inclusions are relatively large (5-20μm across) and often contain a halite salt phase that occupies 2-10% of the inclusion (Fig. 5.2A). In some cases there is evidence for the presence of CO_2. However, primary inclusions are commonly necked and deformed, often in the orientation of the fractures within the sample, therefore, very few were suitable for thermometric analysis. Smaller (1-8μm) secondary inclusions within trails are common (Fig. 5.2B), many being two-phase aqueous inclusions (~70% of secondary population) but some containing a minor NaCl phase (5-10% of inclusion size). A fault-related vein quartz sample from Chingola B (sample CB1) contained a higher proportion of necked primary inclusions, as expected due to scale of deformation around this zone, and in general inclusions were much smaller (3-15μm). A greater proportion of inclusions followed trails and were two-phase aqueous secondary inclusions that were small and oblate-shaped.

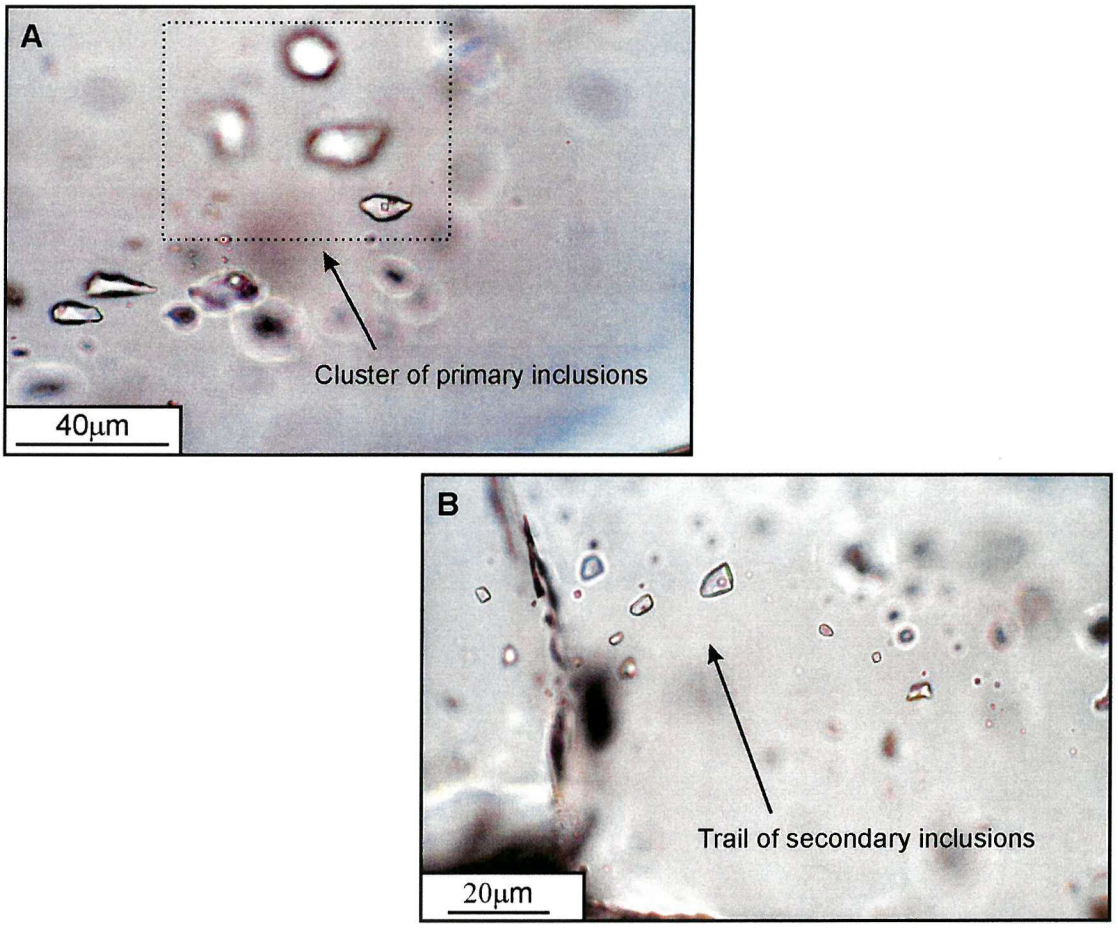

Figure 5.2: Photographs of fluid inclusions within vein quartz from the Lower Orebody 'Transition' unit: (A) primary inclusion with halite daughter phase, and (B) trail of secondary inclusions, mostly aqueous two-phase but some with halite daughter phases.

Vein quartz that hosts sulphides within the Upper Orebody

A typical fluid inclusion population for these samples consists of often isolated and fairly rare primary inclusions (that do not show evidence of necking; 5-20μm across) surrounded by relatively abundant trails of much smaller (normally <10μm, average ~ 3-4μm) secondary inclusions (Fig. 5.3A). Degrees of fill mostly range from 0.85 to 0.98. Evidence of leakage of larger inclusions is common (Fig. 5.3B), often appearing to be in the orientation of fractures (and hence trails of secondary inclusions). Approximately 60-70% of primary inclusions show a halite salt phase (a small number show evidence of a second minor salt phase) whereas fewer secondary inclusions contain any daughter phases. In some cases a moving 'bubble within a bubble' (Shepherd *et al.*, 1985) within primary inclusions represents the presence of CO_2. It is unknown whether this is the case within secondary inclusions due to their very small size.

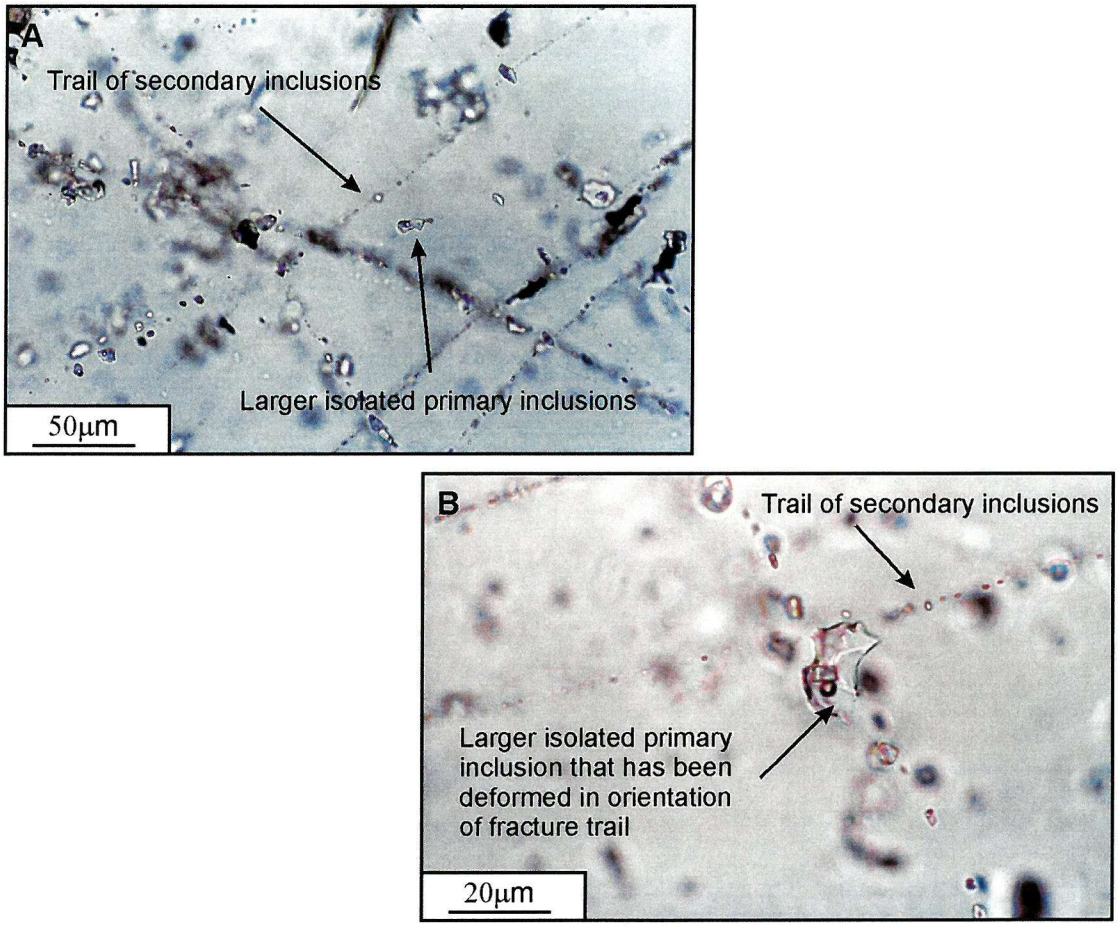

Figure 5.3: Photographs of fluid inclusions within layer-parallel quartz veins that host sulphides within the Upper Orebody: (A) typical population of inclusions with rare, isolated primary inclusions surrounded by trails of secondary inclusions, and (B) evidence of leakage and deformation of larger primary inclusions in the orientation of fractures.

Thrust-related vein quartz ('Banded Sandstone')

Only one sample was suitable for analysis from this group (NOP760-3). It contains a large number of mainly secondary but also several primary inclusions. The latter are commonly the largest within the population (average 10μm; Fig. 5.4A) with degrees of fill in the range of 0.85 to 0.95, although many have been deformed, and contain a halite daughter phases. Much more common are 5 to 12μm secondary inclusions that follow trails and commonly have a halite phase within them (5-10% of the inclusion volume; Fig. 5.4B).

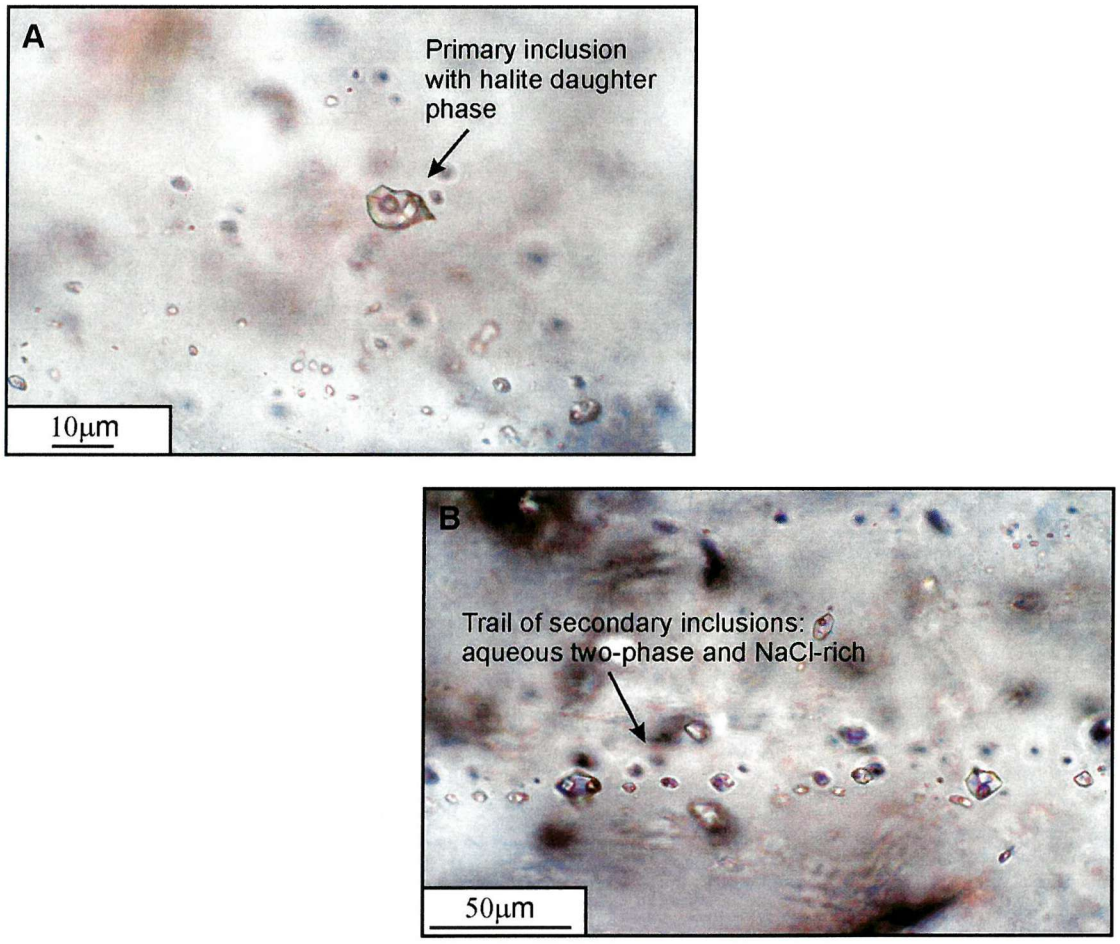

Figure 5.4: Photographs of fluid inclusions within vein quartz from a thrust-related shear-zone in the 'Banded Sandstone' unit: (A) primary inclusion with halite daughter phase, and (B) trail of secondary inclusions, most of them also containing a halite daughter phase.

5.2.3 Results of thermometric analysis

The temperature of first melting (T_{FM}), temperature of homogenization of the vapour phase (T_H), and the temperature of halite dissolution (T_S) were measured during analysis (Appendix C2). Calibration of the measuring equipment was achieved by carrying out thermometric analysis on (1) CO_2 melting within a synthetic CO_2 inclusion (-56.6°C), (2) ice melting of distilled water (0°C), and (3) melting of Phenacetin (135°C). A correction factor of 1.0074

was determined and was used on all thermometric results (Appendix C1). In general, most of the thermometric results are for primary inclusions, due to the small size of many secondary inclusions within trails and inability to accurately observe phase changes.

First melt temperatures (T_{FM} °C)

Due to the very small size of fluid inclusions, first melting temperatures were extremely difficult to measure, and distinguishing between first melt 'crazy paving' texture and the colour change that occurs within inclusions was, in some cases, unachievable. However, a number of T_{FM} measurements were made on the high-angle veins within the granite and arkose and bedding-parallel veins within the Lower and Upper Orebodies, which can be used in conjunction with the expected first melt (eutectic) temperatures listed by Shepherd *et al.* (1985; Table 5.2) for various salt-water systems (data from Borisenko, 1977). The T_{FM} values for high-angle veins within the granite and arkose are spread over a wide range and are somewhat ambiguous (Fig. 5.5). However veins from within the arkose, show two dominant ranges, from –34° to –37°C (n=7) and –51° to –57°C (n=10). These data suggest the presence of Na, Mg, Ca, and possibly Fe chlorides. A greater number of measurements would possibly identify a mode, and may constrain the composition of these fluids further. Solid CO_2 formed during freezing (<100°C) in only one inclusion and yielded a value for CO_2 clathrate melting of –56.8°C, suggesting any gas present was near-pure CO_2 (very close to pure CO_2 melting temperature of –56.6°C).

Salt system	Eutectic Temperature (°C)	Solid phases
H_2O-NaCl-$CaCl_2$	–55	Ice + NaCl.$2H_2O$ + $CaCl_2$.$6H_2O$
H_2O-MgCl2-$CaCl_2$	–52.2	Ice + $MgCl_2$.$12H_2O$ + $CaCl_2$.$6H_2O$
H_2O-KCl-$CaCl_2$	–50.5	Ice + $CaCl_2$.$6H_2O$
H_2O-$CaCl_2$	–49.5	Ice + $CaCl_2$.$6H_2O$
H_2O-Na_2CO_3-K_2CO_3	–37.0	Ice + $(K,Na)_2CO_3$.$6H_2O$ + K_2CO_3.$6H_2O$
H_2O-NaCl-$FeCl_2$	–37.0	Ice + NaCl.$2H_2O$ + $FeCl_2$.$6H_2O$
H_2O-$FeCl_2$	–35.0	Ice + $FeCl_2$.$6H_2O$
H_2O-NaCl-$MgCl_2$	–35.0	Ice + NaCl.$2H_2O$ + $MgCl_2$.$12H_2O$
H_2O-$MgCl_2$	–33.6	Ice + $MgCl_2$.$12H_2O$
H_2O-NaCl-KCl	–23.5	Ice + NaCl.$2H_2O$
H_2O-NaCl	–21.2	Ice + NaCl.$2H_2O$

Table 5.2: Eutectic temperatures of various salt-water systems and solid phases formed during freezing (Shepherd *et al.*, 1985 using the data of Borisenko, 1977).

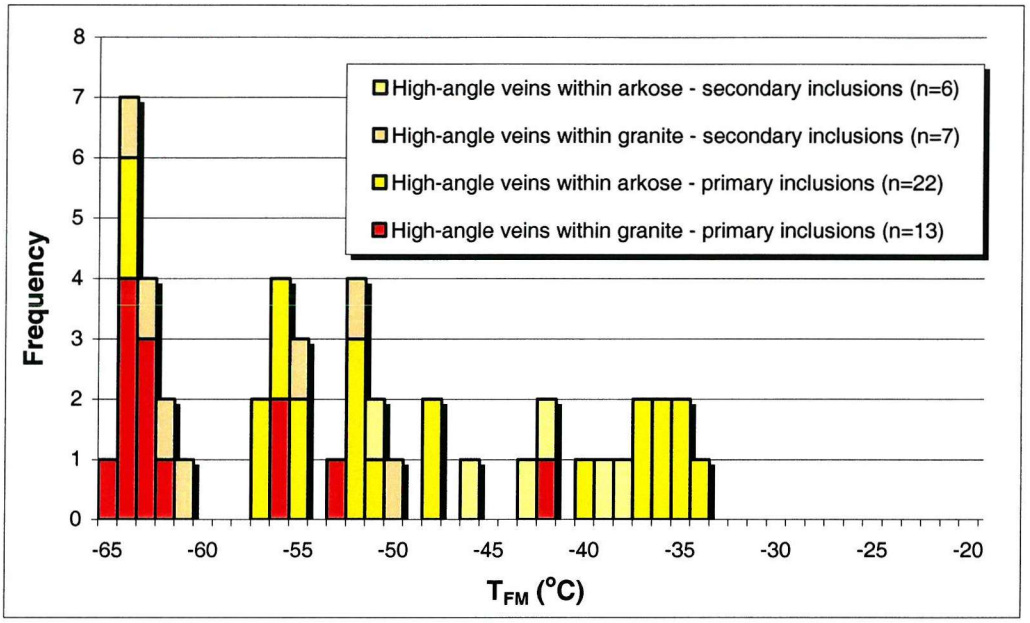

Figure 5.5: First-melt temperatures for primary and secondary inclusions within high-angle veins within the granite and arkose.

The T_{FM} results from the Lower and Upper Orebodies show a slightly more consistent pattern (Fig. 5.6). First melt temperatures from Lower Orebody inclusions tend to cluster around –35° to –37°C, with some more values at –39° to –43°C, although inclusions were rare within these veins and very few measurements could be taken. This again suggests the presence of Na, Mg, and possibly Fe chlorides during freezing and reheating to room temperature.

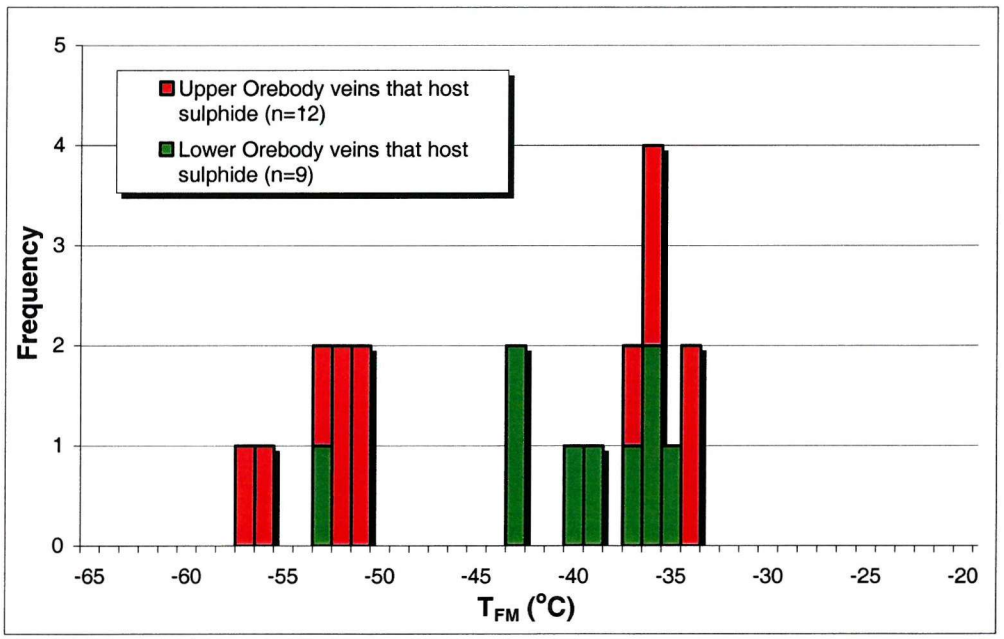

Figure 5.6: First-melt temperatures for primary inclusions within quartz veins from the Lower and Upper Orebodies.

The Upper Orebody T_{FM} values, like the high-angle veins within the arkose, show two dominant ranges from –34° to –36°C and –51° to –53°C (Fig. 5.6). Again these are indicative of the presence of Na, Mg, and Ca chlorides. In general, inclusions were only saturated with respect to NaCl, but the presence of minor, unidentified second daughter phases within a very small number of inclusions within the Upper Orebody may represent salts of one or more of these other components. One inclusion yielded a melting temperature for solid CO_2 of –56.4°C, again suggesting that that gas present was almost pure CO_2.

Homogenization temperatures (T_H °C)

By far the easiest inclusions to measure were those within the high-angle veins within the granite basement and overlying arkose, and in total sixty three primary and thirty secondary inclusions were analysed thermometrically (Fig. 5.7). A broad range of temperatures has been obtained, with primary inclusions within the granite and arkose yielding temperature ranges (for vapour to liquid phases change) of 105°-245°C and 140°-300°C respectively. Secondary inclusions within these veins show T_H ranges of 110°-160°C and 150°-180°C (mode = 170°C).

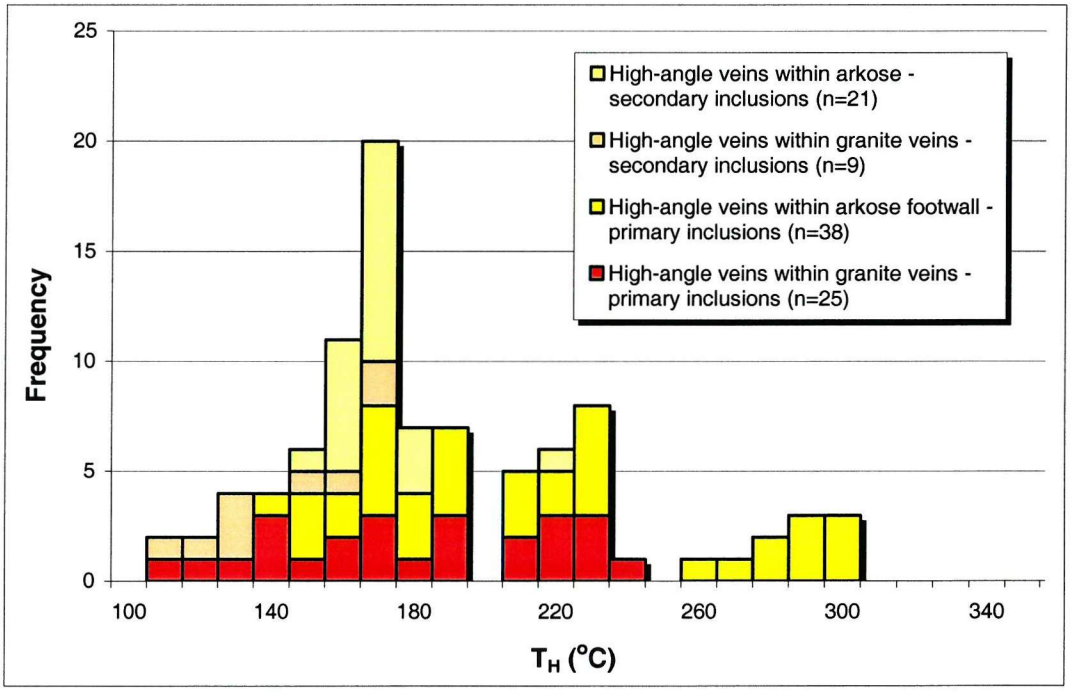

Figure 5.7: Homogenization (T_H) temperatures (for vapour to liquid phase change) for primary and secondary inclusions within high-angle veins from the granite and arkose units.

However, considering the secondary inclusion data, it appears more likely that many of the inclusions that were treated as primary (110°-180°C) may have, in fact, been secondary. If this is true then two more representative populations would be a primary population at 200° to

240°C (with a mode of 230°C) and a secondary population at 110° to 190°C (with a mode of 170°C). It is not known, with the relatively small amount of data, where the higher range of primary-inclusion T_H values within the arkose (260° to 300°C) fits into this. It is possible that they may represent a higher-temperature secondary phase.

Inclusions from within the Lower Orebody 'Transition' unit are rare and so within most samples were either absent or deformed. Only one sample (NE529-6) yielded any results that show a pattern that can be treated with confidence (Fig. 5.8). The data show a range of temperatures (vapour to liquid) from 140° to 220°C, with a clear mode of 180°C. The few results from other samples show no pattern and so are not considered here. However, primary and secondary inclusions from within vein quartz (that hosts sulphides) within the Upper Orebody were much more common and homogenization measurements could be made with more confidence. The T_H (vapour to liquid) data for two samples (Fig. 5.9) show a range of temperatures for primary inclusions of 130° to 220°C (mode of 160°C), and a range of 100° to 150°C (mode of 130°C) for secondary inclusions from within trails. Again the presence of a very small amount of CO_2 in some inclusions may have been the cause for decrepitation before true homogenization.

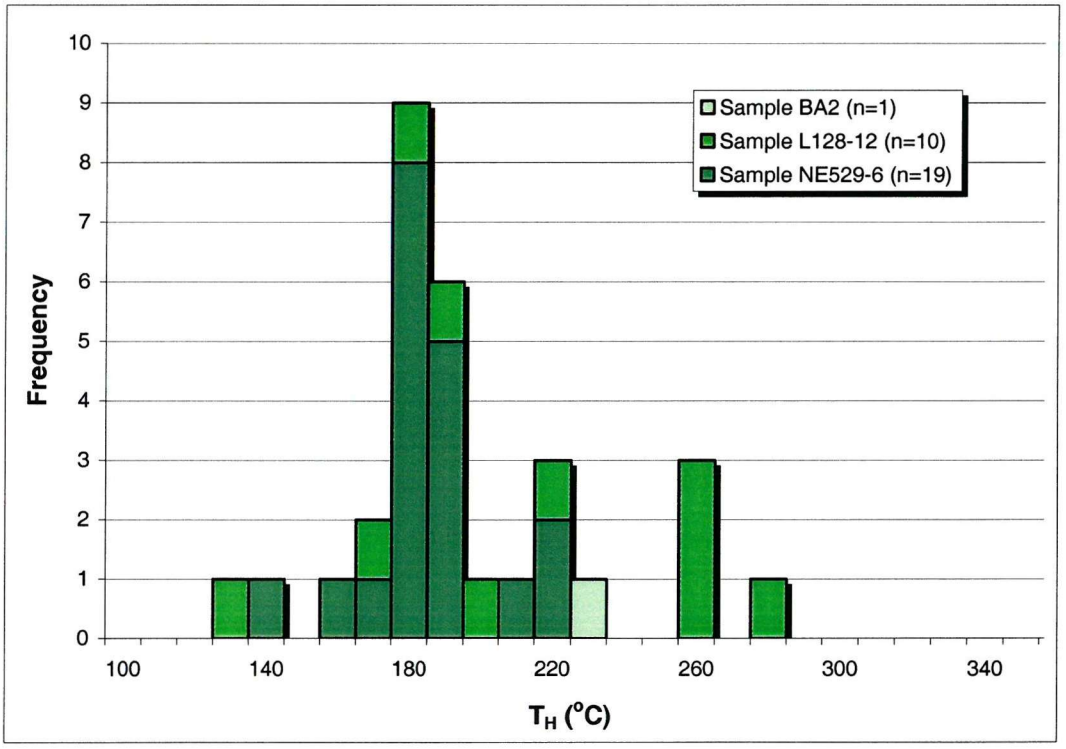

Figure 5.8: Homogenization (T_H) temperatures (vapour to liquid) from primary inclusions within three vein quartz samples from the Lower Orebody 'Transition' unit associated with mineralization.

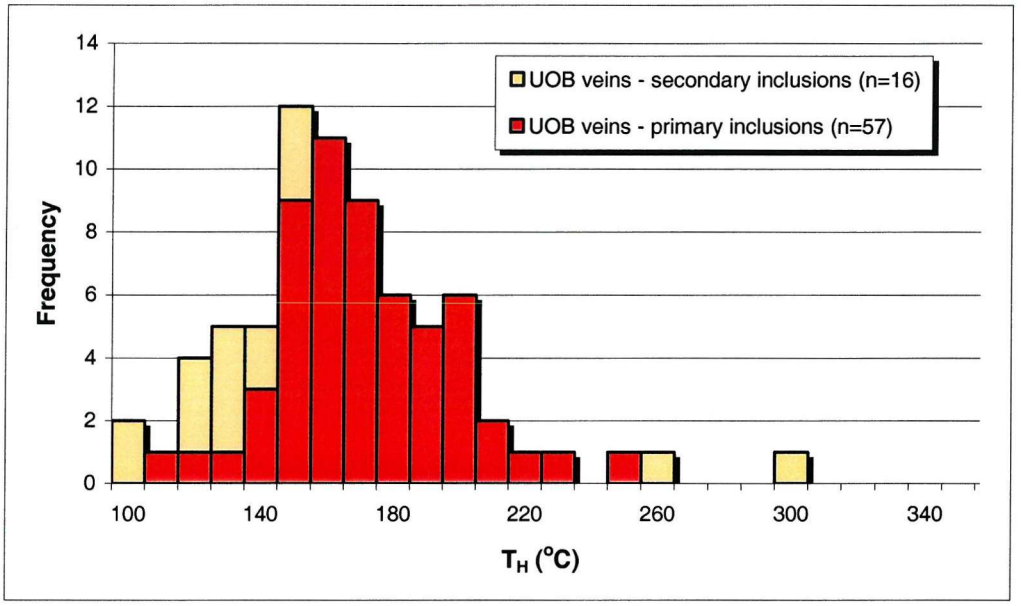

Figure 5.9: Homogenization (T_H) temperatures (vapour to liquid) of inclusions within layer-parallel quartz veins (that host sulphides) from the Upper Orebody (samples NOP128 and NOP741-21).

Finally, one sample (NOP760-3) of vein quartz from a thrust-related shear zone within the 'Banded Sandstone' unit, Nchanga Open Pit, yielded fourteen primary-inclusion homogenization temperatures (no measurements were possible on secondary inclusions). These data revealed slightly higher temperatures than those within the orebodies on either side of this unit (Fig. 5.10) with a clear range of temperatures of 190° to 280°C, and a mode of 240°C.

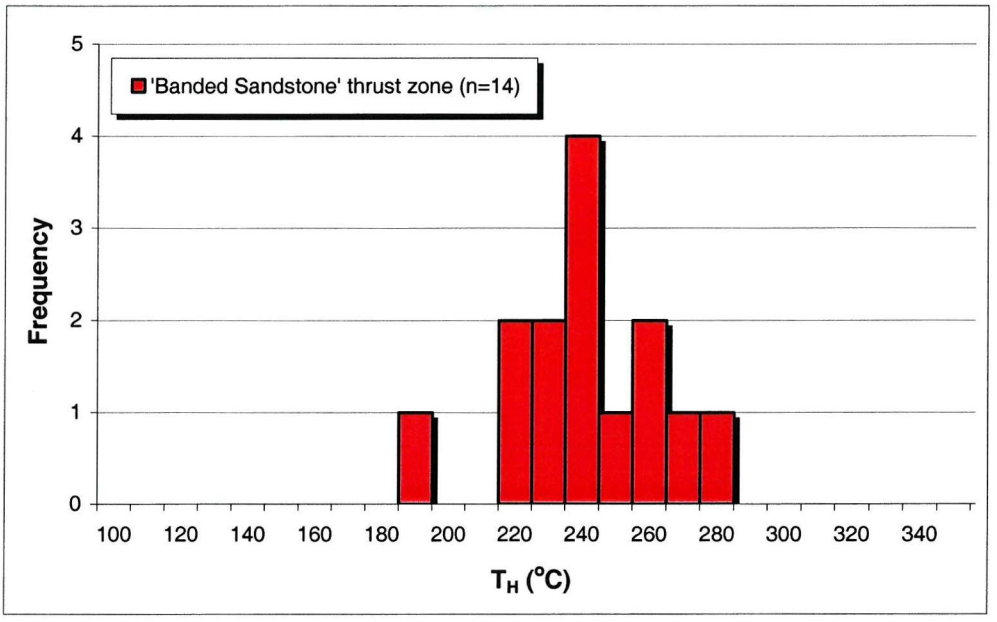

Figure 5.10: Homogenization (T_H) temperatures (vapour to liquid) of inclusions from vein quartz (sample NOP760-3) associated with a thrust zone within the 'Banded Sandstone' unit, Nchanga Open Pit.

Salinity

The salinity of inclusion fluids, unsaturated with respect to halite, can be calculated for the $NaCl-H_2O$ binary system by measuring the freezing point depression, the amount by which the ice melting temperature is decreased by the presence of NaCl (equation 5.1; Bodnar, 1993):

Equation 5.1: $$\text{Salinity (equiv. wt\% NaCl)} = 1.78\theta - 0.0442\theta^2 + 0.000557\theta^3$$

Where θ = the freezing point depression measured as degrees Celsius below 0°C at which ice melts

However, where the fluids are saturated with respect to NaCl a different equation is used to calculate the salinity by measuring the temperature at which halite dissolves during heating (equation 5.2: Sterner *et al.*, 1988).

Equation 5.2: $$\text{Salinity (equiv. wt\% NaCl)} = 26.242 + 0.4928\gamma + 1.42\gamma^2 - 0.223\gamma^3 + 0.04129\gamma^4 + 0.006295\gamma^5 - 0.001967\gamma^6 + 0.0001112\gamma^7$$

Where γ = the dissolution temperature of the halite daughter phases (T°C/100)

Almost all salinity measurements were made on primary inclusions, except for a small number of values for secondary inclusions within vein quartz from high-angle structures within the granite. The salinities recorded in this study are high (generally >30 equivalent wt% NaCl) within each of the vein types described above (Figs. 5.11 & 5.12). The broad range of values for the high-angle veins within the granite and arkose is also reflected in the salinity data (Fig. 5.11) which occupy much broader temperature-salinity fields than the Lower and Upper Orebody and thrust-related quartz vein data (Fig. 5.12). Primary fluid salinities range from ~31-36 equivalent wt% NaCl for granite high-angle veins, ~30-38 equivalent wt% NaCl for arkose high-angle veins, ~33-35 equivalent wt% NaCl for a thrust-related quartz vein, and ~30-32 equivalent wt% and ~30-34 equivalent wt% NaCl for Lower Orebody and Upper Orebody veins respectively. High-angle and thrust-related fault vein samples are hotter and more saline, particularly the thrust-zone sample within the 'Banded Sandstone' unit. In contrast the orebody vein samples generally reveal much more compact distributions and slightly decreased salinities and temperatures (averaging approximately 50°C and 2 equivalent wt% NaCl lower). In reality, the salinity measurement can only be given as approximations as the above calculation (Equation 5.2) is reportedly only accurate

where T_H is after T_S (Wilkinson, *pers. Comm.*), and at T_H temperatures greater than 300°C an error of ~5 wt% NaCl is likely (Sterner *et al.*, 1988)

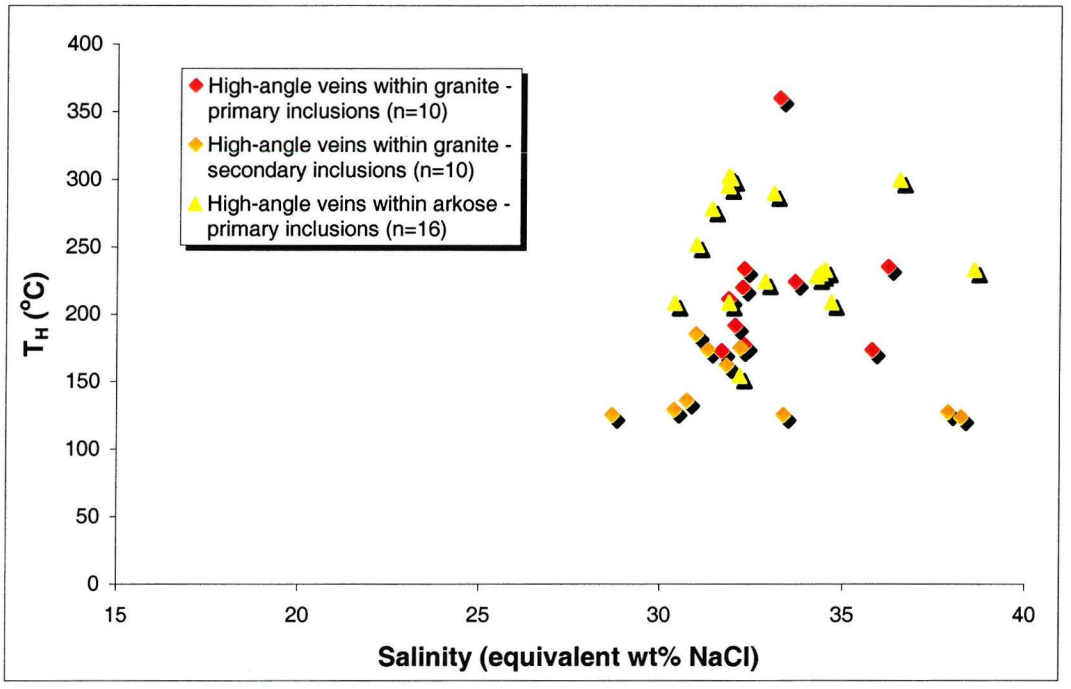

Figure 5.11: Salinity-temperature plot for fluid inclusion data for vein quartz from high-angle fault zones within the granite and arkose units.

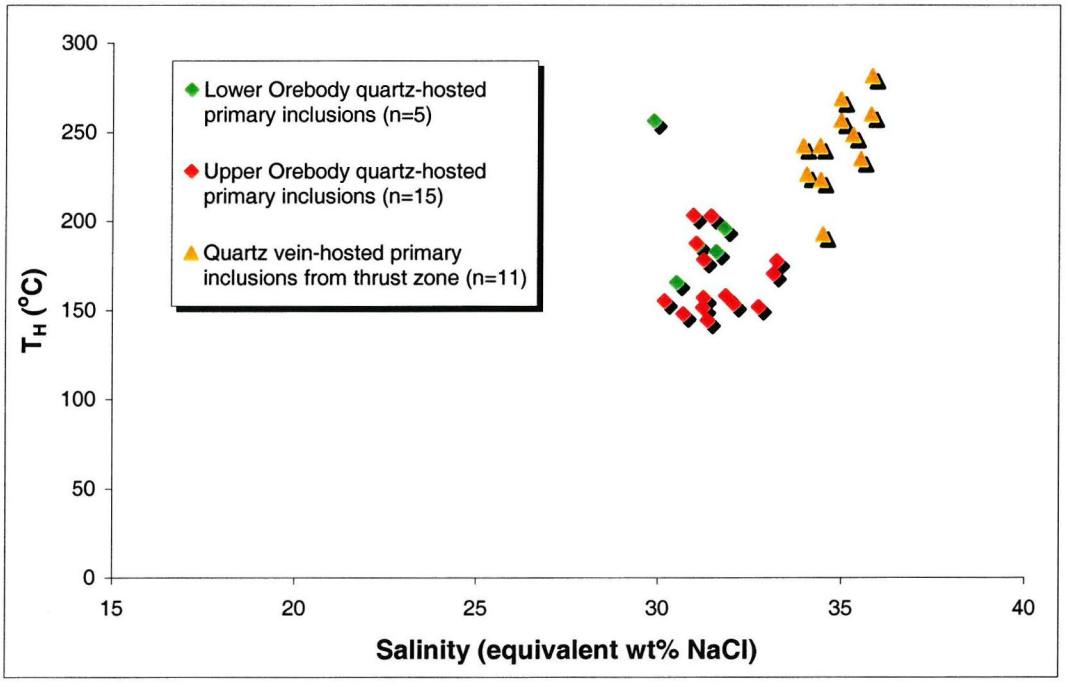

Figure 5.12: Salinity-temperature plot of fluid inclusion data for Lower Orebody 'Transition' quartz veins, Upper Orebody veins that host sulphide, and thrust-related veins.

These relationships are evident in a summary diagram of the various temperature-salinity fields, taking out some of the very high or low results that do not fit into the rest of the data and may have been a result of leakage of inclusions (Fig. 5.13). The similarity between the data from both orebodies is evident, although the Lower Orebody field is only based on four results. The data from high-angle veins and low-angle thrust-related veins appears to occupy similar broad fields.

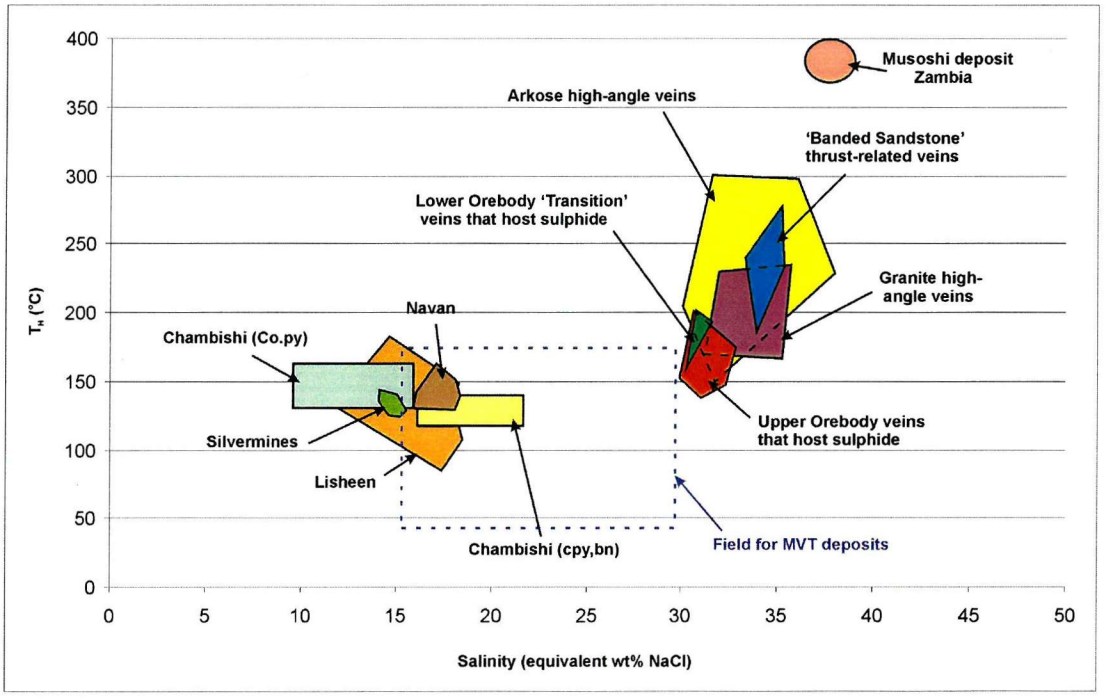

Figure 5.13: Summary diagram and salinity-temperature fields of fluid inclusion data generated during this Nchanga study, compared to fluid inclusion data from the Chambishi and Musoshi deposits, Zambia (Annels, 1989; Richards *et al.*, 1988), some Irish Pb-Zn orefield deposits, and classic Mississippi Valley Type fluids (Trude & Wilkinson, 2001).

5.2.4 Previous Copperbelt fluid inclusion data

Fluid inclusion data for deposits of the Zambian Copperbelt are rare considering the significance of these metal-rich ore horizons and the widespread use of fluid inclusion analysis in the study of ore deposits. Annels (1989) cited the fluid inclusion work of Cunningham (1986) on samples from both Chambishi and Chambishi Southeast, which aimed to investigate the temperature of mineralization using subconcordant quartz veins and nodules that host sulphides, much like the ones described from Nchanga during this study. As has been predicted at Nchanga, Annels (1989) argued that quartz veins (and associated sulphides) are introduced at the same time as 'disseminated' sulphides due to identical mineralogy between host rock and veins and similar sulphur isotope compositions (see section 5.4). Annels (1989) suggested ranges of ore fluid temperatures and salinities of 130°-165°C and 9-

16% for veins associated with 'early' pyrite and carrollite, and 125°-145°C and 16-22% for 'later' copper sulphides (chalcopyrite and bornite; Fig. 5.13), which contrast with the much higher salinity and slightly higher T_H fluids identified at Nchanga. However, the paragenesis of sulphides suggested by Annels (1989) does not conform with the petrography carried out during this study and so care must be taken with the different temperatures that have been determined and how they are compared to the Nchanga data. Richards *et al.* (1988) carried out fluid inclusion studies at the Musoshi deposit in Zambia, obtaining data from vertical quartz-hematite vein arrays from within the footwall arkoses, which, from the description, appear to be very similar to the high-angle structures observed at Nchanga from within the same unit. They suggested that the fluids had a temperature of approximately 395 ± 5°C, with 39wt% NaCl, 15wt% KCl, and minor amounts of CO_2 (Fig. 5.13), which are significantly higher in temperature and slightly higher in salinity than the Nchanga fluids. These temperatures are taken from the dissolution of the halite phase present, which Richards *et al.* (1988) claimed is representative of the true trapping temperature of the fluid, whereas their T_H data ranges from 335° to 380°C (these are quoted as the minimum trapping temperatures). The Nchanga data, when compared to brines from another classic sediment-hosted base metal district, the Irish Pb-Zn orefield, shows much higher salinities and moderately higher temperatures (Fig. 5.13).

5.3 Oxygen isotopes

In total twenty nine samples were selected in order to investigate the $\delta^{18}O$ (relative to Standard Mean Ocean Water, SMOW) of any hydrothermal fluids that had been present within the mineralizing system and, in conjunction with the fluid inclusion results, further understand their source and evolution. The following were investigated: (1) the $\delta^{18}O$ of quartz veins that host ore sulphides to investigate the nature of any potential ore-forming hydrothermal fluid; (2) the $\delta^{18}O$ of the high-angle basement veins compared to that of the veins within the Lower Roan sequence to test whether they are products of the same fluid event and hence the same origin; and (3) the $\delta^{18}O$ of detrital quartz grains, recrystallized quartz grains, and vein quartz to test whether recrystallized grains were formed by the same fluid as the veins. In addition to the quartz separates, $\delta^{18}O$ values have been obtained for alteration dolomite from within the Upper Orebody (six samples) and thrust-related shear zone dolomite (two samples), that is thought to have been introduced at the same time as the vein quartz from within those zones, and marine dolomites (four samples) from the dolomite units higher in the Nchanga sequence. This allows a direct comparison between the different

dolomite types and may determine whether the same fluid could have been responsible for precipitation of both the dolomite and the quartz within these zones.

It is worth noting that $\delta^{18}O$ isotope analysis of minerals would normally be carried out in conjunction with deuterium isotope analysis (δD) of the same samples. This would further constrain the types of fluids within the Nchanga sequence, and would allow a much more detailed comparison with fluids described from other ore deposits in the literature. However, it is a pre-requisite for δD analysis of quartz separates that there must only be one generation of fluid inclusions within the sample (i.e. the primary inclusions). Following optical examination of fluid inclusions within the Nchanga quartz vein samples, it was clear that this could not be achieved with any degree of confidence.

5.3.1 Sample selection and method

Pure quartz separates were handpicked from each of the main vein- and rock-types: (1) high-angle veins within the granite and arkose, (2) veins that host sulphides within both orebodies, (3) thrust-related veins from within the 'Banded Sandstone' unit, (4) veins from within the 'Dolomitic Schist' unit above both orebodies, and (5) detrital and recrystallized quartz from within both the Lower and Upper Orebodies. The same samples that had been investigated for fluid inclusion characteristics were selected where possible. Approximately Img samples were fluorinated using a CO_2 laser and the liberated oxygen reacted with a carbon rod at high temperature to produce CO_2, which is the phase used for determination of the $\delta^{18}O$. Pure separates were obtained for the marine and shear zone dolomite samples, but this could not be achieved for the alteration dolomite samples, for which crushed whole rock samples were used. Although these samples would have contained a large amount of detrital and vein quartz, the $\delta^{18}O$ results solely represent the dolomite, as in sample preparation (see section 5.5.1) carbonates are reacted with 100% phosphoric acid, which does not dissolve silicate minerals. In each case only a few milligrams of sample are required for the analysis.

5.3.2 Results

Different vein samples reveal distinct $\delta^{18}O$ isotope signatures (Fig. 5.14; see Appendix D1 for data). Vein quartz within D1 extensional structures within the basement granite and arkose show $\delta^{18}O$ values of +11.3‰ to +12.5‰, with a mean of +11.9 ± 0.6‰ (n=3). Quartz veins within the Lower Orebody show variable $\delta^{18}O$ values, ranging from +12.3‰ to +21.2‰, with a mean of +17.2 ± 4.4‰ (n=4). However, the field relationships of one sample (BA2, $\delta^{18}O$ = +21.2‰) suggest that it could be a late feature, and so the two heavier values may be late-stage veins (with a mean of +20.5 ± 1.1‰), whereas the two lighter ones may be earlier (with

a $\delta^{18}O$ mean of +14.0 ± 2.3‰). Another possibility is that there is inter-orebody variability as the two heavier values are from the Block A Open Pit whereas the lighter values are from the Luano Open Pit and Chingola B Underground. This would require further investigation.

Low-angle veins (that host sulphides) within the Upper Orebody, show extremely consistent values, ranging from +13.7‰ to +14.5‰, with a mean of +14.0 ± 0.3‰ (n=9). Vein quartz from within the 'Banded Sandstone' units reveals a range of $\delta^{18}O$ of +15.1‰ to +19.2‰, with a mean of +16.8 ± 2.2‰ (n=3). However, again the heavier value represents a sample that appears to be a later-stage vein within the sheared unit ($\delta^{18}O$ = +19.2‰) whereas the two lighter values appear to be thrust-related veins, yielding a new mean of +15.6 ± 0.6‰ (n=2). Finally, quartz veins within the sheared 'Dolomitic Schist' units reveal the heaviest $\delta^{18}O$ values, ranging from +18.7‰ to +23.8‰, with a mean of +20.7 ± 2.7‰ (n=3).

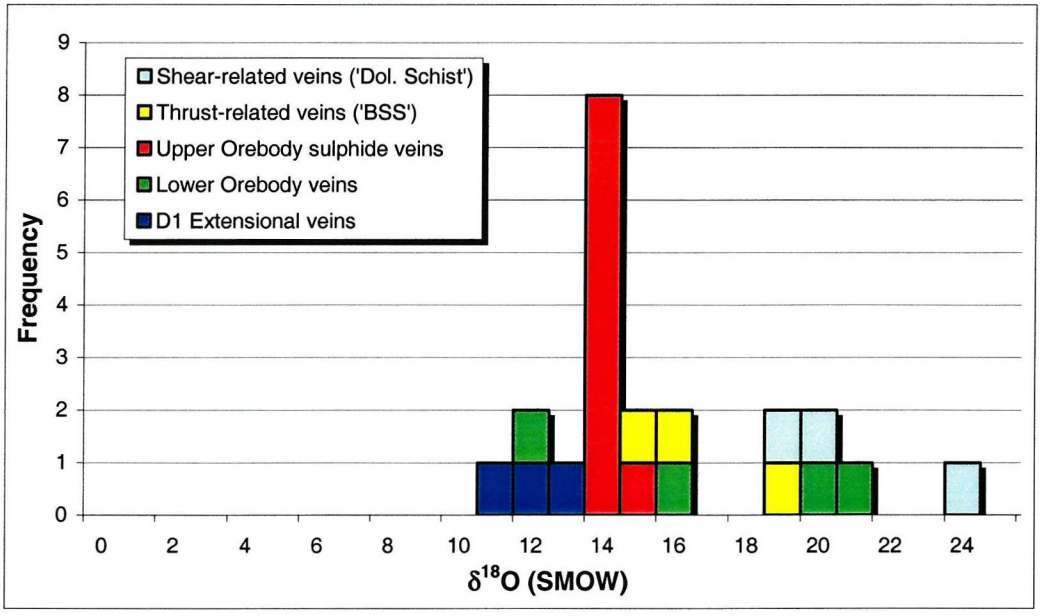

Figure 5.14: All $\delta^{18}O_{quartz}$ values obtained for different quartz vein types at Nchanga, comparing early veins associated with pre-Katangan, high-angle structures with sulphide-rich, thrust-related, and late-stage quartz veins ('BSS' = 'Banded Sandstone' unit).

The $\delta^{18}O$ values of detrital quartz, recrystallized detrital quartz within ore zones, and vein quartz are compared (Fig. 5.15). For each orebody, detrital quartz has the lowest $\delta^{18}O$ with values of +10.7‰ (n=1) for the Lower Orebody and +11.2‰ (n=1) for the Upper Orebody. However, recrystallized quartz within both ore zones has a heavier $\delta^{18}O$ than the detrital material with mean values of +12.7 ± 0.8‰ (n=2) for the Lower Orebody and +13.5 ± 0.8‰ (n=3) for the Upper Orebody, in both cases shifting towards the $\delta^{18}O$ signatures of quartz veins within the ore zones of +14.0 ± 2.3‰ (n=9) and +14.0 ± 0.3‰ (n=2) respectively.

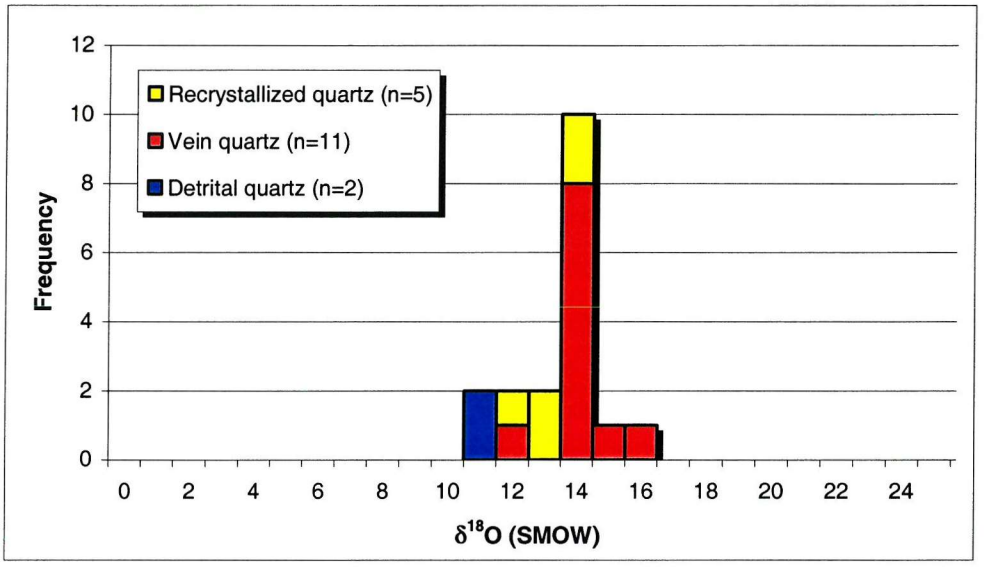

Figure 5.15: Histogram of $\delta^{18}O$ values obtained for quartz vein samples within the Lower and Upper Orebodies compared to detrital quartz from the original host unit and recrystallized quartz from within hydrothermally altered zones.

The $\delta^{18}O$ results from analysis of the dolomite samples (Fig. 5.16) show a clear distinction between the dolomites that are assumed to be marine with a range of +22.4‰ to +23.0‰ and a mean of +22.7 ± 0.2‰ (n=4) and those dolomites within shear-zones, which reveal a range of +16.3‰ to +16.9‰ and a mean of +16.6 ± 0.4‰ (n=2), and the dolomite alteration within the Upper Orebody which range from +11.7‰ to +14.0‰ with a mean of +13.1 ± 0.8‰.

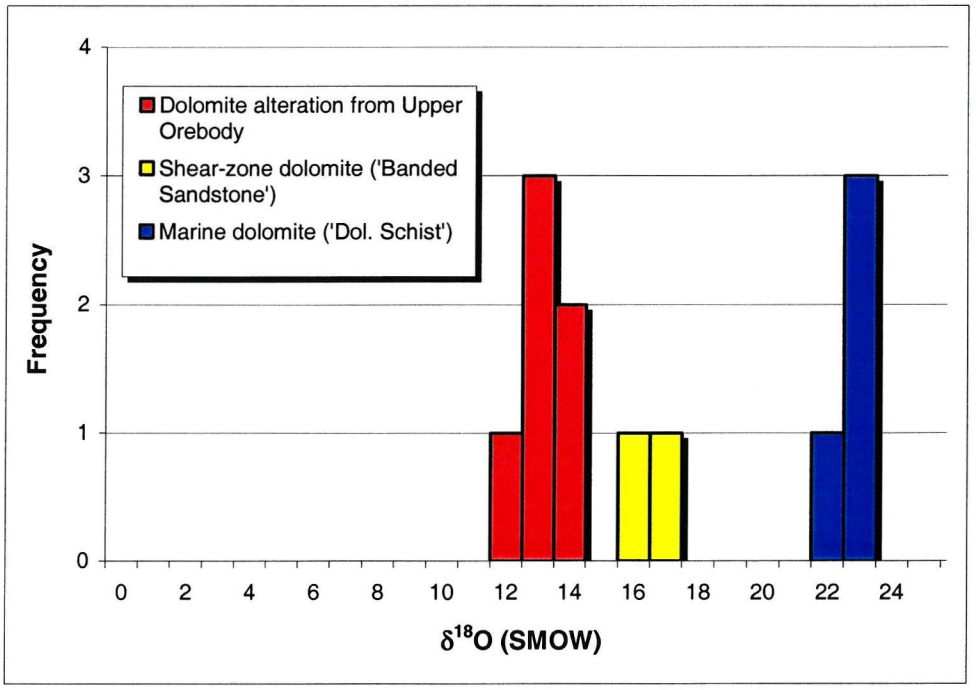

Figure 5.16: Histogram of $\delta^{18}O$ values for a small number of dolomite samples from marine dolomite to dolomite that occurs within ore zones and shear zones to test whether they have a common origin.

5.3.3 Calculation of fluid $\delta^{18}O$ in the quartz-H_2O and dolomite-H_2O systems

The difference in $\delta^{18}O$ values (relative to SMOW) between two phases with equilibrated oxygen and a common reservoir is a function of temperature (Faure, 1986; Taylor, 1979, 1997) and gives the useful approximation (equation 5.3; Faure, 1986; Zheng, 1993):

Equation 5.3: $$\mathbf{1000 \ln \alpha_{1/2} \approx \delta_1 - \delta_2 \approx A(10^6 T^{-2}) + B(10^3 T^{-1}) + C}$$

where: $\boldsymbol{\alpha_{1/2}}$ is the isotopic fractionation factor

$\boldsymbol{\delta_1}$ is the $\delta^{18}O$ value of material 1

$\boldsymbol{\delta_2}$ is the $\delta^{18}O$ value of material 2

T is the calculated temperature of formation (T_H) in degrees Kelvin

A, B and **C** are experimentally derived constants

Therefore, for a measured $\delta^{18}O$ of quartz the $\delta^{18}O$ of the fluid can be calculated for a given temperature (experimentally measured by fluid inclusion analysis) by using the quartz-H_2O equilibrium isotope fractionation. This isotope thermometer is based on three assumptions: (1) the two phases were in equilibrium with each other; (2) no subsequent change to the isotopic compositions took place after equilibrium, and (3) the temperature dependence of the fractionation factors (i.e. the constants in the above calculation) have been determined experimentally (Faure, 1986). A number of different authors have calculated different constants to be inserted into equation 5.3 for the fractionation between quartz and water (Table 5.3), where the constant B (Equation 5.3) is normally given as zero.

Reference	Temp. range °C	A	C	1000lnα if T = 200°C	$\delta^{18}O_{(fluid)}$ if $\delta^{18}O_{(qtz)}$ = 15‰
Friedman & O'Neil (1977)	200-500	3.380	–2.90	12.198	2.8
Matsuhisa *et al.* (1979)	250-500	3.340	–3.31	11.609	3.4
Sharp & Kirschner (1994)	> 100	3.650	–2.90	13.404	1.6
Zhang *et al.* (1989)	180-550	3.306	–2.71	12.057	2.9
Zheng (1993)	0-1200	4.480	1.71	11.640*	3.4

Table 5.3: Different $\delta^{18}O$ fractionation factors for the quartz-H_2O system and the $\delta^{18}O_{(fluid)}$ calculated using them if $\delta^{18}O_{(qtz)}$ = 15‰. (*Zheng (1993) uses a constant for B of –4.770).

Different constants are used in the same equation to calculate the $\delta^{18}O$ of fluids that precipitated dolomite, with the constant B again taken as zero (Table 5.4). Temperatures can be obtained from the same fluid inclusion temperatures taken from vein quartz within the Upper Orebody and 'Banded Sandstone' shear zones, as it is assumed that they formed at the

same time and from the same fluid (i.e. they were in equilibrium during precipitation). The same equations are normally used for temperatures lower than the ones quoted for the calculation of the fractionation factors, although the error involved in this must be taken into account.

Reference	Temp. range °C	A	C	1000lnα if T = 200°C	$\delta^{18}O_{(fluid)}$ if $\delta^{18}O_{(dol)}$ = 15‰
Friedman & O'Neil (1977)	300-510	3.200	–1.50	12.794	2.2
Golyshev *et al.* (1981)	100-650	3.260	–4.51	10.052	4.9
Land (1983)		3.340	–3.34	11.579	3.4
Zheng (1999)	0-1200	4.060	1.71	10.018	5.0

Table 5.4: Different $\delta^{18}O$ fractionation factors for the dolomite-H_2O system and the $\delta^{18}O_{(fluid)}$ calculated using these factors if $\delta^{18}O_{(dol)}$ = +15‰. (*Zheng (1999) uses a constant for B of –4.650).

In this study, the fractionation factors of Matsuhisa *et al.* (1979) and Land (1983) are used. This $\delta^{18}O_{fluid}$-$\delta^{18}O_{mineral}$-temperature relationship can be represented graphically for each mineral (Fig. 5.17) and provides a rapid estimation of the fluid $\delta^{18}O_{fluid}$ when the other parameters are known.

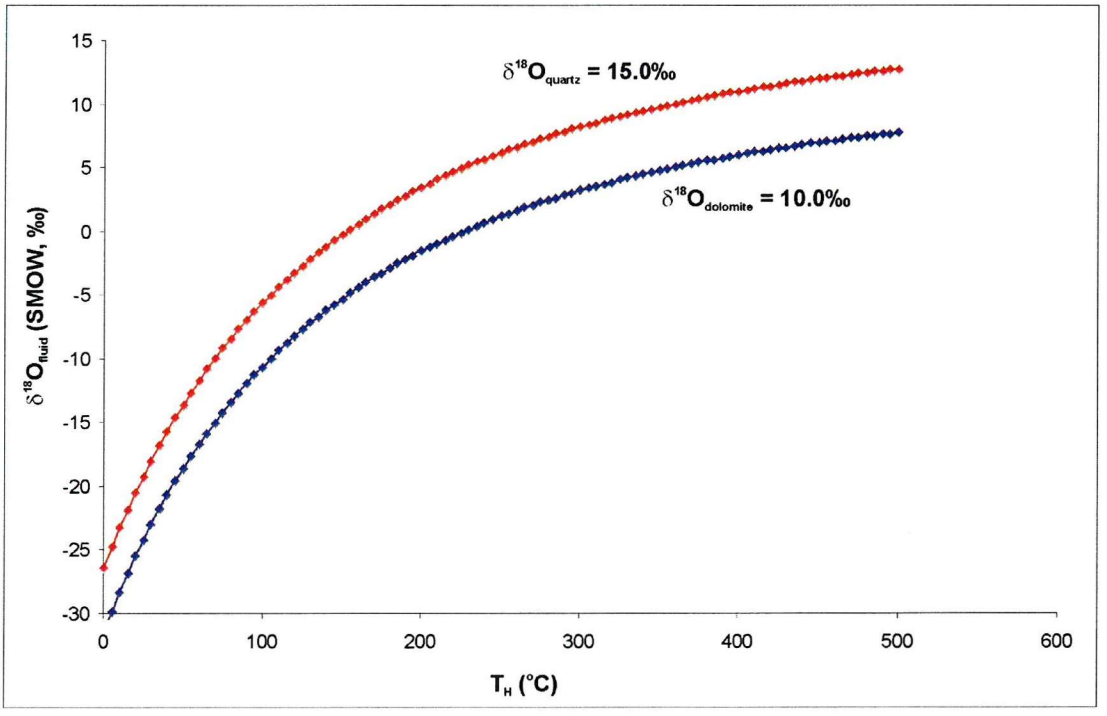

Figure 5.17: Example of the graphical representation of experimentally determined equilibrium oxygen isotope fractionation curves for the quartz-H_2O and dolomite-H_2O systems, using the fractionation factors of Matsuhisa *et al.* (1979) and Land (1983) respectively.

Ranges of $\delta^{18}O$ of fluids have been calculated from the quartz and dolomite $\delta^{18}O_{(mineral)}$ data for the high-angle veins within granite and arkose, Lower and Upper Orebody veins, and thrust-related vein samples for which fluid inclusion temperature data had been collected (calculated data in Table 5.5; graphically represented in Figs. 5.18, 5.19, 5.20, and 5.21). Using the minimum and maximum temperatures recorded during fluid inclusion analysis the range of $\delta^{18}O_{fluid}$ values can be calculated, with modal temperature used to give the most likely true $\delta^{18}O_{fluid}$ value. Temperatures can be assumed to be the same for the dolomite and quartz veins for the Upper Orebody alteration and shear zone samples as they are considered to have formed under the same conditions.

Sample	Range of fluid temperature data (°C) (mode)	$\delta^{18}O_{(mineral)}$ (‰) Quartz or Dolomite	Range of $\delta^{18}O_{fluid}$ values calculated (‰)	Modal value of $\delta^{18}O_{fluid}$ using modal temp.(‰)
High-angle veins	200-240 (230)	+11.9 (qtz)	+0.3 - +2.5	**+2.0**
Lower Orebody	140-220 (180)	+14.0 (qtz)	–2.3 - +3.6	**+1.0**
Thrust-zone	190-280 (240)	+16.8 (qtz)	+4.5 - +9.2	**+7.4**
		+16.6 (dol)	+4.4 - +9.0	**+7.3**
Upper Orebody	130-220 (160)	+14.0 (qtz)	–3.2 - +3.6	**–0.5**
		+13.1 (dol)	–4.1 - +2.7	**–1.4**

Table 5.5: Calculated $\delta^{18}O$ of fluids that are thought to have precipitated quartz (qtz) and dolomite (dol) using the fractionation factors of Matsuhisa *et al.* (1979) and Land (1983) respectively.

Veins from within the Lower and Upper Orebody reveal similar ranges in $\delta^{18}O_{fluid}$ values with most probable true values of +1.0‰ and –0.5‰ respectively based on the modal fluid inclusion temperatures. Although the range of $\delta^{18}O_{fluid}$ values for veins related to D1 high-angle extensional structures (Fig. 5.18) is similar to the orebody data (+2.0‰; Fig. 5.19), the vein samples from thrust-zones (Fig. 5.20) yield much higher $\delta^{18}O_{fluid}$ values of +7.3‰ to +7.4‰. A striking feature of the data is the $\delta^{18}O_{fluid}$ values calculated from the dolomite (Fig. 5.21) compared to the quartz vein results (Fig. 5.20) of both 'Banded Sandstone' shear zones and Upper Orebody veins and alteration. The ranges of $\delta^{18}O$ data for fluids are very similar when calculated separately from the quartz and dolomite (from the same samples) using the appropriate fractionation factors.

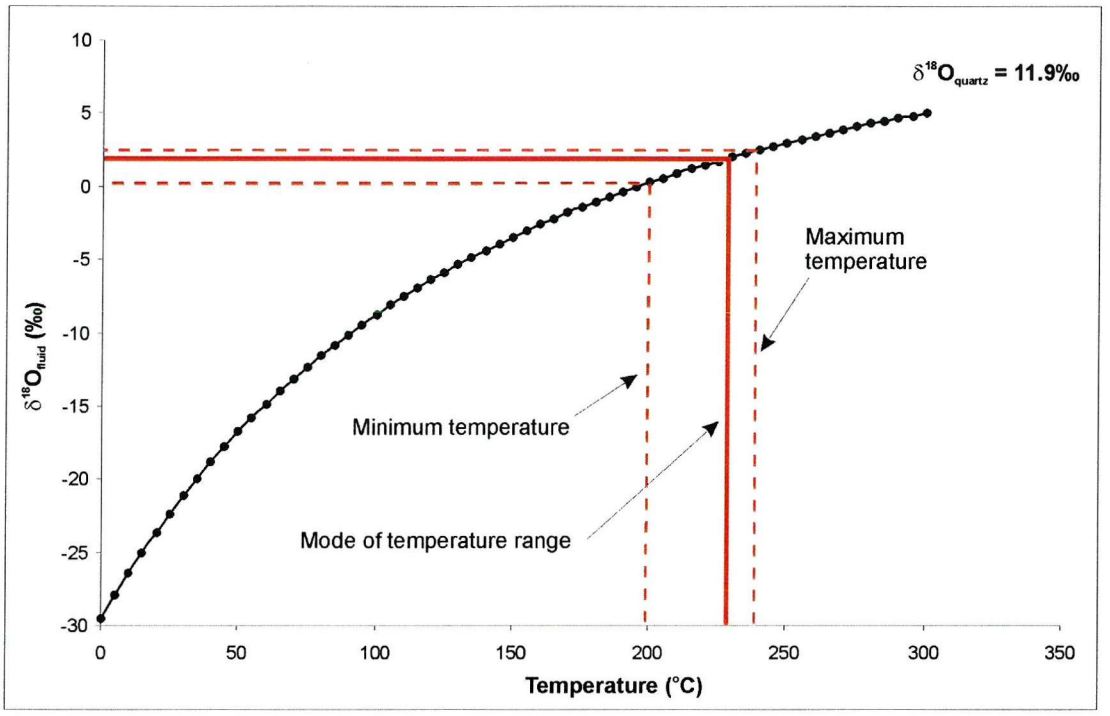

Figure 5.18: Graphical representation of the range of $\delta^{18}O_{fluid}$ values for the quartz vein samples from high-angle D1 extensional structures within the granite and arkose units (Table 5.5) based on the $\delta^{18}O_{quartz}$ data and fluid inclusions results and using the fractionation factors of Matsuhisa *et al.* (1979). The most likely true fluid $\delta^{18}O$ is obtained by using the modal homogenization temperature.

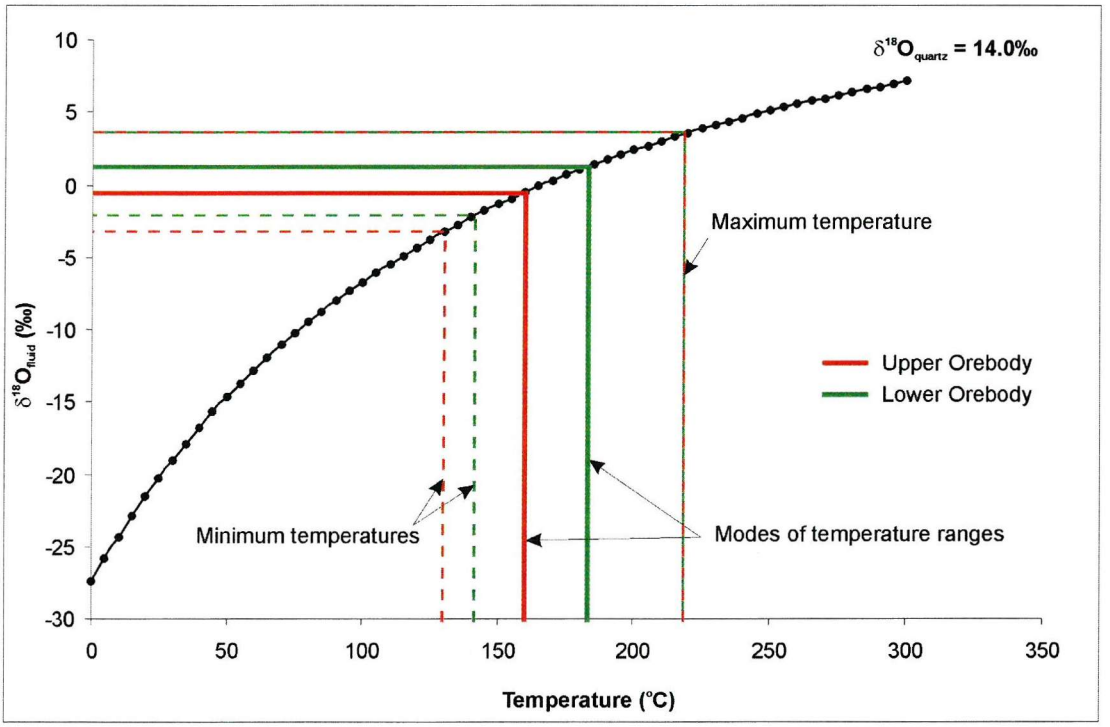

Figure 5.19: Graphical representation of the range of $\delta^{18}O_{fluid}$ values for the quartz vein samples from the Lower and Upper Orebodies (Table 5.5) based on the $\delta^{18}O_{quartz}$ data and fluid inclusions results and using the fractionation factors of Matsuhisa *et al.* (1979). The most likely true fluid $\delta^{18}O$ is obtained by using the modal homogenization temperature.

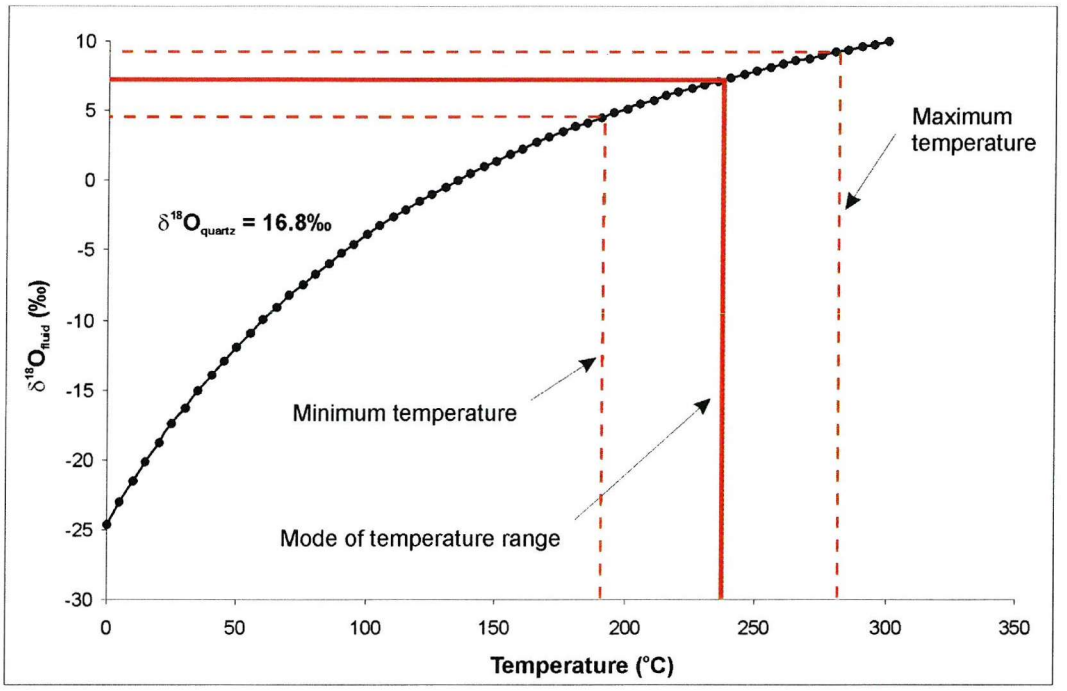

Figure 5.20: Graphical representation of the range of $\delta^{18}O_{fluid}$ values for the quartz vein samples from a thrust zone within the 'Banded Sandstone' unit (Table 5.5) based on the $\delta^{18}O_{quartz}$ data and fluid inclusions results and using the fractionation factors of Matsuhisa *et al.* (1979). The most likely true fluid $\delta^{18}O$ is obtained by using the modal homogenization temperature.

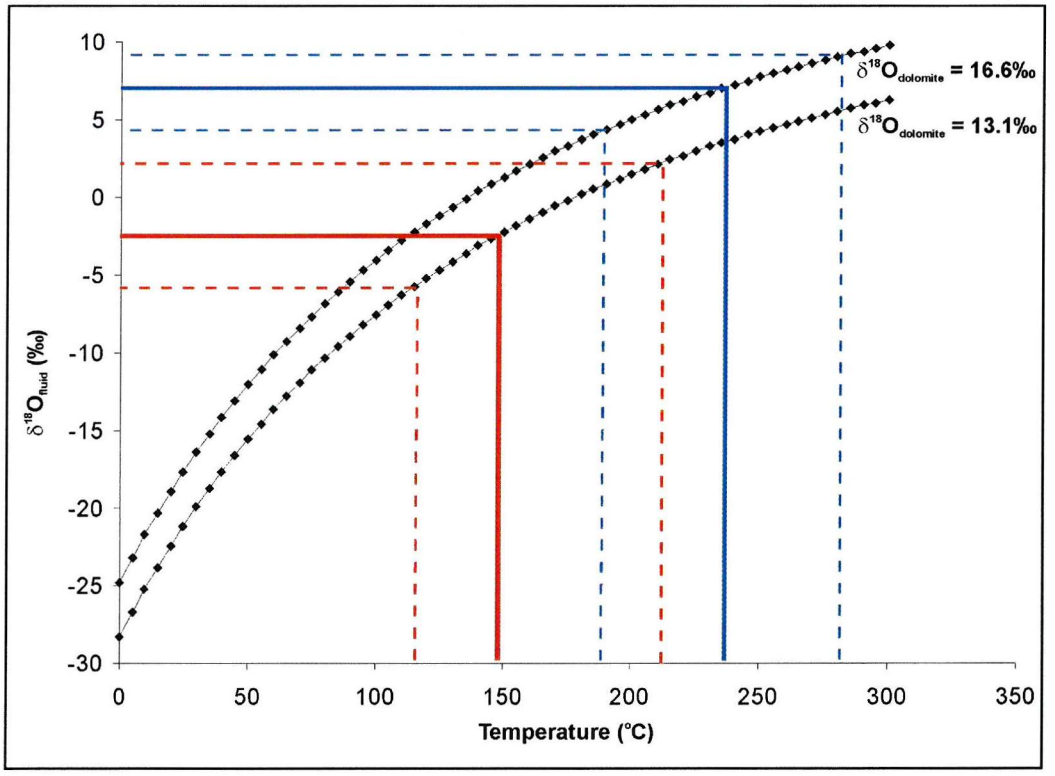

Figure 5.21: Graphical representation of the range of $\delta^{18}O_{fluid}$ values for the dolomite samples taken from the Upper Orebody and a thrust zone, which are thought to have formed at the same time (and more importantly at the same temperature) as the vein quartz from the same locations (Table 5.5), based on the $\delta^{18}O_{dolomite}$ data and fluid inclusions results and using the fractionation factors of Land (1983). The most likely true fluid $\delta^{18}O$ is obtained by using the modal homogenization temperature.

5.3.4 Previous oxygen isotope data

Annels (1989) discussed the oxygen isotope data of Cunningham (1986) for carbonate samples within the sequences of the Chambishi and Chambishi Southeast deposits. The results are similar to those obtained during this study in that 'reef dolomite' samples reveal $\delta^{18}O$ values of approximately +21.3‰, yet vein dolomite that hosts sulphides within the ore zones yields slightly lower values of approximately +18.1‰ (although higher than the +16.6‰ and +13.1‰ values yielded by Nchanga dolomite from shear zones and the Upper Orebody respectively). The value of $\delta^{18}O$ for the fluid in the dolomite-H_2O system for the vein sample is given as approximately +6.3‰ (based on the fractionation calculation of Olson, 1984). However, this work is based on only one sample of vein dolomite and so the range and accuracy of the data are unknown.

5.4 Sulphur isotopes

The sulphur isotope characteristics of Nchanga sulphides was investigated to determine the source of the sulphur component and the mechanisms of ore formation, and compare the results with typical sulphur isotope compositions in nature (Fig. 5.22). Sulphur isotope values are quoted relative to the Canon Diablo Troilite meteorite standard (CDT).

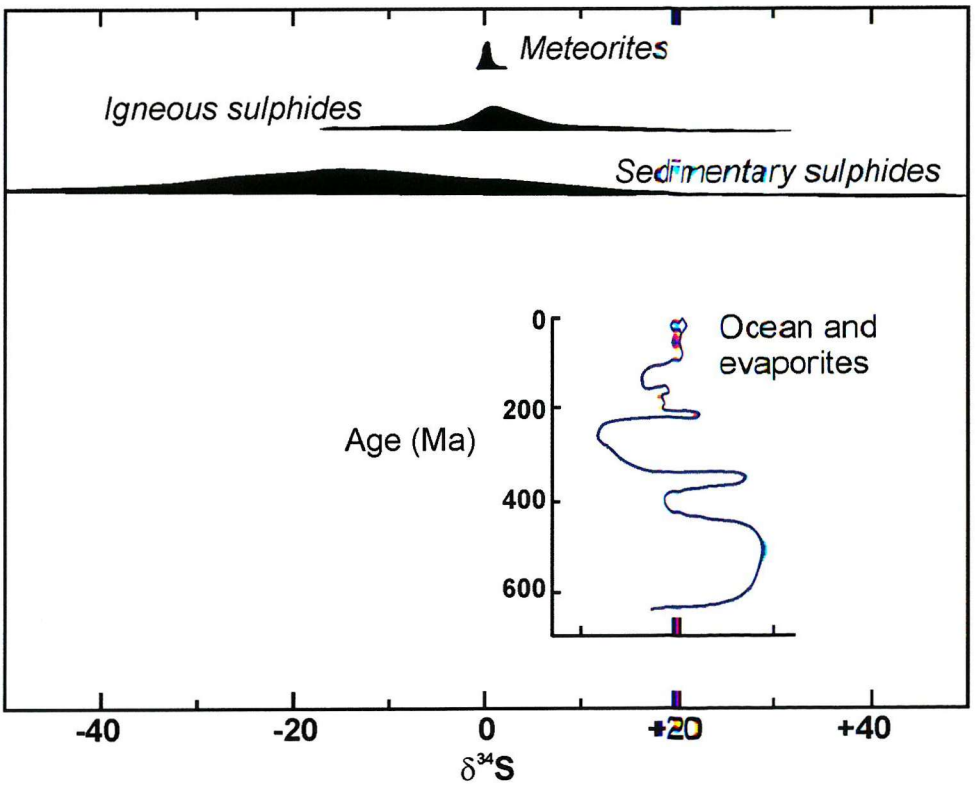

Figure 5.22: Sulphur isotope compositions in nature (Ohmoto & Rye, 1979).

The $\delta^{34}S$ of disseminated, vein-hosted and fracture-hosted copper sulphides from Nchanga was compared with both diagenetic pyrite and late-stage sulphides to determine: (1) the source of the sulphur in the system, and whether diagenetic pyrite has the same source as the later copper sulphides; (2) whether bacteriogenic sulphate reduction (BSR) or thermochemical sulphate reduction (TSR) were the main controls on sulphide precipitation; (3) the provision of a new data set to be compared and contrasted with existing Copperbelt $\delta^{34}S$ data, in particular using the in situ laser technique unavailable during earlier studies; and (4) to generate a new model for the source of the sulphur. On a smaller scale, these data can test whether disseminated host-rock sulphides are part of the same mineralizing event as those that are vein-hosted, and also whether sulphides that reveal replacement textures (e.g. chalcocite that replaces bornite) have the same $\delta^{34}S$ and hence origin.

5.4.1 Sample selection and method

Sulphides were analysed using both conventional and *in situ* laser technique. The former involves the handpicking of sulphides from selected samples whereas laser analysis combusts the sulphide *in situ* within a polished block. The five sulphides sampled in this analysis were pyrite, bornite, chalcopyrite, carrollite and chalcocite, and were selected not only on the basis of mineral type but also paragenesis: e.g. diagenetic pyrite versus chalcopyrite versus secondary chalcocite (Table 5.6). Sampling on this scale is not always possible by the hand-picking method (10mg required for analysis), for example where bornite grains were replaced by minor chalcocite, but the subtlety of the *in situ* laser technique allows a careful dissection of the paragenetically different sulphides. These new developments in sulphur isotope analysis allow a much higher resolution to be achieved; for example, variations within single sulphide grains (<80μm) can be identified.

Paragenesis	Sulphide Mineral	Location	Number of Analyses (conv., laser)
Diagenetic	pyrite	Lower Orebody	**6** (3, 3)
Diagenetic/later	pyrite	Upper Orebody	**8** (0, 8)
Main stage	Bornite	Lower Orebody	**23** (14, 9)
	Chalcopyrite Chalcocite	Upper Orebody	**65** (36, 29)
Late vein	pyrite	Upper Orebody	**3** (3, 0)

Table 5.6: Paragenetically different samples selected during the sulphur isotope study and number of analyses.

Both conventional and laser methods involve the conversion of sulphide sulphur into SO_2, from which sulphur isotope measurements are almost always made (Ohmoto & Rye, 1979; Thode *et al.*, 1971). Handpicked sulphide separates (approximately 10mg) were reacted conventionally with Cu_2O in a vacuum at a temperature of 1075°C (Robinson & Kusakabe, 1975) to perform this conversion in the conventional method. For the in situ laser sulphur isotope analysis, sulphide sulphur was combusted by the use of the laser in the presence of O_2 (Wagner *et al.*, 2002).

5.4.2 Correction factors for *in situ* laser analysis of sulphides

$^{34}S/^{32}S$ isotope ratios have been measured with high analytical precision in a number of studies using the laser method (Crowe *et al.*, 1990; Kelley & Fallick, 1990; Sharp, 1992), although experimental work has shown that, during laser combustion of sulphides, fractionation occurs between the $\delta^{34}S$ of the SO_2 gas produced and the mineral $\delta^{34}S$ (Crowe *et al.*, 1990; Kelley & Fallick, 1990; Huston *et al.*, 1995). This fractionation is influenced by the analytical parameters (e.g. laser power density) and by the nature of the analyzed mineral (Fallick *et al.*, 1992; Wagner *et al.*, 2002). Therefore, under reproducible analytical conditions (i.e. same mass spectrometer and line), the correction factor for this fractionation is mineral specific (Crowe *et al.*, 1990; Huston *et al.*, 1995). The fractionation factors of only a limited number of sulphides have been calculated and calibrated by comparing a number of conventional and laser analyses from the same homogenous sulphide sample. Some common factors are: pyrite, +0.8 ± 0.9‰; chalcopyrite, +0.7 ± 0.3‰; sphalerite, +0.4 ± 0.3‰; and galena, +2.5 ± 0.3‰ (Wagner *et al.*, 2002). In terms of the Nchanga sulphides analysed here, the correction factors, highlighted above, have been used for pyrite and chalcopyrite and also the correction factor of chalcopyrite (+0.7) for bornite. However, it was necessary to determine the fractionation factors for both chalcocite (Cu_2S) and carrollite ($Cu(Co,Ni)_2S_4$), using the isotope facilities at the Scottish Universities Environmental Research Centre (SUERC).

This was achieved by selecting two samples (L128-12 for chalcocite and NOP741-24 for carrollite) with expected homogenous $\delta^{34}S$ values and enough sulphide to carry out both the conventional and *in situ* laser analysis. The $\delta^{34}S$ for conventional and laser analyses were then compared and the weighted means calculated (weighted to the baratron reading on the apparatus) to calculate the overall fractionation factor (Table 5.7).

1 Sample	2 Line No.	3 $\delta^{34}S$ (conv.) (‰)	4 $\delta^{34}S$(laser) (‰)	5 Baratron (B) reading	6 $B/B_{(total)}$ x $\delta^{34}S$	7 Correction factor (‰)
741-24	**SA8947**	13.92		37.5	3.508	
(carrollite)	**SA8948**	13.05		34.76	3.048	
	SA8950	13.38		32.83	2.952	
	SA8951	14.00		43.73	4.114	
			Total	**148.82**	**13.62 ± 0.2 (n=4)**	
	LS5280		13.82	1.96	5.966	
	LS5281		14.34	2.02	6.380	
	LS5288		13.53	0.56	1.669	
			Total	**4.54**	**14.02 ± 0.4 (n=3)**	**-0.4**
L128-12	**SA8944**	5.52		33.37	1.862	
(chalcocite)	**SA8945**	5.59		32.48	1.835	
	SA8946	5.41		33.07	1.809	
			Total	**98.92**	**5.51 ± 0.1 (n=3)**	
	LS5283		5.40	0.91	1.082	
	LS5284		4.92	0.96	1.040	
	LS5285		6.44	0.94	1.333	
	LS5286		5.36	1.73	2.042	
			Total	**4.54**	**5.50 ± 0.6 (n=4)**	**+0.01**

Table 5.7: Calculation of fractionation correction factors for carrollite and chalcocite between conventional and laser $\delta^{34}S$ analysis (see text for explanation).

Columns 3 and 4 are the conventional and laser $\delta^{34}S$ data respectively. An average for these data is then calculated (totals in column 6), which is the total of the $\delta^{34}S$ data weighted to the baratron readings (i.e. column 3 or 4 multiplied by the baratron reading divided by the total of the baratron readings; totals in column 5). The correction factor (column 7) is then calculated by subtracting the weighted average for the laser data from that of the conventional data. The results indicate that a correction factor of –0.4 be added to the carrollite laser data. Although the results also suggest a correction factor of +0.01 be added to the chalcocite laser data, this value would be significantly less than the error involved in obtaining the $\delta^{34}S$ measurement in the first place and the error involved in the above calculation.

5.4.3 Results

In total one hundred and five $\delta^{34}S$ values have been obtained by both conventional and *in situ* laser analysis (Appendix D2). All results plotted together, ignoring the mineral type and paragenesis, show a broad range of $\delta^{34}S$ values from –17‰ to +23‰ (Fig. 5.23). However, distinguishing between different minerals, paragenetically different sulphides, and sulphides from different locations (e.g. Lower versus Upper Orebody), demonstrates significant variability in the data (Fig. 5.24).

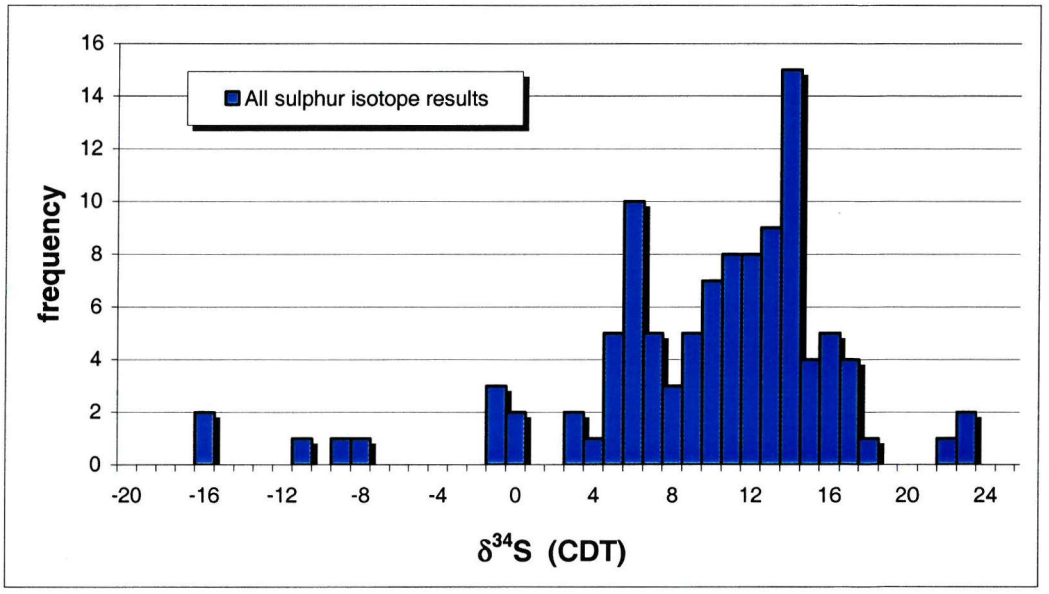

Figure 5.23: All sulphur isotope data collected during this study.

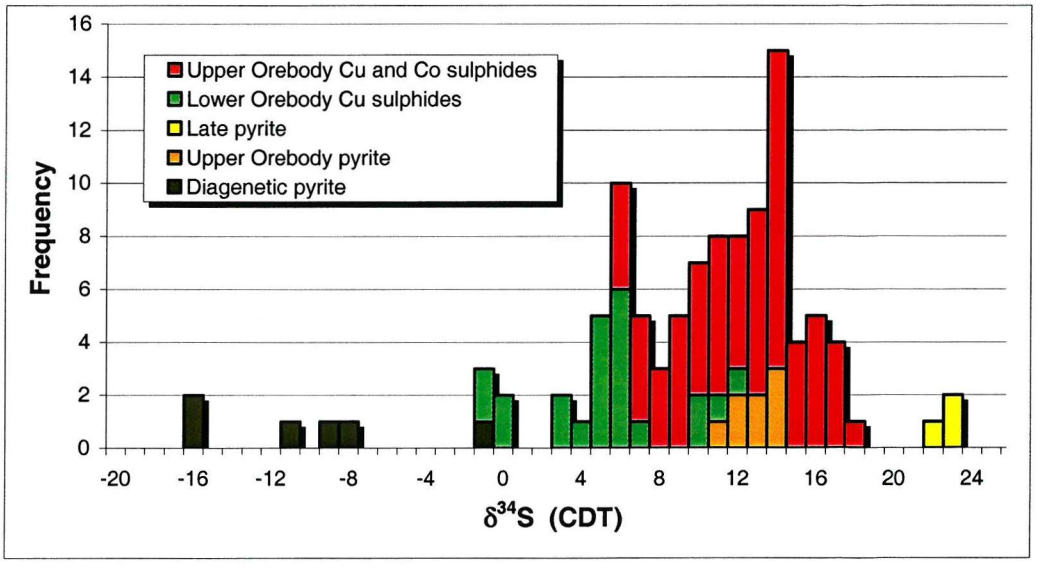

Figure 5.24: All sulphur isotope data collected during this study, with distinction between different sulphide minerals, paragenetically different sulphides, and sulphides from various locations in the Nchanga sequence.

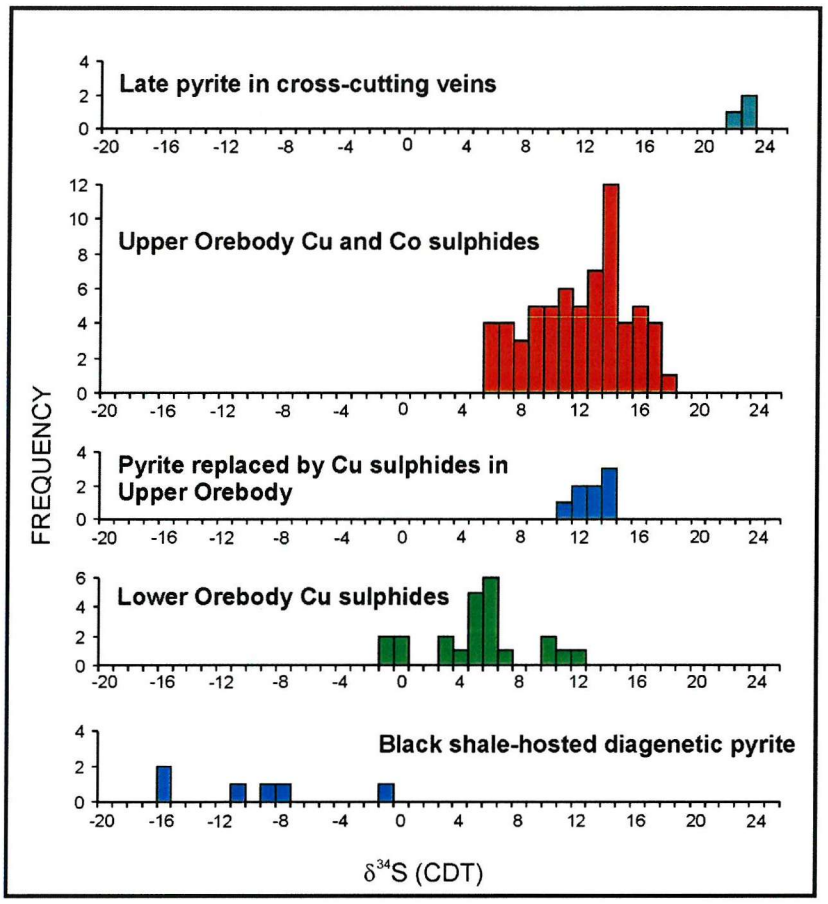

Figure 5.25: All sulphur isotope data collected during this study illustrated as separate histograms to differentiate between paragenetically different sulphide phases and sulphides from various locations in the Nchanga sequence (McGowan *et al.*, in press).

Diagenetic pyrites in the 'Lower Banded Shale' unit show distinct, relatively low sulphur isotope signatures ranging from –1‰ to –17‰ with a mean of –10.2 ± 5.9‰ (n = 6). Arenite- and shale-hosted copper and cobalt sulphides show $\delta^{34}S$ from –1‰ to +12‰ for the Lower Orebody and +5‰ to +18‰ for the Upper Orebody. There is also a clear distinction between the mean of +12.1 ± 3.3‰ (n = 65) for the Upper Orebody compared with +5.2 ± 3.6‰ (n = 23) for the Lower Orebody. The range of values for copper sulphides of the Upper Orebody spans that of the pyrites that they replace (11-15‰). Rare, paragenetically late, pyrites in quartz veins reveal the highest $\delta^{34}S$ of around +22‰ to +23‰.

The subtlety of the *in situ* laser technique provides the capability to measure $\delta^{34}S$ at a higher resolution, e.g. copper sulphides that replace earlier formed pyrite (Fig. 5.26) and chalcocite that replaces bornite in the Upper Orebody (Fig. 5.27). The range of $\delta^{34}S$ values obtained by both the conventional and laser methods are consistent with each other (Fig. 5.28A & B). This suggests that there is no major bias in the laser data to lighter or heavier $\delta^{34}S$ once the correction factor has been added.

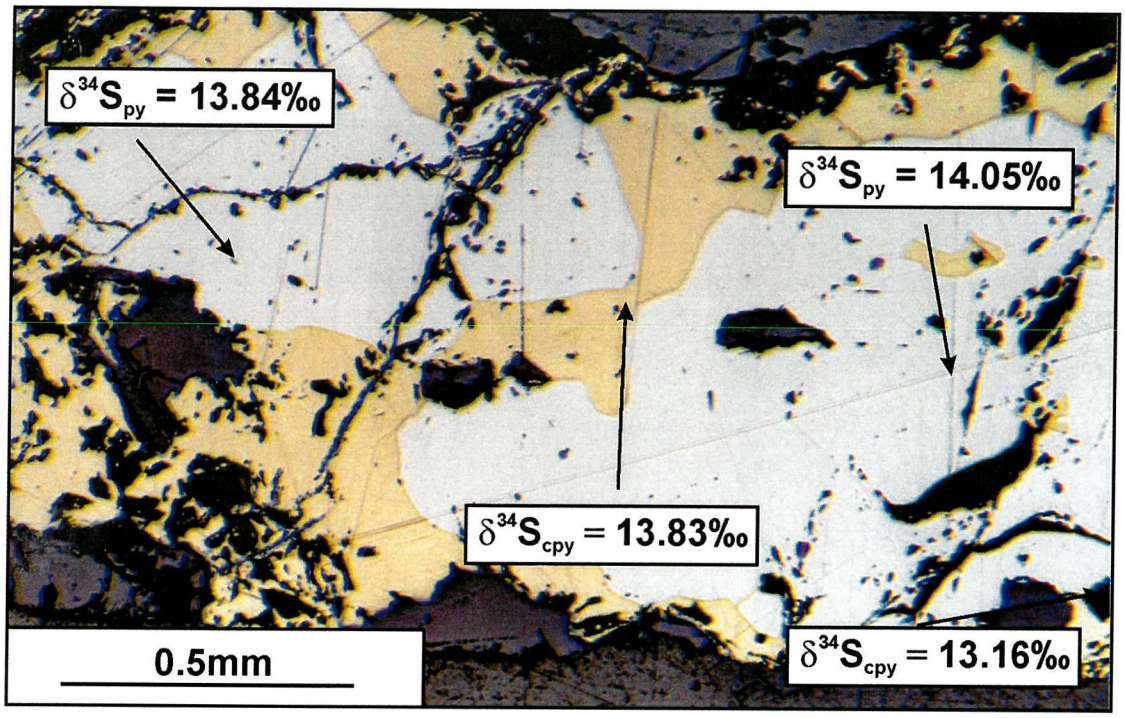

Figure 5.26: The $\delta^{34}S$ values of pyrite replaced by chalcopyrite within the Upper Orebody.

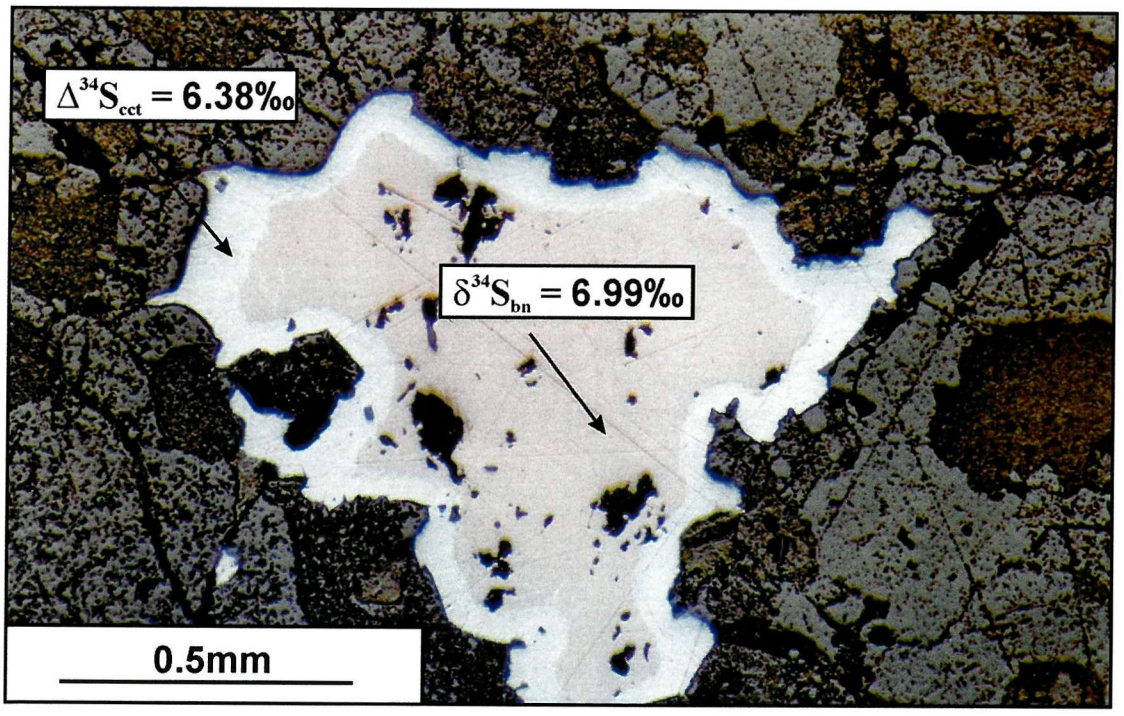

Figure 5.27: The $\delta^{34}S$ of secondary chalcocite that replaces earlier bornite showing similar results.

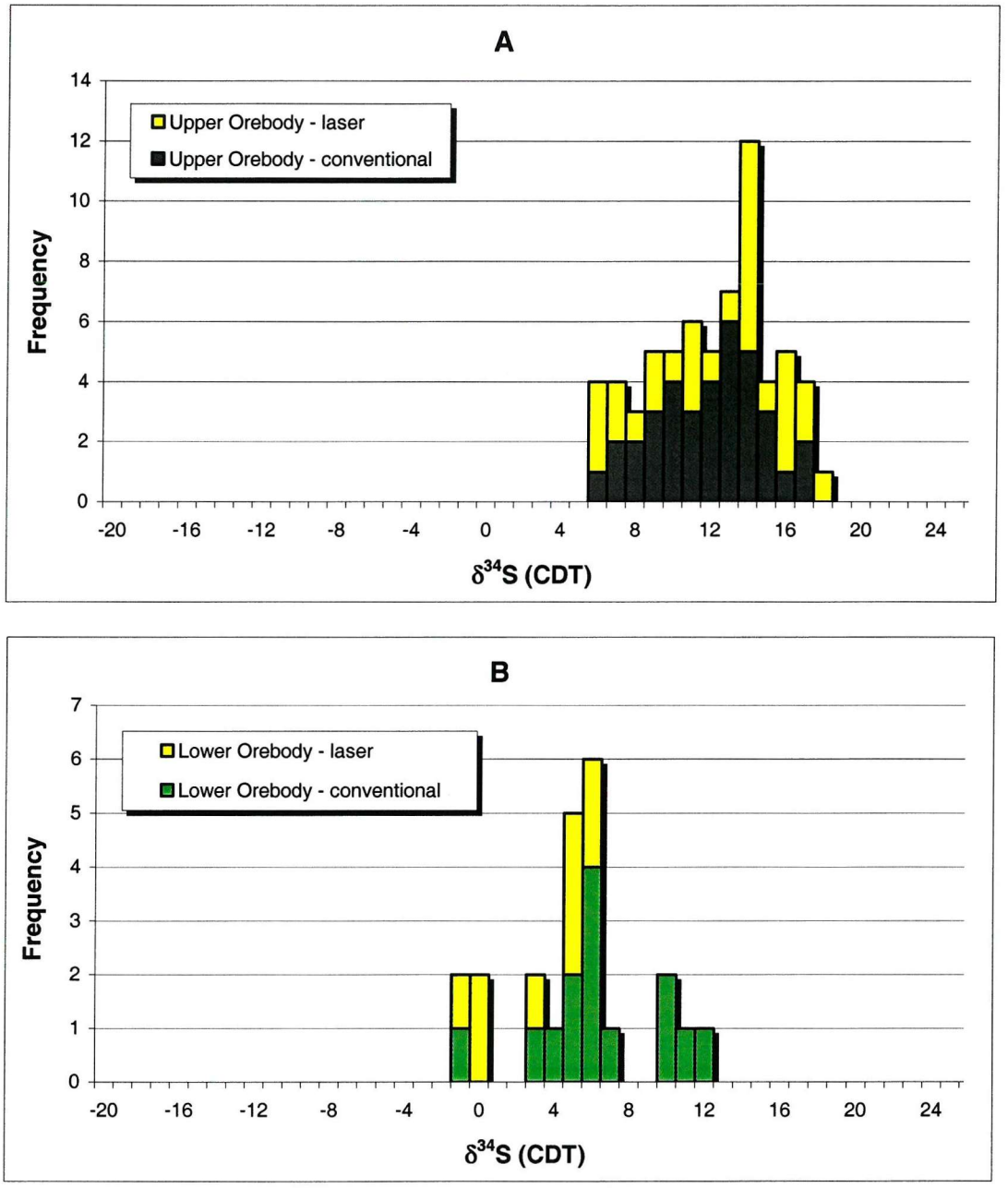

Figure 5.28: Conventional versus *in situ* laser $\delta^{34}S$ data for: (A) Upper Orebody copper and cobalt sulphides, and (B) Lower Orebody copper sulphides.

An interesting feature of the sulphur isotope data is the comparison between sulphides that are disseminated (or fracture-related) within the host rock and those that are hosted by quartz (± dolomite) veins (Fig. 5.29) for which the sulphide (and gangue) mineralogy is always identical for Nchanga samples. The range of data for vein-hosted sulphides is consistent with the data for disseminated sulphides hosted within the lithology of the host unit. This has been tested on a smaller scale by comparing vein sulphides with non-vein sulphides from within the same or adjacent samples (Table 5.8):

Sample	Sample type and mineral	$\delta^{34}S$
NOP741-14	TFQ-hosted / carrollite	12.48
NOP741-20	TFQ vein-hosted / carrollite	13.12
NOP731-13	TFQ-hosted / bornite (+cct)	14.87
NOP731-12	TFQ vein hosted / bornite (+cct)	14.50

Table 5.8: Comparison between TFQ ('The Feldspathic Quartzite')-hosted sulphides and vein-hosted sulphides from within the same unit from the Upper Orebody.

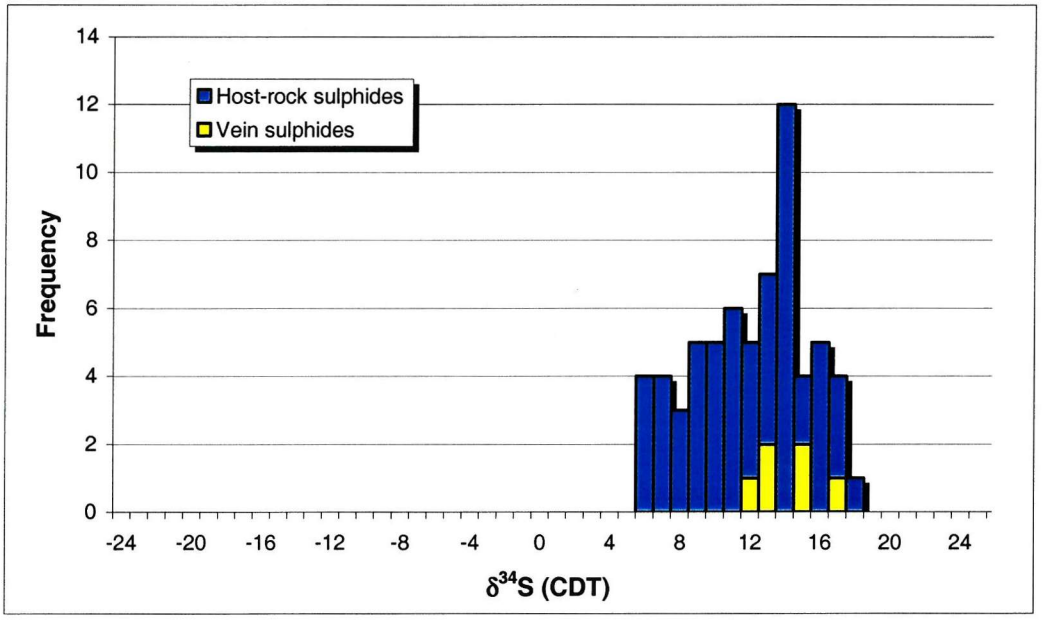

Figure 5.29: Comparison between host-rock sulphides (disseminated and fracture-hosted) and quartz (dolomite) vein-hosted sulphides within the Upper Orebody.

5.4.4 Previous Copperbelt sulphur isotope studies

Published sulphide $\delta^{34}S$ data for various Copperbelt deposits (Fig. 5.30) show ranges of: –11‰ to +11‰ for Chambishi (Annels, 1989); –10.5‰ to +10.9‰ for Mufulira: +2.9‰ to +11.7‰ for Nkana North Limb and +6.5‰ to +15.9‰ for Chibuluma (Dechow & Jensen, 1965), and –7‰ to +9‰ for Konkola (Sweeney *at al.*, 1986). Annels (1989) also claimed that the sulphides hosted by quartz-carbonate veins within Chambishi orebodies were introduced at the same time and under the same conditions as disseminated mineralization due to the identical sulphide and gangue mineralogy and consistent $\delta^{34}S$ signatures of sulphides. Dechow & Jensen (1965) carried out a total of 550 $\delta^{34}S$ analyses of sulphide samples from both the Zambian Copperbelt and Katanga Province of the Democratic Republic of Congo, although no sulphur isotope data has been reported from any of the Nchanga ores. In addition to typical Copperbelt ores, Dechow & Jensen (1965) also studied occurrences of Basement

mineralization, notably including Gray's Quarry, which is situated ten miles northwest of Chambishi and consists of fracture-related and disseminated pyrite and chalcopyrite within the Nchanga Red Granite, and the 'Lamprophyre dyke' body, which is exposed in the Nchanga Open Pit. These sulphides yielded $\delta^{34}S$ signatures of +3.0‰ to +13.3‰, with a mean of +7.6 ± 3.7‰ (n=8), and +3.8‰ to +4.2‰, with a mean of 4.0‰ ± 0.3 (n=2) respectively, whereas Lufubu Schist-hosted mineralization at the Fimpimpa prospect, midway between Mufulira and Konkola, yielded much lighter $\delta^{34}S$ values of –2.3‰ to –10.5‰, with a mean of –5.6 ± 3.5‰ (n=9; Dechow & Jensen, 1965). Existing sulphur isotope data, in light of the data obtained during this study, is discussed in more detail in Chapter 6.

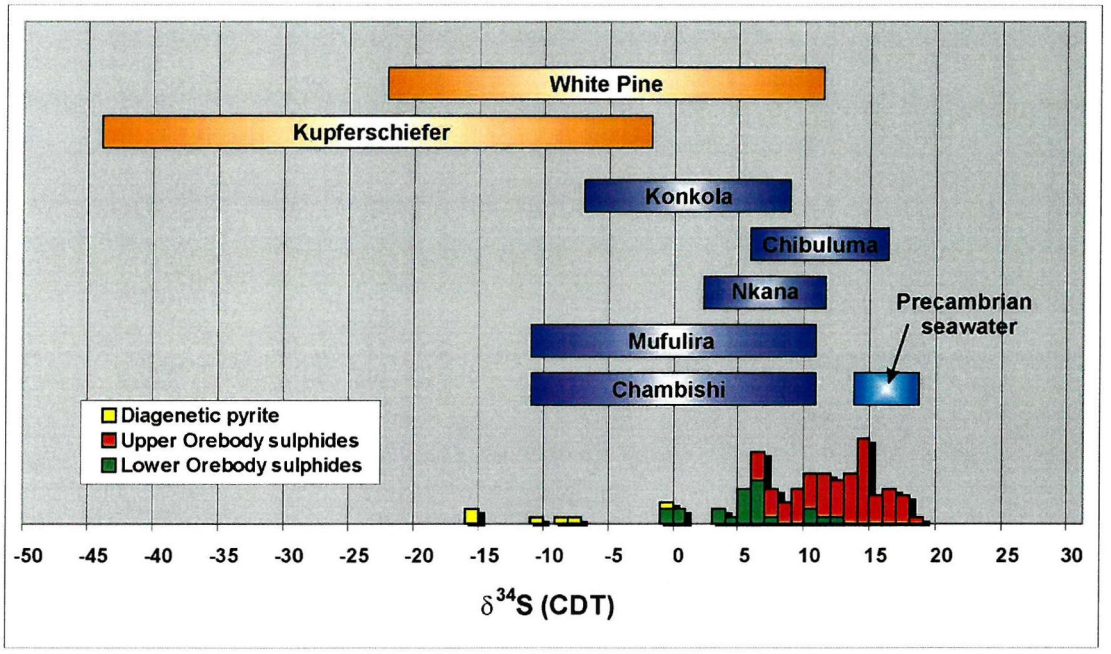

Figure 5.30: Existing $\delta^{34}S$ data for various Copperbelt deposits and the calculated value of Precambrian seawater $\delta^{34}S$ from available literature compared to the range of data collected during this study and some sulphur isotope data from the Kupferschiefer and White Pine sediment-hosted copper deposits. Source of data: Chambishi (Annels, 1989); Mufulira, Nkana North, and Chibuluma (Dechow & Jensen, 1965); Konkola (Sweeney *et al.*, 1986); Kupferschiefer and White Pine (Gustafson & Williams, 1981); PreCambrian seawater (Claypool *et al.*, 1980; Annels, 1989).

In addition to the sulphide sulphur data above, the $\delta^{34}S$ of sedimentary anhydrite from the Lower Roan sequence at individual Copperbelt deposits constrain the $\delta^{34}S$ of Precambrian seawater at the time of Lower Roan deposition, which is thought to range from +14.2‰ to +18.9‰ (Fig. 5.30; Dechow & Jensen, 1965; Claypool *et al.*, 1980; Annels, 1989) with a suggested mean $\delta^{34}S$ of +17.5‰ (Fig. 5.31; Holser & Kaplan, 1966; Claypool *et al.*, 1980).

5.5 Carbon isotopes

Within hydrothermal ore deposits, carbon occurs as carbonate minerals of calcium, magnesium, or iron, and as CO_2 or CH_4 in fluid or gaseous inclusions in ore or gangue minerals (Faure, 1986). The $\delta^{13}C$ values of natural carbon (relative to the Vienna Peedee Formation Belemnite, PDB, standard) are approximately 0‰ for marine carbonates or limestones, –5‰ for igneous carbon, and –25‰ for organic compounds (Ohmoto & Rye, 1979; Faure, 1986; Ohmoto & Goldhaber, 1997). With these typical values in mind, an investigation into the $\delta^{13}C$ of some Nchanga carbonates was initiated to compare the abundant dolomite found within the Upper Orebody alteration assemblage and within the major thrust-related shear zones within the 'Banded Sandstone' unit with the dolomite of the (Upper Roan?) units higher in the sequence. The main aim of this analysis was to test whether the dolomite from each of these locations has the same origin.

5.5.1 Sample selection and method

In total twelve samples were selected (Table 5.9) in order to achieve the above objectives:

Location / type of sample	Sample numbers	Number of analyses
Dolomite units (Upper Roan?)	NOP73, 76, 77, 79	4
Upper Orebody dolomite alteration associated with ore	NOP111, 123, NOP785-8, NOP741-14, -5	6
'Banded Sandstone' shear-zone dolomite	NOP770-2, NOP785-6	2

Table 5.9: Samples selected for $\delta^{13}C$ study, their location, and number of analyses.

In the same way as with sulphur isotopes and SO_2, the $\delta^{13}C$ (along with $\delta^{18}O$) is typically determined from CO_2. The CO_2 from the above samples was liberated from the carbonates by reaction with 100% phosphoric acid at 25°C (Ohmoto & Goldhaber, 1997). In the case of bulk samples like the Upper Orebody alteration, which is a mix of dolomite and silicates, results represent the signature of the dolomite only, as silicates do not dissolve in the acid.

5.5.2 Results

The $\delta^{13}C$ of the selected dolomites from the different locations shows clear differences when plotted together (Figs. 5.31; Appendix D3). The dolomites from the (Upper Roan?) units above the Upper Orebody show $\delta^{13}C$ values of +1.4‰ to +2.5‰ (mean = +2.0 ± 0.5‰, n=4), typical of marine dolomite (Ohmoto & Rye, 1979). However, both the dolomite from the

'Banded Sandstone' shear-zones and the alteration assemblage within the Upper Orebody clearly show much more negative $\delta^{13}C$ values: –2.9‰ to –4.0‰ (mean = –3.5 ± 0.4‰, n=2) and –5.6‰ to –8.3‰ (mean = –7.1 ± 1.1‰, n=6) respectively, further highlighted in a plot of $\delta^{13}C$ and $\delta^{18}O$ results (Fig. 5.32). The implications of these results are discussed in Chapter 6.

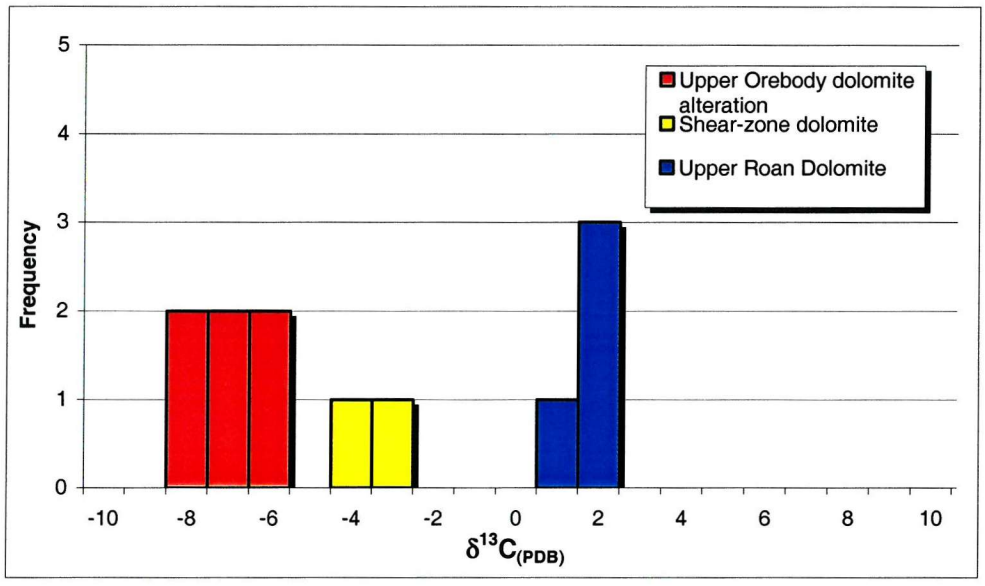

Figure 5.31: Histogram to show the $\delta^{13}C$ of dolomites within the Nchanga sequence, highlighting the difference between marine-derived carbonates (Upper Roan?), shear zone-hosted dolomites, and dolomite alteration within ore zones.

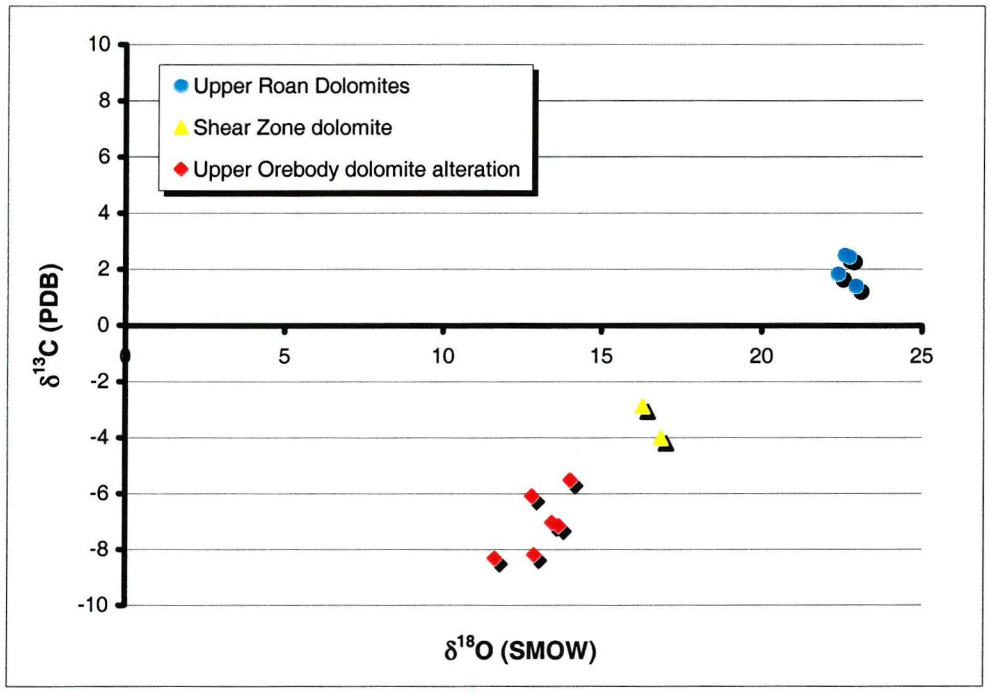

Figure 5.32: Plot to show $\delta^{13}C$ and $\delta^{18}O$ of dolomites within the Nchanga sequence, highlighting the difference between marine-derived carbonates and dolomite alteration within ore zones. $\delta^{18}O(SMOW)$ is calculated by $\delta^{18}O_{(SMOW)} = 1.0391*\delta^{18}O_{(PDB)} + 30.91$.

5.5.3 Previous Copperbelt carbon isotope data

Annels (1989) summarized the results of Cunningham (1986) for carbon and oxygen isotope studies on dolomites from the Chambishi deposits. Reef dolomites revealed $\delta^{13}C$ values of +0.5‰ and –4.5‰ (n=2). Other $\delta^{13}C$ values obtained were –8.6‰ (n=1) for subconcordant dolomite veins, –13.8‰ (n=1) for algal mat dolomites from a carbonaceous shale unit, and also –18.2‰ and –25.2‰ (n=2) for nodular dolomite from the carbonaceous shale unit at Mwambashi B (Annels, 1989). They suggested that the reef dolomite is compatible with Precambrian dolomites as constrained by the $\delta^{18}O_{(PDB)}$ and $\delta^{13}C_{(PDB)}$ values of Veizer & Hoefs (1976) of –4‰ to –8‰ and –1‰ to +3‰ respectively. The subconcordant veins, algal mats, and nodules reveal increasingly lighter $\delta^{13}C$, which was interpreted to indicate a more important role of organic carbon in the precipitation of these dolomites.

5.6 Summary

- First melt temperatures of vein quartz-hosted primary fluid inclusions within orebody and fault samples reveal the presence of Mg, Ca, and Fe chlorides. Thermometric analysis has revealed homogenization temperatures (vapour to liquid) and salinities of 230°C and 30-38 equivalent wt% NaCl for Basement and arkose high-angle veins, 180°C and 30-32 equivalent wt% NaCl for Lower Orebody veins, 240°C and 33-35 equivalent wt% NaCl for thrust-related veins, and 160°C and 30-34 equivalent wt% NaCl for Upper Orebody veins. Pressure-corrected fluid temperatures and the influence of these on the $\delta^{18}O_{fluid}$ signature of the vein-forming fluid are discussed in the next chapter.

- Sulphur isotope analysis has identified a clear distinction in $\delta^{34}S$ between diagenetic Nchanga pyrite (–1‰ to –17‰) and the copper and cobalt sulphides of the Lower and Upper Orebodies (–1‰ to +12‰ and +5‰ to +18‰ respectively). Sedimentary anhydrite reveals a $\delta^{34}S$ of +17.5‰, which is thought to be the signature of Precambrian seawater (Claypool *et al.*, 1980).

- There is a clear difference in carbon isotope signatures of marine (reef) dolomite with a $\delta^{13}C$ of +1.4‰ to +2.5‰, shear zone dolomite with a $\delta^{13}C$ of –2.9‰ to –4.0‰, and dolomite alteration associated with Upper Orebody mineralization with a $\delta^{13}C$ of –5.6‰ to –8.3‰.

The significance of the fluid inclusion and various isotope results is discussed in detail in Chapter 6.

CHAPTER 6:

DISCUSSION

CHAPTER 6: DISCUSSION

6.1 Discussion of observations and results

The principal discussion points, with respect to the new data presented here, are: (i) a new structural model for the Nchanga area, (ii) the relationship of mineralization to lithology and structure and assessment of their relevance to the localization of major ore zones, (iii) the relative timing of mineralization with respect to deformation, alteration, and metamorphism, (iv) the alteration and geochemistry of the host units and implications for fluid chemistry, (v) the p-t-x of the fluids within the deposits, and (vi) a critical evaluation and interpretation of the new stable isotope data.

6.1.1 Structural evolution of the Nchanga host sequence

The thrust and fold model, described in Chapter 3, represents a significant reinterpretation of the mine geology at Nchanga. However, it is not entirely new. Previous authors, including Daly *et al.* (1984) and Molak (1995), described the role that layer-parallel decollements and low-angle structures played in shaping the structural geometry of the Nchanga sequence. Daly *et al.* (1984) recognized the importance of bedding parallel shear zones, also observed during this study (principally the one at the top of the arkose unit and base of overlying shale), and interpreted them as thrusts. They also suggested that the 'ore-shale' was used as a preferred plane of slip by these thrusts. Hitzman (1998) observed similar features at the Chambishi deposit.

Notably, Diederix (1977) suggested the former presence of major evaporites within the sequence, in particular at the top of the arkose unit, where one of these decollements or thrusts now exists. It is possible that such units aided deformation by lubrication of layer-parallel decollement-type structures. This supports the idea that rheological differences between lithological units within the sequence played an important role in the location of major structures and hence the current structural geometry. This is demonstrated by field observations where less competent units, such as the 'Banded Sandstone,' preferentially fold around structures and more competent units, such as 'The Feldspathic Quartzite,' only flex to a limited extent before thrust-breakthrough occurs.

The dominant vergence of structures, measured during the present study at Nchanga, is to the northeast (Fig. 3.13). This supports the Copperbelt-wide observations of Daly *et al.* (1984) who suggested an ENE-directed thrust movement across the whole Lufilian Arc. In addition, the notion that pre-Katangan extensional structures underlie the Lower Roan sedimentary rocks is consistent with the rift models for basin evolution (rifts promoting sediment deposition and distribution) of Raybould (1978), Annels (1984, 1989), and Unrug (1989). Field and geometrical evidence suggests that major basement structures were inverted during compression (Fig. 3.17) and, as a result, controlled the location and development of thrusts (discussed in section 3.5). At Nchanga, inversion on major granite-bounding structures demonstrates that the competence contrasts between the stable granite block and both the less-competent older Lufubu Schists and the younger Lower Roan sediments were major factors in the inversion process.

The timing of these tectonic processes on the Copperbelt is much less well constrained. In light of the current evidence, it is considered that (i) the development of pre-Katangan extensional structures (D1) commenced before 877 Ma (based on the 877 ± 11Ma date of Armstrong *et al.*, 1999) and during the deposition of the footwall arkoses, and that (ii) the main phase of thrusting of the Katangan sequence (and inversion of early extensional structures) on the Copperbelt most likely took place between 550 and 560 Ma (Hanson *et al.*, 1993) during the Lufilian Orogeny, which may have lasted from 656 Ma to 503 Ma (Cahen *et al.*, 1984).

6.1.2 Relationships of mineralization to lithology and structure

The mineralization at Nchanga is almost completely stratabound as it is mostly concentrated within a clearly defined section of the Nchanga sequence from the top of the arkose unit to the base of the 'Upper Banded Shale' unit. However, it is not stratiform, as this would refer to mineralization that is parallel to the principal planar fabric, e.g. bedding or cleavage (Kearey, 1996). On a large scale, mineralization transgresses stratigraphy (e.g. Chingola B; Fig. 3.18) and in some cases fracture-related sulphides dominate over disseminated sulphides (Fig. 4.9A).

Despite a strong stratigraphic control of mineralization, the copper mineralization at Nchanga is not confined to shales or the 'ore-shale' unit (as previously reported in some literature). Anomalous concentrations of copper occur throughout the Lower Roan sequence and economic concentrations are consistently located within arkose or arenite units that are overlain by shale horizons (in many cases the base of the overlying shale is mineralized for a short distance upwards). Therefore the host lithology does appear to play a major role in the

localization of mineralization, both on a Copperbelt scale, where the majority of mineralization occurs within a specific section of the Lower Roan sequence (~60-80m within the 1.9km Katangan sediments, excluding Kundulungu which is generally missing on the Zambian Copperbelt), and on a deposit scale where lithological variations appear to play a role (arenite versus shale).

Despite the stratigraphic control, the strongest evidence for a structural control of copper and cobalt mineralization is the fact that Upper Orebody mineralization only occurs where the thrust-propagation fold structures have developed internally within the Lower Roan at Chingola B and the Nchanga Open Pit. In fact, cobalt, which is exclusively hosted within fold-hinge zones of the fault-propagation structures described in Chapter 3, has a stronger element of structural control on its spatial distribution than copper. This is also the case at the Chibuluma West deposit, central Copperbelt (McGowan, 1999). The low-angle structures at which these thrusts detach are also mineralized both at the top of the arkose (Lower Orebody) and within the 'Banded Sandstone' ('Refractory' or 'vermiculite' ore). The strong correlation between copper concentrations and phlogopite development within 'Banded Sandstone' shear zones was used by Molak (1995) as evidence for a common structural origin of both alteration and copper. These large-scale structural relationships are evident in the geological sections and copper concentration contours presented in section 3.6.1. However, less obvious in these sections is the apparent relationship of higher-grade mineralization and high-angle structures (pre-Katangan extension – D1) within the granite basement. This is suggested by the spatial relationship between increased copper concentrations and one major structure within the Nchanga Open Pit and River Lode Open Pit (section 3.6.2). This is interpreted here as evidence that early extensional structures, represented in the Basement and later inverted during Lufilian compression, may have played an important role in controlling the location and devlopment of significant ore horizons. However, further investigation of the role of basement faults is virtually impossible due to the lack of exposure of such structures within open pit deposits and failure of boreholes to intersect them.

The larger-scale relationships of mineralization to structure and lithology are mirrored on a small scale in the petrographic nature of the ore minerals (section 4.2.3). Both the lithological characteristics of host rocks and the local tectonic fabrics appear to control the location of sulphides. Within shale units, coarser layers are more prone to hosting sulphides (Fig. 4.11G). Within arenite host rocks, sulphides often appear disseminated and interstitial to host detrital grains. These features strongly suggest that host-rock porosity (and possibly even permeability) played a vital role. Yet, sulphides are also commonly orientated along (but not necessarily deformed by) a developed structural fabric or hosted within small fractures. In the

Lower Orebody, the scale of oxidation and weathering of host rocks and primary sulphides has destroyed primary ore mineral textures in many cases. Primary bornite and chalcopyrite occur at deeper levels at Chingola D (Roberts, 2003) and further detailed examination of these ore assemblages would reveal the nature of sulphides with respect to structure and lithology. This not only implies that both natural and structurally-induced porosity (and permeability) controlled the passage of mineralizing fluids through the suitable host rocks, but also has implications for the timing of mineralization. For sulphides to be hosted within bedding-sub-parallel fractures and low-angle microstructures (Fig. 4.11D), they must have been introduced to their current position during structural evolution (post-lithification) and associated fluid movement, during either primary mineralization or remobilization of pre-existing sulphides. Previous authors have claimed that any structural control of mineralization, observed in mine sections, is a result of this remobilization of precursor stratiform sulphides (e.g. Garlick, 1961). This process is considered responsible the formation of 'lateral secretion veins,' which are said to have formed during significant compaction of the host sequence where sulphides (and gangue minerals) are 'squeezed out,' recrystallized, and re-concentrated in small veins that have halos of barren host rock (i.e. no sulphides). This is said to account for the similar sulphide and gangue mineralogy of veins and host rock, and implies no external addition of vein component (i.e. they are all sourced from the host lithology during recrystallization). Although small-scale remobilization (millimetre- to centimetre- scale) has undoubtedly taken place during continued structural evolution and subsequent modification of pre-existing sulphides (e.g. replacement by chalcocite), remobilization on the scale required to generate the broad structural relationships of mineralization at Nchanga (e.g. the Upper Orebody at Chingola B) is rejected on the basis of the present study. The present author has observed none of the 'lateral secretion veins,' although, in reality, the scale of oxidation of primary sulphides within the Lower Orebody could have overprinted any evidence for and against remobilization. Instead, host-rock porosity and fracture-induced porosity/permeability, during structural evolution, are the favoured mechanisms for the flow of mineralizing fluids through the Nchanga host sedimentary rocks.

6.1.3 Ore mineral paragenesis and the copper-cobalt association

The petrographic observations made during this study strongly support an ore mineral paragenesis of pyrite (diagenetic) followed by hypogene chalcopyrite and bornite (± carrollite and chalcocite?) and carrollite, followed by hypogene chalcocite (section 4.2). The copper and cobalt phases may be part of the same mineralizing event; yet in many cases the carrollite shows local replacement of copper sulphides suggesting it is slightly later, particularly in the case of bornite (Fig. 4.6B). Some chalcocite may also have been introduced during the main phase copper mineralization. This temporal relationship from early, diagenetic pyrite to later

addition of copper iron sulphides and even later chalcocite is a common feature of the major sediment-hosted copper deposits (Brown & Chartrand, 1983; Brown, 1984).

These observations are in contrast to details of ore mineralization described by previous authors. For example, Annels *et al.* (1983) and Annels & Simmonds (1984) described co-existing ore mineral assemblages of chalcopyrite, bornite, and carrollite, from various Copperbelt orebodies, including Chibuluma, suggesting no significant temporal differences between the phases. Annels *et al.* (1983) also described early cobalt sulphides completely surrounded by 'later' copper sulphides from the Chambishi South East deposit, alternatively suggesting that the cobalt phase was earlier than the main introduction of copper. This study also has implications for the ore mineral zoning, described from various Copperbelt deposits, that is so often used as substantiation for any syngenetic model. The concept of primary sulphide zonation relies somewhat on the perception that the various sulphides (Fig. 2.8) were precipitated from the same solutions, whether that be seawater or hydrothermal. However, if pyrite and chalcocite are temporally different phases of mineralization (earlier and later respectively) and hence were probably precipitated from different fluids, then a primary zonation related to palaeo-shorelines or any other feature is untenable. These observations also suggest that fluids were active within the Nchanga system after the introduction of the bulk of the copper, leading to modification and possible enrichment of pre-existing sulphides, as indicated by the replacement of chalcopyrite and bornite by chalcocite.

At this stage, there is no evidence to explain why cobalt, although found in low concentrations (100-500ppm cobalt) within all copper-rich rocks, is only economically concentrated (>1% cobalt) within one small part of the southward-verging limb of the Nchanga Syncline. The setting and alteration associated with the cobalt ore minerals appears to be no different to those of copper; yet in one particular thrust-propagated fold zone cobalt occurs as high-grade mineralization. The apparent replacement of copper sulphides by cobalt sulphides may be a function of their relative solubilities and reactions during reduction of a common ore-forming fluid (as discussed below). This has led the present author to believe that both copper and cobalt are part of the same broad phase of mineralization, as no evidence has been found (including alteration, stable isotope, and fluid inclusion; see below) to suggest multiple mineralization and fluid events.

It is worth highlighting the extensive oxidation of primary sulphide mineralization that has taken place at Nchanga, in particular within the Lower Orebody. That the extent of oxidation of mineralization is controlled by proximity to the topographic surface (where sulphide mineralization dominates at deeper levels) supports the notion that malachite and chrysocolla

were formed during supergene processes. Permeable horizons or contacts, such as the top of the arkose unit, would have acted as conduits to fluids up to the present day. This explains the extent of oxidation in the Lower Orebody compared to the Upper Orebody. The latter, even though nearer to ground surface, has undergone relatively little oxidation.

6.1.4 Hydrothermal alteration and geochemistry: implications for fluid chemistry

The field, petrographic, and geochemical observations made during this Nchanga study provide compelling evidence for the passage of hydrothermal fluids through the Nchanga sequence. In addition, the data support a strong relationship between this hydrothermal alteration and the presence of copper and cobalt within the major ore zones.

The alteration assemblages, spatially related to mineralization, have been summarized in Chapter 4. In general terms, the assemblage of biotite plus sericite and quartz (± K-feldspar, rutile) is typical of potassic alteration (Reed, 1997; Jacobs & Parry, 1979). One important point to make is the similarity in the assemblages between the Upper and Lower Orebodies. Phlogopite, sericite, and rutile are consistent between the two, yet dolomite is only found within the Upper Orebody. However, dolomite may once have been present within the host rocks to Lower Orebody mineralization. The evidence for this is two fold: (i) dolomite is present within the Upper Orebody but only where copper sulphides have not been replaced by chalcocite; yet where they are, dolomite is absent; and (ii) minor occurrences of dolomite have been found within the oxidized Lower Orebody, and at even deeper levels abundant dolomite has been found related to rich bornite mineralization (e.g. 460m within borehole NE532, Chingola D, where no oxidation of primary mineralization has taken place; Roberts, 2003). There also appears to be an inverse relationship between the presence of dolomite and malachite. This suggests that dolomite was a component part of the primary alteration assemblage that was later leached and replaced during malachite precipitation (source of CO_3). That the oxidation of primary sulphides and abundance of malachite is enhanced dramatically within the Lower Orebody compared to the Upper Orebody supports this view.

No tourmaline has been found in association with the Upper Orebody, yet it is abundant in some arkose rocks as interstitial fine prismatic crystals and as alteration overgrowths on detrital tourmaline grains. Darnley (1960) identified abundant tourmaline alteration in his study of Copperbelt host rocks, which he interpreted as evidence of regional boron metasomatism. Darnley (1960) also noted sericitic alteration of feldspars, which, together with the tourmaline, he cited as evidence for extensive hydrothermal activity within the Copperbelt system by K- and B-rich fluids. The present author described similar occurrences of interstitial fine-grained and prismatic tourmaline associated with footwall mineralization at

Chibuluma (McGowan, 1999). Rutile is considered here as an accessory mineral associated with both orebodies. Garrard (1972) noted the spatial relationship between copper minerals and rutile in his study of the Chingola area. He claimed that ilmenite, within the host rocks, transformed into pyrite and rutile under reducing conditions (Deer *et al.*, 1966), during diagenesis and introduction of copper minerals. Taking into account the isocon plots (Appendix B6), TiO_2 is only enriched to a minor extent in the arkose unit, and there is little evidence to confirm whether rutile was formed from titanium already present within the arkose (pre-alteration) or introduced by the fluid that caused the alteration.

Another feature of the alteration mineralogy is the significance of the mineral phlogopite and its association with almost all occurrences of mineralization at Nchanga, in the Lower and Upper Orebodies, and also with Basement mineralization and the 'refractory' ore within 'Banded Sandstone' shear zones (section 4.3.1). An abundance of phlogopite is also almost always associated with structures at Nchanga, in particular the low-angle thrusts and shear zones. These features strongly suggest a common structurally-controlled origin for both phlogopite and copper, an observation also recorded by Molak (1995).

Phlogopite chemistry

The mineral chemistry of phlogopites provides insights into the evolution of the ore-forming fluid through the Nchanga sequence. These data suggest that the phlogopites of the Basement faults and thrust-related shear zones within the Lower Roan sequence are geochemically linked and of the same origin as those within the alteration assemblages of mineralized zones. This is because the fault phlogopite data are consistent with the overall up-sequence increase in the Mg/Fe ratios of the phlogopites (Fig. 4.17). The data suggest that the same fluid was responsible for the precipitation of the phlogopite, the Mg/Fe ratios being dependent on the composition of the fluid as it evolved whilst migrating through the Nchanga sequence. This is most likely to happen from depth (Basement) upwards through the sequence, so that Mg/Fe ratios are lowest in the basement, but iron was lost from the fluid when both sulphides (chalcopyrite and bornite: $CuFeS_2$ and Cu_5FeS_4 respectively) and phlogopite were precipitated within the ore zones. Phlogopites in the dolomite unit (above the mineralization and representative of a fluid leaving the mineralizing system) therefore have much higher Mg/Fe ratios. The data also suggest that this all occurred in a closed system: i.e. there was no external supply of iron to the fluid: as iron was consumed during sulphide precipitation, with no subsequent replenishment, the Mg/Fe ratio of the fluid increased.

The occurrence of high concentrations of fluorine within some of the hydrothermal Nchanga phlogopites is intriguing. There appears to be no explanation for why phlogopites within the

Lower Orebody host rocks are so fluorine rich (up to 4.3wt% F) and others are not (Fig. 4.18). The most likely source of fluorine, from what is known of the Copperbelt stratigraphy, is fluorite, which has been described by McKinnon & Smit (1961) within Basement granite rocks. Fluorite may also have been present within footwall siliciclastic rocks, as it can sometimes be found as a cementing mineral in sandstones (Deer *et al.*, 1966). In addition, the site at which these F-rich phlogopites are located may once have been the location for abundant evaporites (Diederix, 1977) with the possibility of fluorite also being present.

Selby & Nesbitt (1998) noted a similar phenomenon within porphyry copper deposits and proposed that the Mg/Fe ratios and fluorine contents of biotites in the Yukon porphyry deposit increase (e.g. become more Mg- and F- rich) within potassic alteration zones, compared to unaltered zones, an observation analogous to the observations made here. Beane (1974) also identified higher Mg-contents within alteration biotite/phlogopite (with potassic zones of copper porphyry deposits), where micas tended towards the phlogopite end-member in the annite-phlogopite-oxyannite solid solution series of ferromagnesium biotites. At the Kipushi Zn-Pb-Cu deposit in the Shaba Province of the Democratric Republic of Congo, Chabu (1995) noted the same relationship, where more fluorine-rich (4.41 to 6.39wt% F) and magnesium-rich (X_{Mg} up to 0.99) phlogopites were found associated with ore-grade mineralization, with the same ratios decreasing away from mineralized zones. Thus there appears to be a common theme of a sequential increase in Mg- and F-contents of phlogopites or biotites within potassic alteration zones and copper-rich rocks within ore deposits.

The magnesium and fluorine content of the phlogopites is also supported by some further work carried out by Roberts (2003) on the Mg/Fe ratios and fluorine contents of detrital tourmalines and their tourmaline overgrowths within the arkose unit and Lower Orebody mineralization at Nchanga. Within the alteration-associated overgrowths the Mg- and F-contents are considerably increased in the vicinity of copper mineralization. Slack (1996) suggested that the Mg-rich nature of tourmalines associated with stratabound deposits commonly indicates a component of either Mg-rich seawater or Mg-rich evaporitic brine. The fluid-inclusion data, presented in this study, also strongly support the presence of an Mg-rich brine within the Nchanga sequence, an aspect that is further discussed in section 6.2.5.

Whole-rock geochemistry

In terms of major element geochemistry, enrichments in MgO and CaO within the Upper Orebody and MgO within the Lower Orebody are significant. These undoubtedly relate to the abundances of phlogopite and dolomite that are commonly found within these zones. This enrichment does not always directly correlate with copper and cobalt but can be observed

physically above or below high concentrations and may, therefore, be representative of a halo of alteration around anomalous concentrations. These observations point to the primary fluid that caused this alteration being principally Mg-rich with significant amounts of calcium, where rock-fluid interactions caused the precipitation of Mg-rich minerals such as phlogopite and dolomite. There is a suggestion, in some downhole plots, of K_2O enrichment across the ore zones (in particular the Upper Orebody). However, this may be a result of an increase in the microcline component within the host unit and the context to which this is related to hydrothermal alteration (phlogopite and sericite) is unknown.

Trace element and base metal concentrations across the Lower Orebody host rocks, particularly at the contact between the arkose and overlying shale suggest that Ba, Bi, U, As (and possibly V) are all enhanced directly at the contact, as well as minor Zn and Mo. The relationship of copper mineralization and alteration with these elements suggests a possible common fluid origin. In light of this, there are two factors which may control their deposition: (i) the change of fluid composition during copper precipitation and wallrock interactions (i.e. reduction of an ore fluid; see later), and (ii) the redox front provided by the arkose shale contact, where elements such as U and Mo are much more mobile in oxidizing fluids (Levinson, 1980) and would precipitate during reduction. Sutton & Maynard (2002) noted increases in barium at the arkose-shale contact, and interpreted this as evidence for a Cu-, K-, Ba-, and Cl-bearing fluid that mixed with a more reducing fluid at the site of the Lower Orebody, and hence caused deposition of Ba in the form of barites. However, without evidence of the presence or mixing of two separate fluids, the natural reduction front of the 'Lower Banded Shale' is a far more feasible control on the deposition of some of these elements.

Implications for fluid composition and chemistry

The geochemical data presented here suggest that the hydrothermal fluids responsible for the alteration (and potentially the copper-cobalt mineralization) within the Nchanga host rocks were principally Mg- and Ca-rich (also indicated by the first melt data of fluid inclusions, see below). Field and petrographic observations within the most intense alteration zones reveal abundant phlogopite (± dolomite) and support the interpretation that Mg- and Ca-rich fluids were present within the system. Lefebvre (1989) also interpreted the hydrothermal alteration assemblages, associated with copper and cobalt mineralization, to be indicative of Mg-rich fluids from the deposits within the Shaba region of the Democratic Republic of Congo.

The dominant mineral assemblage of phlogopite, sericite, and quartz can be used to estimate fluid temperature and chemistry. Sericite and quartz alteration can occur over a wide range of

temperatures (Rose & Burt, 1979). However, phlogopite is reported to be stable in the solid phase between 25° and 350°C (Jasinski, 1988). Inan & Einaudi (2002) described a potassic alteration assemblage consisting of phlogopite, sericite, and quartz associated with quartzite-hosted nukundamite-bearing copper ore in the Bingham porphyry deposit in Utah, an almost identical alteration phase to that observed during this Nchanga study. They interpreted the assemblage to be indicative of fluids at approximately 350°C. The fluids associated with this porphyry deposit were found to be magmatic brines, and so had similar salinities to the Nchanga fluids. This type of potassic alteration (by copper-rich solutions) is also indicative of near-neutral to slightly acidic fluid pH conditions with a typical pH of around 5 (5.3 is the optimum pH for the co-transport of copper, sulphur and iron; Rose & Burt, 1979; Beane, 1974). Darnley (1960) suggested that the alteration assemblages within Copperbelt host rocks, associated with mineralization, indicated temperatures in the region of 400° to 600°C, although he reduced this to 300° to 400°C based on the evidence for sericitization of almost all arenite orebodies. Therefore, the mineral assemblage recorded in this study suggests a temperature of alteration of approximately 300° to 350°C. The higher temperatures would be in proximity to fault zones, e.g. thrust-zones within the 'Banded Sandstone' where phlogopite development is much more extensive, whereas lower temperatures away from fault zones would produce more sericite-dominant assemblages. This may explain why phlogopite within the Upper Orebody is generally developed within fault-propagation fold zones, becoming more scarce away from such zones. These estimates are in good agreement with the pressure-corrected fluid inclusion data (see below).

Previous authors have described greenschist facies metamorphism of the Katangan sedimentary rocks at Nchanga to be represented by the development of biotite, sericite, and scapolite, and the recrystallization of the host quartz component (McKinnon & Smit, 1961; Fleischer *et al.*, 1976). However, the field and petrographic observations presented here suggest that all these features are in fact related to fluid processes occurring during structural evolution of the Nchanga sequence. Distinct metamorphic and alteration assemblages have not been recognized at Nchanga, suggesting either: (i) minerals related to metamorphism have been overprinted or masked by abundant hydrothermal alteration assemblages, or (ii) peak metamorphism (low-grade), alteration, and hence mineralization, occurred simultaneously during structural development within the Nchanga system. The latter is favoured by the present author, based on the petrology carried out during this study. Phlogopite development was reported to be restricted to argillaceous units (McKinnon & Smit, 1961); yet this is clearly not the case, as it has been observed within Basement faults and arenaceous units. Recrystallization of all arkosic or arenitic units is common, and a component of it may be related to metamorphism, although it is more extensive within mineralized and structurally

affected zones. A common assemblage of muscovite, sericite, and chlorite is associated with modification of pre-existing sulphides during replacement by chalcocite. It is feasible, therefore, that this actually represents metamorphism of Katangan sedimentary rocks during continued deformation.

6.1.5 Palaeo-fluid and oxygen isotope analysis: implications for fluid characteristics

The fluid inclusion data presented in section 5.2 revealed homogenization temperatures and salinities of 230°C and 30-38 equivalent wt% NaCl for Basement and arkose high-angle veins, 180°C and 30-32 equivalent wt% NaCl for Lower Orebody veins, 240°C and 33-35 equivalent wt% NaCl for thrust-related veins, and 160°C and 30-34 equivalent wt% NaCl for Upper Orebody veins. The homogenization data (T_H), however, may only represent minimum temperatures of formation, and may not be representative of the true fluid temperature at the time of vein precipitation, which is dependent on pressure (a function of depth of formation) and the density of the trapped fluid (Shepherd *et al.*, 1985). As discussed above, the thrust-fold development of the Nchanga sequence most likely took place during the Lufilian Orogeny, ~550 to 560 Ma (300 Ma after the deposition of the Lower Roan). The veins, hosted within the Lower Roan and sampled for fluid inclusion analysis, are thought to be syn-tectonic with this structural phase, and so it follows that they probably formed under considerable burial depth during basin-scale deformation. This depth of burial (relating to lithostatic pressure) has a major influence on the true formation temperature of the vein, and the homogenization data must be corrected accordingly, which will also impact on the oxygen isotope results.

Pressure correction

The density of the trapped fluid can be calculated by knowing the average degree of fill and volumetric proportion of any salt phases present (equation 6.1; Shepherd *et al.*, 1985):

Equation 6.1: $$\rho_{TOT} = (V_V * \rho_V) + (V_S * \rho_S) + (V_L * \rho_L)$$

Where

- V_V, V_S, and V_L are the volumetric proportions of the vapour, solid (NaCl), and liquid respectively
- P_V, ρ_S, and ρ_L are the density of the vapour (0), solid (NaCl; 2.16), and liquid (1.2) at room temperature respectively

Taking average values for the volumetric proportions, this yields average densities for the fluids of 1.24 g/cm^3 for high-angle veins, 1.24 g/cm^3 for Lower Orebody veins, 1.22 g/cm^3 for thrust-related veins, and 1.24 g/cm^3 for Upper Orebody veins.

Determining the actual depths of entrapment is complex. Some previous authors have estimated burial depths and from these it is possible to estimate corresponding lithostatic pressures. Annels (1989) estimated the thickness of rocks overlying the stratigraphic position of mineralization to be between 4.7 and 6.9km, based on the observations of the Katangan sequence in Zambia and the Shaba province of the Democratic Republic of Congo of Garlick (1961), Demesmaeker (1961), and Francois (1974). For the purposes of this correction a minimum value of 4.7km will be used, which is approximately equivalent to a lithostatic pressure of 1200 bars (Yardley, 1989). This equates to pressure corrections on the homogenization temperatures of approximately 50° to 70°C for all vein types (using the pressure correction equation of Bodnar & Vityk, 1994). These are quoted as approximations only due to the error involved in the calculations, including estimating the depth of burial and the calculation of lithostatic pressure, which would vary depending on the bulk composition of the overlying rocks (e.g. clastics versus carbonates). This correction suggests that the actual fluid temperatures, during formation of the veins within the Nchanga system, could have been much higher than the homogenization temperatures originally suggested in section 5.2.3 (Table 6.1; Fig. 6.1):

Vein Type	T_H (°C) range	Modal T_H (°C)	Press. corr. (°C)	Corr. T (°C)
High-angle	200-240	230	~70	~300
Lower Orebody	140-220	180	~60	~240
Thrust-related	190-280	240	~70	~310
Upper Orebody	130-220	160	~60	~220

Table 6.1: Corrected homogenization temperatures with respect to pressure to give estimated true formation temperature of fluids (based on the pressure correction curve presented in Shepherd *et al.*, 1985).

Considering the depth to which the rocks, hosting these veins, were buried and the fact that the veins appear to be syn-tectonic and related to regional compression (i.e. basin-wide deformation and thrust-related thickening equates to increased burial depths), the higher, pressure-corrected modal T_H temperatures are favoured. The results of Richards *et al.* (1988), in their study of the Musoshi deposits, Zambia, support the higher range of temperatures suggested here with temperatures of 395 ± 5°C for high-angle veins within the footwall to

mineralization (equivalent to the high-angle veins measured at Nchanga). With the correction applied the Nchanga results are closer to these temperatures.

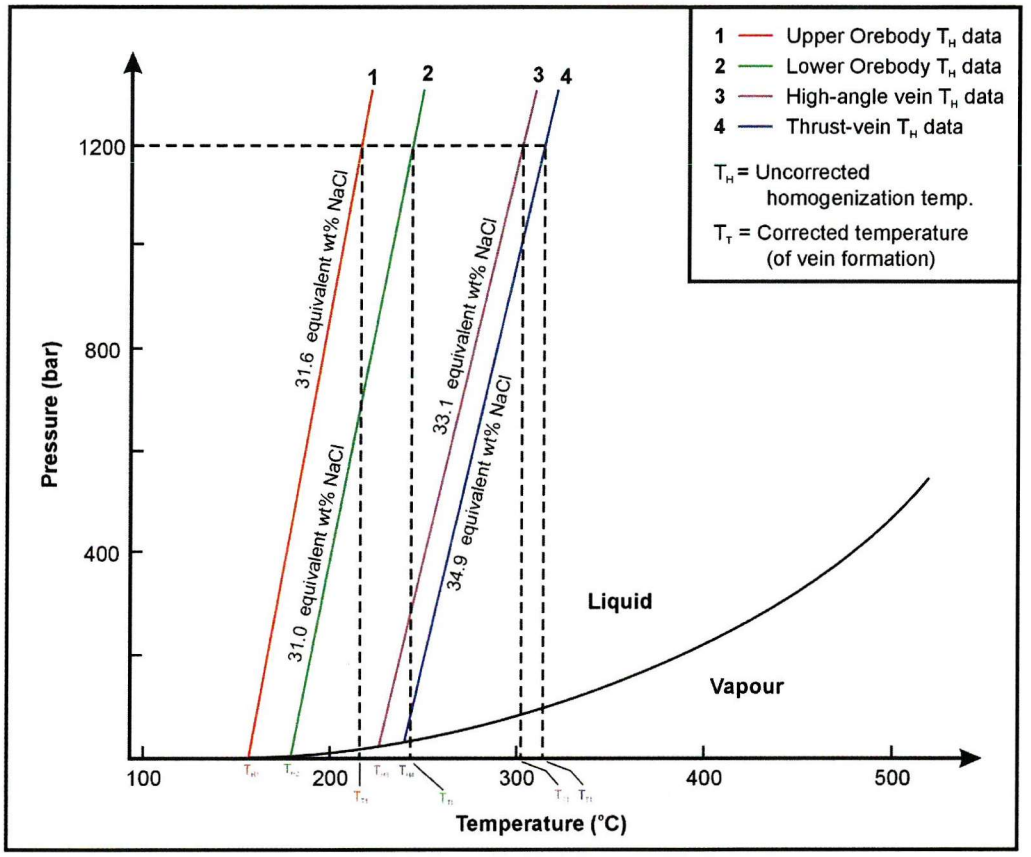

Figure 6.1: Isochore diagram to show the correction applied to the homogenization results for each vein type collected during this study based on the composition and depth of burial of the fluids during their formation (using mean salinities, modal T_H values, and the pressure-temperature equation of Bodnar & Vityk, 1994).

Interpretation

The corrected homogenization data suggest that the vein-forming fluid within ore zones was a high-salinity and fairly medium-temperature variety, and indicates a composition relating to the H_2O-NaCl-$MgCl_2$ and H_2O-NaCl-$CaCl_2$ systems. Secondary fluids within the Upper Orebody vein types were slightly lower temperature (pressure corrected = ~200°C) with similar compositions. No salinity data were recorded for secondary inclusions. Analysis of fault-related samples from high-angle structures within the granite and arkose (below the Lower Orebody) and low-angle thrust zones within the 'Banded Sandstone,' reveal fluids that are similar in salinity and composition (evidence for $MgCl_2$ and $CaCl_2$ as well as NaCl), but higher temperature (~50°C higher). This evidence alone suggests that the fluids that precipitated these veins, within each of the locations studied, could have a common origin. Fluids from fault zones (i.e. the original conduit) are likely to be hotter than fluids that have diffused into the surrounding wallrock over time. Further supporting the pressure-corrected

temperatures are the hydrothermal alteration assemblages that suggest temperatures of <250°C, consistent with the abundance of phlogopite within fault zones.

The evidence suggests that these mineralized quartz veins and the copper mineralization have the same fluid source and formed at the same time. The identical sulphide and gangue mineralogy between veins and host rock and that both disseminated and vein-hosted sulphides have similar sulphur isotope compositions support this interpretation, an observation also noted by Annels (1989). Therefore, copper (and cobalt) was probably transported to the current site of deposition by high-salinity, $MgCl_2$- and $CaCl_2$-rich brines that ranged in temperature from 220° to 310°C. Although it cannot be confirmed with current available data, the secondary fluids, with a similar composition but lower temperatures (180°-200°C), may have been responsible for the later replacement and modification of pre-existing sulphides, i.e. chalcocite replacement of bornite and chalcopyrite.

Temperature-corrected oxygen isotope data

The pressure-corrected fluid inclusion temperatures must also be applied to the calculation of fluid $\delta^{18}O$ as it will have some effect on the values obtained. The plots of T_H against $\delta^{18}O_{fluid}$ (Figs. 5.18 to 5.21) show that higher temperatures will yield higher $\delta^{18}O_{fluid}$ values for the given $\delta^{18}O_{quartz}$ values (Table 6.2).

Vein type	Temp. (°C) (mode)	Mean $\delta^{18}O_{quartz}$ (‰)	$\delta^{18}O_{fluid}$ (‰) uncorrected	$\delta^{18}O_{fluid}$ (‰) corrected
High-angle veins	300 (Q)	+11.9	+2.0	**+5.0**
Lower Orebody	240 (Q)	+14.0	+1.0	**+4.6**
Thrust-zone	310 (Q)	+16.8	+7.4	**+10.3**
	310 (D)	+16.6	+7.3	**+10.1**
Upper Orebody	220 (Q)	+14.0	–0.5	**+3.6**
	220 (D)	+13.1	–1.4	**+2.7**

Table 6.2: Calculated $\delta^{18}O$ of fluids that are thought to have precipitated quartz or dolomite using the fractionation factors of Matsuhisa *et al.* (1979) and temperatures adjusted for a pressure correction to the fluid inclusion homogenization data. Q = quartz, D = dolomite.

One striking feature of the data, when comparing the $\delta^{18}O_{fluid}$, calculated from the measured $\delta^{18}O_{quartz}$ and $\delta^{18}O_{dolomite}$, is the similarity between the calculated fluid values. Petrographic observations suggest that the quartz vein material within thrust-related shear zones has a common source with the dolomite from those zones, as both are restricted to deformed rocks. In the same way the quartz vein material (± dolomite) within the Upper Orebody arenite appears to be genetically related to the dolomite alteration that is spatially associated with ore

sulphides. In both cases the oxygen isotope data support these observations and indicate a common fluid origin for the vein quartz and abundant dolomite within these zones.

When compared to the $\delta^{18}O_{fluid}$ of typical natural waters (Fig. 6.2), the corrected $\delta^{18}O_{fluid}$ values for Nchanga veins (indicating high salinity brines) lie in the field occupied by metamorphic and magmatic waters but more significantly also lie in the field of basin-derived brines or 'formation' waters (Sheppard, 1986; Taylor, 1997). Surface waters (including meteoric types and seawater) have had consistent $\delta^{18}O_{fluid}$ values of around 0‰ for the past 2.5Ga (Sheppard, 1986). Basinal brines typically yield $\delta^{18}O_{fluid}$ signatures that indicate an original surface source (Wilkinson *et al.*, 1999), with increasingly positive values resulting from water-rock interaction and exchange (Fritz, 1976; Sheppard, 1986). One such example of these are bittern brines which can form by dissolution of pre-existing evaporites (Kesler *et al.*, 1995; Wilkinson *et al.*, 1999).

In light of the geological observations made and current knowledge of Copperbelt geology, a magmatic source for these high-salinity brines is considered unlikely, although the $\delta^{18}O_{fluid}$ values could lie in the field for magmatic fluids (depending on δD values which are not available; Fig. 6.2). Instead the medium temperature, high-salinity, and syn-tectonic character of the high-angle, Lower Orebody, and Upper Orebody veins (and Upper Orebody dolomite alteration) are consistent with basinal fluids, in this case a surface-derived fluid that has undergone significant interaction with rocks to now yield increased $\delta^{18}O_{fluid}$ values. These were most likely fluids that were generated within the host basin and then were expelled, during subsequent compression and deformation, towards the basin margins (Oliver, 1986; Hanor, 1979; Garven & Raffensperger, 1997). The fluid inclusion first-melt temperature data also point to these fluids being $MgCl_2$-rich as well as containing significant amounts of $CaCl_2$ and NaCl. The thrust-related veins from within the 'Banded Sandstone' unit yield slightly higher temperatures and increased $\delta^{18}O_{fluid}$ values, yet they appear to be similar in terms of salinity and composition ($MgCl_2$-rich). However, the fluid inclusion and oxygen isotope data for the latter are based on one and two samples respectively and a more detailed investigation of a greater number of samples would further constrain the fluid source. With the similar composition and salinity they are thought to represent the same fluid as identified within the Upper and Lower Orebodies.

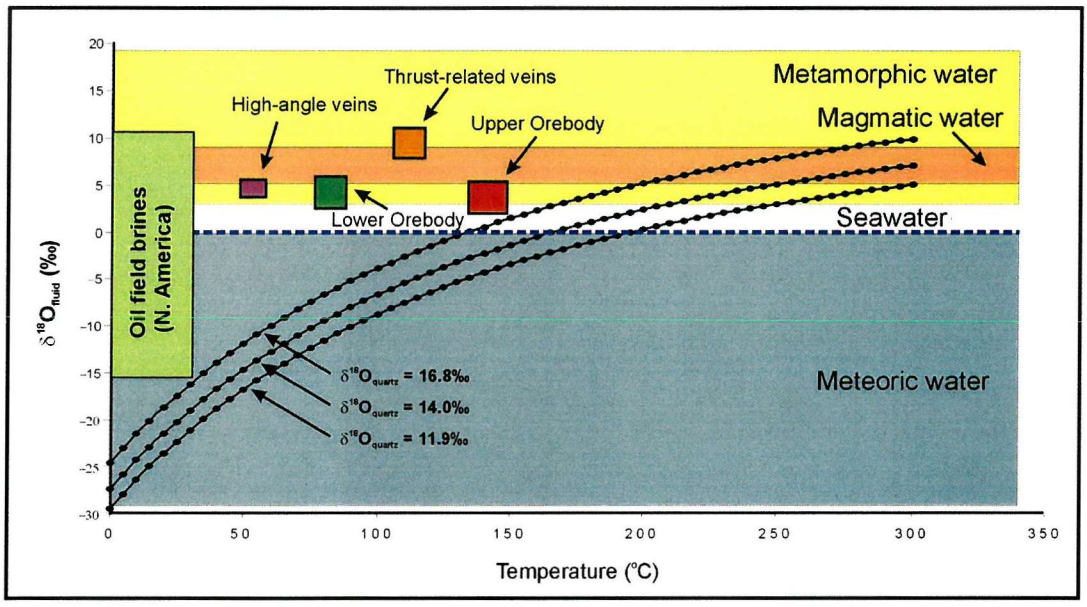

Figure 6.2: Comparison of $\delta^{18}O_{fluid}$ data (corrected following pressure correction of T_H data) from Nchanga with typical natural waters (Sheppard, 1986; using data of Clayton *et al*, 1966; Hitchon & Friedman, 1969; and Kharaka *et al.*, 1973). Fields for Nchanga fluids apply for $\delta^{18}O$ values only (not temperature).

Interestingly, the $\delta^{18}O_{fluid}$ results, calculated with uncorrected homogenization temperatures, would also lie in the field for basinal or oilfield brines. These would be similar fluids, with a less positive $\delta^{18}O_{fluid}$ signature, indicating less extensive water-rock interaction. However, for the reasons outlined above, the pressure-corrected temperatures and higher $\delta^{18}O_{fluid}$ values (indicating more extensive water-rock interaction) are favoured.

Detrital versus recrystallized quartz

The $\delta^{18}O_{quartz}$ data for detrital, recrystallized, and vein samples highlight a clear difference between the three sample types. In the case of each orebody the $\delta^{18}O_{quartz}$ of detrital quartz shifts to heavier values, towards quartz-vein $\delta^{18}O$, once it has been recrystallized. Considering these results and the fact that the veins analysed are the only evidence of major fluid infiltration and quartz introduction into the host rocks, it seems likely that the fluid responsible for vein quartz formation (with heavier $\delta^{18}O_{quartz}$) was also responsible for the recrystallization of the host detrital quartz. Recrystallization of the host arenites or arkoses is strongly spatially associated with the major concentrations of copper and cobalt mineralization of the Lower and Upper Orebodies. Therefore, the concept that quartz veins that host sulphides and disseminated sulphides have a common fluid source, and that this fluid was the transporting medium for copper to its current site of deposition, is strengthened.

6.1.6 Sulphur and carbon isotope analysis

Compared to the published data from the Copperbelt (e.g. Dechow & Jensen, 1965; Fig. 5.30), the Nchanga data reveals similar ranges of $\delta^{34}S$ for all sulphide data. However, the subtlety of the *in situ* laser technique, used in the present study, has extended the range of $\delta^{34}S$ values from the Copperbelt (this study shows the highest and lowest data published to date), and has also yielded a better understanding of the variation of $\delta^{34}S$ with paragenesis. In addition, these data contrast with those determined for other well-studied sediment-hosted deposits; for example, White Pine ranging from –22‰ to +12‰ (Burnie *et al.*, 1972), and Kupferschiefer ranging from –44‰ to -2‰ (Marowsky, 1969; Bechtel *et al.*, 2001; Fig. 5.30). Precambrian seawater $\delta^{34}S$, at the time of Lower Roan deposition, has been estimated at 17.5‰ (Holser & Kaplan, 1966; Claypool *et al.*, 1980).

Previous authors have suggested that a major component of Copperbelt mineralization gains its sulphur from bacterially-reduced seawater during diagenesis. The $\delta^{34}S$ value of any bacteriogenic sulphide available for deposition of early diagenetic sulphides depends on: (i) the $\delta^{34}S$ value of this seawater sulphate, (ii) the kinetic isotope effect associated with bacterial sulphate reduction, and (iii) the open or closed nature of the system (Schwarcz & Burnie, 1973; Ohmoto, 1986). The observed $\Delta_{SO4\text{-}Sulphide}$ for Precambrian diagenetic pyrites (with $\delta^{34}S$ of –1‰ to –18‰) at Nchanga averages around 30‰, which is consistent with open-system bacterial reduction of contemporaneous seawater sulphate (Ohmoto 1986; Machel *et al.*, 1995).

Dechow & Jensen (1965) explained the heavy and sometimes narrow range of $\delta^{34}S$ of the copper sulphides by suggesting metamorphic homogenization of original sedimentary $\delta^{34}S$ signatures (Gustafson and Williams, 1981). However, the distinct range of diagenetic $\delta^{34}S$ from shale units and the contrasting signatures of the Upper and Lower orebodies reported in this study suggest this is not the case. Furthermore, metamorphic re-equilibration of sulphides at this low grade results only in homogenization, if any, on a millimetre scale (Willan & Coleman, 1983; Crowe *et al.*, 1990; Skauli *et al.*, 1992; Velasco *et al.*, 1998), with large-scale, pre-metamorphic $\delta^{34}S$ variation generally being preserved (Rye & Ohmoto, 1974). In addition, during conditions of burial metamorphism, simple re-equilibration of sulphides would have occurred with the diagenetic pyrites within the 'Lower Banded Shale,' if this were, in fact, the process that generated these $\delta^{34}S$ signatures. Instead, the $\delta^{34}S$ of copper sulphides is more indicative of sulphide derived from the thermochemical reduction of a sulphate-enriched fluid (Machel *et al.*, 1995). The different fields of bacterially-produced, organic, and thermochemically-produced sulphide are graphically represented by

Emery & Robinson (1993) where the latter occupies a heavier and more narrow range of $\delta^{34}S$ values (consistent with Nchanga sulphides) compared to the much broader and generally negative range of bacterially produced sulphide (Fig. 6.3). In such systems, the likely sulphate source would have been remobilized evaporite minerals (e.g. Sverjensky, 1987; Naylor *et al.*, 1989).

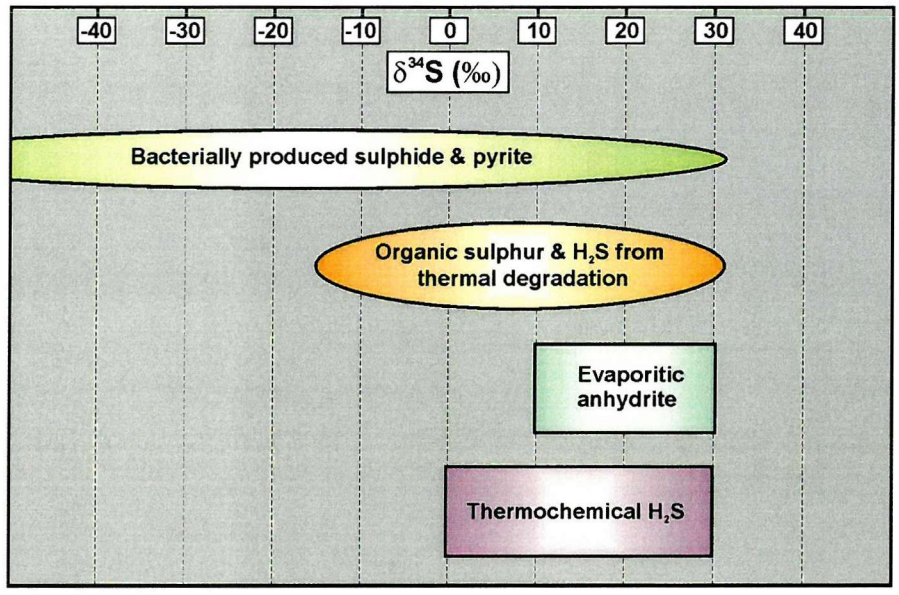

Figure 6.3: The $\delta^{34}S$ signature of various sulphur sources and sulphides (Emery & Robinson, 1993).

A clear distinction between the range of values for Lower Orebody, Upper Orebody, and late sulphides has been made in this study. Upper Orebody sulphides, with $\Delta_{SO4\text{-}Sulphides}$ (from the value of Precambrian seawater sulphate of +17.5‰) of only 5‰ compared to 10-15‰ for Lower Orebody sulphides suggest sequential reduction in an increasingly closed system. In light of this, the isotopically heavy pyrite in crosscutting veins may represent even later-stage mineralization, which is consistent with their discordant nature. Machel *et al.* (1995) claimed that fractionations of ~15‰ and ~10‰ $\delta^{34}S$ represent thermochemical sulphate reduction (TSR) at temperatures of 150°C and 200°C respectively. This implies that the lesser the fractionation the hotter the conditions under which TSR took place. Applying this to the $\delta^{34}S$ values from Nchanga would suggest that Upper Orebody sulphides were precipitated at temperatures greater than 200°C, and that Lower Orebody sulphides were precipitated at slightly lower temperatures.

The interpretation of closed-system reduction suggests that the amount of sulphate to be reduced, due to precipitation of sulphides, became more and more limited within the system. Supporting the notion of a closed system are the iron and magnesium concentrations within

phlogopites from Nchanga, which suggest the passage of a fluid though the sequence and the consumption of iron, with no replenishment from an external source. Considering the relationship of the phlogopites to the sulphides, it seems reasonable to assume that the same fluid precipitated both as it evolved in this closed system. An alternative explanation for lighter $\delta^{34}S$ values for Lower Orebody sulphides is the fact that copper sulphides within the arkose and 'Lower Banded Shale' replace earlier formed diagenetic pyrite, which has a range typical of bacterially-reduced sulphate corresponding to $\delta^{34}S$ of –17‰ to –1‰. Therefore, if there is an element of bacteriogenic sulphide incorporated into copper sulphides during this replacement process (as well as thermochemically-reduced sulphate), the resultant $\delta^{34}S$ of the Lower Orebody sulphides would appear lower.

Thermochemical sulphate reduction of an ore-fluid requires oxidation of organic matter as part of the redox process, which liberates H_2S via the reaction (Equation 6.2):

Equation 6.2: $\mathbf{CaSO_4 + CH_4 \rightarrow CaCO_3 + H_2S + H_2O}$ (Warren, 1999).

Common reaction products include carbonate, oxidized hydrocarbons, and base metal sulphides, although no solid bitumen is found where methane is the main or only reactive hydrocarbon (Machel *et al.*, 1995). This latter point is significant regarding the Nchanga study as no solid or pyrolised bitumens have been found within any samples at Nchanga. This suggests that a gaseous hydrocarbon (i.e. methane), derived from thermal maturation of solid or liquid hydrocarbons, may be the reducing agent of a potential ore-fluid (a notion also suggested by Brown, 1978). This theory is supported by the range of $\delta^{34}S$ obtained here which is very similar to the range of $\delta^{34}S$ for H_2S from various gas fields (Ohmoto & Rye, 1979; Fig. 6.4), and made more plausible by the fact that the host units of the Nchanga sulphides (e.g. arenites and arkoses) commonly form clastic reservoirs for hydrocarbon gases. In addition, the antiformal structures, formed during deformation, would have increased porosity and hence the amount of methane that could have been held within those zones would also be increased. Thermochemical sulphate reduction (TSR), with geologically feasible reaction rates, occurs above a minimum temperature of 100-140°C (Machel, 2001), which is well below the homogenization temperature (T_H) data collected during this study.

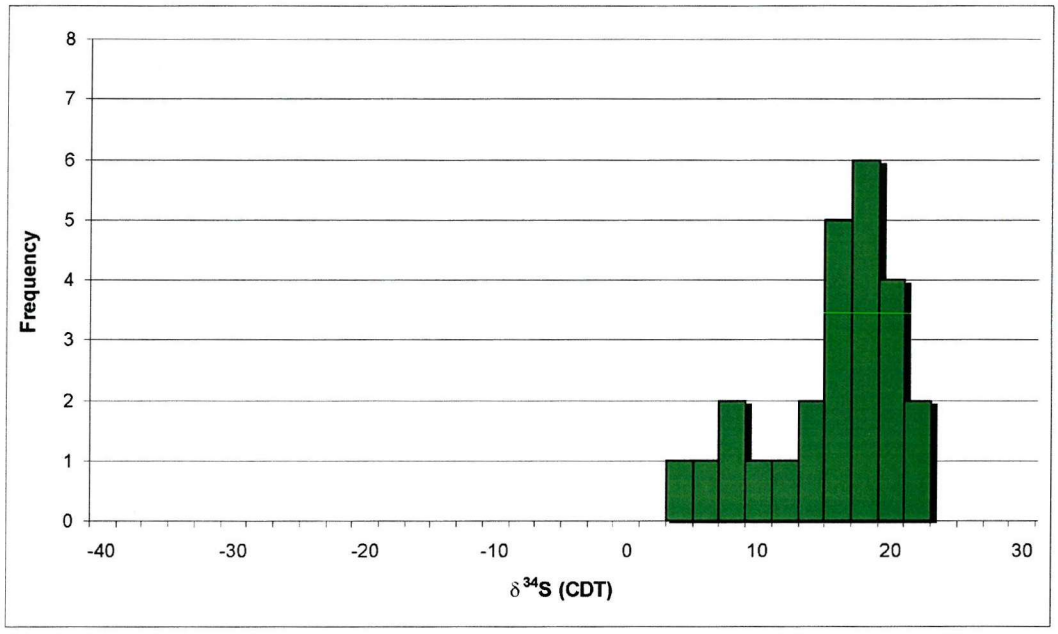

Figure 6.4: The $\delta^{34}S$ (‰) signature of H_2S from various gas fields (including the Sour Gas Field, Big Horn Basin, Smackover, Alberta Basin, and Aquitaine Basin; Ohmoto & Rye, 1979).

As demonstrated above, carbonate is a common reaction product of thermochemical reduction in these kinds of systems (Machel, 1987; Machel *et al.*, 1995). Anderson & Garven (1987) constrained this a little further by claiming that dolomite precipitation, as a reaction product, is consistent with *in situ* thermochemical reduction of a sulphate-rich fluid. Rye & Ohmoto (1974) discussed the variation of $\delta^{13}C$ values of carbonate gangue minerals for a number of hydrothermal ore deposits. The data reveal generally negative $\delta^{13}C$ values for carbonates precipitated during sulphide deposition from the original ore-forming fluid, including –3‰ to –8‰ for the Providencia deposit and –3‰ to –9‰ for Casapalca. These values are interpreted to represent a deep-seated source for the hydrothermal carbon. However, potentially significant for this Nchanga study, Rye & Ohmoto (1974) identified an increase in $\delta^{13}C$ through time, interpreted as reflecting the dissolution of host limestones by the ore-forming fluid during deposition of the mineralization. Therefore, only the early $\delta^{13}C$ values actually reflect the primary hydrothermal fluid (Rye & Ohmoto, 1974). These results are based on carbon species already present within the ore-forming fluid, either as CO_2 or CH_4, yet in the Nchanga situation it is more likely that a carbon-bearing phase was already present within the host sequence and that sulphide (and carbonate) precipitation was triggered by the reduction of an ore fluid by that carbon. Dissolution of marine-derived dolomites within the sequence (e.g. Upper Roan dolomites from this study with $\delta^{13}C$ signature of +1‰ to +2‰) may have pushed the $\delta^{13}C$ of the dolomite alteration within the Upper Orebody to more positive values, as observed by Rye & Ohmoto (1974). If this were the case the $\delta^{13}C$ of this dolomite alteration would represent a mix of organic carbon (typically less than –15%) and marine

carbon (typically ~0‰), the former being the original $\delta^{13}C$ of the dolomite alteration, the latter being introduced during dissolution of marine limestones or dolomites over time. The $\delta^{13}C$ data for dolomite alteration within the Nchanga Upper Orebody are therefore consistent with dolomite formed during thermochemical reduction of an oxidized fluid, in this case carrying significant amounts of copper (and cobalt), and incorporating a contribution from organic carbon as well as remobilized marine carbon. This contrasts with marine (reef?) dolomites that are typical of marine carbon source where CO_2 (atmospheric CO_2 has $\delta^{13}C$ of –7‰) is dissolved in seawater as HCO_3^-, which is approximately +7‰ to 10‰ enriched in $\delta^{13}C$ with respect to CO_2 (Ohmoto & Rye, 1979) and yield $\delta^{13}C$ values of about 0‰.

6.2 Ore genesis

The discussion of any genetic model for a mineral deposit or province concerns the various aspects of source, migration, and trap. This section deals with ore genesis from the source of ore-forming components to local controls on mineralization, based on the results of this present study.

6.2.1 Source of metals

The source of the vast amount of metal contained within the Copperbelt is perhaps the most fundamental question when dealing with the genesis of these spectacular orebodies. However, it is probably the most complex issue and is least likely to be solved by a mine-based study. Sweeney & Binda (1994) summarized the suggested sources of the copper and cobalt of the Copperbelt, which include magmatic (Darnley, 1960), metamorphic (McNaughton, 1953), rifting-induced exhalations (Annels 1989), erosion of basement anomalies (Garlick, 1961), leaching of basement (Sweeney *et al.*, 1986), deep-derived hydrothermal fluids and leaching at deep crustal levels (Raybould, 1978), and leaching of footwall red beds (Hoeve & Quirt, 1989). It has also been claimed that the cobalt was sourced from mafic volcanics (Annels & Simmonds, 1984; Brown, 1984), by leaching of the basement (Sweeney & Binda, 1994), or was basinal in origin (Sweeney, 1985, from Sweeney & Binda, 1994).

In light of the results and interpretations presented here, the most likely source for the copper (and cobalt) is either leaching of Basement or leaching of the thick sequence of footwall siliciclastic rocks. Anomalous concentrations of copper within the basement have, in the past, been described as pre-Katangan porphyry copper deposits and hence have been identified as potential sources of metals for the Copperbelt-style, stratiform deposits within the Lower Roan (e.g. the Samba 'porphyry; Wakefield, 1978). However, in their studies of the Samba

and Lumwana deposits respectively, Sillitoe (*pers comm.*, 2002) and Nisbett (*pers comm.*, 2002) both considered the mineralization to be Copperbelt style, but hosted in Basement rocks, which could have been introduced at the same time as the major ore occurrences on the Copperbelt. That major, deep-rooted extensional structures (later inverted) may have played a role in the migration of copper- and cobalt-rich solutions to the sites of mineralization opens up the possibility that copper may have been sourced from the extensive leaching of major volumes of Basement rocks. This remains the most likely source for the copper and cobalt of the Copperbelt.

6.2.2 Source of fluids and the role of evaporites

Previous authors have suggested that oilfield brines, as potential ore-forming solutions, played a major role in the formation of stratiform and vein deposits, in particular with reference to Mississippi Valley-type deposits (Barnes, 1979; Wilkinson, 1990). The basinal brine model of ore formation involves the genesis of hot, saline solutions deep within the sedimentary basin, and the subsequent migration of these fluids along major aquifers or structures, where they form ore deposits at varying distances (often greater than 100km) from their source (Sverjensky, 1984, 1989; Wilkinson, 1990; Garven & Raffensberger, 1997). As the formation or oilfield brine migrates, the composition may change, as a result of water-rock interactions (e.g. with red beds or evaporite sequences), to the composition of the final ore-forming solution (Sverjensky, 1984). High salinity, Na-Ca-Cl brines are commonly located within deep sedimentary basins and are potential ore-forming fluids (also Mg-rich in the case of Nchanga). There are a number of mechanisms to generate this high salinity, including the evaporation of seawater (prior to brine development) and dissolution of evaporite sequences (during brine migration). This mechanism is significant in order to generate the metal-carrying capabilities of the fluid, discussed further in section 6.3.3.

Considering the oxygen isotope results of this study, the most likely source of the ore-forming fluid is surface-derived (a combination or one of seawater, meteoric, or connate waters) that has evolved within the host basin (i.e. became a brine) and subsequently been expelled during compression and deformation. The fact that the brines were principally Mg-rich and also Ca-rich suggests either a seawater or evaporite source. Taking into account the geology of Zambia, dissolution of evaporites within the host basin, to form Mg-rich brines, is the favoured mechanism for the generation of the mineralizing fluids (Eugster, 1980). The relatively medium-temperature, high salinity, and $MgCl_2$ and $CaCl_2$ character of the fluids is more typical of basin-derived fluids than any other of the potential sources (e.g. metamorphic, magmatic) and the $\delta^{18}O_{fluid}$ is consistent with this interpretation (Wilkinson *et al.*, 1999). Evaporites can play a major role in the formation of basin-hosted copper deposits. Not only

are they a potential source for the high salinity and oxidized sulphur (in the form of sulphate SO_4^{2-}), but they may also be crucial to the development of fO_2 conditions required to transport copper and cobalt in ore-forming concentrations (see section 6.3.3; Sverjensky, 1987).

6.2.3 Transport of copper and cobalt and fluid characteristics

The 'ideal' ore fluid for transporting copper is a Cl-rich brine of intermediate redox state where cuprous-chloride complexing promotes very high copper solubilities (Sverjensky, 1984; Rose, 1989; Seward & Barnes, 1997). Strong complexes are formed between Cl^- and Cu^+, e.g. $CuCl_2^-$ and $CuCl_3^{2-}$, which are most stable under intermediate redox conditions and allow fluid concentrations of >100ppm copper (Rose, 1976, 1989). However, these studies were for solutions at a temperature of only 100°C. Xiao *et al.* (1998) studied the Cu^+ chloride complexing in hydrothermal solutions at 40° to 300°C and determined the same complexes as Rose (1989) as well as $CuCl_{(aq)}$. They also claimed that chloride brines at temperatures less than 250°C are incapable of transporting significant quantities of copper unless 'unusually' oxidized, i.e. cooling a fluid to <250°C will cause precipitation of most of the contained copper. This can be explained by oilfield brines that commonly contain very low concentrations of copper; yet when they interact with evaporites (on a basin scale; Warren, 1997) they can be transformed into much more oxidized fluids, with fO_2 levels necessary to transport the required concentrations of copper in order to form major ore deposits (Sverjensky, 1987).

Crerar & Barnes (1976) investigated the solubilities of chalcopyrite and chalcocite assemblages in hydrothermal solutions at temperatures of 200° to 350°C for application to porphyry copper deposits (Fig. 6.5). Like the study of Xiao *et al.* (1998), they concluded that, at temperatures of 350°C and near-neutral to mildly acid pH conditions, copper and iron dissolve in Cl^--rich fluids at concentrations up to 1000ppm, but this is dramatically reduced (by 90 to 99%) to concentrations of only 10-100ppm at a temperature of 250°C. Rose (1970) suggested fluids at a temperature of 350°C can carry concentrations of copper up to 1000ppm if the pH of the solution is no more than one pH unit below neutrality, although this does not necessarily agree with other studies (e.g. Crerar & Barnes, 1976) which suggest that copper can be transported at slightly more acidic pH conditions (Fig. 6.5).

If these known constraints are applied to this Nchanga study, it becomes clear that the modal pressure-corrected estimates of vein temperatures within either fault-hosted veins within the basement or thrust-related shear zones of approximately 300° and 310°C respectively represent fluids that were capable of transporting anomalous concentrations of copper but not necessarily in ore-forming concentrations, suggesting that oxidation of the ore-fluid may have

been required to increase its copper-carrying potential. Further supporting the argument for the metal-carrying potential of these fluids is their very high salinity, i.e. high Cl^- content, and the fact that alteration associated with this fluid suggests neutral to slightly acidic pH conditions.

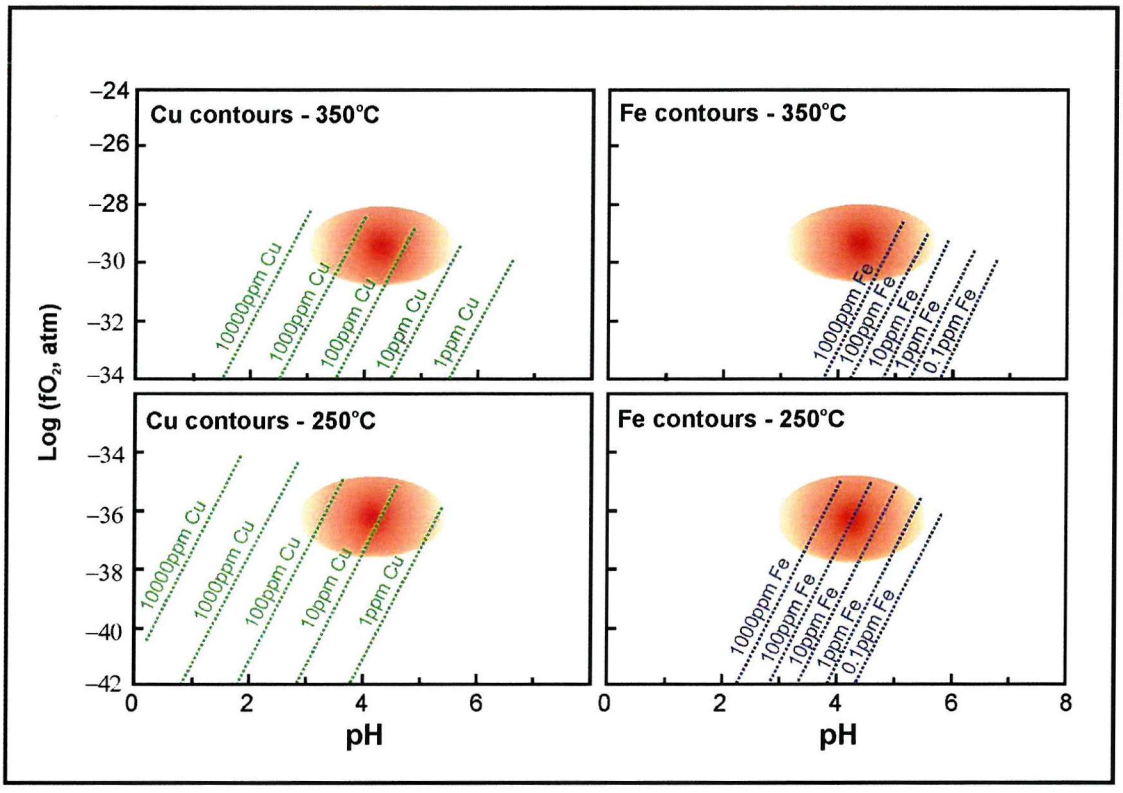

Figure 6.5: Solubility (in ppm concentrations) of copper and iron as chloride complexes (CuCl and $FeCl^+$ respectively) within hydrothermal NaCl solutions, as a function of pH and oxygen fugacity, at temperatures of 250° and 350°C (Crerar & Barnes, 1976). Area shaded in red is a typical ore-fluid from porphyry copper systems within the sericite stability field showing the temperature dependence of both metals, in particular copper. Although the fluids involved in porphyry copper deposits and the Zambian Copperbelt may have different sources, the transporting capabilities and the metal solubility-controlling properties of the ore-forming fluids will be subject to the same constraints.

Taking this a little further, Brimhall & Crerar (1987) claimed that to form a sizable ore deposit, metals must be structured in tetrahedral complex ions, in this case aqueous chloro-complexes of copper and cobalt (Fig. 6.6). They suggested that when copper (or cobalt) is taken up in tetrahedral complexes, the greater amount of metal can be contained in the fluid. This boils down to fluids, at greater temperature and often higher salinity, carry more metal, where deposition of the metal is more subtly controlled by these factors and hence ore deposits are more easily formed (Fig. 6.6). The data shown for the Zambian Copperbelt (taken from Susak & Crerar, 1985) show similar salinities to the fluid inclusion data presented here, and similar temperatures to the uncorrected (with respect to pressure and depth of formation)

homogenization data and suggests that copper and cobalt are transported in the fluid via tetrahedral chloro-complexes.

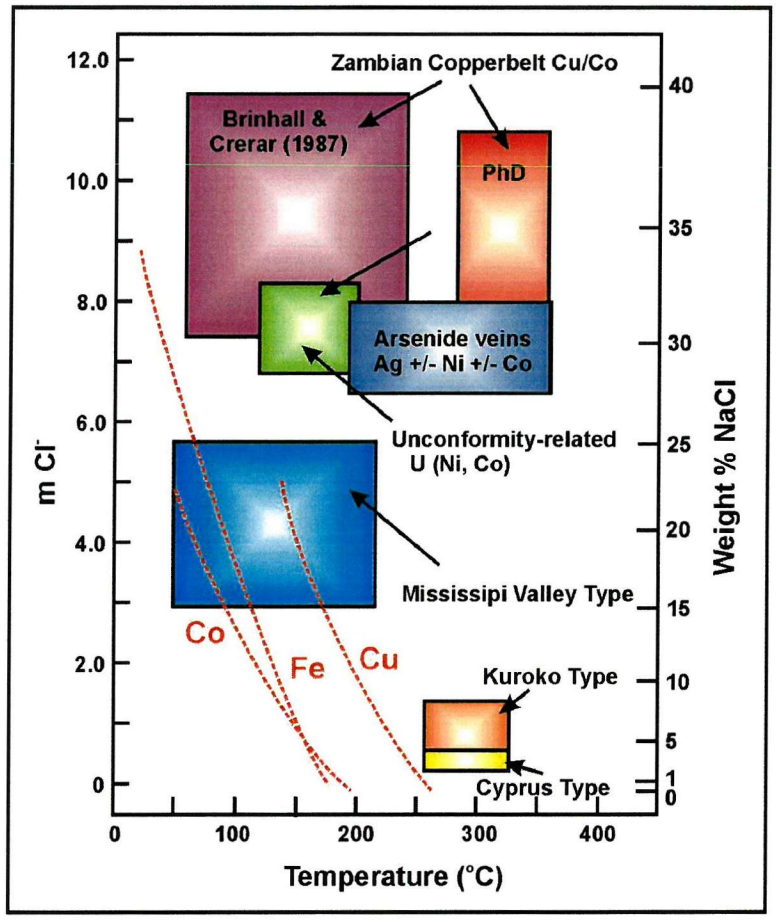

Figure 6.6: The appearance of tetrahedral complex ions for chloro-complexes of Co, Fe, and Cu. Octehedral complexes dominate to the left of the red dashed lines, whereas tetrahedral complexes dominate to the right. Temperature-salinity fields for ore-forming fluids from major deposit types (including the Zambian Copperbelt) are plotted showing the dominance of tetrahedral complexes at higher temperatures and in most cases higher salinities (Susak & Crerar, 1985; Brimhall & Crerar, 1987). The red shaded area represents the fluid inclusion data (pressure-corrected) collected for Nchanga during this study, for comparison.

The fact that the same fluids may have transported significant concentrations of both copper and cobalt puts constraints on the possible composition, pH, temperature, Cl content, and redox state of the ore-forming fluid (Rose, 1989). Previous authors have investigated the relative mobility of copper and other base metals at low temperatures, often found in association in sediment-hosted copper deposits. For example, Rose (1989) determined a 'transport field' for copper at 25°C reflecting the probable chemistry of mineralizing brines in these kinds of systems, where it is transported as chloride complexes. Cobalt is soluble as Co^{2+} in most of the transport field, except for pH values of greater than 7.6 and along the most reducing edge of the field (Rose, 1989). This suggests that a fluid, transporting ore-forming

concentrations of both copper and cobalt (1000ppm and 200ppm respectively; Haynes & Bloom, 1987), must be more oxidizing and have a lower pH (of approximately 7) than would normally be required for the transport of copper alone. Haynes & Bloom (1987) quantified this by claiming that copper and cobalt solubilities are dependent on oxygen fugacity with potential ore-forming concentrations achieved within a near-neutral solution at >1000ppm copper and 200ppm cobalt at fO_2 conditions between 10^{-55} and 10^{-35} bars. The results obtained here suggest the fluids may have been as high as 300°C, but the transport fields for copper and cobalt (as chloride complexes) at these temperatures indicate the same controls (Fig. 6.7). At these higher temperatures, the fluid must have a pH less than 7 for the transport of cobalt as Co^{2+}, whereas copper can be transported over a wider range of pH conditions. However, for a fluid to transport both of these metals in ore-forming concentrations, it must achieve higher fO_2 conditions than for copper alone. Therefore, the possibility of increasing the oxygen fugacity state of the fluid and hence the solubility of copper by the dissolution of evaporites (Sverjensky, 1987) must be taken into account when considering the capabilities of any potential ore-forming fluid to carry both copper and cobalt.

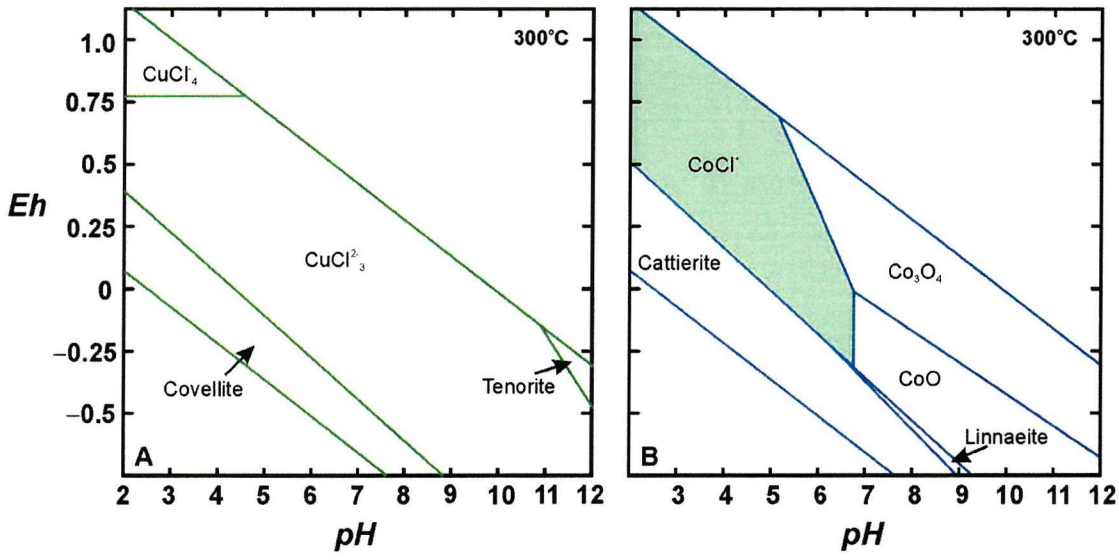

Figure 6.7: Eh-pH diagrams for (A) copper and (B) cobalt, at 300°C and PCO_2 = 0.01 atm (1 kPa). The shaded area on (B) represents Co solubility (activity) greater than 10^{-5} M. The intersection of the transport field for copper on (A) and the shaded area on (B) represents the Eh-pH conditions required for a fluid to carry ore-forming concentrations of both metals.

The results of the present study suggest that the ore-forming fluid carried significant quantities of both copper and cobalt. Rose (1989) considered the processes occurring during reduction (bacterial or thermochemical) of sulphate, contained within a fluid transporting both of these metals. He suggested that if H_2S (from sulphate reduction) were available after copper has been precipitated, then cobalt sulphides would subsequently precipitate. This may be significant in explaining why carrollite at Nchanga commonly appears to locally replace

copper sulphides, without any evidence of it being a completely separate phase of mineralization (i.e. different fluid). It suggests that copper could have precipitated first out of any fluid, during sulphate reduction, followed by cobalt precipitation from the same fluid once the copper had been used up. Importantly, this offers a possible explanation for the occurrence of cobalt within one thrust-propagation fold-zone on the south limb of the Nchanga Syncline. The antiformal structure, within which the cobalt is hosted, is probably one of the largest of these internal folds at Nchanga. It therefore makes sense that if this antiform held trapped methane, it probably held more than anywhere else, as it would have been such an effective trap for hydrocarbon gas. For all the copper to have been precipitated from the fluid, reduction must have continued for longer than at other sites of mineralization which would have required increased volumes of the reducing medium, in this case methane. This could have been the most likely place for this to happen at Nchanga, and therefore once the copper had been used up, there was remaining methane to continue reduction and the precipitation of cobalt sulphides was triggered. Based on the current evidence, this may be the most likely explanation for the copper-cobalt association at Nchanga.

6.2.4 Migration of hydrothermal fluids

The evidence presented here suggests that Basement high-angle faults and thrust structures control the location of significant concentrations of copper and cobalt. Therefore, these structures may have played a major role in the migration of mineralizing fluids to the current sites of deposition. This aspect of the early extensional structures acting as conduits for hydrothermal solutions has been considered by previous authors (Annels, 1984; Lefebvre, 1989; Unrug, 1989), where they were considered as early rift faults (of a failed aulacogen) that supplied mineralizing solutions from deep crustal levels to variously compacted cover sequences. The thrusts have also been interpreted as structurally developed pathways to hydrothermal copper- (and cobalt)-rich solutions in the past (Molak, 1995). The pre-Katangan extensional structures within the Basement and thrusts within the Lower Roan have often treated as two separate structural regimes. However, if inversion tectonics is a significant process in the structural evolution of the Nchanga sequence, then they are much more closely linked that previously considered. This makes the idea that both sets of structures were major conduits for metal-rich fluids more feasible and may explain the association of metals to both structural regimes.

On a smaller scale (e.g. 10-20m), the migration of fluids is controlled by both structures and lithology. The latter is clearly important when considering the two major orebodies. The evidence suggests that the shale units overlying both arenite host rocks (arkose and 'The Feldspathic Quartzite') may have acted as seals or permeability barriers to mineralizing

fluids. This may have promoted lateral flow of fluids through the more permeable sandstones. However, the fluids were most likely transported to the host strata, on this scale, via structures, in particular via the internal thrusts within the Lower Roan sequence. They may have then been allowed to permeate laterally, once a unit such as 'The Feldspathic Quartzite' had been intersected by a thrust and fracture networks developed. The sandstones themselves were more than likely permeable to fluids before deformation, but, based on the evidence, fracture-induced permeability may have played a vital role in the passage of hydrothermal solutions within the host rocks. This is supported by the fact that thrust-related fold zones (where fracture-permeability may be at its greatest) are commonly most heavily mineralized.

6.2.5 Deposition of copper and cobalt

Precipitation of copper (and cobalt) sulphides from this type of basinal brine could be triggered by a number of changes in fluid chemistry or composition (Barnes, 1979), including:

- A decrease in fluid temperature
- An increase in fluid pH
- A decrease in Cl^- activity
- A decrease in the oxygen fugacity (fO_2) state of the fluid

The results of this Nchanga study, in particular the stable isotope and fluid inclusion evidence, are consistent with deposition and precipitation of sulphides being triggered by one or both of: (i) reduction of an oxidized ore fluid by thermochemical processes (rapid decrease in oxygen fugacity), and/or (ii) a decrease in fluid temperature (Rose, 1989). The sulphur isotope data suggest thermochemical reduction of the ore fluid was the principal control. For the reasons outlined in section 6.2.6, reduction of the oxidized fluid species, carrying copper, is considered to have occurred on interaction of the fluid with gaseous hydrocarbons (methane), which were present within the host sandstone units. In addition, and accompanying the thermochemical reduction process, a decrease in temperature, indicated in the homogenization data from fluid inclusions within fault-related vein quartz and mineralized vein quartz, most likely occurred during the thermochemical reduction process when the ore-forming hydrothermal fluids mixed with the methane. In the case of Nchanga a decrease of approximately 60°-90°C, from 300°-310° (fault zones) to 220°-240°C (ore zones), could have potentially triggered the precipitation of some copper contained within the fluid (in agreement with Crerar & Barnes, 1976).

A pre-requisite, which must be taken into account, for each of these mechanisms for ore deposition is that sufficient space must have been available (or generated through water-rock interactions) within any potential host rock. Host rocks to the majority of sulphides at Nchanga are arenites (sandstones), which feasibly had an element of host rock and fracture-induced porosity (and permeability) that appears to have exerted a control on the location of major orebodies. Within some units (e.g. the 'Lower Banded Shale' and arkose) there is evidence that evaporites (probably anhydrite) were once present and that sulphides may have replaced them. Therefore further space generation may have occurred within Nchanga host rocks during dissolution of minor anhydrite within the sequence.

The zonation of sulphides with respect to supposed palaeo-shorelines is widely described from the Copperbelt (e.g. Garlick, 1961; Vink, 1972; Skripchenko, 1986) and also from other major sediment-hosted copper deposits such as White Pine in Michigan (Brown, 1971). Darnley (1960) suggested that palaeo-shorelines were representative of deeper-seated crustal structures, and that it was actually these that control any primary zoning. For example, major pre-Katangan extensional structures (as the principal basin-forming mechanism) would probably control where palaeo-shorelines were located, and so the close association between early (inverted) extensional structures and copper mineralization at Nchanga would support such an interpretation.

6.3 Genetic model for the Nchanga copper-cobalt deposits

The evidence collected during this Nchanga study suggests a significant reinterpretation of the models for genesis of these copper-cobalt deposits. The main stages of a new genetic model for the Nchanga deposits, discussed in section 6.2, are summarized below:

Basin scale:

- Generation of hot saline fluids, possibly similar in composition to oilfield brines, within the deepest parts of the Zambian sedimentary basin, potentially one of or a mixture of meteoric water, seawater, or connate waters (Fig. 6.8).

- Migration of these fluids towards the basin margins during early (Lufilian-age; 550-560 Ma) compression of the host basin, either along major aquifers or structures (Fig. 6.8).

- Dissolution of continental evaporite sequences (source of Cl and salinity, Mg, Ca, fO_2, and SO_4^{2-}) during migration of the fluids rendering the fluid very oxidizing and generating a Na-Ca-Mg-Cl basinal brine that was also rich in oxidized sulphate. This

stage produces a fluid that is then capable of transporting both copper and cobalt in ore-forming concentrations, and significantly is capable of taking into solution metals that it interacts with.

- Leaching of copper (and cobalt) from basal clastics or basement rocks during migration of the highly saline fluids to basin margins.
- Large volumes of mineralizing fluids focused through the deforming margin basin, with re-precipitation of copper (and cobalt) within relatively small volume of rock (on a basin-scale).

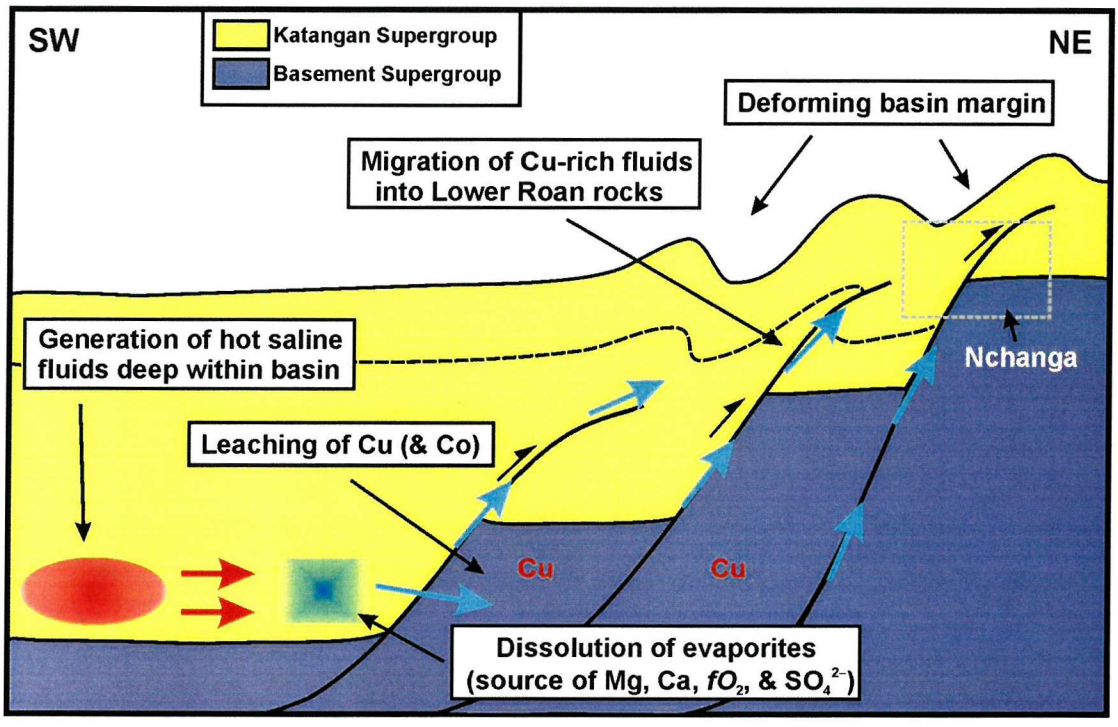

Figure 6.8: Basin-scale schematic model for the generation of hot, saline brines in the deepest parts of the Zambian sedimentary basin, and subsequent migration of these brines to the basin margins (through continental clastics and evaporites and basement rocks) during compression of the host basin.

Nchanga deposit scale:

- Migration of ore-forming fluids, to the Lower Roan host rocks, along Basement (inverted) structures and major low-angle thrust structures.

- Migration of fluids into the top parts of permeable and porous arenite units (increased by fracturing of these competent units during fold-thrust development), where lateral

flow was promoted by overlying shale units acting as seals to mineralizing solutions (Fig. 6.9A).

- Rapid reduction of the ore fluid when it reacts with methane, where arenite units have acted as local gas-rich hydrocarbon reservoirs (Fig. 6.9A & B), and precipitation of ore sulphides (copper followed by cobalt). A decrease in temperature most likely accompanied the reduction process when hot fluids mixed with methane, and potentially contributed to the precipitation of sulphides.

- Further fold and thrust evolution to form folded orebodies, with associated modification of sulphides (e.g. replacement of primary sulphides by chalcocite).

- Near-surface supergene processes (particularly within natural aquifers or along permeability horizons such as the contact between the arkose and overlying 'Lower Banded Shale' unit) causing leaching (and potential enrichment) of copper. Dissolution of dolomite alteration may have contributed to the precipitation of malachite during this process.

This epigenetic model involves the mineralization process occurring during structural evolution of the host sequence, most probably during the Lufilian Orogeny. However, even if the mineralization was diagenetic (and subsequently remobilized to form the structural relationships of copper and cobalt) many of the same controls, based on the evidence presented here, would still apply to the model, including: the fluid characteristics, source, and migration (except for thrusts), the same restriction of fluids to arenite units with overlying shale acting as natural fluid seals as a result of grain size differences, and the same precipitation controls involving the role of methane. The main evidence for an epigenetic model and not a diagenetic model includes: (i) the spatial association between mineralization and thrust structures and hydrothermal alteration; and (ii) the presence of hydrothermal alteration assemblages and fluid inclusions that suggest that fluids were between 280° and 360°C, temperatures more appropriate to a thrust model.

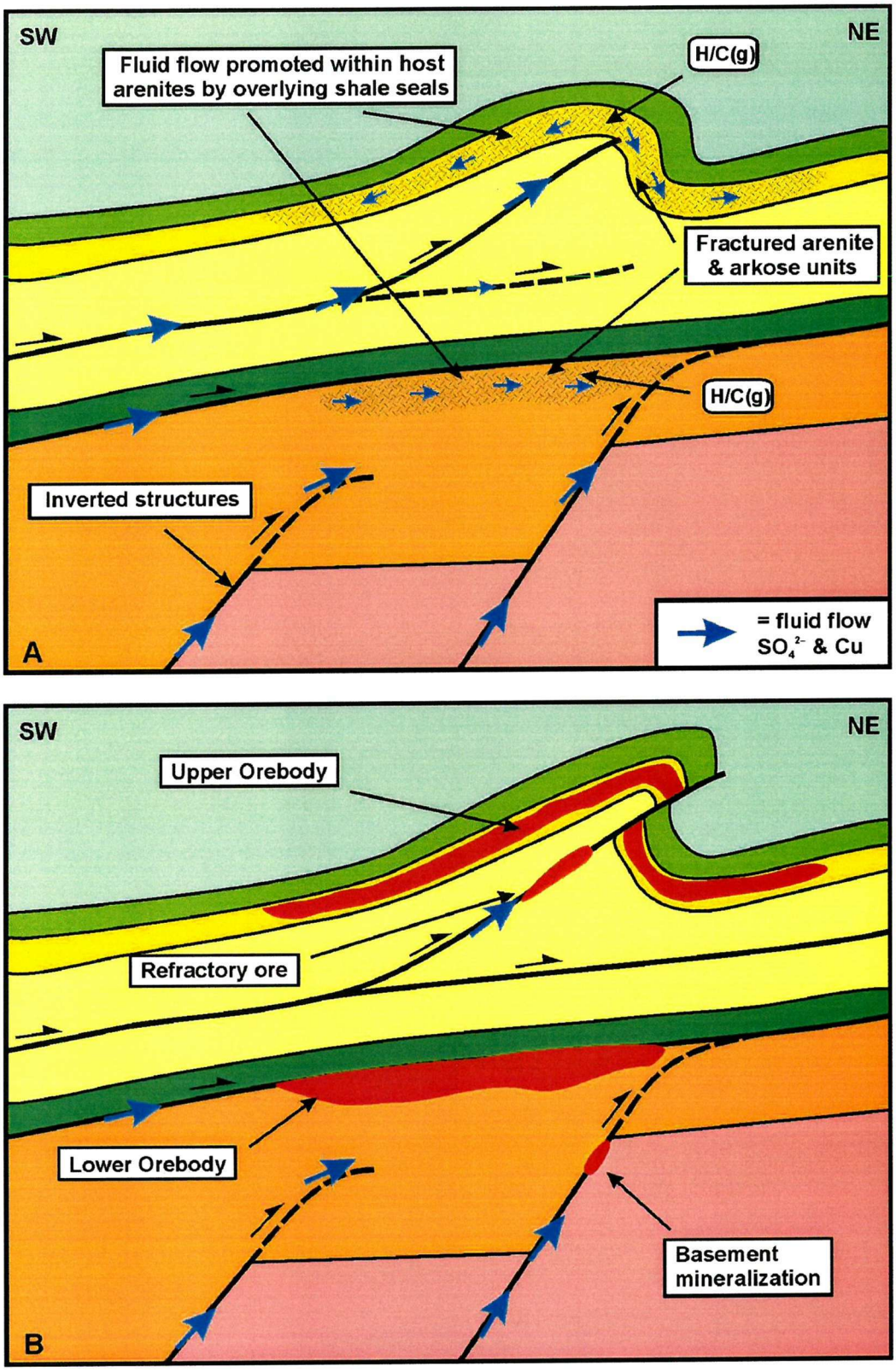

Figure 6.9: Nchanga deposit-scale schematic model for (A) the migration of mineralizing copper- and cobalt-rich brines into fractured arenite host rocks and (B) the subsequent precipitation of sulphides on rapid reduction of the ore fluid by methane.

CHAPTER 7:

CONCLUSIONS

CHAPTER 7: CONCLUSIONS

7.1 Conclusions

The main conclusions to be drawn from this Nchanga-based study are summarized below:

- The structural evolution of Nchanga occurred over two main stages: (i) early, pre-Katangan extension (> 880 Ma), represented by high-angle structures within the Basement, followed by (ii) inversion on high-angle structures and internal thrust-propagation fold development within the basal part of the Katangan sequence (Lower and Upper Roan Groups) during the main phases of the Lufilian Orogeny (550 to 560 Ma), with the structural geometry strongly controlled by competence contrasts between different lithologies.

- High-grade copper and cobalt are consistently located within the top parts of arenite and arkose units that are overlain by shale units, and are spatially associated with bedding-parallel detachment surfaces, low-angle structures, thrust-propagation fold structures, and high-angle Basement faults.

- Ore mineral paragenesis consists of diagenetic/early pyrite (that may have replaced earlier anhydrite) replaced by primary copper sulphides chalcopyrite and bornite (± chalcocite), followed by carrollite, where present, and subsequent replacement by chalcocite. All sulphides are overprinted by supergene oxidation of primary mineralization (in particular the Lower Orebody), indicated by an abundance of malachite and chrysocolla.

- A potential ore-forming fluid has been identified with the following characteristics:

    - Medium temperature of 220° to 240°C with ore zones and 300°C to 310°C within fault zones (pressure-corrected; T_H data is 160°-180°C and 230°-240°C respectively)
    - Near-neutral to slightly acidic pH (5 to 7)
    - High-salinity and Cl-rich (30 to 38 equivalent wt% NaCl)

- High concentrations of Mg and Ca components
- A range of $\delta^{18}O_{fluid}$ (SMOW) of +2.7‰ to +10.3‰, representing basinal brines that have undergone significant water-rock interaction to achieve increased values (from 0‰)

- These mineralizing hydrothermal fluids were responsible for a potassic alteration assemblage consisting of phlogopite, sericite, and quartz (± tourmaline, rutile, and K-feldspar) and recrystallization of detrital components, developed in association with the mineralization and adjacent to structures, and may also have carried Bi, Ba, U, Mo, and As.

- Measured $\delta^{34}S$ (CDT) data of –1‰ to +18‰ for copper-cobalt sulphides contrasts considerably with values of –1‰ to –17‰ for diagenetic pyrite (typical of bacterial sulphate reduction), suggesting that precipitation of copper-cobalt sulphides occurred on thermochemical reduction of the sulphate-enriched fluid within a closed system (i.e. limited source of sulphate and fluid).

- Alteration dolomite, found consistently with primary copper sulphides, reveals $\delta^{13}C$ (PDB) values indicating an organic carbon component (–5.6‰ to –8.3‰) compared with dolomite from the Upper Roan that reveals a clear marine source (+1.5‰ to +2.5‰).

- Brines were most likely generated deep within the host basin and expelled during regional deformation (compression and inversion) towards the basin margins. During fluid migration, significant interaction with, and dissolution of, evaporite sequences, would have provided a source of high salinity, sulphate, Mg, and Ca, and a mechanism for achieving suitable fO_2 conditions, necessary for the transport of copper and cobalt as chloride complexes in ore-forming concentrations. The fluid would then have been capable of leaching metals from the Basement during its migration to the sites of mineralization.

- Oxidizing, metal-bearing hydrothermal fluids were introduced, during fold-thrust development, into fractured and porous quartzo-feldspathic units that were sealed during deformation by overlying shale caps. Precipitation of sulphides occurred on thermochemical reduction of the ore fluid by methane present within sandstones, a reaction that also triggered the precipitation of dolomite. Cobalt sulphide precipitation would have occurred once copper had been stripped from the fluid.

These new data highlight the link between processes occurring during basin evolution and ore formation for the sediment-hosted copper-cobalt deposits of the Zambian Copperbelt. This new model represents a significant reinterpretation of the genesis of a major component of Copperbelt mineralization and may have an impact, not only on our understanding of the origin of other major sediment-hosted copper provinces, but also on future exploration in the region.

7.2 Implications for future exploration

The implications of this study for future exploration initiatives on the Copperbelt are as follows:

- Future exploration must address the role of tectonics and associated fluids in the origin of these world class deposits.

- Mineralization may not necessarily be restricted to the Lower Roan Group of the Katanga sequence, and deposits could potentially be located at deeper levels within the Katangan sequence and the Basement, more than likely associated with structures.

- Major structures may be more useful in identifying targets on a regional scale than previously considered, in particular early extensional structures that may have been inverted during Lufilian compression. These might help to locate internal thrust-fold systems (internal to Lower Roan) that may have played a crucial role in the migration of fluids to the eventual sites of metal deposition.

- Certain features of the geology and mineralization at Nchanga can be used to create vectors to mineralization, in particular potassic alteration and high-salinity fluids, which appear to represent the necessary p-t-x conditions of fluids to transport ore-forming concentrations of copper and cobalt.

- The role of hydrocarbons may be significant in the generation of Copperbelt mineralization. Plausible clastic reservoirs, in particular to gaseous hydrocarbons, may be common hosts to mineralization, with dolomite alteration as a common indicator of thermochemical reduction processes.

- The potential for Pb-Zn mineralization within the region, as the identified ore-forming fluid was also capable of transporting them in significant quantities.

7.3 Recommendations for future work

The following broad suggestions for future research are proposed:

- A test of the above model at other major Copperbelt localities, by employing similar study methods, to determine whether aspects of the same alteration, fluid, or isotope characteristics are present.

- Expansion of the study on a regional level to incorporate the deposits of the Democratic Republic of Congo. This would allow a study of the controls of mineralization within the whole Lufilian Arc, which should be treated as one mineralizing system (not just copper and cobalt). In addition, the much more common cobalt deposits in the D.R.C. may lend a further insight into the copper-cobalt association.

- Hydrogen and oxygen isotope analysis of phlogopites and other micas to determine temperatures of formation, but more importantly, by measuring the δD and $\delta^{18}O$ of minerals in equilibrium, test whether the same fluid is responsible for the precipitation of sulphide-hosting veins and hydrothermal alteration minerals.

- Dating of hydrothermal alteration minerals associated with mineralization and structures, in particular the phlogopite by the Ar-Ar method to determine a precise age for hydrothermal activity and potentially for copper and cobalt mineralization.

- Strontium isotope analysis of carbonates and micas within mineralized sequences to further understand the fluids responsible for their deposition, and in particular determine the interaction of the fluid with the Basement.

- Halogen geochemistry of fluid inclusions in order to determine the source of the high salinity fluids and investigate modifications to that fluid during water-rock interactions. The use of halogen tracers and chlorine isotopes would provide insights into the origin and evolution of the base metal mineralizing brines, and in particular define the role of seawater or evaporites in the mineralization process.

- Boron isotope analysis of tourmalines and hydrothermal fluids in order to determine the role of boron within these systems. In particular, the distinctively heavy $\delta^{11}B$ of seawater can be used as a tracer of marine inputs into various systems as well as determining the contributions from marine and non-marine evaporites and continental crust.

REFERENCES

REFERENCES

ACKERMANN, F. & FORSTER, A. 1960. Grundzuge der stratigraphie and struktur des Irumidien Orogens. *21st International Geological Congress, Norden, Copenhagen*, **18**, 182-192.

ANDERSON, G.M. & GARVEN, G. 1987. Sulphate-sulphide-carbonate associations in Mississippi-Valley Type lead zinc deposits. *Economic Geology*, **82**, 482-488.

ANNELS, A.E. 1974. Some aspects of the stratiform ore deposits of the Zambian Copperbelt and their genetic significance. *In:* BARTHOLOME, P. (ed.) *Gisements stratiformes et provinces cupriferes.* Centenaire Societe Geologique Belgique, Liege, 235-254.

ANNELS, A.E. 1984. The geotectonic environment of Zambian copper-cobalt mineralization. *Journal of the Geological Society of London*, **141**, 279-289.

ANNELS, A.E. 1989. Ore genesis in the Zambian Copperbelt, with particular reference to the northern sector of the Chambishi Basin. *In:* BOYLE, R.W., BROWN, A.C., JEFFERSON, C.W., JOWETT, E.C., & KIRKHAM, R.V. (eds) *Sediment-Hosted Stratiform Copper Deposits.* Geological Association of Canada Special Paper 36, 427-452.

ANNELS, A.E. & SIMMONDS, J.R. 1984. Cobalt in the Zambian Copperbelt. *Precambrian Research*, **25**, 75-98.

ANNELS, A.E., VAUGHAN, D.J., & CRAIG, J.R. 1983. Conditions of ore mineral formation Zambian Copperbelt deposits with special reference to the role of cobalt. *Mineralium Deposita*, **18**, 71-88.

ARMSTRONG, R.A., ROBB, L.J., MASTER, S., KRUGER, F.J., & MUMBA, P.A.C.C. 1999. New U-Pb age constraints on the Katangan sequence, Central African Copperbelt. *Journal of African Earth Sciences*, **28 (4A)**, 6-7.

BARNES, H.L. 1979. Solubilities of ore minerals. *In:* BARNES H.L. (ed.) *Geochemistry of hydrothermal ore deposits, 2nd edition.* John Wiley & Sons, Inc., New York, 404-460.

BARR, M.W.C., CAHEN, L., & LEDENT, D. 1977. Geochronology of syntectonic granites from Central Zambia: Lusaka Granite and Granite NE of Rufunsa. *Annales de la Societe Geologique de Belgique*, **100**, 47-54.

BASSETT, W.A. 1958. Copper vermiculites from Northern Rhodesia. *The American Mineralogist*, **43**, 1112-1133.

BEANE, R.E. 1974. Biotite stability in the porphyry copper environment. *Economic Geology*, **69**, 241-256.

BECHTEL, A., SUN-YUZHUANG, PUETTMANN, W., HOERNES, S., & HOEFS, J. 2001. Isotopic evidence for multi-stage base metal enrichment in the Kupferschiefer from the Sangerhausen Basin, Germany. *Chemical Geology*, **176**, 31-49.

BELKIN, H.E., CAVARRETTA, G., DE VIRO, B., & TECCE, F. 1988. Hydrothermal phlogopite and anhydrite from the SH2 well, Sabatini volcanic district, Latium, Italy: fluid inclusions and mineral chemistry. *American Mineralogist*, **73**, 775-797.

BINDA, P.L. 1975. Detrital bornite grains in the Late Precambrian B greywackes of Mufulira, Zambia. *Mineralium Deposita*, **10**, 101-107.

BINDA, P.L. 1995. Stratigraphy of Zambian Copperbelt orebodies. *Journal of African Earth Sciences*, **19**, 251-264.

BINDA, P.L. & MULGREW, J.R. 1974. Stratigraphy of Zambian Copperbelt orebodies. *Journal of African Earth Sciences*, **19**, 251-264.

BINDA, P.L. & PORADA, H. 1995. Observations on the Katangan breccias in Zambia. *In:* WENDORFF, M., & TACK, L. (eds) *Late Proterozoic Belts in Central and Southwestern Africa.* Proceedings IGCP302, Annales Musee Royal Afrique, Central Tervuren Belgique, 49-62.

BODNAR, R.J. 1993. Revised equation and table for determining the freezing point depression of H_2O-NaCl solutions. *Geochimica et Cosmochimica Acta*, **57**, 683-684.

BODNAR, R.J. & VITYK, M.O. 1994. Interpretation of microthermometric data for H_2O-NaCl fluid inclusions. *In:* DE VIVO, B & FREZZOTTI, M.L. (eds) *Fluid inclusions in minerals: methods and applications.* Short Course of the Working Group (IMA), Virginia Tech, Blacksburg, 117-130.

BORISENKO, A.S. 1977. Study of the salt composition of solutions in gas-liquid inclusions in minerals by the cryometric method. *Soviet Geology and Geophysics*, **18**, 11-19.

BOYLE, R.W. 1974. Elemental associations in mineral deposits and indicator elements of interest in geochemical prospecting. *Geological Survey of Canada*, **74-5**, 40p.

BOYLE, R.W., BROWN, A.C., JEFFERSON, C.W., JOWETT, E.C., & KIRKHAM, R.V. 1989. *Sediment-Hosted Stratiform Copper Deposits.* Geological Association of Canada Special Paper 36, 710p.

BRIMHALL, G.H. & CRERAR, D.A. 1987. Ore fluids: magmatic to supergene. *In:* CARMICHAEL, I.S.E. & EUGSTER, H.P. (eds) Thermodynamic modeling of geological materials: minerals, fluids and melts. *Reviews in Mineralogy*, **17**, 235-322.

BROWN, A.C. 1971. Zoning in the White Pine Copper Deposit, Ontonagon County, Michigan. *Economic Geology*, **66**, 543-573.

BROWN, A.C. 1978. Stratiform copper deposits – evidence for their post-sedimentary origin. *Minerals Science Engineering*, **10**, 172-181.

BROWN, A.C. 1981. The timing of mineralization in stratiform copper deposits. *In:* WOLF, K.H. (ed.) *Handbook of Stratabound and Stratiform Ore Deposits, Volume 9.* Elsevier Scientific Publishing Company, Amsterdam, 1-23.

BROWN, A.C. 1984. Alternative sources of metals for stratiform copper deposits. *Precambrian Research*, **25**, 61-74.

BROWN, A.C. & CHARTRAND, F.M. 1983. Stratiform copper deposits and interactions with co-existing atmospheres, hydrospheres, biospheres, and lithospheres. *Precambrian Research*, **20**, 533-542.

BURNIE, S.W., SCHWARCZ, H.P., & CROCKET, J.H. 1972. A Sulphur isotope study of the White Pine Mine, Michigan. *Economic Geology*, **67**, 895-914.

CAHEN, L., DELHAL, J., DEUTSCH, S., GROGLER, N., & PASTEELS, P. 1970. The age of the Roan Antelope and Mufulira granites. *Musee Royal de L'Afrique Centrale – Tervuren, Belgiques Annales – Serie in 8° - Sciences Geologiques*, **65**, 15-37.

CAHEN, L. & SNELLING, N.J. 1966. *The geochronology of Equatorial Africa.* North Holland, Amsterdam, 195p.

CAHEN, L., SNELLING, N.J., DELHAL, J., VAIL, J.R., BONHOMME, M., & LEDENT, D. 1984. *Geochronology and Evolution of Africa.* Clarendon, Oxford, 512p.

CAILTEUX, J., BINDA, P.L., KATEKESHA, W.M., KAMPUNZU, A.B., INTIOMALE, M.M., KAPENDA, D., KAUNDA, C., NGONGO, K., TSHIAUKA, T., & WENDORFF, M. 1994. Lithostratigraphical correlation of the Neoproterozoic Roan Supergroup from Shaba (Zaire) and Zambia, in the central African copper-cobalt metallogenic province. *Journal of African Earth Sciences*, **19(4)**, 265-278.

CHABU, M. 1995. The geochemistry of phlogopite and chlorite from the Kipushi Zn-Pb-Cu deposit, Shaba, Zaire. *The Canadian Mineralogist*, **33**, 547-558.

CHAPPELL, B.W. & WHITE, A.J.R. 1974. Two contrasting granite types. *Pacific Geology*, **8**, 173-174.

CLAYPOOL, G.E., HOLSER, W.T., KAPLAN, I.R., SAKAI, H., & ZAK, I. 1980. The age curves of sulphur and oxygen isotopes in marine sulphate and their mutual interpretation. *Chemical Geology*, **28**, 199-260.

CLAYTON, R.N., FRIEDMAN, I., GRAF, D.L., MAYEDA, T.K., MEENTS, W.F., & SHIMP, N.F. 1966. The origin of saline formation waters: 1 isotopic composition. *Journal of Geophysical Research*, **71**, 3869-3882.

CLEMMEY, H. 1974. Sedimentary geology of a late Precambrian copper deposit at Kitwe, Zambia. *In:* BARTHOLOME, P. (ed.) *Gisements stratiformes et provinces cupriferes.* Centenaire Societe Geologique Belgique, Liege, 255-265.

CLIFFORD, T.N. 1967. The Damaran episode in the Upper Proterozoic-Lower Proterozoic structural history of southern Africa. *Geological Society of America Special Paper 92*, 100p.

COLLER, D. 2000. *Phase 1: Structural orientation program of the Nchanga Cu and Co mineralization system.* ERA Maptec/Zamanglo Prospecting Services Unpublished Report, 10p.

COLLER, D. & WANI, L. 2001. *Developing a robust model for exploration of the Zambian Copperbelt: Phase 3 structural appraisal of Nchanga Mine.* ERA Maptec/Zamanglo Prospecting Services Unpublished Report, 13p.

COOPER, M.A. & WILLIAMS, G.D. 1989. Inversion Tectonics. *Geological Society of London Special Publication*, **44**, 376p.

COSI, M., DE BONIS, A., GOSSO, G., HUNZIKER, J., MARTINOTTI, G., MORATTO, S., ROBERT, J.P., & RUHLMAN, F. 1992. Late Proterozoic thrust tectonics, high-pressure metamorphism and uranium mineralization in the Domes Area, Lufilian Arc, northwestern Zambia. *Precambrian Research*, **58**, 215-240.

COWARD, M.P. & DALY, M.C. 1984. Crustal lineaments and shear zones in Africa: their relationship to plate movements. *Precambrian Research*, **24**, 27-45.

CRAIG, J.R. & VAUGHAN, D.J. 1981. *Ore microscopy and ore petrography.* John Wiley & Sons, Canada, 406p.

CRERAR, D.A. & BARNES, H.L. 1976. Ore solution chemistry V. Solubilities of chalcopyrite and chalcocite assemblages in hydrothermal solutions at 200° to 350°C. *Economic Geology*, **71**, 772-794.

CROWE, D.E., VALLEY, J.W., & BAKER, K.L. 1990. Micro-analysis of sulphur-isotope ratios and zonation by laser microprobe. *Geochimica et Cosmochimica Acta*, **54**, 2075-2092.

CUNNINGHAM, M.J. 1986. *Copper-cobalt mineralization in the northern portion of the Chambishi Basin, Zambia.* Unpublished Ph.D. thesis, University College, Cardiff.

DALGLEISH, K.V. 1977. *The Nchanga 'Lamprophyre.'* Unpublished Report N.C.C.M (Chingola Division), 12p.

DALY, M.C. 1986. Crustal shear zones and thrust belts: their geometry and continuity on Central Africa. *Philosophical transactions Royal Society London*, **A317**, 111-128.

DALY, M.C., CHAKROBORTY, S.K., KASOLO, P., MUSIWA, M., MUMBA, P., NAIDU, B., NAMATEBA, C., NGAMBI, O., & COWARD, M.P. 1984. The Lufilian Arc and Irumide Belt of Zambia: results of a geotraverse across their intersection. *Journal of African Earth Sciences*, **2**, 311-318.

DARNLEY, A.G. 1960. Petrology of some Rhodesian Copperbelt orebodies and associated rocks. *Transactions of the Institution of Mining and Metallurgy*, **69**, 137-173.

DAVIDSON, C.M. 1931. The geology and ore deposits of Chambishi, Northern Rhodesia. *Economic Geology*, **26**, 131-154.

DECHOW, E., & JENSEN, M.L. 1965. Sulphur isotopes of some central African sulphide deposits. *Economic Geology*, **60**, 894-941.

DEER, W.A., HOWIE, R.A., & ZUSSMAN, J. 1962. *Rock-forming minerals: volume 3 sheet silicates.* Longman: London.

DEER, W.A., HOWIE, R.A., & ZUSSMAN, J. 1966. *An introduction to the rock-forming minerals.* Longman: London.

DEMESMAEKER, G. 1961. The Katanga System in Katanga. *In:* MENDELSOHN, F. (ed.) *The Geology of the Northern Rhodesian Copperbelt.* Macdonald: London, 55.

DE SWARDT, A.M.J. 1962. Structural relationships in the N. Rhodesian Copperbelt: an alternative explanation. *Geological Survey of Northern Rhodesia Occasional Paper 30.*

DE SWARDT, A.M.J. & DRYSDALL, A.R. 1964. Precambrian geology and structure in central Northern Rhodesia. *Memoirs Geological Survey North Rhodesia*, **2**, 82p.

DIEDERIX, D. 1977. *The Geology of the Nchanga Mining Licence Area.* Unpublished Company Report – Nchanga Consolidated Copper Mines Limited Chingola Division, 59p.

DRYSDALL, A.R., JOHNSON, R.L., MOORE, T.A., & THIEME, J.G. 1972. Outline of the geology of Zambia. *Geologie en Mijnbouw*, **51 (3)**, 265-276.

DUANE, M.J. & SAGGERSON, E.P. 1995. Brine expulsion, fluid transport and metallization spanning 2 Gyr in basins of southern and central Africa. *Basin Research*, **7**, 97-108.

EMERY, D. & ROBINSON, A. 1993. *Inorganic Chemistry: Applications to Petroleum Geology.* Blackwell Science Publications, Oxford, 254p.

EUGSTER, H.P. 1980. Geochemistry of evaporitic lacustrine deposits. *Annual Reviews of Earth and Planetary Sciences*, **8**, 35-63.

FALLICK, A.E., MCCONVILLE, P., BOYCE, A.J., BURGESS, R., & KELLEY, S.P. 1992. Laser microprobe stable isotope measurements on geological materials: some experimental considerations (with special reference to $\delta^{34}S$ in sulphides). *Chemical Geology*, **101**, 53-61.

FAURE, G. 1986. *Principles of isotope geology, 2nd edition.* John Wiley & Sons: New York, 350p.

FISHER, J.F.C. & NOTEBAART, C.W. 1976. Metallurgical treatment of Chingola cupriferous mica ores. *Transactions of the Institution of Mining and Metallurgy*, **C85**, 15-22.

FLEISCHER, V.D. 1984. Discovery, geology, and genesis of copper-cobalt mineralization at Chambishi southeast prospect, Zambia. *Precambrian Research*, **25**, 119-133.

FLEISCHER, V.D., GARLICK, W.G., & HALDANE, R. 1976. Geology of the Zambian Copperbelt. *In:* WOLF, K.H. (ed.) *Handbook of Stratabound and Stratiform Ore Deposits, Volume 9.* Elsevier Scientific Publishing Company, Amsterdam, 223-352.

FRANCOIS, A. 1974. Les mineralisations du Shaba meridional et leur environment lithologique et tectonique. *In:* BARTHOLOME, P. (ed.) *Gisements stratiformes et provinces cupriferes.* Centenaire Societe Geologique Belgique, Liege, 79-102.

FRIEDMAN, I. & O'NEIL, J.R. 1977. Compilation of stable isotope fractionation factors of geochemical interest. *In:* FLEISCHER, M. (ed.) *Data of geochemistry (6th edition).* U.S. Geological Survey Professional Paper 440-KK, 12p.

FRITZ, P. 1976. ^{18}O and ^{13}C in hydrothermal systems. *In:* WOLF, K.H. (ed.) *Handbook of Stratabound and Stratiform Ore Deposits, Volume 2.* Elsevier Scientific Publishing Company, Amsterdam, 191-218.

GARLICK, W.G. 1961a. The Syngenetic Theory. *In:* MENDELSOHN, F. (ed.) *The Geology of the Northern Rhodesian Copperbelt.* Macdonald: London, 146-165.

GARLICK, W.G. 1961b. The Chambishi-Nkana Basin. *In:* MENDELSOHN, F. (ed.) *The Geology of the Northern Rhodesian Copperbelt.* Macdonald: London, 281-297.

GARLICK, W.G. 1972. Sedimentary environment of Zambian copper deposition. *Geologie en Mijnbouw*, **51 (3)**, 277-298.

GARLICK, W.G. 1973. The Nchanga Granite. *Special Publication of the Geological Society of South Africa*, **3**, 455-474.

GARLICK, W.G. 1976. Syngenesis versus epigenesis. *In:* FLEISCHER, V.D., GARLICK, W.G., & HALDANE, R. (eds) *Geology of the Zambian Copperbelt. In:* WOLF, K.H. (ed.) *Handbook of Stratabound and Stratiform Ore Deposits Volume 9.* Elsevier Scientific Publishing Company, Amsterdam, 323-352.

GARLICK, W.G. & BRUMMER, J.J. 1951. The age of the granites of the Northern Rhodesian Copperbelt. *Economic Geology*, **46**, 478-497.

GARLICK, W.G. & HALDANE, R. 1976. Nchanga. *In:* FLEISCHER, V.D., GARLICK, W.G., & HALDANE, R. (eds) *Geology of the Zambian Copperbelt. In:* WOLF, K.H. (ed.). *Handbook of Stratabound and Stratiform Ore Deposits, Volume 9*, Elsevier Scientific Publishing Company, Amsterdam, 256-274.

GARRARD, P. 1972. *The geology of the Chingola area, Zambia.* Unpublished PhD thesis, Imperial College, London, 240p.

GARVEN, G. & RAFFENSPERGER, J.P. 1997. Hydrogeology and geochemistry of ore genesis in sedimentary basins. *In:* BARNES H.L. (ed.) *Geochemistry of hydrothermal ore deposits, 3rd edition.* John Wiley & Sons, Inc., New York, 125-189.

GOLYSHEV, Y.F., PADALKO, N.L., & PECHENKIN, S.A. 1981. Fractionation stable oxygen and carbon isotopes in carbonate systems. *Geochemistry International*, **18**, 85-99.

GRANT, J.A. 1986. The Isocon Diagram – a simple solution to Gresens' Equation for metasomatic alteration. *Economic Geology*, **81**, 1976-1982.

GRESENS, R.L. 1967. Composition-volume relationships of metasomatism. *Chemical Geology*, **2**, 47-55.

GUSTAFSON, L.B. & WILLIAMS, N. 1981. Sediment-hosted stratiform deposits of copper, lead, and zinc. *Economic Geology 75th Anniversary volume*, 138-178.

HANOR, J.S. 1979. The sedimentary genesis of hydrothermal fluids. *In:* BARNES H.L. (ed.) *Geochemistry of hydrothermal ore deposits, 2nd edition.* John Wiley & Sons, Inc., New York, 137-189.

HANSON, R.E., WARDLAW, M.S., WILSON, T.J., & MWALE, G. 1993. U-Pb zircon ages from the Hook Granite Massif and Mwembeshi dislocation: constraints on Pan-African deformation, plutonism, and transcurrent shearing in central Zambia. *Precambrian Research*, **63**, 189-209.

HANSON, R.E., WILSON, T.J., & WARDLAW, M.S. 1988. Deformed batholiths in the Pan-African Zambezi Belt, Zambia: age and implications for regional Proterozoic tectonics. *Geology*, **16**, 1134-1137.

HARRIS, N.B.W. & INGER, S. 1986. Trace element modeling of granites. *Contributions to Mineral Petrology*, **110**, 46-56.

HAYNES, D.W. & BLOOM, M.S. 1987. Stratiform copper deposits hosted by low-energy sediments: III aspects of metal transport. *Economic Geology*, **82**, 635-648.

HEINRICH, E.W. 1946. Studies in the mica group; the biotite-phlogopite series. *American Journal of Science*, **244**, 836.

HITCHON, B. & FRIEDMAN, I. 1969. Geochemistry and origin of formation waters in the western Canada sedimentary basin: stable isotopes of hydrogen and oxygen. *Geochimica et Cosmochimica Acta*, **33**, 1321-1349.

HITZMAN, M.W. 1998, Petrographic ore studies of 'ore shale' from the Zambian Copperbelt – implications for models of ore formation. *Geological Society America Abstracts Program*, **30**, 19.

HITZMAN, M.W. 2000. Source basins for sediment-hosted stratiform Cu deposits: implications for the structure of the Zambian Copperbelt. *Journal of African Earth Sciences*, **30**, 855-863.

HOEVE, J. & QUIRT, D. 1989. A common diagenetic hydrothermal origin for unconformity type uranium and stratiform copper deposits. *In:* BOYLE, R.W., BROWN, A.C., JEFFERSON, C.W., JOWETT, E.C., & KIRKHAM, R.V. (eds) *Sediment-Hosted Stratiform Copper Deposits.* Geological Association of Canada Special Paper 36, 151-172.

HOLSER, W.T. & KAPLAN, I.R. 1966. Isotope geochemistry of sedimentary sulfates. *Chemical Geology*, **4**, 93-155.

HUNTER, D.R. & PRETORIUS, D.A. 1981. Structural framework (of southern Africa). *In*: HUNTER, D.R. (ed.) *Precambrian of the Southern Hemisphere.* Amsterdam, Elsevier, 397-422.

HUSTON, D.L., POWER, M., GEMMELL, J.B., & LARGE, R.R. 1995. Design, calibration and geological application of the first operational Australian laser ablation sulphur isotope microprobe. *Australian Journal of Earth Science*, **42**, 549-555.

INAN, E.E. & EINAUDI, M.T. 2002. Nukundamite ($Cu_{3.38}Fe_{0.62}S_4$)-bearing copper ore in the Bingham porphyry deposit, Utah: result of upflow through quartzite. *Economic Geology*, **97**, 499-515.

JACKSON, G.C.A. 1932. The geology of the Nchanga district. *Quarterly Journal of the Geological Society of London*, **88**, 443-514.

JACOBS, D.C. & PARRY, W.T. 1979. Geochemistry of biotite in the Santa Rita porphyry copper deposit, New Mexico. *Economic Geology*, **74**, 860-887.

JASINSKI, A.W. 1988. Activity diagrams for the MgO-Na_2O-K_2O-SiO_2-Al_2O_3-H_2O-HCl system in the temperature range 298 to 623 K and 1 bar pressure: application to the 1900 Ma phlogopite-Mg-chlorite-sericite schists of W. Bergslagen, Sweden. *Geologie en Mijnbouw*, **67**, 379-395.

JOWETT, E.C. 1989. Effects of continental rifting on the location and genesis of stratiform copper-silver deposits. *In:* BOYLE, R.W., BROWN, A.C., JEFFERSON, C.W., JOWETT, E.C., & KIRKHAM, R.V. (eds) *Sediment-Hosted Stratiform Copper Deposits.* Geological Association of Canada Special Paper 36, 427-452.

KAMPUNZU, A.B. & CAILTEUX, J. 1997. Tectonic evolution of the Lufilian Arc (Central Africa Copperbelt) during Neoproterozoic Pan-African Orogenesis. *Abstracts, Intraplate Magmatism and Tectonics of Southern Africa Conference, Harare*, 25-26.

KAMPUNZU, A.B. & CAILTEUX, J. 1999. Tectonic evolution of the Lufilian Arc (Central Africa Copperbelt) during Neoproterozoic Pan-African Orogenesis. *Gondwana Research*, **2**, 401-421.

KAMPUNZU, A.B., KANIKA, M., KAPENDA, D., & TSHIMANGA, K. 1993. Geochemistry and geotectonic setting of late Proterozoic Katangan basic rocks from Kibambale in Central Shaba (Zaire). *Geologische Rundschau*, **82**, 619-630.

KEARNS, L.E., KITE, L.E., LEAVENS, P.B., & NELEN, J.A. 1980. Fluorine distribution in the hydrous silicate minerals of the Franklin Marble, Orange County, New York. *American Mineralogist*, **65**, 557-562.

KEAREY, P. 1996. *Dictionary of Geology.* Penguin Books Ltd., London, 369p.

KELLEY, S.P. & FALLICK, A.E. 1990. High precision spatially resolved analysis of $\delta^{34}S$ in sulphides using a laser extraction technique. *Geochimica et Cosmoschimica Acta*, **54**, 883-888.

KESLER, S.E., APPOLD, M.S., MARTINI, A.M., WALTER, L.M., HUSTON, T., & KYLE, .R. 1995. Na-Cl-Br systematics of mineralizing brines in Mississippi Valley-type deposits. *Geology*, **23**, 641-644.

KHARAKA, Y.K., BERRY, F.A.F., & FRIEDMAN, 1. 1973. Isotopic composition of oil field brines from Kettleman north dome, California, and their geologic implications. *Geochimica et Cosmochimica Acta*, **37**, 1899-1108.

KINGSTON, D.R., DISHROON, C.P., & WILLIAMS, P.A. 1983. Global basin classification system. *American Association Petroleum geology Bulletin*, **67**, 2175-2193.

KIRKHAM, R.V. 1976. *Sediment-hosted stratiform copper deposits: an overview.* Ministry of Energy and Mines, Government of British Columbia, website: http://www.em.gov.bc.ca/Mining/Geolsurv/EconomicGeology/metallicminerals/depmodel/3-sedhst.htm.

KIRKHAM, R.V. 1989. Distribution, settings, and genesis of sediment-hosted stratiform copper deposits. *In:* BOYLE, R.W., BROWN, A.C., JEFFERSON, C.W., JOWETT, E.C., & KIRKHAM, R.V. (eds) *Sediment-Hosted Stratiform Copper Deposits.* Geological Association of Canada Special Paper 36, 3-38.

LAND, L.S. 1983. The application of stable isotope studies to the origin of dolomite and to the problems of diagenesis of clastic sediments. *In:* LAND, L.S. (ed.) *Stable isotopes in sedimentary geology.* Society of Economic Palaeontologists and Mineralogists, Short Course 10, 4.1-4.22.

LEFEBVRE, D.V. & ALLDRICK, D.J. 1996. Sediment-hosted CuAgCo. *In:* LEFEBVRE, D.V. & Hŷ, T. (eds) *Selected British Columbia Mineral Deposit profiles, Volume 2 – Metallic Deposits*, 13-16.

LEFEBVRE, J.J. 1989. Depositional environment of copper-cobalt mineralization in the Katangan sediments of southeast Shaba, Zaire. *In:* BOYLE, R.W., BROWN, A.C., JEFFERSON, C.W., JOWETT, E.C., & KIRKHAM, R.V. (eds) *Sediment-Hosted Stratiform Copper Deposits.* Geological Association of Canada Special Paper 36, 401-426.

LEVINSON, A.A. 1980. *Introduction to exploration geochemistry.* Applied Publishing Ltd., Illinois, 889p.

LUPONELO, J. 2001. *The distribution of copper and cobalt in the Nchanga Open Pit.* Website: http://www.unza.zm/mines/articles/nchanga.html.

MCCLAY, K.R. & BUCHANAN, P.G. 1992. Thrust faults in inverted extensional basins. *In:* MCCLAY, K.R. (ed.) *Thrust Tectonics.* Chapman & Hall, London, 93-104.

MCCLAY, K.R., INSLEY, M.W., & ANDERTON, R. 1989. Inversion of the Kechika Trough, Northeastern British Columbia, Canada. *In:* COOPER, M.A. & WILLIAMS, G.D. (eds) Inversion Tectonics. *Geological Society of London Special Publication*, **44**, 235-257.

MCGOWAN, R.R. 1999. *Controls of Cu-Co mineralization at the Chibuluma West deposit, Zambian Copperbelt.* Unpublished MGeol report, University of Southampton, 102p.

MCGOWAN, R.R., ROBERTS, S., FOSTER, R.P., BOYCE, A.J. & COLLER, D. in press. Origin of the copper-cobalt deposits of the Zambian Copperbelt: an epigenetic view from Nchanga. *Geology.*

MCKINNON, D.M. & SMIT, N.J. 1961. Nchanga. *In:* MENDELSOHN, F. (ed.) *The Geology of the Northern Rhodesian Copperbelt.* Macdonald: London, 234-274.

MCNAUGHTON, J.H.M. 1953. The origin of the Northern Rhodesian copper deposits. *Transactions of the Institution of Mining and Metallurgy*, **62**, 113-124.

MACHEL, H.G., KROUSE, H.R., & SASSEN, R. 1995. Products and distinguishing criteria of bacterial and thermochemical sulphate reduction. *Applied Geochemistry*, **10**, 373-389.

MACHEL, H.G. 1987. Saddle dolomite as a by-product of chemical compaction and thermochemical sulphate reduction. *Geology*, **15**, 936-940.

MACHEL, H.G. 2001. Bacterial and thermochemical sulphate reduction in diagenetic settings – old and new insights. *Sedimentary Geology*, **140**, 143-175.

MAIDEN, K.J., INNES, A.H., KING, M.J., MASTER, S., & PETTITT, I. 1984. Regional controls on the localization of stratabound copper deposits: Proterozoic examples from Southern Africa and South Australia. *Precambrian Research*, **25**, 99-118.

MAROWSKY, G. 1969. Sulphur, carbon, and oxygen isotope studies on the Permian "Kupferschiefer." *Contributions to Mineralogy and Petrology*, **22**, 290-334.

MATSUHISA, Y., GOLDSMITH, J.R., & CLAYTON, R.N. 1979. Oxygen isotopic fractionation in the system quartz-albite-anorthite-water. *Geochimica et Cosmochimica Acta*, **43**, 1131-1140.

MENDELSOHN, F. 1961. *The Geology of the Northern Rhodesian Copperbelt.* Macdonald: London, 423p.

MENDELSOHN, F. 1961. Ore Genesis. *In:* MENDELSOHN, F. (ed.) *The Geology of the Northern Rhodesian Copperbelt.* Macdonald: London, 130-145.

MINISTRY OF MINES AND MINERAL DEVELOPMENT. 1998. Zambia: *Investment opportunities in the mining industry.* Ministry of Mines and Mineral Development, Zambia, 33p.

MOLAK, B. 1995. Some structural and petrological aspects of the Cu (Co) mineralization in the Copperbelt and northwestern provinces of Zambia. *Royal Museum of Central Africa (Belgium) Annales de la Societe Geologique*, **101**, 95-102.

NAYLOR, H., TURNER, P., VAUGHAN, D.J., BOYCE, A.J., & FALLICK, A.E. 1989. Genetic studies of red bed mineralization in the Triassic of the Cheshire Basin, northwest England. *Journal of the Geological Society of London*, **146**, 685-699.

NGOYI, K., LIEGEOIS, J.P., DEMAIFFE, D., & DUMONT, P. 1991. Late-Ubendian age (Lower Proterozoic) for the granitic domes of the Zairian-Zambian Copperbelt. *Comptes Rendus de L'Academie des Sciences, Serie 2, Mecanique, Physique, Chimie, Sciences de L'Univers, Sciences de la Terre*, **313**, 83-89.

NISBETT, B.W. 1996. *Notes on the Nchanga Mine, Zambia.* Unpublished Company Report, Equinox Resources, 14p.

NOTEBAART, C.W. 1978. Cupriferous micas from the Chingola area, Zambian Copperbelt. *Transactions of the Institution of Mining & Metallurgy*, **B87**, 74-78.

OHMOTO, H. 1986. Stable isotope geochemistry of ore deposits. *In:* VALLEY, J.W., TAYLOR, H.P., & O'NEIL, J.R. (eds) Stable Isotopes and High temperature Geological Processes. *Reviews in Mineralogy*, **16**, Mineralogical Society of America, 460-491.

OHMOTO, H. & RYE, R.O. 1979. Isotopes of sulphur and carbon. *In:* BARNES H.L. (ed.) *Geochemistry of hydrothermal ore deposits, 2nd edition.* John Wiley & Sons, Inc., New York, 509-567.

OHMOTO, H. & GOLDHABER, M.B. 1997. Sulphur and carbon isotopes. *In:* BARNES, H.L. (ed.) *Geochemistry of hydrothermal ore deposits, 3rd edition.* John Wiley and Sons, Inc., New York, 517-611.

OLIVER, J. 1986. Fluids expelled tectonically from orogenic belts: their role in hydrocarbon migration and other geologic phenomena. *Geology*, **14**, 99-102.

OLSON, R.A. 1984. Genesis of palaeokarst and stratabound zinc-lead sulphide deposits in Proterozoic dolostone, northern Baffin Island, Canada. *Economic Geology*, **79**, 1056-1103.

O'MEARA, A.E. 1959. *Petrography of the Basement Complex rocks and the Bwana Mkuba Series, Katanga System.* Unpublished Company Report – M.C.M. Ltd.

OSZCZEPALSKI, S. 1989. Kupferschiefer in southwestern Poland: sedimentary environments, metal zoning, and ore controls. *In:* BOYLE, R.W., BROWN, A.C., JEFFERSON, C.W., JOWETT, E.C. & KIRKHAM, R.V. (eds) *Sediment-hosted stratiform copper deposits.* Geological Association of Canada Special Paper 36, 571-600.

PEARCE, J.A., HARRIS, N.B.W. & TINDLE, A.G. 1984. Trace element discrimination diagrams for the tectonic interpretation of granitic rocks. *Journal of Petrology*, **25**, 956-983.

PEPPER, L.J. 1999. *Zambian regional granitoid study: a petrological and geochemical investigation.* Unpublished MGeol report, University of Southampton, 66p.

PETERSEN, E.U., ESSENE, E.J., & PEACOR, D.R. 1982. Fluorine end-member micas and amphiboles. *American Mineralogist*, **67**, 538-544.

PETTIJOHN, F.J., POTTER, P.E., & SIEVER, R. 1987. *Sand and Sandstone.* Springer-Verlag, Berlin, 617p.

PIENAAR, P.J. 1961. Mineralization in the basement. *In:* MENDELSOHN, F. (ed.) *The Geology of the Northern Rhodesian Copperbelt.* Macdonald: London, 30-40.

PITCHER, W.S. 1979. Comments on the geological environments of granites. *In:* ATHERTON, M.P. & TARNEY, J. (eds) *Origin of granite batholiths: geochemical evidence.* Shiva Publishing Ltd., U.K., 1-8.

PORADA, H. 1989. Pan-African rifting and orogenesis in Southern to Equatorial Africa and Eastern Brazil. *Precambrian Research*, **44**, 103-136.

PORADA, H. & BERHORST, V. 2000. Towards a new understanding of the Neoproterozoic-Early Palaeozoic Lufilian and northern Zambezi belts in Zambia and the Democratic Republic of Congo. *Journal of African Earth Sciences*, **30,** 727-771.

RAYBOULD, J.G. 1978. Tectonic controls on Proterozoic stratiform copper mineralization. *Transactions of the Institution of Mining and Metallurgy*, **B87**, 79-86.

REED, M.H. 1997. Hydrothermal alteration and its relationship to ore fluid composition. *In:* BARNES H.L. (ed.) *Geochemistry of hydrothermal ore deposits, 3rd edition.* John Wiley & Sons, Inc., New York, 303-366.

RICHARDS, J.P., KROGH, T.E., & SPOONER, E.T.C. 1988. Fluid inclusion characteristics and U-Pb rutile age of late hydrothermal alteration and veining at the Musoshi stratiform copper deposit, Central African Copperbelt, Zaire. *Economic Geology*, **83**, 118-139.

ROBERTS, S. 2003. *Investigating the hydrothermal alteration of Copperbelt mineralization; Nchanga Mine, Zambia.* Unpublished report, University of Southampton, 18p.

ROBINSON, B.W. & KUSAKABE, M. 1975. Quantative preparation of sulphur dioxide for $^{32}S/^{34}S$ analyses from sulphides by combustion with cuprous oxide. *Analytical Chemistry*, **47**, 1179-1181.

ROEDDER, E. & BODNAR, R.J. 1997. Fluid inclusion studies of hydrothermal ore deposits. *In:* BARNES, H.L. (ed.) *Geochemistry of hydrothermal ore deposits, 3rd edition.* John Wiley and Sons, Inc., New York, 657-698.

ROSE, A.W. 1970. Zonal relations of wall rock alteration and sulphide distribution of porphyry copper deposits. *Economic Geology*, **65**, 920-936.

ROSE, A.W. 1976. The effect of cuprous chloride complexes in the origin of red-bed copper and related deposits. *Economic Geology*, **71**, 1036-1048.

ROSE, A.W. 1989. Mobility of copper and other heavy metals in sedimentary environments. *In:* BOYLE, R.W., BROWN, A.C., JEFFERSON, C.W., JOWETT, E.C., & KIRKHAM, R.V. (eds) *Sediment-Hosted Stratiform Copper Deposits.* Geological Association of Canada Special Paper 36, 97-110.

ROSE, A.W. & BURT, D.M. 1979. Hydrothermal alteration. *In:* BARNES H.L. (ed.) *Geochemistry of hydrothermal ore deposits, 2nd edition.* John Wiley & Sons, Inc., New York, 173-235.

RYE, R.O & OHMOTO, H. 1974. Sulphur and carbon isotopes and ore genesis: a review. *Economic Geology*, **69**, 826-842.

SANZ, J. & STONE, W.E.E. 1979. NMR study of micas, II. Distribution of Fe^{2+}, F^-, and OH^- in the octahedral sheet of phlogopites. *American Mineralogist*, **64**, 119-126.

SCHWARCZ, H.P. & BURNIE, S.W. 1973. Influence of sedimentary environments on sulphur isotope ratios in clastic rocks – review. *Mineralium Deposita*, **8**, 264-277.

SELBY, D. & NESBITT, B.E. 1998. Biotite chemistry of the Casino Porphyry Cu-Mo-Au occurrence, Dawson Range. *In: Yukon Exploration and Geology* (1997), Exploration and Geological Services Division, Yukon, Indiana Northern Affairs, Canada, 83-88.

SEWARD, T.M. & BARNES, H.L. 1997. Metal transport by hydrothermal ore fluids. *In:* BARNES H.L. (ed.) *Geochemistry of hydrothermal ore deposits, 3rd edition.* John Wiley & Sons, Inc., New York, 435-486.

SHARP, Z.D. 1992. In situ laser microprobe techniques for stable isotope analysis. *Chemical Geology*, **101**, 3-19.

SHARP, Z.D. & KIRSCHNER, D.L. 1994. Quartz-calcite oxygen isotope thermometry: a calibration based on natural isotopic variations. *Geochimica et Cosmochimica Acta*, **58**, 4491-4501.

SHEPHERD, T.J., RANKIN, A.H., & ALDERTON, D.H.M. 1985. *A practical guide to fluid inclusion studies.* Blackie: London, 239p.

SHEPPARD, S.M.F. 1986. Characterization and isotopic variations in natural waters. *In:* VALLEY, J.W., TAYLOR, H.P., & O'NEIL, J.R. (eds) Stable Isotopes and High temperature Geological Processes. *Reviews in Mineralogy*, **16**, Mineralogical Society of America, 165-184.

SIMMONDS, J. 1998. The Central African Copperbelt: tectonic overview, metallogeny and analysis of current research. *Geological Society of Australia, Abstracts No. 50: The Assembly and Breakup of Rodinia*, Perth, 57-59.

SKAULI, H., BOYCE, A.J. & FALLICK, A.E. 1992. A sulphur isotope study of the Blaekvassli Zn-Pb-Cu deposit, Nordland, North Norway. *Mineralium Deposita*, **27**, 284-292.

SKRIPCHENKO, N.S. 1986. Zoning and concentration of mineralization in sandstone- and shale-hosted copper deposits. *International Geology Review*, **28**, 1313-1326.

SLACK, J.F. 1996. Tourmaline associations with hydrothermal ore deposits. *In:* GREW, E.S. & ANOVITZ, L.M. (eds) Boron: mineralogy, petrology, and geochemistry. *Reviews in Mineralogy*, **33**, 585-637.

STANTON, R.J. 1966. The solution brecciation process. *Geological Society of America Bulletin*, **77**, 843-847.

STERNER, S.M., HALL, D.L., & BODNAR, R.J. 1988. Synthetic fluid inclusions. V. solubility relations in the system NaCl-KCl-H_2O) under vapor-saturated conditions. *Geochimica et Cosmochimica Acta*, **52**, 989-1005.

STRECKEISEN, A. (1976). To each plutonic rock its proper name. *Earth Science Reviews*, **12**, 1-33.

SUPPE, J & MEDWEDEFF, D.A. 1990. Geometry and kinematics of fault-propagation folding. *Eclogae Geologicae Helveticae*, **83**, 409-454.

SUSAK, N. & CRERAR, D. 1985. Spectra and coordination changes of transition metals in hydrothermal solutions: implications for ore genesis. *Geochimica et Cosmochimica Acta*, **49**, 555-564.

SUTTON, S.J. & MAYNARD, J.B. 2002. Fluid mixing model for the Zambian Copperbelt. *In:* ROBB, L.J. & MOUNTJOIE, R. (eds) *Extended Abstracts Proceedings 11th Quadrennial IAGOD Symposium and Geocongress 2002.* (CD ROM), Geological Survey of Namibia, Namibia.

SVERJENSKY, D.A. 1984. Oilfield brines as ore-forming solutions. *Economic Geology*, **79**, 23-37.

SVERJENSKY, D.A. 1987. The role of migrating oil-field brines in the formation of sediment-hosted copper-rich deposits. *Economic Geology*, **82**, 1130-1141.

SVERJENSKY, D.A. 1989. Chemical evolution of basinal brines that formed sediment-hosted Cu-Pb-Zn deposits. *In:* BOYLE, R.W., BROWN, A.C., JEFFERSON, C.W., JOWETT, E.C., & KIRKHAM, R.V. (eds) *Sediment-hosted stratiform Copper deposits.* Geological Association of Canada Special Paper 36, 111-126.

SWEENEY, M.A. 1985. *Diagenetic processes in ore formation with special reference to the Zambian Copperbelt and Permian Marl Slate.* Unpublished PhD dissertation, University of Aston, Birmingham, UK, 270p.

SWEENEY, M.A. & BINDA, P.L. 1989. The role of diagenesis in the formation of the Konkola Cu-Co Orebody of the Zambian Copperbelt. *In:* BOYLE, R.W., BROWN, A.C., JEFFERSON, C.W., JOWETT, E.C., and KIRKHAM, R.V (eds) *Sediment-hosted stratiform Copper deposits.* Geological Association of Canada Special Paper 36, 499-518.

SWEENEY, M.A. & BINDA, P.L. 1994. Some constraints on the formation of the Zambian Copperbelt deposits. *Journal of African Earth Sciences*, **19 (4)**, 303-313.

SWEENEY, M.A., BINDA, P.L. & VAUGHAN, D.J. 1991. Genesis of the ores of the Zambian Copperbelt. *Ore Geology Reviews*, **6**, 51-76.

SWEENEY, M.A., TURNER, P., & VAUGHAN, D.J. 1986. Stable isotope and geochemical studies of the role of early diagenesis in ore formation, Konkola Basin, Zambian Copperbelt. *Economic Geology*, **81**, 1836-1852.

TAYLOR, H.P. 1979. Oxygen and hydrogen isotope relationships in hydrothermal mineral deposits. *In:* BARNES H.L. (ed.) *Geochemistry of hydrothermal ore deposits, 2nd edition.* John Wiley & Sons, Inc., New York, 236-277.

TAYLOR, H.P. 1997. Oxygen and hydrogen isotope relationships in hydrothermal mineral deposits. *In:* BARNES H.L. (ed.) *Geochemistry of hydrothermal ore deposits, 3rd edition.* John Wiley & Sons, Inc., New York, 229-302.

TAYLOR, R.G. 1994. *Ore Textures, volume 2: Alteration.* National Library of Australia, 58p.

TEMBO, F., KAMPUNZU, A.B. & PORADA, H. 1999. Tholeiitic magmatism associated with continental rifting in the Lufilian Fold Belt of Zambia. *Journal of African Earth Sciences*, **28**, 403-425.

THODE, H.G., CRAGG, C.B., HULSTON, J.R., & REES, C.E. 1971. Sulphur isotope exchange between sulphur dioxide and hydrogen sulphide. *Geochimica et Cosmochimica Acta*, **35**, 35-45.

TRUDE, K.J. & WILKINSON, J.J. 2001. A mineralogical and fluid inclusion study of the Harberton Bridge Fe-Zn-Pb deposit, County Kildare, Ireland. *Journal of the Geological Society of London*, **158**, 37-46.

UNRUG, R. 1983. The Lufilian Arc: A microplate in the Pan-African collision zone of the Congo and the Kalahari Cratons. *Precambrian Research*, **21**, 181-196.

UNRUG, R. 1988. Mineralization controls and source of metals in the Lufilian Fold Belt, Shaba (Zaire), Zambia, and Angola. *Economic Geology*, **83**, 1247-1258.

UNRUG, R. 1989. Landsat-based structural map of the Lufilian fold belt and the Kundelungu aulacogen, Shaba (Zaire), Zambia, and Angola, and the regional position of Cu, Co, and U. *In:* BOYLE, R.W., BROWN, A.C., JEFFERSON, C.W., JOWETT, E.C., & KIRKHAM, R.V. (eds) *Sediment-hosted stratiform Copper deposits.* Geological Association of Canada Special Paper 36, 519-524.

VALLEY, J.W., PETERSEN, E.U., ESSENE, E.J., & BOWMAN, J.R. 1982. Fluorphlogopite and fluortremolite in Adirondack marbles and calculated C-O-H-F fluid compositions. *American Mineralogist*, **67**, 545-557.

VAN EDEN, J.G. 1974. Depositional and diagenetic environment related to sulphide mineralization, Mufulira, Zambia. *Economic Geology*, **69**, 59-79.

VAN EDEN, J.G. & BINDA, P.L. 1972. Scope of stratigraphic and sedimentologic analysis of the Katanga Sequence, Zambia. *Geologie en Mijnbouw*, **51(3)**, 321-328.

VELASCO, F., SÁNCHEZ-ESPANA, J., BOYCE, A.J., FALLICK, A.E., SÁEZ, R. & ALMODOVAR, G.R. 1998. A new sulphur isotopic study of some IPB deposits: Evidence of a textural control on sulphur isotope composition. *Mineralium Deposita*, **34**, 4-18.

VEIZER, J. & HOEFS, J. 1976. The nature of O^{18}/O^{16} and C^{13}/C^{12} secular trends in sedimentary carbonate rocks. *Geochimica et Cosmochimica Acta*, **40**, 1387-1395.

VERGES, J., MUNOZ, J.A., & MARTINEZ, A. 1992. South Pyrenean fold-and-thrust belt: Role of foreland evaporitic levels in thrust geometry. *In:* MCCLAY, K.R. (ed.) *Thrust Tectonics.* Chapman & Hall, London, 255-264.

VINK, B.W. 1972. Sulphide mineral zoning in the Baluba Orebody, Zambia. *Geologie en Mijnbouw*, **51**, 309-313.

VOET, H.W. & FREEMAN, P.V. 1972. Copper orebodies in the basal Lower Roan meta-sediments of the Chingola open-pit area, Zambian Copperbelt. *Geologie en Mijnbouw*, **51 (3)**, 299-308.

WAGNER, T., BOYCE, A.J., & FALLICK, A.E. 2002. Laser combustion analysis of $\delta^{34}S$ of sulfosalt minerals: Determination of the fractionation systematics and some crystal-chemical considerations. *Geochimica et Cosmochimica Acta*, **66**, 2855-2863.

WAKEFIELD, J. 1978. Samba: a deformed porphyry-type copper deposit in the basement of the Zambian Copperbelt. *Transactions of the Institution of Mining and Metallurgy*, **87**, B43-52.

WARREN, J.K. 1997. Evaporites, brines and base metals: fluids, flow and 'the evaporite that was.' *Australian Journal of Earth Sciences*, **44**, 149-183.

WARREN, J.K. 1999. *Evaporites: Their Evolution and Economics.* Blackwell Science, 282p.

WATSON, J. 1973. Influence of crustal evolution on ore deposition. *Transactions of the Institution of Mining and Metallurgy*, **B82**, 107-113.

WENDORFF, M., KAMPUNZU, A.B., CAILTEUX, J., & BINDA, P.L. 2000. Tectono-sedimentary evolution of the Central African Copperbelt. *31st International Geological Congree Extended Abstracts of the Neoproterozoic Symposium F-7, Rio de Janeiro* (CD ROM).

WESTRICH, H.R. 1981. F-OH exchange equilibria between mica-amphibole mineral pairs. *Contributions to Mineralogy and Petrology*, **78**, 318-323.

WHITE, A.J.R. & CHAPPELL, B.W. 1977. Ultrametamorphism and granitoid genesis. *Tectonophysics*, **43**, 7-22.

WHYTE, R.J. & GREEN, M.E. 1971. Geology and palaeogeography of Chibuluma West Orebody, Zambian Copperbelt. *Economic Geology*, **66**, 400-424.

WILKINSON, J.J. 1990. *The origin and evolution of Hercynian crustal fluids, South Cornwall, England.* Unpublished PhD thesis, University of Southampton, 298p.

WILKINSON, J.J., BOYCE, A.J., EARLS, G., & FALLICK, A.E. 1999. Gold remobilization by low-temperature brines: evidence from the Curraghinalt gold deposit, Northern Ireland. *Economic Geology*, **94**, 289-296.

WILLAN, R.C.R. & COLEMAN, M.L. 1983. Sulphur isotope study of the Aberfeldy barite, zinc, lead deposit and minor sulphide mineralization in the Dalradian Metamorphic Terrain, Scotland. *Economic Geology*, **78**, 1619-1656.

XIAO, Z., GAMMONS, C.H., & WILLIAMS-JONES, A.E. 1998. Experimental study of copper(I) chloride complexing in hydrothermal solutions at 40 to 300°C and saturated water vapour pressure. *Geochimica et Cosmochimica Acta*, **62**, 2949-2964.

YARDLEY, B.W.D. 1989. *An introduction to metamorphic petrology.* Longman Group Ltd., 248p.

ZHANG, L., LIU, J., ZHOU, H., & CHEN, Z. 1989. Oxygen isotope fractionation in the quartz-water-salt system. *Economic Geology*, **84**, 1643-1650.

ZHENG, Y.F. 1993. Calculation of oxygen isotope fractionation in anhydrous silicate minerals. *Geochimica et Cosmochimica Acta*, **57**, 1079-1091.

ZHENG, Y.F. 1999. Oxygen isotope fractionation in carbonate and sulphate minerals. *Geochemical Journal*, **33**, 109-126.